Understanding the Potential for Nitrate Attenuation from Paddock to Stream using Dual Nitrate Isotopes.

A thesis

submitted in partial fulfilment

of the requirements for the Degree of

Doctor of Philosophy

at

Lincoln University

by

Sephrah Amy Rayner

Lincoln University

2019

Abstract of a thesis submitted in partial fulfilment of the requirements for the Degree of Doctor of Philosophy.

Understanding the Potential for Nitrate Attenuation from Paddock to Stream using Dual Nitrate Isotopes

by

Sephrah Amy Rayner

Ruminant urine deposition can result in nitrate (NO_3^-) leaching from soil to groundwater under agricultural systems. Nitrous oxide (N_2O) emissions from ruminant urine patches are also a major concern as N_2O is a potent greenhouse gas and contributes to ozone depletion. New Zealand agriculture is dominated by grazed-pasture systems, where ruminant urine deposition has become a significant environmental concern. Attenuation (removal) of NO_3^- from the system through biological denitrification, reducing it to the inert gas dinitrogen (N_2), is one way to reduce NO_3^- leaching losses and N_2O emissions from agriculture. Understanding temporal and spatial variations in NO_3^- attenuation capacity that occurs within the landscape, between the site of ruminant urine deposition and stream or groundwater contamination, may provide a key mitigation tool. The general goal of this PhD programme was to use isotope analysis and soil physics to increase our knowledge of when, 'hot moments', and where, 'hot spots', of NO_3^- attenuation occur under grazed agricultural soils.

Soil physical properties; soil moisture, defined as soil matric potential (Ψ), and relative gas diffusivity (D_p/D_0) play key roles in the amount and rate of NO_3^- attenuation that occurs in the soil. These properties were explored under controlled laboratory conditions for two pasture soils (both A and B horizons), to identify the key Ψ for holding D_p/D_0 at a previously identified threshold for peak denitrification to occur (Chapter 4). The identified key Ψ was then used to analyse the effect of soil type on dual NO_3^- isotope signatures under laboratory conditions (Chapter 5). Another factor that could affect dual NO_3^- isotope signatures is the presence or absence of plants in the soil under bovine urine (BU) patches. This was assessed using lysimeters in a field setting over time, to also better understand temporal isotope dynamics (Chapter 6). All findings were then taken into consideration in a field context, where temporal and spatial variation in N attenuation was measured at two contrasting field sites in Southland, New Zealand using dual NO_3^- isotope signatures and soil physical properties (Chapter 7).

Significant results were found in laboratory trials indicating that peak N_2O emissions occurred at D_p/D_0 values < 0.006, allowing for the D_p/D_0 values associated with NO_3^- attenuation to be extrapolated to field sites, to provide a general overview of what D_p/D_0 values we expect to see in the field when attenuation is occurring. Spatial variation in dual nitrate isotopes was found to be significantly different between soil A and B horizon soils. The A horizon soils played a key role in N processing, showing an isotopic fractionation rate +14‰ greater than in B horizon soils. However, these findings were confounded by diluted expression of NO_3^- attenuation, as prolonged water logging shifted the isotopic signature from enrichment to depletion. This was thought to be due to heterotrophic nitrification changing isotopic N signals in the soil under extended periods of high soil water. The lysimeter study showed $\delta^{15}N\text{-}NO_3^-$ and $\delta^{18}O\text{-}NO_3^-$ to vary temporally, with evidence of denitrification enrichment of isotopes. Plant presence or absence was also found to significantly influence isotope signatures, but only when BU was not applied, indicating that denitrification may be driven by a plant derived C supply at very low NO_3^- concentrations. However, the proportion of N leached under such low NO_3^- concentrations will be minimal and therefore the influence of plant presence will have negligible impact on interpreting drainage $\delta^{15}N$ values. Field study sites demonstrated highly dynamic NO_3^- isotope composition, and that N attenuation hotspots were strongly influenced by spatial variation (soil type) and extended rainfall events, as evidenced by modelled D_p/D_0 values. Dilution of the denitrification isotope signal by mineralisation of soil N and/or nitrification occurred, reinforcing the role of soil processes in realigning the NO_3^--N isotope signal back to a soil-N signal as NO_3^- moves through the soil profile.

This research has clearly shown that $\delta^{15}N\text{-}NO_3^-$ and $\delta^{18}O\text{-}NO_3^-$ show potential for identifying NO_3^- sources and soil processes forming and removing NO_3^-. Further ground-truthing of in situ NO_3^- attenuation, determined by D_p/D_0 values < 0.02 is warranted, as this could potentially provide an economic way for farmers and policy makers to both recognise and even engineer 'hot moments' and 'hot spots' of N attenuation occurring in the landscape.

Keywords: Nitrate, denitrification, attenuation, grazed pastures, stable isotopes, Rayleigh fractionation, diffusion, biogeochemistry, nitrogen leaching, relative soil gas diffusivity, D_p/D_0, soil oxygen, bovine urine, perennial ryegrass (*Lolium perenne* L), ^{15}N isotope.

Acknowledgements

Thanks to my supervisors Tim Clough, Troy Baisden and Jim Moir. To my primary supervisor Professor Tim Clough, thank you for your support, valuable feedback and advice throughout this whole process. Your limitless fountain of knowledge and quoting of references never failed to impress me. Jim, thanks for sticking with me throughout my thesis, honours and undergraduate degree, giving me the needed nudges of motivation, your review and valuable feedback was greatly appreciated.

The best technicians a student could ask for; Neil and Nigel. Always there to help with technical disasters and provide interestingly curious conversation along the way. Neil, you are one of a kind and deserve every word of appreciation that I can think of. Your help with every step of the technical set up of my field trials and the running of them, I could not have done without. I'll never forget your generosity, of being available for me to call on the weekend when yet another sensor had stopped working and I was freezing my arse off in the field, with my head in the datalogger on the phone to you trying to figure it out. Priceless.

Thank you to the people at Lincoln's Analytical Services team, including but not limited to; Leanne Hassall, Qian Liang, Emily Huang, with a special thanks to Roger Creswell. Your willingness to help and the genuine care you had for students and their projects does not go un-noticed, you are a star of a human! Leanne you are the bomb, thanks for all you help and listening to my ramblings, it helped no end. Amal Torky, I don't think anyone in the department would function without you, a true angel and mother to all, thanks for all your hugs and support.

Shout out to my funders who made this whole thing possible; GNS Science, Wellington, Environment Southland, Invercargill and Lincoln University. Special thanks to Environment Southland, where I spent many a month tinkering away with my field trial, taking up valuable desk space and time. Welcoming me into your work community and letting me present my work as it progressed kept me going both emotionally and mentally, you really have a great team! Spending time in Southland is epic, wouldn't have wanted to run a field trial anywhere else (well, maybe somewhere warmer), but what an epic landscape to explore!

Family and friends, your patience, kindness and support gave me the motivation and determination I needed to get through this roller coaster of a project. I couldn't have done it without you all. Mum, Phebs and Jonny, you are truly gorgeous, behind me 100% of the way with the kindest words and lots of love, couldn't have asked for a better support team. Connor, for supporting me and putting up with all the ups and downs, I don't know how you do it but I'm really glad that you've had the patience, don't know where I'd be without you. Thanks to the whole Edwards family for adopting me, you make Wellsford a warmer place.

Table of Contents

List of Tables

List of Figures

List of Images

Acronyms & Abbreviations

ρ_b	Soil bulk density (Mg m^{-3})
ρ_d	Soil particle density (Mg m^{-3})
D_p	Gas Diffusion coefficient in soil (cm^3 soil air cm^{-1} soil s^{-1})
D_0	Gas Diffusion coefficient in air (cm^2 air s^{-1})
D_p/D_0	Relative Gas Diffusivity
ψ	Matric potential (-kPa)
Φ	Total porosity (m^3 void m^{-3} soil)
Ɛ	Air-filled porosity (m^3 air m^{-3} soil)
Ɛ/ Φ	Relative air-filled porosity
WFPS	Water-filled pore space
θg	Gravimetric water content (g water g^{-1} dry soil)
θv	Volumetric water content (m^3 water m^{-3} soil)
C	Carbon
CO_2	Carbon dioxide
OC	Organic carbon
DOC	Dissolved organic carbon
N	Nitrogen
NO_3^-	Nitrate
NO_2^-	Nitrite
NH_4^+	Ammonium
NH_3	Ammonia
N_2	Dinitrogen
N_2O	Nitrous oxide
KNO_3	Potassium nitrate
O_2	Oxygen
$(NH_4)^2SO_4$	Ammonium sulfate
KCl	Potassium chloride
Ar	Argon
DNRA	Dissimilatory nitrate reduction to ammonium
SEM	Standard error of mean
DI	Deionized water
ε	Fractionation enrichment factor
BU	Bovine urine

Chapter 1

Introduction

Grass-fed stock are a key component of agriculture, especially in New Zealand (Clough et al., 2005). However, grazed pasture systems are also the source of substantial greenhouse gas emissions (IPCC, 2014b). Anthropogenic emissions of N_2O, a greenhouse gas, are associated with the deposition of ruminant urine (Selbie et al., 2015) and in addition it is currently the dominant anthropogenic ozone-depleting substance emitted (Ravishankara et al., 2009). Ruminant urine deposition is also associated with NO_3^- leaching, which contaminates waterways, reducing water quality for recreation and freshwater ecosystems (Daughney & Randall, 2009; Galloway et al., 2015; McLaren & Cameron, 1996; Parfitt et al., 2012) and it is the main contaminant in New Zealand groundwater (Close et al., 2016).

The Southland region has the largest number of dairy herds in the South Island of New Zealand, with 989 herds covering an effective land area of 209,133 ha, totalling 563,017 dairy cows (SIDDC, 2017). There has been a considerable increase in dairy cow numbers since the 1980's (Drewry & Paton, 2000): between 1990 and 1999 alone, cow numbers in Southland increased by 513% (Hamill & McBride, 2003). With a rapid decline in sheep numbers due to the conversion to dairying (Figure 1.1). Concerns over the contamination of ground and surface water systems, from agricultural N sources, have led to the introduction of a number of reforms in freshwater management (Close et al., 2016), including but not limited to, a National Policy Statement for Freshwater Management, which contains a legislative framework for freshwater nutrient limits, including NO_3^- (Environment, 2014). Southland's increased number of dairy cows (Figure 1.1) and the land area associated (36% of the region is pastoral land, 8% of the national total, Ledgard (2013)) make it an important region to focus on, in terms of understanding NO_3^- attenuation within the landscape.

Figure 1.1: Stock numbers in the Southland Region from 1860 to 2011, (Ledgard, 2013).

To understand the primary controls on catchment scale NO_3^- export, multiple observations across spatial and temporal scales are required due to the complex interactions between hydrological and biogeochemical processes (Ocampo et al., 2006). Prior research indicates that NO_3^- attenuation via denitrification occurs predominately in headwater catchments (Alexander et al., 2000; Jahangir et al., 2012). However, research is lacking with respect to New Zealand systems. Due to the difficulty of subsurface groundwater sampling there is relatively little knowledge on the spatial and temporal distribution of groundwater reducing zones and associated rates of denitrification (Close et al., 2016) and, as such, available data are predominantly limited to groundwater sampled from existing wells. Extrapolation of this limited data to regional scale has been attempted by Close et al. (2016), following work by Stenger et al. (2008) and Clague et al. (2015b), with varying degrees of success. Isotope analysis (Baisden et al., 2016b; Mudge et al., 2013; Stevenson et al., 2010; Wells et al., 2015; Wells et al., 2016) and relative soil gas diffusivity (Balaine et al., 2016b; Balaine et al., 2013) are also tools that have been used to try and further understand NO_3^- attenuation at various scales.

1.1 Research Objectives & Thesis Structure

This project will focus on understanding NO_3^- transfers and transformations from grazed pastures, focusing on NO_3^- attenuation in the landscape. Identifying key changes in isotopic composition and diffusivity, both spatially and temporally in the landscape, to quantify and identify “hot moments” and “hot spots” of N attenuation. With the aim to fill gaps in the current knowledge about topsoil and subsoil NO_3^- attenuation rates at both spatial and temporal scales in Southland, in addition to directly improving our understanding of soil impacts on NO_3^- dynamics for flows entering and passing through New Zealand’s ground and surface water.

The research outlined in this thesis examines soil NO_3^- attenuation using stable isotopes as an attenuation measurement tool. This study will look at the soil type effects on NO_3^- attenuation at spatial (various soils) and temporal scales (over time as affected by environmental events).

The key research objectives are:

- Identification of spatial "hot spots" and triggers of denitrification in the landscape using repacked soil cores. Specifically, trying to identify if there is an expected shift in $\delta^{15}N$ and $\delta^{18}O$ for a given decrease in NO_3^- across different soil types.

- Identify if there is variation in NO_3^- isotope fractionation with and without plants. What role do plants play? How does the presence of plants/plant growth influence the isotope signature of NO_3^-?

- Define and quantify temporal influences on N attenuation and N isotope signatures. Identifying "hot moments", their duration and the location of the "hot spot" in the soil when they occur.

There is limited knowledge about the capacity of landforms to attenuate NO_3^- concentrations both temporally and spatially in agricultural landscapes within New Zealand. The experiments that follow will be used to identify the key factors that influence temporal and spatial variation of N attenuation in the landscape.

This thesis is comprised of eight chapters, following this introductory chapter. Relevant literature Is reviewed, summarising literature relevant to N attenuation in the landscape (**Chapter 2**). This includes a review of isotope and soil physical properties that affect N attenuation, and how this varies both spatially and temporally in the New Zealand landscape and identification of research gaps. Some chapter introductions repeat segments of the literature review, to add to and reinforce points made. An overview of the general methods used in experiments is given (**Chapter 3**) and is referenced in the following chapters.

Chapters 4 to 7 present experiment outlines, methods, the results and discussion for research undertaken during this PhD. Chapter 6 is presented as a manuscript.

Chapter 4, Experiment 1 focuses on spatial variation in N attenuation using different soil types. It introduces the concept of relative gas diffusivity (D_p/D_0).

Experiment 1 was a laboratory trial conducted at Lincoln University using repacked soil cores, tension tables and diffusivity chambers. This assessed different soil types at different levels of soil Ψ as well as modelling D_p/D_0 to identify N attenuation effects. This trial aimed to further refine the concept of the

denitrification threshold as it relates to D_p/D_0 in order to better understand if D_p/D_0 can provide an accurate predictor for different soil types.

Experiment 1 concluded that peak N_2O emissions for all soil types were found to occur at modelled D_p/D_0 values of <0.006, similar to those previously reported. This further expresses the ability for D_p/D_0 to be used as a key indicator of denitrification thresholds. No significant soil type effect was found on D_p/D_0 values at the very wet end of the soil moisture spectrum (-0.5 kPa to -2 kPa), which is when denitrification is occurring, and therefore soil type does not influence the D_p/D_0 denitrification threshold.

Chapter 5, Experiment 2 also focuses on spatial variation using different soil types. It attempts to use dual NO_3^- isotope signatures to quantify and identify N attenuation processes alongside D_p/D_0.

Experiment 2 was a laboratory trial conducted at Lincoln University using repacked soil cores, tension tables and diffusivity chambers. This assessed different soil types and changes in D_p/D_0 and dual NO_3^- isotope signatures over a three-week period to identify N attenuation effects over time. Soil moisture was held at -0.5 kPa as identified in Chapter 4, to ensure peak denitrification occurred. It was hypothesised that the denitrification fractionation factor would vary spatially due to different soils providing different levels of C, NO_3^- and O_2 which are key factors controlling denitrification.

Experiment 2 concluded that there was spatial variability in NO_3^- isotope signatures with soil horizon, with the A horizon playing a dominant role. Another key finding was the shift in the residual NO_3^- pool from being progressively enriched over time to a situation where the NO_3^- pool becomes progressively depleted. Based on previous studies it is hypothesised that heterotrophic nitrification rates were in excess of denitrification rates and/or denitrification had ceased in order to cause this effect. It was concluded that prolonged saturation of the A horizon caused this shift in the NO_3^- pool, with the resulting depletion of NO_3^- isotope signatures confusing the expression of NO_3^- attenuation.

Chapter 6, Experiment 3 focuses on temporal variation in isotope composition under BU patches in the presence or absence of plants. Dual NO_3^- isotope signatures were measured in leachate to quantify and identify N attenuation processes.

Experiment 3 was a lysimeter field study at Lincoln University using lysimeters containing intact soil columns collected from the Central Plains area in Southland, New Zealand. This experiment assessed changes in dual NO_3^- isotope signatures of leachate under different levels of BU over a 9-month period to identify treatment effects on N attenuation over time, with the presence or absence of plants. The objectives of this study were to determine if pasture plants influenced the isotope signature of leached

NO_3^- following deposition of ruminant urine onto pasture and determine if the isotope signature of leached NO_3^- exhibited any temporal variability.

Experiment 3 concluded that; the presence of pasture induced strong isotopic shifts in $\delta^{15}N\text{-}NO_3^-$ for antecedent NO_3^- in the absence of any BU loading and that $\delta^{15}N\text{-}NO_3^-$ increases over time due to denitrification of NO_3^-. Temporal variation in NO_3^- isotopic signatures were negligible, with key influences being N loading and associated factors controlling microbial activity.

Chapter 7, Experiment 4 focused on temporal and spatial variation in N attenuation under BU patches in a field setting. Dual NO_3^- isotope signatures were measured in soil solution samples, along with soil physical conditions; soil O_2, soil moisture and soil temperature and environmental factors in an attempt to quantify and identify N attenuation processes.

Experiment 4 was a field trial carried out at two sites in the Five Rivers area in the Southland region of New Zealand. This experiment assessed changes between two contrasting soils, at four soil depths, over a two-year period. Measurements of dual NO_3^- isotope signatures and soil physical conditions; O_2, moisture and temperature were performed, as well as the collection of climate data over the two-year period. This information was used to model diffusivity to identity "hot spots" within the soil and temporal "hot moments" of increased N attenuation. Corresponding isotope analysis was used in an attempt to identify which N processes were occurring, along with the N source and the N attenuation rate. It was hypothesised that field data would show 'hot moments' (duration) and 'hot spots' (location) within the soil profile of N attenuation that corresponded with modelled D_p/D_0 and NO_3^- isotope values.

Experiment 4 demonstrated that the NO_3^- isotopic composition, over the study period, was highly dynamic and that D_p/D_0 values were strongly influenced both spatially (soil type and depth) and temporally (periods of extended rainfall). Dilution of the denitrification signal by soil N processes (mineralisation and/or nitrification) was evident, warranting future work looking at nitrification rates and mechanisms at different depths and soil horizons under varying soil moisture contents. Extending the period of sampling to encompass the full BU derived NO_3^- breakthrough curve is also needed to get a full picture of any change in denitrified isotope signatures after the soil has had more time to process N.

Chapter 8 provides a summary and comparison of the experiments performed in this thesis, concluding with future research suggestions.

A map of the experiments is presented below in Figure 1.2, showing the flow of key experimental questions in the thesis.

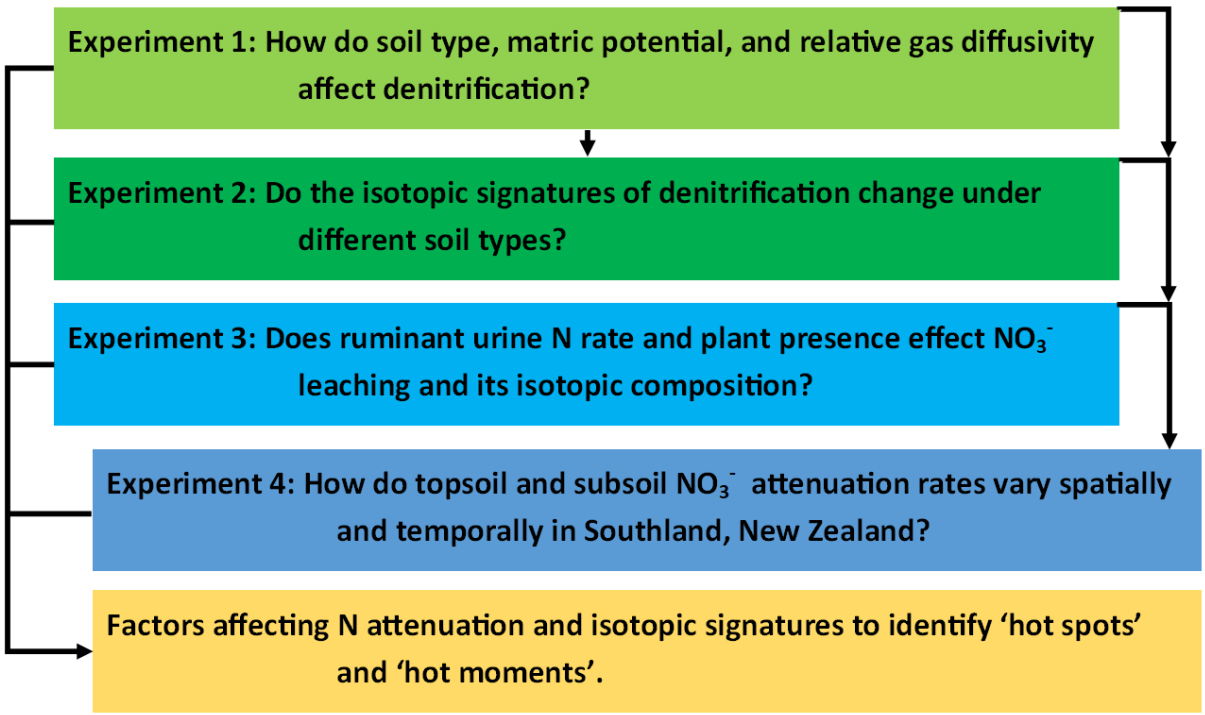

Figure 1.2: Flow of the thesis outline, showing the key research question for each experiment and how they link together to show how one informs the other.

Chapter 2

Literature Review

This literature review focuses on stable isotopes, soil physical and chemical properties, their relationships to soil NO_3^- attenuation (the removal of NO_3^- from the environment) and the potential use of such relationships to measure NO_3^- attenuation. Stable isotopes are defined, dual-isotope methods and their use as a measurement tool are examined. Nitrate attenuation and denitrification are reviewed. Possible management strategies for dealing with NO_3^- leaching are also discussed.

2.1 Implications of Increasing N Levels in the Environment

The main contaminant in New Zealand groundwater is NO_3^- (Close et al., 2016), which is becoming increasingly problematic in areas of intensively grazed and/or fertilised pasture (Cameron & Haynes, 1986; Stark & Richards, 2008). Excess nutrient levels, predominately NO_3^-, result in reduced water quality for recreation, and freshwater ecosystems, due to eutrophication of surface waters (Galloway et al., 2015; McLaren et al., 1996; Parfitt et al., 2012). Nitrate contamination reputedly causes human and animal health issues through aquifer contamination and reduced drinking water quality, all of which are costly to mitigate, but this remains controversial (Addiscott & Benjamin, 2004). Methemoglobinemia and cancer are the two most widely discussed human health problems associated with NO_3^- (Addiscott et al., 2004; Schullehner et al., 2018). Nitrate has been dismissed as the cause of methemoglobinemia, as it is a side-effect of gastroenteritis caused by nitric oxide not NO_3^- which is associated with the bacterial pollution of wells (Addiscott et al., 2004). Nitrate as a cause of cancer in humans is also still widely debated, with research both supporting and dismissing it (Addiscott et al., 2004; Schullehner & Hansen, 2014; Schullehner et al., 2018). In the environment the immediate impact of NO_3^- contamination is eutrophication of water bodies, causing algal or cyanobacterial blooms which can cause hypoxia, disrupt ecosystems and can also be toxic (Conley et al., 2009; Dodds & Smith, 2016). The role of N in different water bodies and its control on eutrophication is an ongoing point of discussion in research (Dodds et al., 2016; Howarth & Marino, 2006; Smith et al., 2016).

Sources of NO_3^- in groundwater potentially include sewage, atmospheric N deposition, fertiliser-N and animal excreta sourced-N from pasture grazing systems (Malcolm et al., 2014a). Uptake of NO_3^- by biomass such as pasture or its removal through denitrification, hereafter termed ‘attenuation’ is desirable, as this can reduce the amount of NO_3^- entering waterways (Clough et al., 1998a; Clough et al., 2005).

Nitrate attenuation in ground and surface waters can potentially occur through many different pathways that include: dilution (Mengis et al., 1999), nitrifier-denitrification, biological denitrification (Wrage-Mönnig et al., 2018) chemo-denitrification (Robertson & Groffman, 2007) and coupled denitrification (An & Joye, 2001). However, denitrification (microbial reduction of NO_3^-, Wrage et al. (2001)) is the primary mechanism for NO_3^- attenuation (Clément et al., 2003). It is influenced by biological (soil microbial community structure and function), physical and chemical factors (soil moisture, O_2 supply, substrate (C and N) supply, temperature and pH (Balaine et al., 2016b; Clague et al., 2015a; Clough et al., 2005; Firestone & Davidson, 1989; Keeney & Fillery, 1979; Knowles, 1982; Mathieu et al., 2006; Neira et al., 2015; Robertson et al., 2007).

Stable isotope methodologies potentially enable the relative source contributions to ground or surface water NO_3^- in the environment to be identified (Seiler, 2005; Widory et al., 2004). This is because different sources of NO_3^- often have isotopically distinct N and O isotopic compositions (Liu et al., 2006). In addition, biological cycling of N fractionates isotopic ratios in predictable and recognizable directions, as light and heavy isotopes react at different rates, creating product and reactant pools of varying isotopic composition (Kendall, 1998). During denitrification, the change in isotopic composition can be directly related to the reaction rate using a Rayleigh model of kinetic fractionation by measuring the change in isotope composition and NO_3^- concentration relative to the original NO_3^- pool using a denitrification fractionation factor (Wells et al., 2016; Xue et al., 2009), assuming that the product pool is continuously removed and there is a constant degree of isotopic discrimination (Kendall & Caldwell, 1998). Potentially, this enables the isotope signatures of the NO_3^- molecule to be used at the landscape scale in order to assess the potential for landscape attenuation of NO_3^-. New Zealand's low atmospheric N inputs, additions of N based fertilisers and intensive pastoral agriculture potentially allow the use of dual NO_3^- isotopes to differentiate soil and effluent sources of N (Baisden et al., 2016a).

Research into the removal of NO_3^- from agricultural ecosystems is important in New Zealand agriculture as pasture systems are dominated by year-round grazing of live-stock (De Klein et al., 2006), detrimentally affecting water quality (Parfitt et al., 2012; Smith et al., 1993). In New Zealand there remains a lack of knowledge surrounding the process, rates and the quantification of denitrification that potentially occurs in soil water below the root zone, in the vadose zone, and in the saturated zones prior to soil water discharge into groundwater (Clague et al., 2015b). Several studies have examined the relationship between catchment characteristics (soil texture, drainage, base flow index and geology) and freshwater quality (Alexander et al., 2002; Davies & Neal, 2007; Heathwaite & Johnes, 1996; Jarvie et al., 2002; Monaghan & Smith, 2004) using average water quality, flow data and N leaching rates from farms, and the river nutrient load divided by the N lost from the root zone (Clothier et al., 2007). However, these studies lacked the ability to define and quantify the potential occurrence of N attenuation, between application/deposition of N on the soil surface and subsequent leaching

into a freshwater body, where a significant amount of N can be attenuated depending on soil biological and physical factors (Ledgard et al., 1999; Wells et al., 2016).

It is not understood if NO_3^- isotope fractionation changes (i) with soil type or depth, (ii) what the spatial and temporal variation in NO_3^- fractionation is, or (iii) if NO_3^- isotope fractionation changes during the course of a NO_3^- leaching event following ruminant urine deposition.

Thus, the use of stable isotopes to understand NO_3^- attenuation within New Zealand agricultural landscapes has been extremely limited and requires further research. The aim of the review is to identify gaps in the current knowledge of soil N attenuation between pasture and stream, and how this varies both spatially and temporally in the New Zealand landscape.

2.2 Nitrate-N Attenuation

There are many ways in which N is cycled in a soil/plant system with different processes of gain, loss and transformations (Figure 2.1). Nitrogen is gained through natural processes such as biological fixation of N by symbiotic bacteria in legume roots, animal excreta or through atmospheric returns. But the main gain of N in most New Zealand agricultural systems is through human addition of N fertilisers such as urea (46% N). Nitrogen is predominantly lost or removed from the soil through the export off the farm of plant and animal products, gaseous losses or leaching (Cameron et al., 2013). The main loss of N is through it leaching out of the soil under animal urine patches as NO_3^-.

Figure 2.1: The soil/plant N cycle (Cameron, 1992).

A better understanding of the potential for NO_3^--N attenuation, defined here as the "removal" of NO_3^--N from the soil-groundwater continuum, and the rates involved, could assist in improving the sustainable management of agricultural intensification. More research would provide data for modelling used in planning and legislation, as well as a tool to aid farm management to increase attenuation rates.

2.2.1 Biological Mechanisms for NO_3^- Attenuation

Nitrate attenuation may occur via nitrifier-denitrification, biological denitrification (Wrage et al., 2001), chemo-denitrification (Robertson et al., 2007), coupled denitrification (An et al., 2001) or DNRA (Denk et al., 2017). The pathways of N oxidation (nitrification) and reduction (denitrification and nitrifier-denitrification) are illustrated below (Figure 2.2). The occurrence and rate of these different pathways of N attenuation will depend on the different soil physical and chemical conditions present at any given time.

Figure 2.2: Transformations of mineral N in soil. Taken from Wrage et al. (2001).

An updated review by Wrage-Mönnig et al. (2018) adds to the understanding of N oxidation and reduction pathways, with NO now known to be an obligate intermediary in nitrification (Figure 2.3).

Figure 2.3: Suggested pathways (black boxes and arrows) and enzymes of N_2O production by nitrification (grey) and nitrifier denitrification (black). (Wrage-Mönnig et al., 2018).

A broad range of soil bacteria carry out N attenuation, over 50 genera with more than 120 denitrifying species have been identified (Robertson et al., 2007). These include organotrophs, chemotrophs and photolithotrophs, N_2 fixers, thermophiles and halophiles. Denitrifying microorganisms are predominantly heterotrophic and facultative anaerobes that use NO_3^- as an electron acceptor for respiration under low O_2 conditions (Wrage et al., 2001).

The key to successful N attenuation is the completion of denitrification to produce N_2, an inert atmospheric gas (Buckthought et al., 2015a; Clague et al., 2015b; Clough et al., 1996; Wells et al., 2016). Partial completion of these pathways leads to the production of N_2O, a greenhouse gas stated to be the "single most important ozone-depleting emission" currently contributing to ozone destruction and it is expected to remain so throughout the 21st century (IPCC, 2014a; Ravishankara et al., 2009).

Biological Denitrification

Denitrification is the only biotic process capable of reducing NO_3^- to the benign N_2 gas (Firestone et al., 1989), and is thus a potential tool for reducing NO_3^- concentrations in ground and surface waters, mitigating environmental impacts (Clough et al., 2005; Fischer, 2014; Robertson et al., 2007).

Denitrification is the reductive microbiological process that reduces NO_3^- and NO_2^- to the gaseous N species, NO, N_2O, or N_2 (Wrage et al., 2001) by facultative aerobes that switch to denitrification under O_2 limited conditions, when there is an available N oxide to be used instead of O_2 as a terminal electron acceptor (Zhu et al., 2013). Enzymes catalyse each step in the denitrification pathway (Figure 2.4). Intermediates; NO and N_2O can be set free at each stage. The N_2O/N_2 ratio that is released from biological denitrification increases with a low pH, and higher NO_3^- and O_2 levels. These factors are the main controls on denitrification (Firestone et al., 1989; Tiedje et al., 1983), changing the ratios of end

products through the changes in optimum conditions for denitrification to occur, i.e. a neutral pH has a positive effect on N_2 as an end productive (Šimek et al., 2002), increased NO_3^- and O_2 availability have a negative effect (Knowles, 1982; Tiedje et al., 1983).

Material removed due to copyright compliance

Figure 2.4: Denitrification: an outline of the pathway involved and enzymes at each step of the process. Taken from Hochstein and Tomlinson (1988).

Coupled denitrification

Coupled denitrification occurs when the nitrifying bacteria directly provide the oxidised N source for the denitrifiers (Abbasi & Adams, 2000; An et al., 2001). Denitrifiers reduce the NO_2^- or NO_3^- produced by nitrifiers (Figure 2.5)(Kool et al., 2011a). This occurs when favourable conditions for both nitrification and denitrification occur in adjacent microhabitats in the soil (Hutchinson & Davidson, 1993; Wrage et al., 2001), especially at aerobic-anaerobic interfaces (Baldwin & Mitchell, 2000; Wrage et al., 2001). These pockets of coupled denitrification can result in a large degree of variation in spatial and temporal N_2O emissions (Hergoualc'h et al., 2007; Kuenen & Robertson, 1994).

Material removed due to copyright compliance

Figure 2.5: Depiction of the major pathways of N_2O formation (Kool et al., 2011a). Production of N_2O by nitrifiers is distinguished as by-product of ammonia oxidation, i.e. nitrifier nitrification (NN), and through nitrifier denitrification (ND), and from denitrifiers by reduction of NO_3^- by reduction of applied NO_3^- produced from nitrification, i.e. nitrification-coupled denitrification (NCD), and, i.e. fertilizer denitrification (FD). Note current research also shows NO in the NN pathway as per Figure 2.3.

Nitrifier-denitrification

Nitrifier denitrification is a nitrification pathway where NH_3 is oxidised to NO_2^-, which is then reduced to NO, N_2O and N_2 by nitrifiers who also have the genetic ability to denitrify (Wrage-Mönnig et al., 2018). Nitrifier denitrification has been reported to contribute significantly to soil N_2O production (Kool et al., 2011a; Wrage et al., 2005; Zhu et al., 2013), and it is now known to be a key N_2O production pathway in biogeochemistry (Wrage-Mönnig et al., 2018).

Figure 2.6: Environmental factors influencing nitrifier denitrification. Grey arrows indicate the pathway, the large white arrows show proximate factors and normal arrows other factors influencing nitrifier denitrification. The same applying to the boxes. Taken from Wrage et al. (2001).

A recent review by Wrage-Mönnig et al. (2018) now highlights that NO is an obligate intermediate in nitrifier denitrification (Figure 2.3), with the reduction of NO now also identified as a source of N_2O under conditions low in O_2 (Caranto & Lancaster, 2017).

The review by Wrage et al. (2001) states that approximately 30% of total denitrification can be attributed to nitrifier denitrification, with 100% of N_2O emissions from NH_4^+ thought to be from nitrifier denitrification (Wrage-Mönnig et al., 2018). Zhu et al. (2013) found nitrifier denitrification to be responsible for between 39 - 49.7% of the N_2O produced under O_2 concentrations of 0.5% when urea or $(NH_4)^2SO_4$ were applied to a clay loam soil. Under 0% O_2, heterotrophic denitrification was responsible for 100% of the N_2O produced. Even though nitrifier denitrification was found to produce a high percentage of the N_2O under low O_2 levels, the total volume of N_2O produced was much less. When O_2 levels were at 0.5%, a total of 440 ng N g^{-1} was produced whereas with O_2 levels at 0%, 2683 ng N g^{-1} was produced. Nitrifier denitrification was the main source of N_2O from ammonia fertiliser under low O_2 concentrations (Zhu et al., 2013).

However, there is some debate as to the reliability of these results (aforementioned Zhu et al. (2013)) attributing such high amounts of N_2O production to nitrifier denitrification, with gross over estimation of nitrifier denitrification because heterotrophic denitrification is included (Bakken & Frostegård, 2017). The use of the method developed by Kool et al. (2011b) using dual isotope tracing is based on the assumption that NO_2^- produced by NH_3 oxidising bacteria is denitrified by them, but not by heterotrophic organisms. This assumption does not hold as many heterotrophs reduce both NO_2^- and NO_3^- (Liu et al., 2013), with some only able to reduce NO_2^- as they lack the gene to reduce NO_3^- (Lycus et al., 2017). Thus, the role and significance of nitrifier denitrification remains contentious.

Chemo-denitrification

Chemo-denitrification is a non-biological reaction (Van Cleemput & Baert, 1984), a "non-enzymatic NO_2^- decomposition" associated with N-gas production (Heil et al., 2016), originally proposed by Clark (1962) and is closely linked to nitrification (Martikainen & de Boer, 1993). Chemo-denitrification is the chemical decomposition of the products produced during the oxidation of NH_4^+ to NO_2^-, or of NO_2^- with organic or inorganic compounds (Wrage et al., 2001) to produce N_2O, N_2 and NO gases (Firestone et al., 1989; Robertson et al., 2007). It can occur in several different aerobic pathways (Robertson et al., 2007). Chemo-denitrification is thought to be a minor N loss pathway in most ecosystems. It has been reviewed by Heil et al. (2016) and is not a focus of the current study.

DNRA

Dissimilatory NO_3^- reduction to NH_4^+, is the stepwise reduction of NO_3^- to NO_2^- (Denk et al., 2017) and subsequently NH_4^+ while producing N_2O as a way to avoid toxic levels of NO_2^- (Rütting et al., 2011). Low O_2 conditions are DNRA inducive, similar to that of denitrification, with soil organic matter content thought to be the best predictor of DNRA. The ratio of OC/NO_3^- has been suggested as a key environmental determinant for partitioning NO_3^- between DNRA and denitrification, as high C availability stimulates heterotrophic soil respiration, which in turn lowers the soil redox potential and changes the NO_3^- consumption from denitrification to DNRA (Friedl et al., 2018). Typically, this process is found in O_2 limited environments such as riparian wetlands and lake sediments (Matheson et al., 2002).

2.2.2 Spatial NO_3^- Attenuation

Denitrification is influenced by the soil's three-dimensional matrix comprised of solid, liquid and gaseous phases that receive pulsed inputs of water (and therefore alterations in O_2 supply) via rainfall or irrigation, N via fertilisers and N-fixation, and OC via plant residues and root exudation (Firestone, 1982; Knowles, 1982) which all vary spatially within the landscape. The main factors controlling denitrification are O_2, NO_3^- and C availability (Kraft et al., 2014; Yoon et al., 2015). Other factors affecting N attenuation discussed below include spatial variation in factors such as; soil moisture, soil

pH, soil depth, soil gas diffusivity, soil type and landscape position, as well as temporal variation; temperature and rainfall. Each factor can either positively or negatively influence the N_2O/N_2 ratio produced (Table 2.1), for example, when there is an increasing level of NO_3^- or NO_2^- then the amount of N_2O produced increases relative to N_2.

Table 2.1: The relationship between biological processes that produce N_2O and N_2, and environmental variables. The direction of the relationship either increases (indicated by ↑) or decreases (indicated by ↓). Modified from Owens (2016).

Variable	Nitrification	Nitrifier-Denitrification	Denitrification	N_2O	N_2
C		↓	↑	↑	↓
NO_3^-			↑	↑	↓
NH_4^+	↑				
NO_2^-		↑		↑	
pH	↑	↓	↑	↑	↑
Soil moisture	↓	↑	↑	↑	↑
O_2	↑	↓	↓	↓	↓
Temperature	↑	↑	↑	↑	↓

Soil Moisture & O_2

Soil pores hold either water or gas, which can, under extreme conditions be completely filled with one of the other. Total soil porosity is a function of both soil structure and ρ_b. Soil pores may be filled with either gas or water, and soil porosity can thus be delineated as being air-filled porosity or WFPS, with the latter a function of soil moisture (Assouline, 2006; Zuraidah et al., 2011). The ratio of water or gas in the soil influences which biological processes can occur, for example the aerobic and anaerobic N cycling processes of nitrification and denitrification. Rates of microbial and enzymatic activity decrease as soils dry out (Linn & Doran, 1984b; Moyano et al., 2013; Šnajdr et al., 2008).

Soil properties such as moisture status and the degree of aeration influence denitrification (Moldrup et al., 2000; Neira et al., 2015) since denitrification occurs under anaerobic conditions. The enzyme N_2O reductase, which reduces N_2O to N_2 is especially sensitive to O_2 and its efficacy declines as O_2 concentrations increase (Firestone, 1982). Due to the positive relationship between soil moisture and N_2O fluxes, the introduction of irrigation into an agricultural system is expected to increase N_2O emissions (Trost et al., 2013). However, there have been mixed reports, with some research stating the contrary, that irrigation will reduce the amount of N_2O emissions (Liu et al., 2011; Maharjan et al., 2014). While Zhu et al. (2013) advocates for agricultural practices that maintain aerobic soil conditions to mitigate N_2O emissions by reducing the anaerobic microbial production of N-gases.

Wetting up of soils is found to increase labile C which stimulates heterotrophic respiration (Franzluebbers et al., 2000; Moyano et al., 2013). Heterotrophic respiration was found to lower soil redox potential, which triggered a shift from denitrification to DNRA consumption of NO_3^- under

anaerobic conditions, with DNRA the most dominant NO_3^- reducing process after wetting up (Friedl et al., 2018). Pasture soils contain high levels of labile C and experience repeated wetting and drying cycles, which may be selecting specific microbial groups, i.e. DNRA verse denitrifiers, which in turn will significantly affect NO_3^- partitioning (Reverey et al., 2018). It is suggested that DNRA dominates at low soil moisture (Rütting et al., 2011), is less sensitive to abruptly changing redox conditions (Sgouridis et al., 2011), and correlates positively with high labile C (Reverey et al., 2018; Song et al., 2014). This supports findings of DNRA dominance in pastural soils after wetting up (Friedl et al., 2018), influencing the retention of N in agricultural soils (Putz et al., 2018).

Total porosity and pore size distribution play a key role in how much water a soil holds (Zuraidah et al., 2011). The total volume of pores dictates how much water a soil can hold and the pore size distribution, determines how much 'tension' is required to remove water from a soil. The smaller the soil pores are, the more tension there is on water through capillary action and the greater the suction required to remove it, this can be referred to as tortuosity (Moldrup et al., 2001). This means that for heavy soils (i.e. clays), the denser the soil is, the less total water it will hold but the tighter it will hold it, with the net effect being that the soil moisture content increases (Assouline, 2006), since the volume of pores that remain water-filled is greater at a more negative Ψ as well as the concurrent decrease in large aerated pores, creating more favourable anaerobic conditions for denitrification (Chamindu-Deepagoda et al., 2019).

Oxygen has been recognised as an important controlling factor of N_2O and NO (Firestone et al., 1989; Wrage et al., 2001). The three main factors influencing O_2 concentration in the soil are; O_2 consumption rate, diffusion rate and the tortuosity of the diffusion pathway (Knowles, 1982). The latter two are a function of the soil's water content. The N_2O reductase enzyme that controls the reduction of N_2O to N_2 is the most sensitive to the presence of O_2 out of the enzymes in the denitrification cascade (Morley & Baggs, 2010). Nitrogen oxide reductase repression by O_2 becomes ineffective within 40 minutes to 3 hours after the removal of O_2 (Knowles, 1982; Payne, 1973; Payne et al., 1971).

The depth or the location of the reactive site within a soil can alter the influence of O_2 on the reaction. Oxygen availability is the main factor controlling denitrification in soils that are close to the surface or well drained, whereas in anaerobic conditions NO_3^- availability is the controlling factor (Firestone et al., 1989). In waterlogged soils the O_2 gradient and the thickness of this oxidised layer at the soil surface determine the rate of nitrification, which in turn influences the quantity of NO_3^- available to the underlying zone of denitrification (Engler et al., 1976; Knowles, 1982; Patrick Jr & Gotoh, 1974; Van Kessel, 1977; Watanabe & Furusaka, 1980).

Soil C & N Substrate

The underlying microbial processes responsible for N attenuation are influenced by C and N substrate availability (Andersen & Petersen, 2009). Carbon is used as the electron donor during denitrification, and N-oxides as the acceptors for energy production (Morley et al., 2010). At low concentrations NO_3^- controls the rate of denitrification (Knowles, 1982), through limitation of N substrate for denitrifiers. Without sufficient OC, heterotrophic denitrifiers cannot reduce NO_3^-, thus when NO_3^- is present but the OC source is limited there is significantly less denitrification (Figure 2.7). Increased NO_3^- also sifts the N_2/N_2O ratio, increasing N_2O production as the end product of denitrification, as NO_3^- is favoured as an electron acceptor over N_2O (Dendooven & Anderson, 1995). When there is an increase in available soil OC, it causes a positive correlation with the production of N_2 as the final product of denitrification (Mathieu et al., 2006). Higher available OC and soil moisture levels cause denitrification to progress to completion with a greater N_2/N_2O ratio seen under these conditions.

Figure 2.7: Cumulative denitrification ($N_2O + N_2$) from three different treatments as influenced by NO_3^- only (T1); NO_3^- + glucose C, (T2) and NO_3^- + DOC, (T3) and soil horizons during the 17-day incubation period. Taken from Jahangir et al. (2012)

Increases in labile C after wetting up of soils triggered heterotrophic soil respiration, this was found to reduce redox potential, changing NO_3^- consumption from denitrification to DNRA (Friedl et al., 2018). This change alters N loss pathways, reducing denitrification attenuation of N to N_2, and increasing N_2O and NH_4^+ production through DNRA. Therefore, labile C availability can change the ratio of N_2/N_2O produced under high soil moistures.

Plant growth (Jia & Zhou, 2009), plant diversity (Dias et al., 2010) and photosynthesis after translocation of photosynthates to roots (Bahn et al., 2009; Moyano et al., 2007), can affect available C in the soil and strongly influence microbial activity (Balogh et al., 2011).

A study in New Zealand, looking at soils under different irrigation treatments (62 year field trial) found that the control (no irrigation) and the soil receiving minimal irrigation inputs (260 mm yr^{-1} average) both contained significantly greater amounts of soil C (peaking at 32 Mg ha^{-1} more) than the higher irrigation treatment (770 mm yr^{-1} average)(Condron et al., 2014). This is contrary to the hypothesis that irrigation significantly increases plant and animal production, and therefore will also increase soil C. The reduced soil C was attributed to increased C loss through higher stocking rate product removal (Soussana et al., 2004) and drainage (Ghani et al., 2010), as well as accelerated decomposition of OC due to soil moisture levels being maintained through the season (Fierer & Schimel, 2003a; Miller et al., 2005; Schipper et al., 2013).

The increased removal of C under irrigation or highly productive pasture that is not limited by soil moisture, may create an imbalance in C/N ratios. This may lead to further N saturation and loss of NO_3^- from the system due to a lack of available C source for it to be denitrified. Therefore, maintaining soils at a soil moisture level that promotes denitrification as an N attenuation practice to remove NO_3^- before it reaches waterways, may in turn also lead to loss of soil OC (Liu et al., 2011; Maharjan et al., 2014).

Previous research shows that soil depth also plays a role in the availability of C, as the movement of C down a soil profile is slow, therefore C is limiting at depth. Jahangir et al. (2012) used intact soil cores taken from different soil depths to look at subsurface denitrification (Figure 2.8). Treatments of either additional N, N with glucose-C or N with DOC were applied to the cores. Nitrous oxide flux rates were found to be greater in the A horizon (0.77 to 2.38 mg N kg^{-1} d^{-1}) than in the C horizon (0.04 to 0.09 mg N kg^{-1} d^{-1}, Jahangir et al. (2012)). Although the total denitrification rate was lower in the subsoils, they had higher $N_2O/(N_2O+N_2)$ ratios which indicates their potential for complete denitrification to N_2 was limited. Thus, the addition of a C source to the subsoil may significantly increase the subsurface soils potential for denitrification (Clough et al., 1998a; Jahangir et al., 2012; Qin et al., 2017).

Material removed due to copyright compliance

Figure 2.8: Mean N_2O fluxes from two soil horizons, A (a) and C (c) as influenced by NO_3^- only (T1); NO_3^- + glucose C, (T2) and NO_3^- + DOC, (T3). Taken from Jahangir et al. (2012).

National soil C concentrations in New Zealand are reportedly declining (Parsons et al., 2009; Schipper et al., 2007), with a study by Schipper et al. (2010) reporting soil C stocks declining by -1.2 Mg C ha^{-1} y^{-1} on dairy grazed land, no decline for drystock flat-land and an increase of approximately 1 Mg C ha^1 y^{-1} for drystock hill-country (top 0.9 m of soil, sites sampled n = 83). Dairy grazed land C stocks were thought to be declining due to increased grazing removing C (Parsons et al., 2013) and/or cow urine solubilising OC causing C decomposition or leaching (Lambie et al., 2012a; Lambie et al., 2012b), with the gains in hill-country due to the rebuilding of topsoil that had been previously lost to erosion (Parfitt et al., 2013). Further research by Schipper et al. (2010) constrained C losses on flatland to soil orders, Allophanic and Gley Soils, losing -1.37 kg C ha^1 y^{-1} and -0.78 kg C ha^1 y^{-1}, respectively. The decline in C stocks and increase in N through both animal excreta and fertiliser may lead to even further N saturation of soils and a decline in net immobilisation (Schipper et al., 2004).

Soil Depth

Soil depth can influence N attenuation through the limitation of controlling factors; O_2/moisture availability, OC and NO_3^- as they vary throughout a soil profile (Moldrup et al., 2000; Neira et al., 2015). Soil depth also influences ρ_b, as generally the deeper the soil the greater the ρ_b, reducing soil porosity and therefore its ability to hold O_2 or water (Zuraidah et al., 2011).

Most soil research focuses on the root zone, where NO_3^- transformations are well documented (Ibendahl & Fleming, 2007), but understanding of NO_3^- transformation and movement in the subsoil is lacking (Jahangir et al., 2012). There is a gap in knowledge of the processes occurring between NO_3^- leaving the root zone and moving into the vadose and saturated zones, before it enters waterways (Clague et al., 2015b). Previous work in the Waikato found large spatial variation between sites only 250 m apart (Clague et al., 2015a; Clague et al., 2015b). There is also little to no information for this

zone in Southland, New Zealand, as previous research focuses on isotope data from wells and ground and surface water bodies that are easier to access and sample (Baisden et al., 2016a; Rissmann, 2011, 2012). Work by Rogers et al. (2017) provides the most information on Southland soils, analysing soil samples down to 0.7 m for NO_3^- concentration and NO_3^- isotope signatures.

Spatial variability in leaching losses, flow paths and attenuation processes make it difficult to measure and quantify NO_3^- attenuation occurring in this zone, between the bottom of the roots and groundwater (Groffman et al., 2009; Hesser et al., 2010; Woodward et al., 2013; Wriedt & Rode, 2006).

Soil pH

Denitrification is positively related to soil pH, with an optimum pH range of 7 to 8 (Delwiche & Bryan, 1976; Knowles, 1982; Müller et al., 1980; Nömmik, 1956; Van Cleemput & Patrick, 1974; Wijler & Delwiche, 1954). At low (< 4) pH N_2O-reductases are repressed, causing a decrease in the overall rate of denitrification but increases in the fraction of N_2O produced, N_2O is the major product at a pH less than four (Nömmik, 1956; Wijler et al., 1954). Bakken et al. (2012) suggest that liming could be a way of reducing N_2O emissions as under acidic conditions there is an increase in the N_2O/N_2 product ratio of denitrification. Recent work by Bakken et al. (2017) summaries that in most cases the N_2O to N_2 ratio of denitrification products seems to increase under acidic pH. As most organisms cannot assemble N_2O reductase in acidic conditions, however once assembled it does function at low pH (Liu et al., 2014). However, there is a poor understanding of the mechanisms involved with pH's influence on denitrification and more research is needed (Bakken et al., 2017).

Soil Type

There are many factors that influence and determine a soil type's physical and chemical structure; ρ_b, texture and mineralogy, climate, landscape position, organic matter supply (manures & crops), management of tillage, grazing and machinery (Gould et al., 2016; Six et al., 2004). These different properties effect the soil and its capacity to attenuate NO_3^-, making it a difficult process to measure and understand all of the variables and mechanisms involved (Groffman et al., 2009).

Soils are comprised of varying fractions of sand, silt and clay, or textures (McLaren et al., 1996). These textural fractions can influence a soils ability to attenuate N, for example a sandy soil maintains better drainage than a clay soil which in turn may promote denitrification under poorly drained/anaerobic soil conditions. The relationship between water held in soil pores and the suction it is under is presented as a soil moisture curve in Figure 2.9. Suction has an inverse relationship to the water content of the soil, meaning suction increases as soil moisture decreases (Miller et al., 2002). This also relates to the texture of a soil, as the finer the soil texture (> clay%) the smaller the pores, the greater

the suction required to remove it, the longer the pores will stay waterfilled and therefore more anaerobic, creating conducive conditions for attenuation to occur.

Figure 2.9: Typical soil-water characteristic curve illustrating the relationship between soil moisture and suction (Miller et al., 2002).

There are many factors that can affect soil ρ_b; as clay content increases so does soil ρ_b, depth increases compaction due to pressure, while adverse management that allows over-grazing and pugging can also increase soil ρ_b. As soil ρ_b increases, Φ declines due, predominately, to reduced macro-porosity, resulting in decreased ε. Consequently, water inputs result in relatively higher anaerobic conditions which favour denitrification (Beare et al., 2009).

Transport of NO_3^- via advection, dilution and dispersion within the landscape, depending on soil type and associated soil textures, and the effect transient characteristics of water runoff and pathways have on that transport are generally neglected when assessing the variability of NO_3^- attenuation (Cirmo & McDonnell, 1997; Ocampo et al., 2006).

Physiographic Zones

Land use alone does not account for variability in water quality (Rissmann et al., 2018), a key indicator of N levels in the environment, with more than twice the variability in water quality accounted for by spatial variability in landscape attributes (Becker et al., 2014; Hale et al., 2004; King et al., 2005; Shiels, 2010). Recent research in Southland New Zealand examines how landscape attributes contribute to water quality (Pearson et al., 2018; Rissmann et al., 2018; Rissmann et al., 2016). This research

fundamentally uses a physiographic approach to understand water quality and hydro-chemical composition by "identifying and mapping the spatial coupling between process signals in water and landscape attributes" (Rissmann et al., 2018).

Physiographic zones are defined using various parameters, with four different process-attribute layers representing key processes; atmospheric, hydrological, redox and weathering, with water quality and hydrochemistry data used as response variables (Rissmann et al., 2018) which are then compared with geospatial layers within a capture zone to test the hypothesis (Rissmann et al., 2018; Rissmann et al., 2016). An example of how these four key processes are combined to estimate spatial hydrochemistry is shown in Figure 2.10. Different combinations of layers are used to produce physiographic zones that share the same characteristics for a specific objective, i.e. identifying areas of NO_3^- contamination using field data associated with a given surface or groundwater monitoring site such as, soil drainage class, soil C content and electron donor abundance (Rissmann et al., 2018). This allows for the estimation of spatial variation in groundwater NO_3^- at the process level despite similar levels of land use intensity (Hughes et al., 2016; Rissmann et al., 2016; Snelder et al., 2016).

Figure 2.10: Diagram depicting how the conceptual physiographic model combines the four key drivers to estimate hydrochemistry spatially (Rissmann et al., 2016).

Identification and understanding of processes that lead to accumulation or reduction of N in the landscape are complex and need multi-level analyses to be able to identify what or how they are occurring. However, understanding of landscape attributes that influence N attenuation would be helpful in reducing NO_3^- loss and freshwater contamination.

2.2.3 Temporal NO_3^- Attenuation

Seasonal variation in rainfall and temperature (wetting and drying cycles) influence the rate and quantity of soil N attenuation by promoting nitrification followed by denitrification (Knowles, 1982).

Denitrification commonly occurs once water from rainfall or irrigation fills up soil pore space, reducing O_2 availability (Robertson et al., 2007), with WFPS of 60% or greater often cited as leading to increased denitrification rates (Linn and Doran, 1984). Attenuation of N was found to be highly responsive to rainfall, accounting for 93% of calculated attenuation (20 kg NO_3^- N ha^{-1} yr^{-1}) in a catchment study, where the land-use was dominated by pasture production over a two year period in Canterbury, New Zealand (Wells et al., 2016).

In a study by Clague et al. (2015b), in the Waikato region of New Zealand, higher soil solution NO_3^- concentrations were found in early winter (June and July), due to a build-up in the top soil over summer, and the subsequent flush of autumn rain with the seasonal wetting up of soils. Isotopic composition of NO_3^- samples taken by Clague et al. (2015b) also reflected this temporal variation, June and July NO_3^- samples ($\delta^{15}N$- NO_3^- +3.8‰) were not as enriched in ^{15}N as those from late winter to early spring (August and September, $\delta^{15}N$- NO_3^- +11.1‰) at a 0.7 m depth. Frequent simulated rainfall events (5-day intervals), were found to cause soil NO_3^- concentrations to limit N turnover (microbial transformation), rather than soil O^2 content (Gu & Riley, 2010). The consistent anaerobic conditions limit nitrification and therefore NO_3^- production. Whereas under prolonged dry periods (15-day intervals) nitrification was facilitated, increasing soil NO_3^- concentrations and denitrification becoming limited by aerobic conditions.

The further reduction of N_2O to N_2 is potentially enhanced when percolating water traps N_2O in the soil (Clough et al., 2005). The potential for N_2O to be trapped after rainfall events may prove to reduce N_2O emissions by stimulating further denitrification to N_2. The opposite may also occur with an influx of water into the soil. Rather than reduce N_2O emissions, water infiltration into the soil may cause N_2O that was trapped in the soil air to bubble out to the soil surface, releasing a pulse of N_2O (Clough et al., 2005).

The Southland region experiences annual rainfall averages anywhere from 750 mm up to 7000 mm (Ledgard, 2013). However, these high rainfall areas (4000 - 7000 mm) are found on the West Coast, Fiordland Region, which is predominantly conservation land. Low land and coastal areas along the Southern coast experience annual rainfall from 1000 to 1250 mm year, with rainfall volumes steadily declining further inland and eastwards from Fiordland, with the Waimea basin averaging 750 mm of rainfall a year.

Temperature readily affects microbial activity (Braker et al., 2010), therefore influencing the rate of N attenuation. Denitrification and temperature are positively correlated, with shifts in denitrifier community composition at different temperatures. N_2O production is greater at high and low temperatures (Nömmik, 1956), NO is also dominant at low temperatures (Bailey, 1976). Denitrification slows at lower temperatures but is still measurable at temperatures of 0 to 5°C (Bailey & Beauchamp, 1973; Bremner & Shaw, 1958; Ryden, 1986; Smid & Beauchamp, 1976). Temperature may limit dentification in the Southland region which experiences temperatures below freezing in winter (June - August), especially in inland basins where frosts and snowfall are a regular occurrence during winter (Ledgard, 2013).

In an isotope catchment scale study in the State of New York, USA (Burns et al., 2009) temperature was also found to have a positive effect on denitrification. Denitrification was found to be most prominent during periods of warm air temperatures and low streamflow during summer and early fall, coinciding with the lowest stream NO_3^- concentrations ($r^2 = 0.87$). Phillips et al. (2015) found more apparent N_2 as a denitrification end product at under higher temperatures (35°C compared to 19°C) while studying a New Zealand pasture soil. However, this was thought to be due to enhanced mineralisation of organic matter at higher temperatures increasing heterotrophic denitrification rather than a direct influence of temperature. When studying several contrasting dairy-pasture sites Luo et al. (2000) did not find denitrification to be limited by cold winter temperatures, but temperatures at experimental sites didn't drop below the reported critical temperature of 5°C which is said to limit denitrification.

Bailey et al. (1973) conducted a laboratory trial to look at the effects of temperature on the reduction of N species in soil. The reduction rate of NO_2^- and NO_3^- was found to decrease with decreasing temperatures (30°C to 5°C). At 5°C NO_3^- reduction was completely inhibited. Decreasing temperatures did not affect the production of N_2O, but were found to reduce the production of N_2 and to increase the production of NO (Table 2.2), where the increased production of NO was attributed to chemo-denitrification of NO_2^-.

Table 2.2: Nitrogenous gases produced from saturated soil treated with NO_3^- (500 µg N g^{-1} air dried soil as KNO_2), incubated anaerobically at 30, 15 and 5°C. Adapted from Bailey et al. (1973).

Nitrogenous Gases	NO_3^- Treatment		
	30°C	15°C	5°C
	(µg N g^{-1} air-dried soil)		
N_2	250.7	223.1	0.0
N_2O	196.3	196.0	0.0
NO	45.1	74.0	0.0

2.2.4 Plant Effect on NO_3^- Attenuation

Perennial ryegrass (*Lolium perenne*) dominates New Zealand pastoral systems (Crush et al., 2005) and is often sown with white clover (*Trifolium repens*)(King et al., 2012). Perennial ryegrass seasonal growth peaks occur in autumn and spring with variation in heading date between cultivars (Fleming, 2003). Seasonal changes, low temperatures in winter or low soil moisture in summer can affect plant growth and therefore N uptake. Temperature effects plant growth, optimum growth temperature ranges from 20 - 25°C for most temperate species, which stop actively growing below temperatures of 5 - 10°C (White & Hodgson, 1999). Seasonal temperatures range from an average of 22°C in summer (December - February) to 0°C in winter (June - August) in Southland, New Zealand (Macara, 2014). Lower areas towards coastal areas in Southland experience a mean annual temperature of between 10 - 11°C. Inland areas average between 9 - 10°C annual temperature and experience minimum temperatures that drop below 0°C from April through to October (Macara, 2014).

Perennial ryegrass is a shallow rooted pasture species with 80% of its roots in the top 0 - 15 cm of soil (Bolinder et al., 2002). NO_3^- is rapidly leached through the profile and out of this zone giving the plant only a short time for optimal uptake. Research looking at pasture N concentrations found that annual pasture N uptake was more strongly influenced by high animal urine N deposition than pasture N concentration, as this greatly increased plant N uptake (Moir et al., 2016). It was suggested by Crush et al. (2005) that greater densities of roots deeper in the soil would decrease NO_3^- leaching, as deeper rooting plants have greater access to soil N than those that are shallow rooting. Lucerne for example can root to depths of three meters, which allows it to take up more N than a plant such as potatoes which leave an excess of N in the soil and which is readily leached (Webb et al., 1997). The life span and persistence of roots against disease and drought could also influence their N uptake efficiency (Wu et al., 2005). Plants roots can affect more than just N removal by uptake, they can also influence soil structure, change hydraulic conductivity, increase aeration, stabilise soil (Gould et al., 2016; Macleod et al., 2013; Stokes et al., 2009), as well as stimulate microbial and fungal activity by exuding root exudates (polysaccharides and proteins)(Leifheit et al., 2014).

2.3 Gas Diffusivity

The main mechanism of gas movement through soil is diffusion (Penman 1940), “diffusion is proportional to the gas concentration gradient” according to Fick’s Law. Soil gas diffusion is represented by relative soil diffusivity (D_p/D_0), where D_p is the soil-gas diffusion coefficient (cm^3 soil air cm^{-1} soil s^{-1}) and D_0 is the diffusion coefficient of the same gas in free air (cm^2 air s^{-1})(Moldrup et al., 2000). Many models of soil D_p/D_0 have been developed relating it to Ɛ and Φ (Buckingham, 1904; Marshall, 1959; Millington & Quirk, 1961; Penman, 1940), as measuring D_p is more difficult, requiring special equipment and conditions in the laboratory or in situ (Rolston & Moldrup, 2002). More recent

models also incorporate soil ρ_b (Chamindu Deepagoda et al., 2011b) to account for the large range of ρ_b that exists between soil types.

The role of O_2 in the regulation of NO and N_2O production has been difficult to explain (Bollmann & Conrad, 1998; Khalil et al., 2004; Venterea, 2007). Oxygen is rarely measured and used as an indicator of denitrification (Linn & Doran, 1984a; Zhu et al., 2013). However, O_2 is one of the main controlling factors affecting the onset of denitrification and subsequent denitrification rates and products (Firestone et al., 1989). Soil gas diffusion is the main mechanism of O_2 transport in soil (Neira et al., 2015) and therefore an important influence on the potential for NO_3^- attenuation. Fick's law of diffusion is used to describe the gas diffusion flux in free air, as follows:

$$J_g = -D_g^a \partial C_g / \partial z$$ **Equation 2.1**

where Cg is the concentration of the gas (g cm^{-3} of air), z is the distance over which diffusion occurs (cm), and D_g^a (cm^2 s^{-1}) is the binary gas diffusion coefficient in free air. However, this equation (2.1) overestimates the gas diffusivity in soil as it doesn't account for the tortuosity of soil pores increasing gas pathway length. A gas diffusion coefficient term was developed, modifying the diffusion in air by a gas tortuosity factor (ξ_g), where D_g^S replaces D_g^a in equation 2.2:

$$D_g^S = \xi_g D_g^a$$ **Equation 2.2**

Soil gas diffusion is influenced by soil physical properties such as soil ρ_b, texture, structure, pore size distribution and pore connectivity. Soil organic matter (Neira et al., 2015), compaction and water saturation can also modify the soil physical properties, affecting the transport of gases within the soil (Moldrup et al., 2000). This in turn affects the rate at which the soil can process N due to O_2 availability. For example, decreasing Ψ (increasing soil water content) can increase the rate of NO_3^- attenuation, especially as ρ_b increases (Figure **2.11**)(Balaine et al., 2013).

Figure 2.11**: Effect of soil bulk density on mean N_2O-N fluxes for 11 levels of matric potential. Plotted lines are derived from a three-parameter Gaussian model fitted to the N_2O-N flux and matric potential data. Numbers in the legend indicate soil bulk density treatments applied (Mg m^{-3}). Error bars = SEM, n=4. Taken from Balaine et al. (2013).**

Soil moisture, expressed as WFPS has been historically used as a preferred soil moisture parameter for predicting N_2O losses (Beare et al., 2009; Dobbie et al., 1999; Dobbie & Smith, 2001), with it also used to better understand how microbial activities vary in soils of differing soil ρ_b (Aulakh et al., 1991; Linn et al., 1984b). Peak N_2O emissions are classically reported to occur between 50 and 70% WFPS (Bateman & Baggs, 2005; Davidson et al., 2000; Dobbie et al., 1999) which is generally an approximation of field capacity for a soil, with N_2 becoming the main end-product once WFPS is greater than 80% (Bowman & Steltzer, 1998). However, as quoted by Farquharson and Baldock (2008) "while adequate for describing processes in a single soil with a constant ρ_b, the use of WFPS across a single soil or different soils varying in ρ_b is problematic.". Water filled pore space quantifies the proportion of pores that are filled with water, without accounting for the change in pore space between soils with different ρ_b, and therefore it does not measure the volume of the soil that is filled with air or water (Figure 2.12). This makes it dimensionless and a poor predictor for the movement of solutes and gases that regulate processes in soils with different porosities.

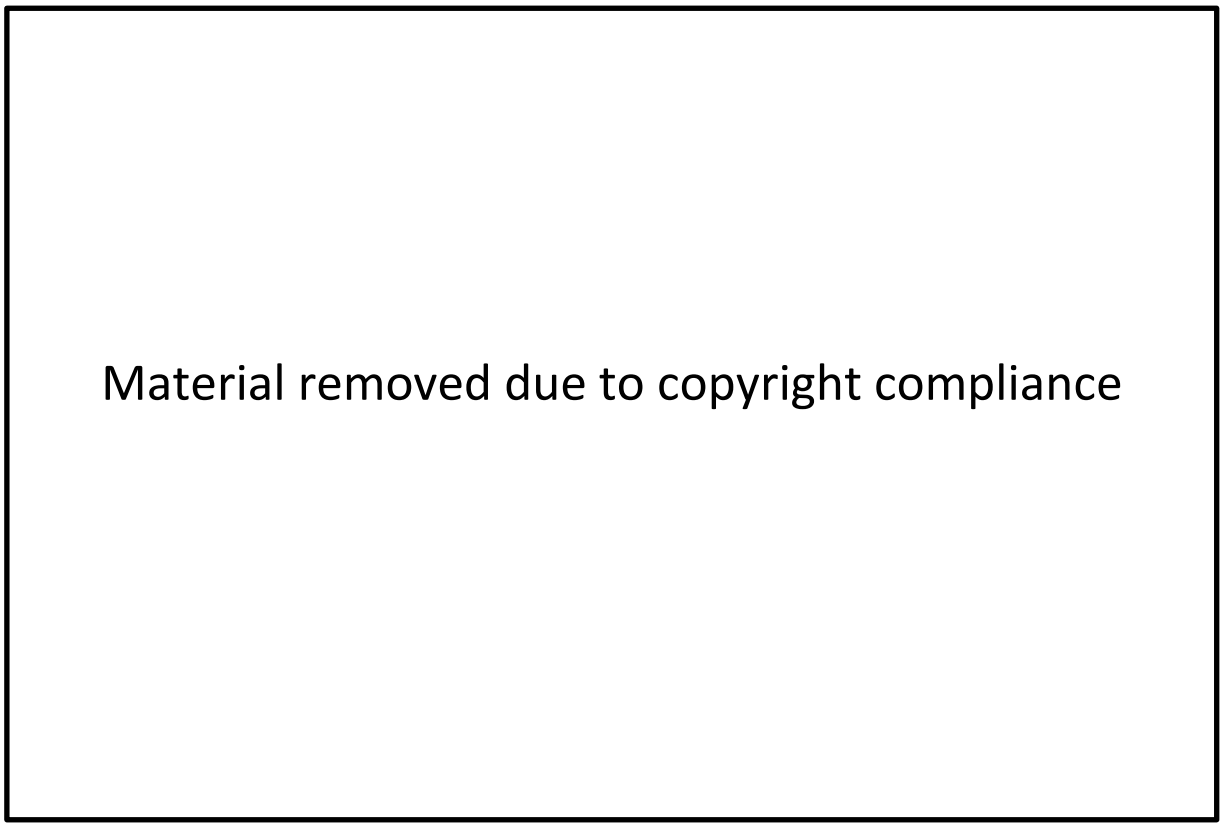

Figure 2.12: Variations in the volume fractions of air and water with water filled pore space (WFPS) for soils at different bulk densities (ρ_b g cm^{-3}). For a given WFPS the volume fractions of air or water vary depending on the ρ_b of soil. Left axis: volume fraction of air, right axis: volume fraction of water (Farquharson and Baldock (2009).

Anderson and Peterson (2009) suggested that D_p/D_0 could be a better predictor of N_2O emissions from soils than the commonly used WFPS after conducting research using repacked, nutrient amended soil under three soil Ψ (-1.5 to -10 kPa). Further research by van der Weerden et al. (2012) went on to also demonstrate a strong relationship between D_p/D_0 and N_2O emissions from soils amended with NO_3^-. More recent research relates BU, urea, or NO_3^- derived N_2O and N_2 emissions to D_p/D_0, as well as examining the interaction between soil ρ_b and soil Ψ (Balaine et al., 2016b; Balaine et al., 2013; Chamindu-Deepagoda et al., 2019; Owens et al., 2016).

Balaine et al. (2013) found that D_p/D_0 was a key indicator of soil N_2O emission potential, with maximum N_2O emissions occurring at a D_p/D_0 value of 0.006 (Figure 2.13). The N_2O fluxes were found to increase rapidly as D_p/D_0 decreased to a value of 0.006, before declining rapidly due to complete denitrification, expressed as an increase in N_2 (Balaine et al., 2013). N_2O production peaked with declining levels of Ψ (-1.5 to -6 kPa) and increasing levels of ρ_b (1.1 to 1.5 Mg m^{-3}) as the proportion of micro-pores in the soil increased (Balaine et al., 2013). N_2O fluxes and Ψ were found to be highly related to air entry potential ($r^2 = 0.96$). When comparing soils of varying ρ_b Balaine et al. (2016b) found that a soil's D_p/D_0 was better than WFPS at explaining peak fluxes in both N_2O and N_2. This was because D_p/D_0 accounts for the interactive effect of soil ρ_b and soil water content on functional pore space within the soil. The

study by Balaine et al. (2016b) infers that there is a potential threshold for peak N_2O emissions which can be defined using soil D_p/D_0. This variable D_p/D_0, has the potential to be a beneficial agricultural management tool, if soil and irrigation management can be used to maximise the D_p/D_0 threshold for N attenuation.

Figure 2.13: The relationship of measured N_2O-N flux with relative soil gas diffusivity (D_p/D_0) at varying soil bulk densities (Mg m^{-3}). Numbers in the legend indicate bulk density treatments applied. Error bars = SEM, n = 4. Taken from Balaine et al. (2013).

Owens et al. (2017) also showed declining D_p/D_0 linked to enhanced N_2O emissions in a field study in Canterbury, New Zealand. Modelled D_p/D_0 has also been shown to link N_2O emissions with low D_p/D_0 values (Friedl et al., 2017). Friedl et al. (2018) found that in the first 24 hours there was a strong relationship between log D_p/D_0 and log N_2O, however on day two, N_2O reaches its peak and starts to decline at a D_p/D_0 of 0.0068, as reduction to N_2 becomes dominant. This confirms the critical threshold for maximum N_2O fluxes of 0.006 (Balaine et al., 2013).

Better understanding of the hydro-geochemical system and its effect on denitrification is needed to better understand, predict and manage the impact of agricultural practices on NO_3^- contamination of ground and surface waters (Böhlke et al., 2007) and the impact on N_2O emissions (van der Weerden et al., 2012). Attenuation of N in the soil under grazing systems in Southland is poorly understood, with previous research focusing on ground and surface water N concentrations, with modelled estimations of a soils ability to remove N and limited physical quantification. This is highly important in terms of management and implementation of new regional and national laws to improve the state of New Zealand's environment. Soil properties used and models are general, but do not account for temporal change and are spatially broad on their approach.

Gas diffusivity could provide a useful tool in farm and policy management as it could provide real time data showing N attenuation through the measurement of soil O_2 using sensors placed in soils where

in-situ ρ_b measurements have been taken. This would allow for the modelling of D_p/D_0 and identification of attenuation moments showing when and where NO_3^- attenuation occurs.

2.4 Stable Isotopes

"Isotopes are forms of the same element that differ in the number of neutrons in the nucleus," (Fry, 2007). Many elements come in different forms, behaving in only subtly different ways. However, out of the 3100 isotopic forms of elements that exist 90% of them undergo radioactive decay, meaning that there are only 283 stable isotopes. Stable isotopes potentially provide a way to trace natural element cycling, acting as 'natural dyes' that can be followed through natural systems. Stable isotope values are usually reported as delta (δ) values in units of parts per thousand, or permil (‰), as natural variation in isotope abundance occurs on a very small scale, relative to a standard of known isotopic composition (Fry, 2007).

δ values are calculated as follows:

$$\delta X\ (‰) = (R_x / R_s - 1) \times 1000 \qquad \textbf{Equation 2.3}$$

where R is the ratio of the heavy to light isotope (e.g., $^{15}N/^{14}N$), R_x is the ratio of heavy to light isotopes in the sample and R_s is the ratio of heavy to light isotopes in the standard (Kendall et al., 1998).

Light stable-isotopic compositions are reported with respect to international standards. Atmospheric N (‰ v.AIR) is used as a standard for $^{15}N/^{14}N$ because it is isotopically constant over a wide geographical area (Amundson et al., 2003). Standards are large natural steady state pools that provide a point of stability in overall isotope circulation, such as Standard Mean Ocean Water (‰ v.VSMOW) for hydrogen (H) and O_2 isotopes. Natural abundance samples generally have δ values ranging from -100 to +50‰ (with the exception of H). The more negative the δ value, the more depleted in the heavy isotope the sample is compared to the standard, while a positive δ value means that the sample is more enriched in the heavy isotope relative to the standard. The dual isotope composition of NO_3^- for example, provides a means of measuring sources and sinks of N in the environment as both N and O isotopes exist in infinite amounts (N is made up of 99.6337‰ ^{14}N, "light" isotope, and 0.3663‰ ^{15}N, "heavy" isotope and O is 99.759‰ ^{16}O "light", 0.037‰ ^{17}O and 0.024‰ ^{18}O "heavy" (Fry, 2007)).

2.4.1 Nitrate Isotopes

The isotopic composition of NO_3^- ($\delta^{15}N/^{14}N$‰ and $\delta^{18}O/^{16}O$‰) can provide an indication of either sources or sinks of N in the landscape (Austin & Vitousek, 1998; Heaton, 1986), as biogeochemical processes distribute them in predictable unequal ratios across the landscape (Kendall, 1998; Seiler, 2005; Widory et al., 2004). Kinetic fractionation (α) of isotopes during biogeochemical processing

causes this unequal distribution, as heavy isotopes have a slower reaction rate (k_2) than light isotopes (k_1), (Kendall et al., 1998):

$$\alpha_k = k_1 / k_2 \qquad \textbf{Equation 2.4}$$

Precipitation (atmospheric deposition), fertilisers, soil N, sewage and manures are the major NO_3^- sources that have been well documented in terms of their NO_3^- isotopic compositions and respective ranges (Figure 2.14, Fischer (2014)). Synthetic N fertilisers have a low $\delta^{15}N$ (~0‰) and a high $\delta^{18}O$ (~+20‰), sitting to the left on the $\delta^{15}N$ and $\delta^{18}O$-NO_3^- cross plot, while NO_3^- that has been partially denitrified sits to the right, increasing in the enrichment of N and O isotopes along a slope of 2:1 or 1:1 (Figure 2.14).

Figure 2.14: Typical isotopic ranges for the $\delta^{15}N$ and $\delta^{18}O$ of NO_3^- of various sources. Boxes indicate the broad range of possible values of $\delta^{15}N$ and $\delta^{18}O$-NO_3^- (Kendall, 1998; Kendall et al., 2007; Nestler et al., 2011; Xue et al., 2009). The arrows indicate commonly expected slopes (1:1 or 2:1) of enrichment due to denitrification and assimilation (Granger et al., 2008; Granger et al., 2004; Sigman et al., 2001). The arrows shown are for an initial $\delta^{15}N$ and $\delta^{18}O$ of 6 and -9 ‰, but this could occur within any initial source value. Taken from Fischer (2014).

Distinguishable ratios of the dominant N species allow for the identification of the NO_3^- source (Liu et al., 2006). Nitrogen fertilisers, atmospheric deposition, manure and sewage for example, have $\delta^{15}N$-NO_3^- signatures that range from -6‰ to +6‰, -13‰ to +13‰, +5‰ to +25‰ and +4‰ to +19‰,

respectively (Figure 2.14, Xue et al. (2009)). Reported isotope ranges for $\delta^{18}O$ differ significantly between atmospheric (from +52.5‰ to +60.9‰) and soil derived (from +0.8‰ to +5.8‰) NO_3^- sources (Durka et al., 1994). Rates of atmospheric deposition of NO_3^-, with $\delta^{18}O$ values from +20‰ to +100‰ (Figure 2.14), are considered negligible in New Zealand (Parfitt et al., 2012). The identification of N sources, using NO_3^- isotopic signatures, in the environment is limited by a poor understanding of the controls on denitrification fractionation, with reported ranges varying between publications due to changes in biochemical processing rates and environmental conditions. Other drivers of ecosystem variation in isotope values include, but are not limited to; soil age, climate and topography (Amundson et al., 2003; Craine et al., 2009).

Internationally, the $\delta^{15}N$ signature of NO_3^- leached from pasture soils has been reported to sit between +0.3‰ to +6.6‰ (Minet et al., 2012; Oelmann et al., 2007; Rock et al., 2011) and pasture soil leachate in New Zealand has been found to sit within this range (Mudge et al., 2013; Stevenson et al., 2010). Isotope analyses of two long-term New Zealand pasture trials gave ranges of +2.8‰ to +4.6‰ across all irrigation and fertiliser treatments from soils between 1958 and 2009 (Mudge et al., 2013), while another study of 210 soils across different land uses within New Zealand found $\delta^{15}N$ values ranged from +3.8‰ to +5.4‰ for dry-stock and dairy cattle, respectively (Stevenson et al., 2010). A wider range of $\delta^{15}N\text{-}NO_3^-$ values, from -3.38‰ to +19.2‰, was reported in a trial based in Canterbury, New Zealand, where pasture soils were subjected to different rates of BU or urea-N (Wells et al., 2015). The expected $\delta^{15}N\text{-}NO_3^-$ range for a urea or urine source has been reported to range from -5‰ (Wells et al., 2015) to +1.2‰ (Frank et al., 2004).

Nitrate leached from under pastoral agriculture originates from a mixture of urea fertilisers and BU (Buckthought et al., 2015b; Romera et al., 2012) which have been reported to be normalised to a range of between -10‰ to +10‰ for both $\delta^{15}N$ and $\delta^{18}O$ during transport through agricultural soil (Granger et al., 2008; Oelmann et al., 2007; Rock et al., 2011). Recent research in Canterbury, New Zealand by Wells et al. (2015) also states that $\delta^{15}N\text{-}NO_3^-$ isotopes values as low as -10‰ should be considered to be from a urine source to account for post-deposition soil N cycling.

Clague et al. (2015b) identified seasonal denitrification in a Typic Recent Gley Soil (New Zealand Soil Classification) (Hewitt, 1998) in an agricultural catchment in the Waikato region of New Zealand using NO_3^- isotope values. Periodic saturation of the soil profile was observed with $\delta^{15}N\text{-}NO_3^-$ values reaching +28.5‰ and $\delta^{18}O\text{-}NO_3^-$ values of up to +19.6‰. While isotope values of soils in Southland, New Zealand show a range of $\delta^{15}N$ values from +0.3‰ to +12.9‰ across a regional transect (Rogers et al., 2017), values increased from west to east, moving from indigenous forest to more intensively farmed areas (Figure 2.15). Which was consistent with the $\delta^{15}N$ values of the most intensive farm managements, dairy farming and cropping, found by Stevenson et al. (2010), averaging values of +5 to +6‰ (±3‰

SD). Surface soils $\delta^{15}N$ values from agricultural areas of Southland averaged +4 to +8.8‰ (Rogers et al., 2017; Stevenson et al., 2010), with an outlier of 12.9‰. These contrasting values show variation in soil isotope values across New Zealand, changing spatially and temporally. The two sites in the Waikato, only 250 m apart varied greatly in their denitrification capacities, 425 kg N ha^{-1} yr^{-1} and 56 kg N ha^{-1} yr^{-1}, respectively, for a Morrinsville (Typic Orthic Granular, NZSC (Hewitt, 1998)) and Kereone (Typic Orthic Allophanic, NZSC (Hewitt, 1998)) soil, illustrating just how spatially variable denitrification can be (Clague et al., 2015a; Clague et al., 2015b).

Figure 2.15: Nitrogen isotope abundance ($\delta^{15}N$ ‰) across a transect of Southland, New Zealand (167.0 - 167.4 longitude). Highest isotope values are found in the Oreti and Mataura River Basins. The solid line represents the A horizon sampling depth of 0 - 30cm, the dotted line represent the B horizon sampling depth of 50 - 70cm. Grey grass on white = native forest/tussock, grey square pattern = pasture/farming, solid grey = exotic forest/pine plantations (Rogers et al., 2017).

Interpretation of NO_3^- concentrations may vary as reductions in NO_3^- concentrations can indicate denitrification has occurred, or that there has been dilution with NO_3^- free water (Groffman et al., 2006). Therefore the use of isotope data is a useful tool to identify processes, as measuring the isotope signatures of initial and residual pools can indicate if denitrification has occurred (Clague et al., 2015b). Isotope signatures of NO_3^- will plot along the 2:1 or 1:1 denitrification vector, due to fractionation of isotopes during denitrification enriching the residual pool (Baily et al., 2011; Mengis et al., 1999).

2.4.2 Fractionation

Fractionation is the process that controls the distribution of isotopes on earth, it is “an agent of change” (Fry, 2007). Patterns of fractionation, the separation of isotopes into two products and then their mixing, to form a single product once again can be predicted. Isotopes follow a common pattern

during these processes, allowing us to trace nutrient cycling through the biosphere. Ecosystem processes; chemical, physical or biological have significant isotope fractionations, which are either reversible equilibrium reactions or irreversible kinetic reactions. Kinetic fractionation generally results in a product that is lighter than the reactant, as lighter isotopes react quicker than heavy isotopes, whereas equilibrium fractionation can produce products that are either heavier or lighter than the original reactant (Kendall, 1998). Isotope fractionation factors (α) can be defined as the ratios of the heavy to light isotope (R) in the product (p) and substrate (s) (Kendall et al., 1998), as shown in this equation:

$$\alpha = R_p / R_s \qquad \textbf{Equation 2.5}$$

Metabolic processes that occur in the N-cycle, such as denitrification, have irreversible unidirectional kinetic fractionation effects and are highly variable depending on microbial processes and environmental conditions (Figure 2.16, Kendall et al. (1998)).

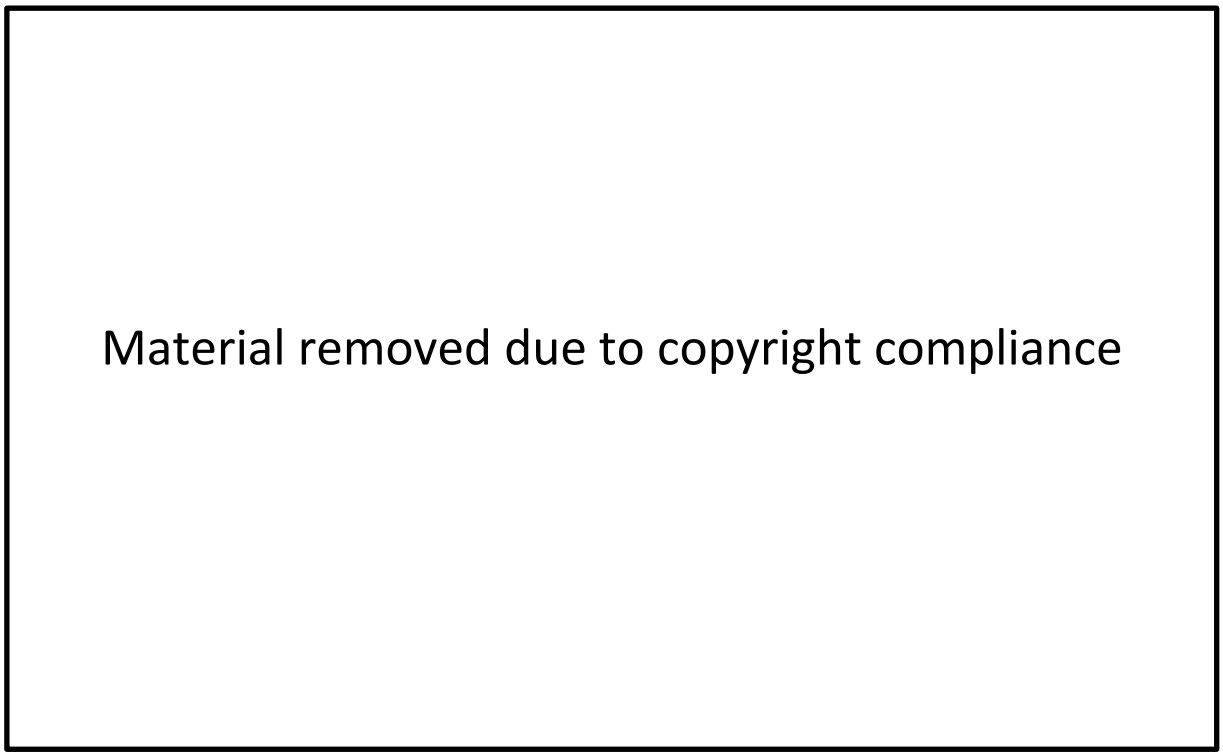

Figure 2.16: Nitrogen transformations and processes affecting $\delta^{15}N$ values in forest systems. (Kendall, 1998; Nadelhoffer & Fry, 1994).

During denitrification, both N and O of the residual NO_3^- pool are progressively enriched during the reduction of NO_3^- to NO_2^-. This fractionation of the NO_3^- isotope as it is reduced to NO_2^- allows for the quantification of substrate removed using the Rayleigh equation (Kendall et al., 1998):

$$R/R_0 = (C/C_0)^{1/(\alpha\ denit-1)}$$ **Equation 2.6**

The Rayleigh model uses the slope of linear regression lines given by the correlation of $\delta^{15}N$- NO_3^- with the natural logarithm of the fraction of residual NO_3^- to estimate microbial denitrification rates (Figure 2.17). As the residual (R) NO_3^- pool compared to the original (R_0) can be quantified relative to the corresponding change in substrate concentration (C_t/C_0), assuming a constant degree of isotopic discrimination.

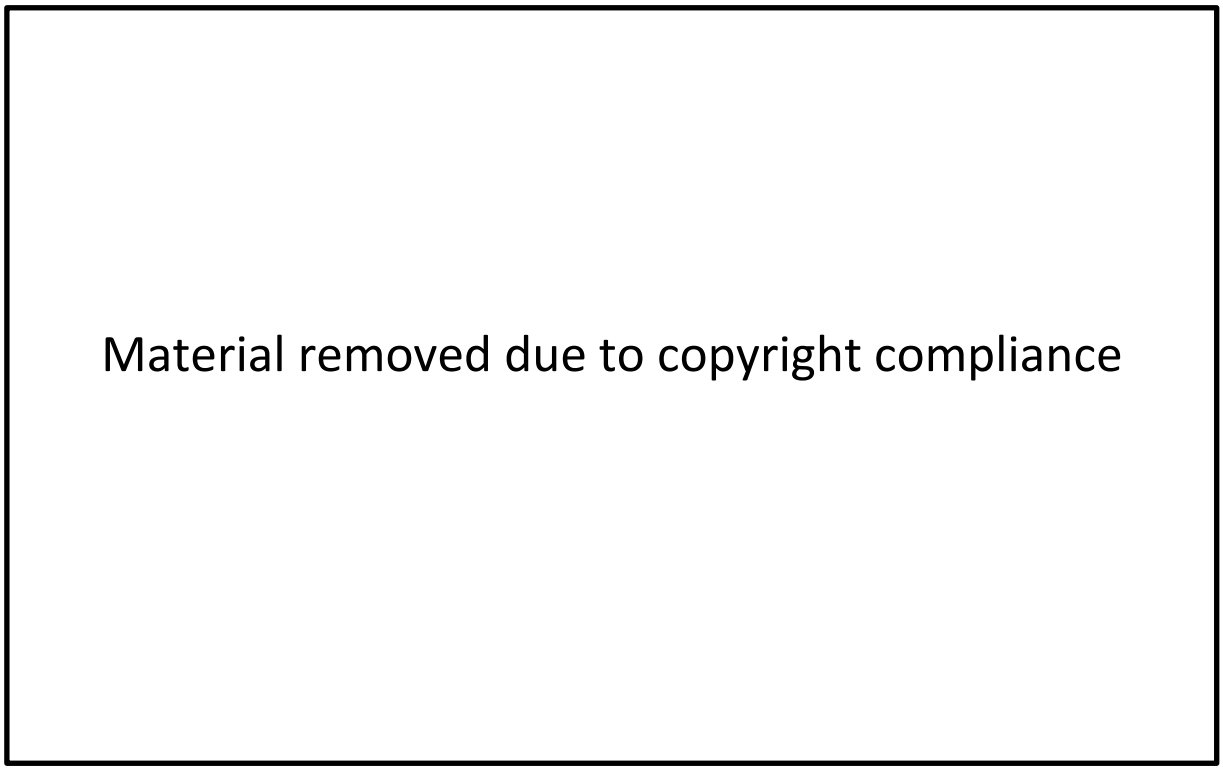

Figure 2.17: Illustration of the linear regression of a Rayleigh calculation used by Warneke et al. (2011) to calculate the $\delta^{15}N$-NO_3^- fractionation factor (-19‰). Showing the $\delta^{15}N$-NO_3^- verses the log of the ratio of C_t/C_0, where C_t is the NO_3^- concentration at a given time (t) and C_0 is the initial NO_3^- concentration.

The enrichment factor is used to calculate the fraction of substrate remaining, based on the changes in corresponding isotopic composition. An isotope enrichment factor, ε, can be defined as (Kendall et al., 1998):

$$\varepsilon_{p\text{-}s} = (\alpha\text{-}1) \times 1000$$ **Equation 2.7**

The more negative the enrichment factor, the greater the magnitude of fractionation, the closer it is to 0, the lower the effect. For example, the relative enrichment factors for N and O range from 0.5 to 1.0 as during denitrification, as they enrich in parallel (Figure 2.14).

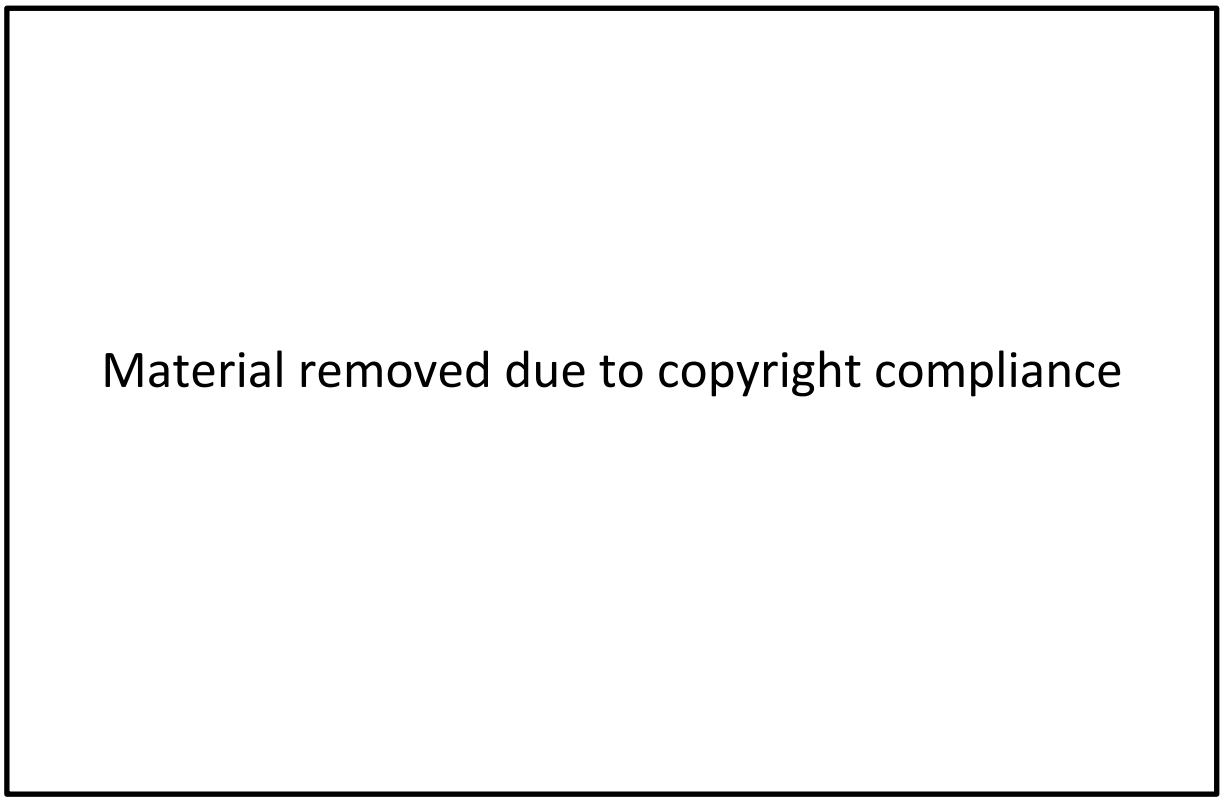

Figure 2.18: Rayleigh fractionation (α) of NO_3^- during denitrification, showing the relative changes in $\delta^{15}N$ during a complete reaction in a closed system (Högberg, 1997; Mariotti et al., 1981), against the concentration change of the substrate remaining (C) relative to the initial substrate concentration (C_0). (Wells, 2013).

Fractionation of NO_3^- isotopes also allows for the fingerprinting and identification of significant denitrification, as the presence of increasingly "heavier" $\delta^{15}N$ indicates that NO_3^- removal has been due to denitrification (Savard et al., 2007; Wells et al., 2016), with the failure to find a relationship between NO_3^- concentration and $\delta^{15}N$ ruling out the presence of significant denitrification (Figure 2.18).

The transportation and mixing of isotopes in the landscape can lead to errors in interpreting isotope signatures. Light isotopes can fractionate during transport as they can easily diffuse between aerobic and anaerobic zones in a flow path (Abe & Hunkeler, 2006; Aeppli et al., 2009) decreasing the expression of denitrification enrichment (Ueda et al., 2006). Therefore, fractionation due to diffusion can occur, as lighter molecules can diffuse at a different rate.

The mixing of two sources in a flow path can distort the expression of reaction rates and isotopic fractionation since the resulting pool is a mix of the two NO_3^-sources their respective concentrations and their isotopic signatures (Fry, 2007). For example, the mixing of an aerobic source with low enrichment and an enriched anaerobic source can reduce the expression of reaction rates in the enriched source. To determine the effect of different sources on the isotopic signature of NO_3^- a standard two-pool isotope mixing model can be used, as the isotopic composition of the mixture is an intermediate between the composition of the endmembers (Kendall, 1998):

$$M_C = S_1 + S_2 \quad \textbf{Equation 2.8}$$

$$\delta^{15}M_c \times M_c = \delta^{15}S_1 \times S_1 + \delta^{15}S_2 \times S_2 \quad \textbf{Equation 2.9}$$

Where the $\delta^{15}N$ value of the mixture (M_c) can be calculated from the two known sources (S_1 and S_2) and their respective $\delta^{15}N$ values. Where M_c, S_1 and S_2 are routinely given in units of concentration or moles.

2.4.3 Variation in Isotope Signatures

The $\delta^{18}O$ of NO_3^- varies geographically due to the isotopic signatures of $\delta^{18}O$-H_2O and $\delta^{18}O$-O_2, as both H_2O and O_2 contribute O to NO_3^- formation (Pellerin et al., 2009). The $\delta^{18}O$-H_2O varies latitudinally due to variation in global meteoric waters, while $\delta^{18}O$-O_2 varies locally with microbial respiration and primary O_2 production. Atmospheric deposition is relatively high in $\delta^{18}O$, generally greater than +60‰ (Elliott et al., 2007). Nitrifiers use two O atoms from H_2O ($\delta^{18}O$ -25 to +5‰) and one atom from O_2 ($\delta^{18}O$ ≈+23‰) to form NO_3^- (Amberger & Schmidt, 1987), resulting in NO_3^--$\delta^{18}O$ derived from nitrification being generally in the range of -10 to +10‰ (Burns & Kendall, 2002; Sebestyen et al., 2008). Factors that can increase $\delta^{18}O$ signatures include nitrification in soil water with high $\delta^{18}O$ due to evaporation, or O_2 with a high $\delta^{18}O$ due to respiration (Kendall et al., 2007; Pellerin et al., 2009).

Biological processes are comprised of a number of steps (e.g., denitrification: $NO_3^- \rightarrow N_2O \rightarrow N_2$), with each step having the potential for fractionation, which are often dependant on environmental variables; size of reservoir pools (O_2, NO_3^-), soil pH, species of organism etc. All of these variables increase the complexity of natural system fractionation (Kendall et al., 2007).

Microbial assimilation of N in soils shows a minimal fractionation range between -1.6‰ to +1.0‰ (Hübner, 1986), mineralisation of organic-N to NH_4^+ also has very little isotope fractionation effect (Kendall & Aravena, 2000). Nitrification has a much wider range, depleting NO_3^- in ^{15}N by -5 to -35‰, with respect to the NH_4^+ source (Kendall et al., 2000; Mariotti et al., 1980a). Denitrification causes exponential increase in ^{15}N as NO_3^- concentrations decrease, with enrichment factors under controlled laboratory conditions ranging from -29.4‰ to -24.6‰ (Kendall et al., 2000). Meaning the denitrification produced N_2 is lower than NO_3^- by these numbers.

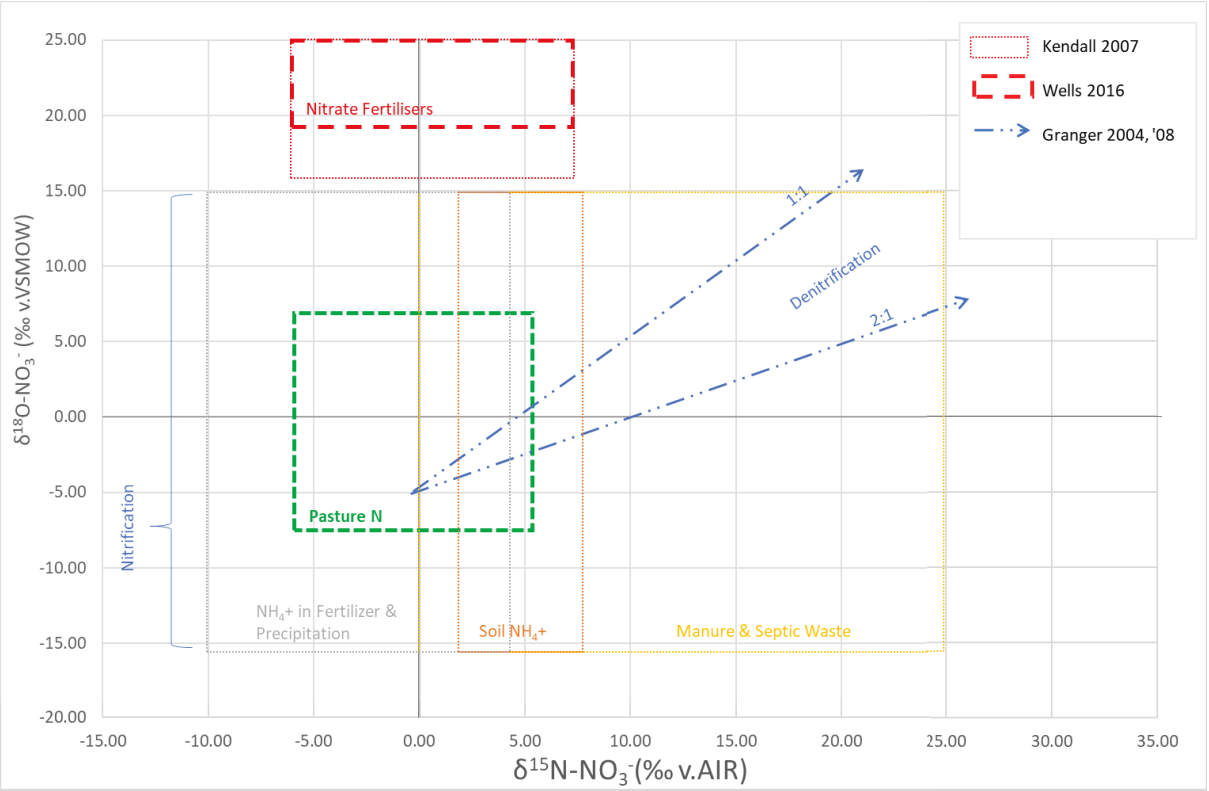

Figure 2.19: Summary of NO_3^- isotope ratios for identifying NO_3^- sources as reported by Granger et al. (2008), Granger et al. (2004), (Kendall et al., 2007) and Wells et al. (2016)

However, the reported ratios of NO_3^- isotopes, used for identifying sources of N, vary (Figure 2.14 and Figure 2.19), and there is a poor understanding of factors controlling kinetic fractionation thought to be responsible for this disparity (Curtis et al., 2011; Nestler et al., 2011; Xue et al., 2009). There are multiple factors that can influence the isotopic composition of NO_3^- environmental samples (NO_3^- source, transformation, transport and mixing processes) and these need to be considered when studying source apportionment or NO_3^- attenuation (Figure 2.20). There is minimal knowledge on how these multiple factors affect NO_3^- isotopic composition in Southland. More research is required to define isotope values that identify N-cycle processes in the environment. This would allow for N-cycle processes to be identified, quantified in relation to specific areas in the landscape.

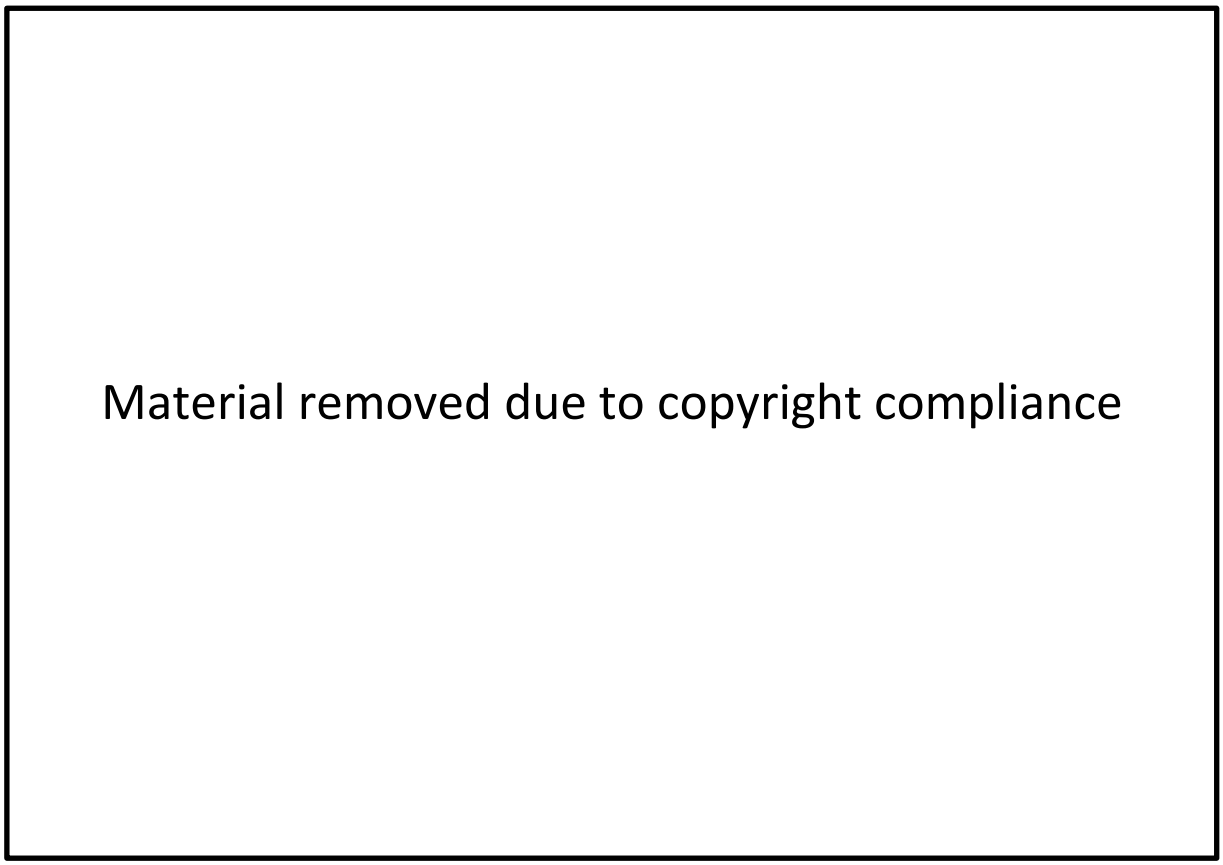

Figure 2.20: Summary of processes that affect the isotopic composition of the NO_3^-, taken from Nestler et al. (2011). ANAMMOX: Anaerobic ammonium oxidation; DNRA: Dissimilatory reduction of ammonia.

In New Zealand systems for example, the NO_3^- source ranges plot in clearly designated zones on a $\delta^{18}O$:$\delta^{15}N$ plot (Figure 2.21), where denitrification shifts the ^{18}O and ^{15}N ratio along a 1:1 slope. This plot provides a basic understanding of the biogeochemical processes that occur in New Zealand environments, with negligible expression of high $\delta^{18}O$ values from atmospheric deposition (Parfitt et al., 2012).

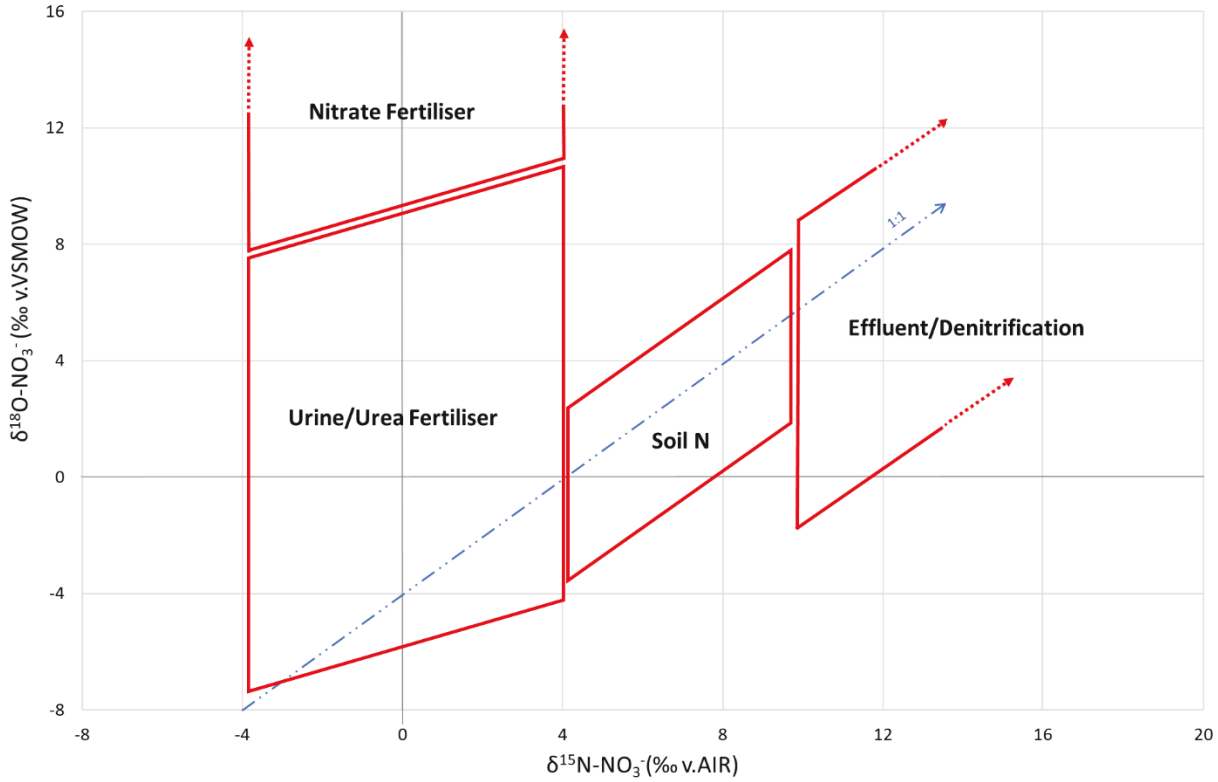

Figure 2.21: Red parallelograms represent ranges presented by Baisden et al. (2016b) based on a board range of research across New Zealand agricultural systems.

The potential of pasture plants to influence the soil N-isotope signature, and the $\delta^{15}N$ of NO_3^- that may be subsequently leached has not been widely researched. It also remains to be seen if temporal variation occurs in the isotopic signature of urine-NO_3^- leached from a pasture system. Temporal $\delta^{15}N$-NO_3^- variation may confound the interpretation of such data when modelling N attenuation in the landscape. While previous research has found pasture production to correlate positively ($r^2 = 0.77$, P = 0.02) with the rate of $\delta^{15}N$-NO_3^- enrichment, this was due to the influence of fertilizer and irrigation on production and their respective effects on $\delta^{15}N$ rather than the pasture growth (Mudge et al. 2013). Rock et al. (2011) found an average $\delta^{15}N$ shift of ~+5‰ $\delta^{15}N$, between the range of +0.3 and +8‰, when comparing soils under legume (Lucerne, (*Medicago sativa* L.)) and non-legume treatments, with the legume having lower $\delta^{15}N$ but greater $\delta^{18}O$ (up to +7‰) due to fixation of atmospheric N_2. Ranges of $\delta^{15}N$-NO_3^- from 0‰ to +19‰ and +9‰ to +18‰ for plant N assimilation of NO_3^- and NH_4^+ into organic N, respectively, were also previously reported (Högberg, 1997; Robinson, 2001).

Isotopic fractionation can be biochemically driven (intrinsic fractionation), with fractionation rates varying between different microbial strains (Bryan et al., 1983; Granger et al., 2008; Kritee et al., 2012; Shearer & Kohl, 1988). Even under ideal denitrifying environmental conditions; non-limiting C, anaerobic and warm, denitrification enrichment was found to vary between -5‰ to -31‰ (Wells, 2013). Environmental factors, particularly O_2 concentration and C substrate have been found to alter

the magnitude of denitrifier strain fractionation, with decreased response as environmental stresses are increased (Kritee et al., 2012).

It is also noted that there is an inverse relationship between denitrification fractionation and enrichment (Bates & Spalding, 1998; Korom et al., 2012). Increasing fractionation decreases the magnitude of denitrification enrichment, as increasing environmental stresses reduce the strength of discrimination against heavy isotopes (Bullen & Kendall, 1998; Kritee et al., 2012).

The function and distribution of microbial communities for a given location need to be better understood to better define isotopic denitrification enrichment in the field, as well as how local denitrifier populations are affected by environmental conditions.

2.5 Key Outcomes

It is known worldwide that there needs to be a change in how N is managed to reduce its environmental impact. But the large spatial and temporal variation in denitrification across the landscape is difficult to quantify, with many different environmental and chemical factors influencing the magnitude of attenuation during biological denitrification and its influence on freshwater bodies.

Spatial variation between soil types and their effect on isotope signatures is poorly understood but may play a key role in identifying ”hotspots” and “hot moments” of N attenuation in the landscape. There is also a lack of quantified data relating to the N attenuation processes occurring below the root zone before N reaches freshwater systems.

Soil O_2 and ρ_b are known to play a key role in controlling biological processes in the soil. But it is poorly understood how these factors, involved in N attenuation, influence the amount of N that moves from the soil into waterways. Dual isotope analysis of NO_3^- potentially allows for the identification of N source and can also allow for quantification of N removed, however, the fractionation of isotopes is strongly dependant on local conditions and therefore they cannot be readily used to analysis processes in different locations.

Thus, further research focusing on N attenuation in the vadose zone, and identifying key interactions between soil environmental factors, such as soil O_2 and ρ_b could allow for N attenuation processes to be quantified in relation to time and place in the landscape. The recent use of gas diffusivity as a potential variable for explaining the onset of anaerobic conditions has not been used to explore NO_3^- attenuation and NO_3^- isotope dynamics, but has the potential to enable further understanding of conditions suitable for NO_3^- attenuation, both temporally and spatially within the landscape.

Key research gaps:

- Isotope analysis provides a tool to identify N-cycling processes and N source. There is a current gap in knowledge surrounding soil dual stable isotope analysis of NO_3^-, particularly below the root zone.

- The Southland region has an abundance of freshwater isotope data, both ground and surface, the addition of soil isotope data would potentially allow for a more detailed picture of N attenuation across the landscape. This region of New Zealand is of importance due to the large increases in farming intensity and therefore is at high risk of environmental contamination.

- Isotope analysis has become more widely used as a way to understand environmental processes in the landscape. However, the use of isotopes to identify temporal and spatial variability in NO_3^- leached under urine patches, a primary NO_3^- source, has not been widely researched. Understanding the influences of urine patches on NO_3^- isotope signatures would provide a better understanding of the effects of agricultural intensification on the state of the environment.

- Soil properties, such as air-filled pore space and ρ_b have been used to model or measure soil D_p/D_0, and in field and laboratory studies this correlates well with surface denitrification fluxes. However, no studies have examined this in the context of NO_3^- isotope dynamics.

- Soil O_2 plays a key role in the variation in N-gas emissions, which vary with soil ρ_b. These two key physical soil parameters may allow for the measurement of D_p/D_0 in the field to be used as a N management tool.

Building on these research gaps this thesis attempts to further understand N attenuation within the landscape, using dual stable isotope signatures and the key soil physical parameter of diffusivity. The following chapters will present original findings on N attenuation dynamics:

- Soil physical properties; soil Ψ and gas diffusivity, of two soils (A and B horizons) on N attenuation under controlled laboratory conditions (Chapter 4).

- Soil type effect on gas diffusivity and dual NO_3^- isotope signatures under controlled laboratory conditions (Chapter 5).

- Plant presence and temporal effect on dual NO_3^- isotope signatures under a urine patch, using lysimeters in a field setting (Chapter 6).

- Temporal and spatial variation in N attenuation at two contrasting field sites in Southland, New Zealand using dual NO_3^- isotope signatures and soil physical properties (Chapter 7).

Chapter 3

General Methods

3.1 Soil Properties & Soil Water

In-situ soil bulk density (ρb, Mg m^{-3}) was determined by taking intact soil cores: stainless steel cylinders (7.3 cm i.d., 4 cm deep) which were slowly inserted into the ground to avoid disturbing the soil profile and then carefully removed, keeping the soil core intact. Back in the laboratory the intact soil cores were oven dried at 105°C until at a constant weight, and then the mass of soil and the internal cylinder volume were used to determine soil ρ_b:

$$\rho_b = M_s/V_s \qquad \textbf{Equation 3.1}$$

Where: ρ_b = soil bulk density (Mg m^{-3}), M_s = mass of dry soil (g), V_s = volume of the soil core (m^3)

Bulk density of repacked soil cores were also checked using the equation above.

Total porosity was determined as:

$$\Phi = \left(1 - \left(\frac{\rho_b}{\rho_d}\right)\right) * 100 \qquad \textbf{Equation 3.2}$$

Where: Φ = Total porosity (%), ρ_d = particle density (2.65 Mg m^{-3})

Gravimetric soil moisture (θ_g) was determined using the weights before and after drying. Soil sub-samples were taken to calculate soil gravimetric moisture content by weighing a 10 g moist soil sample, placing it in the 105 °C oven for 24 hours then weighing it again to calculate the percentage of water held in the soil at the time of sampling (Blackmore et al., 1987). Calculated as:

$$\theta_g = (M_w - M)/M \qquad \textbf{Equation 3.3}$$

Where: θ_g = Gravimetric soil moisture (g water g^{-1} oven dry soil), M_w = the mass of wet soil (g), M = the mass of oven dry soil (g).

Volumetric water content (θ_v) was determined as:

$$\theta_v = \theta_g * \rho_b \qquad \textbf{Equation 3.4}$$

Where: θ_v = Volumetric water content (m^3 m^{-3}), θ_g = Gravimetric soil moisture (Mg), ρ_b = soil bulk density (Mg m^{-3})

Water-filled pore space (WFPS) was calculated as:

$WFPS = \theta_v / \Phi$ **Equation 3.5**

Where: WFPS = water-filled pore space (m^3 m^{-3}), θ_v = Volumetric water content (m^3 m^{-3}), Φ = Total porosity (%).

Air-filled pore space (Ɛ) was calculated as:

$\varepsilon = \Phi - \theta_v$ **Equation 3.6**

Where: Ɛ = Air-filled pore space (m^3 m^{-3}), Φ = Total porosity (%), θ_v = Volumetric water content (m^3 m^{-3}).

Soil particle size analyses were performed at the University of Waikato using a Laser Diffraction Particle Analyser (Mastersizer 3000 v3.50, Malvern Panalytical Ltd.).

3.2 Repacking Soil Cores

The re-packed soil cores used in the laboratory experiments used air-dried soil sieved to 2 mm. After determining the soil gravimetric water content of the air-dried, sieved soil, stainless steel cylinders (7.3 cm i.d., 4 cm deep) were packed to a constant volume, at soil ρ_b values of 1 and 1.2 Mg m^{-3}, representative of soil A and B horizons, respectively. The following calculation was used to determine the amount of soil needed to reach the desired bulk density of each core:

$M_s = \rho_b * V_s + \theta_g * \rho_b * V_s$ **Equation 3.7**

Where: M_s = mass of dry soil (g), V_s = volume of the soil cores (m^3), θ_g = gravimetric water content (g water g^{-1} dry soil).

To maintain a uniform soil ρ_b through the core, the soil was compressed 1 cm depth at a time (Plate 3.1). A nylon mesh was stretched over the bottom of the stainless-steel cylinder, prior to soil packing, to prevent soil loss.

Plate 3.1: Solid steel weights used for repacking the soil cores (the four from the left) and a core with nylon mesh in place (right).

3.3 Soil Physical & Chemical Data

3.3.1 Preliminary Soil Sampling & Chemical Data Analysis

Preliminary chemical data for all the soils used in trials was performed on sub-samples of soils collected from Southland, New Zealand between the 16th to the 18th of November 2016 (Table 3.1 and Figure A.1). There were five field sampling sites in the Southland region:

Table 3.1: Site information for soils used in experiments, soils classified to the New Zealand Soil Classification (Hewitt, 2010). All soils were collected from Southland, New Zealand.

In text	Soil Name	Classification	Site Location	Experiments
CP	**Braxton**	Typic Orthic Gley	Central Plains	Lysimeter & Laboratory
GM	**Gore**	Acidic Orthic Brown	Five Rivers	Field Trial
DH	**Acton**	Melanic Orthic Gley	Five Rivers	Field Trial
AG	**Acton**	Melanic Orthic Gley	Five Rivers	Laboratory

Field soil sampling methodology consisted of digging a soil pit at each site and taking a 5 cm x 5 cm x 5cm sample down the full depth of the soil pit face for each horizon. Samples from each horizon were then air dried for 4 days at 30°C, sieved to 2 mm and well mixed by hand, to allow for a homogenized sample down through each soil horizon. Sub-samples of each horizon were then sent for chemical analysis at Hills Laboratories, Hamilton and particle analysis at Massey University, Palmerston North, New Zealand.

The field trial sites were sampled more intensively (Gore and Acton), with each 5 cm increment analysed separately to give a more detailed overview of the soil's chemical composition. As well as a 50 m transect sampling to 7.5 cm depth, with a 7.5 cm soil core taken every metre. All transect cores were air dried for 4 days at 30°C, sieved to 2 mm and combined before a well-mixed sub-sample was

sent to Hills Laboratories for chemical analysis. Field bulk density cores were taken at each site, 3 cores from each horizon (A and B) (Section 3.1, Equation 3.1).

Soil chemical analyses were performed by Hill Laboratories (Hamilton, New Zealand). Soil pH (1:2 (v/v) soil: water slurry followed by potentiometric determination of pH)(Blackmore et al., 1972), Olsen P (Olsen extraction followed by Molybdenum Blue colorimetry: Flow Injector Analyser; Tecator Inc., Sweden)(Olsen et al., 1954), Total C and N (Dumas combustion)(Horneck & Miller, 1998) were determined using an elementar 'Vario' MAX CN Analyser (Elementar Analysensysnane, GmbH).

Soil particle analysis was performed by the Earth Sciences Department, Faculty of Science and Engineering at the University of Waikato, New Zealand, using laser-based particle size analysis (Malvern Matersizer 2000).

Initial soil $\delta^{15}N$ values were determined on air dried and sieved (<2 mm) soil with visible organic material removed, that had been ground to < 200 μm prior to analyse on a Sercon GSL/20-22 Isotope Ratio Mass Spectrometer.

Detailed chemical and physical information for each soil type can be found in Appendix A.

3.3.2 Study Soil Chemical Data Analysis

Analysis of chemical data on soil and/or leachate samples from laboratory, lysimeter and field experiments for this thesis were performed as follows.

Soil inorganic N (NO_3^-, NO_2^- and NH_4^+) was determined by extracting a soil subsample with KCl (potassium chloride) (4 g of wet soil: 40 mL of 2 M KCl) by shaking for 1 h, then centrifuging for 10 mins at 2000 rpm. The extract was filtered (Whatman 41) and analysed for inorganic N content using an Alpkem FS3000 twin channel Flow Injection Analyser (FIA) as described by Blackmore et al. (1987). Leachate samples were also analysed for inorganic N using the FIA.

Field trial samples that were less than 5 mL volume were analysed for NO_3^--N and Br concentrations by ion chromatography (Dionex ICS-2100, Thermo Fisher Scientific, Sunnyvale, CA, USA), which had a 50 mm long guard column (4 mm internal diameter), a 250 mm long analytical column (4 mm internal diameter, IonPac AS9-SC), a self-regenerating anion suppressor (Dionex AERS 500) and a conductivity detector. Both, FIA and Dionex analyses, were carried out at Lincoln University, Lincoln, New Zealand.

Soil pH was taken using a flat surface pH electrode (Broadley James Corp., Irvine CA.).

Dissolved organic carbon was determined using cold water extractions (Ghani et al., 2003). Soil and DI were combined, 10 g soil:100 mL DI water and mixed on a side-by-side shaker at 75 rpm for 1 hr, then

centrifuging for 20 mins at 3300 rpm Samples were then passed through a 0.45 µm syringe filter, frozen after extraction until analysis on a Total Organic Carbon Analyser (TOC 5000A, Shimadzu, Australia).

3.4 Tension Table Construction

Construction of tension tables was performed, according to Romano et al. (2002), as follows; first a filter (Whatman 42) was placed over the top of the water outlet in the tray to prevent egress of sand, followed by a two cm layer of brick-layers sand, evenly spread into the base of the tray. At this point the siphon between the bottle and the tray was created using the weight of the water to draw it down into the bottle, making sure there were no air bubbles present in the tube to ensure there was a continuous column of water. A silica flour slurry made up of a 2:1 ratio of silica flour to water was then poured into the tray on top of the sand. This step was completed before all the water was drained out of the sand to ensure there was no air trapped in the silica flour. Silica flour slurry was added in layers until it was approximately 4 cm thick. Then tension tables were set to their designated soil matric potential treatments (Plate 3.2). The silica flour slurry settles out and creates a surface that allows the soil in the core to connect to the water column created by the hanging bottle, this allows the manipulation of the soil water to generate different soil matric potentials.

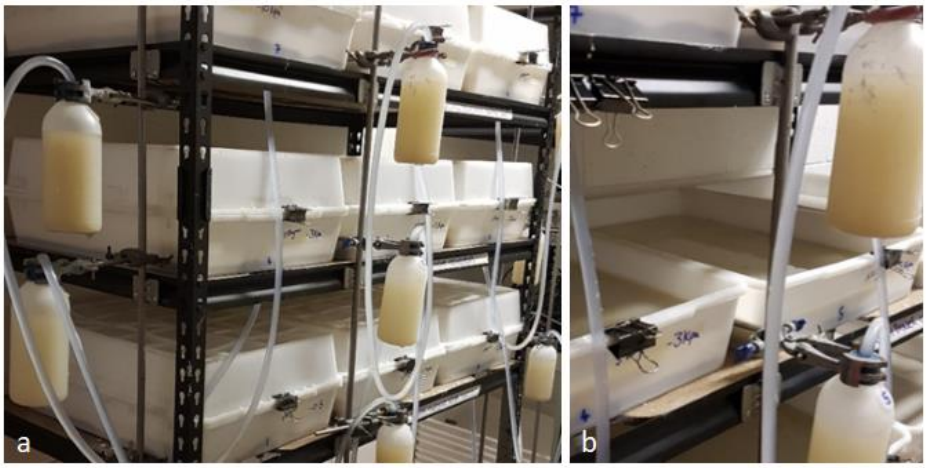

Plate 3.2: The tension table set up showing tray, tube and bottle (a). The silica flour layer in the tension table trays that creates a surface for the soil cores to connect to the water column and generate different soil matric potentials (b).

3.5 Nitrous Oxide Gas Sampling

The N_2O fluxes were determined by placing the soil cores in 1 L air-tight mason jar (Plate 3.3). Gas samples were taken at time 0, 20 and 40 minutes after the jars were sealed using a 20 mL glass syringe fitted with a 3-way tap and a 25-gauge 0.5 by 16 mm needle (Precision Glide; Becton-Dickinson, Franklin Lakes, NJ)(Plate 3.3) as described by Balaine et al. (2013).

Plate 3.3: Jars with soil cores sealed inside them during N_2O flux determinations. Glass syringe in foreground.

Extracted N_2O samples were transferred to pre-evacuated (-0.1013 MPa) 6 mL vials (Exetainer; Labco Ltd., Lampeter, UK). Nitrous oxide fluxes were determined at Lincoln University using an automated GC (8610, SRI Instruments, Torrance, CA) interfaced to an autosampler (Gilson 222XL, Middleton, WI) as described by Clough et al. (2006). Nitrous oxide concentrations were quantified with a ^{63}Ni electron capture (ECD) operated at 310°C. The N_2O fluxes (mg m^{-2} h^{-1}) were calculated using the 'Ideal Gas Equation' [Eq. 3.8], rearranged to solve for *n* [Eq. 3.9] and equation Eq. 3.10:

PV = nRT **Equation 3.8**

n = PV/RT **Equation 3.9**

where:

P = 1 atmosphere (atm)

V = volume of N_2O = GC output (t_2-t_0, total cover period - start of cover period, µL L^{-1}) x headspace volume of sampling containers (1 L container - volume of soil core and ring (0.16 L)).

n = moles of N_2O (µmoles).

R = Gas constant (L.atm K^{-1} mol^{-1}) 0.08201

T = temperature (K) (273.15 plus the laboratory temperature in °C)

$$\mathbf{F_{N2O}} = \frac{a_m t_h (\mathrm{m}/a_{cm}/t_f)}{m_\mu} \qquad \textbf{Equation 3.10}$$

where:

F_{N2O} = N_2O flux (µg m^{-2} h^{-1})

m = mass N_2O-N (µg N_2O-N) = n (moles of N_2O, equation 3.9)* molecular weight of N_2O-N (28.0134)

a_{cm} = area of soil core (cm^2)

t_f = minutes / hour (60)

a_m = conversion from cm^2 to m^2 (10,000)

t_h = conversion from minutes to hours (60)

m_μ = conversion from mg to µg (1000)

3.6 Isotopic Sample Analysis

Measurements of leachate NO_3^- $\delta^{15}N$ and $\delta^{18}O$ were performed at the National Isotope Lab, Geological and Nuclear Science, Wellington, New Zealand, using the cadmium-azide method (McIlvin & Altabet, 2005). Isotope values were analysed using a GVI Isoprime coupled with an AquaPrep for water samples. The reference standard used for $\delta^{18}O$ analyses was VSMOW for waters (Vienna Standard Mean Ocean Water, absolute isotope ratio (2005.20 ± 0.45) x 10^{-6} (Baertschi, 1976), with a measurement precision of 0.1‰. The reference standard used for $\delta^{15}N$ analyses was Air (atmospheric N gas, absolute isotope ratio (3676 ± 4) x 10^{-6} (Coplen et al., 1992; Junk & Svec, 1958), with precision of 0.3‰. All isotope results are reported in respect to internationally recognised standards:

$$\delta\,‰ = (R_{sample} - R_{standard})/R_{standard} \times 1000 \qquad \text{Equation 3.11}$$

The $\delta^{15}N$ composition of the BU treatment input was determined by pipetting two replicate 5 mL aliquots into tin capsules filled with Chromosorb W (Supelco, Bellefonte, PA)(Cheng et al., 2011). The $\delta^{15}N$ composition of the soil was determined on air dried and sieved (<2 mm) soil with visible organic material removed, analysed on a Sercon GSL/20-22 Isotope Ratio Mass Spectrometer.

3.7 Relative Soil Gas Diffusivity

The diffusivity of the cores was measured using diffusivity chambers that were constructed at Lincoln University following the procedure of Rolston et al. (2002).

This system uses a fully sealed chamber, containing O_2 sensors (KE-25, Figaro Engineering Inc., Osaka, Japan), that only allows air to enter the chamber by diffusion through the soil core (Plate 3.4).

When using the chambers, the soil cores are first placed into the lids and the chambers are sealed. Petroleum jelly is used to make sure there are no leaks around soil core cylinders. The chambers are purged with an O_2 free gas mixture (90% Ar and 10% N_2) so that there is no O_2 present in the chambers. Measurements are started once O_2 levels have dropped below 0.02% in the chambers. The sensors and datalogger record the change in O_2 over time as it diffuses through the soil core over a period of 120 to 180 min.

Plate 3.4: Soil diffusivity chamber with soil core in place, chamber closed to record O_2 change over time.

This information is then used to calculate the diffusivity of the soil, expressed as D_p/D_0, which is the normalised ratio of diffusion through soil:air based on soil properties (Balaine et al., 2016b; Balaine et al., 2013). The value of D_p is the gas diffusion through soil, calculated using the natural log plot of relative O_2 concentration (eq. 3.12) over time (hrs). Where C represents different points of gas (in this experiment O_2) concentration in the diffusivity chamber set-up over time, C_g is the concentration of gas in the chamber at any t, C_s is the concentration of gas in the soil at $t = 0$, and C_0 is the concentration of gas in the chamber at $t = 0$:

$$lnC_r = ln(C_g-C_s)/(C_0-C_s) \qquad \textbf{Equation 3.12}$$

Analysis of the slope of the regression equation of the natural log plot of relative O_2 concentration over time allows the measured soil O_2 diffusion coefficient to be calculated according to Rolston et al. (2002) (eq. 3.13 to 3.16). Equation 3.13 is transformed into equation 3.14 to calculate D_p, where k is the slope of the regression equation of lnC_r (eq. 3.12) plotted against time, Ɛ is the soil AFP and α is determined using eq. 3.15 and 3.16 (where a is the volume of the chamber by the area of the soil core) to find hl and the corresponding αl from reference table (Table 4.3-1 Rolston et al. (2002)). Where l is core length and the table lists the first 6 roots of $\alpha_n l$ equal to αl tan αl, the roots of the equation are real if hl >0.

$$-D_p\alpha_1^2/Ɛ \qquad \textbf{Equation 3.13}$$

$$D_p = k*Ɛ/\alpha_1^2 \qquad \textbf{Equation 3.14}$$

$$a = V_{chamber}/A_{soil\ core} \qquad \textbf{Equation 3.15}$$

$$h = Ɛ/a \qquad \textbf{Equation 3.16}$$

The method assumes that error in measured D_p due to O^2 consumption is negligible (Rolston et al., 2002).

The value of D_0 equates to the diffusivity of O_2 through air at 20°C and equals 0.205 $cm^2\ s^{-1}$ (Currie, 1960; Rolston et al., 2002), calculated using equation 3.17. Where D_{T2} and D_{T1} are the diffusion coefficients at temperatures T_2 and T_1 (Kelvin). The value of the exponent of 1.75 was used by Fuller et al. (1966). Gas diffusion coefficient of the measured gas needs to be known, binary diffusion coefficients of common gases are listed in table 4.3-2 by Rolston et al. (2002). Oxygen diffusion through air is 0.178 $cm^2\ s^{-1}$ at 0°C (Gliński & Stępniewski, 1985).

$$\mathbf{D_{T2} = D_{T1}\ (T_2/\ T_1)^{1.72}} \qquad \textbf{Equation 3.17}$$

The aforementioned equations were then used to calculate measured D_p/D_0.

3.8 Modelling Relative Soil Gas Diffusion

Modelled D_p/D_0 was calculated using total porosity (Φ) and air-filled porosity (Ɛ), where C_m is the media complexity factor which takes into consideration the soil density and therefore Φ. The model is based on the original WLR (water-induced linear reduction) concept (Moldrup et al., 2000), with the adoption of C_m creating the SWLR (structure-dependant water-induced linear reduction) model:

$$\boldsymbol{D_p/D_0 = \varepsilon^{(1+C_m\,\Phi)}(\varepsilon/\Phi)} \qquad \textbf{Equation 3.18}$$

A media complexity factor of C_m = 1 was used as previous research shows it to be a good predictor of D_p/D_0 for repacked soils (Moldrup et al., 2013).

Chapter 4

Lab Experiment - Part One: Soil Physical Properties.

4.1 Introduction

Grass-feed stock are a key component of agricultural systems, especially in New Zealand (Clough et al., 2005). However, grazed pasture systems are also a substantial source of greenhouse gas emissions (IPCC, 2014b). Nitrous oxide is a greenhouse gas and is currently the dominant anthropogenic ozone-depleting substance emitted (Ravishankara et al., 2009). In grazed pastures it is predominantly associated with the deposition of ruminant urine (Selbie et al., 2015). Ruminant urine deposition is also associated with NO_3^- leaching, which contaminates waterways, reducing water quality for recreation and freshwater ecosystems (Daughney et al., 2009; Galloway et al., 2015; McLaren et al., 1996; Parfitt et al., 2012) and is the main contaminant in New Zealand groundwater (Close et al., 2016). Denitrification, with respect to these environmental issues, is both a problem and a solution. It potentially provides a solution as the process denitrifies NO_3^-, attenuating NO_3^- in the environment, thus removing the issue of NO_3^- pollution (Clough et al., 1998a; Seitzinger et al., 2006). If denitrification goes to completion the process reduces NO_3^- to N_2, an environmentally benign gas, however, incomplete reduction is a problem as it generates N_2O (Cannavo et al., 2004). Denitrification also represents a significant economic loss of N if ca. 25% of ruminant urinary-N inputs are lost as N_2 (Clough et al., 1998b). In New Zealand there remains a lack of knowledge surrounding the process, rates and the quantification of denitrification that potentially occurs in soil water below the root zone, prior to soil water discharge into groundwater (Clague et al., 2015b), better understanding of denitrification in the landscape would allow for better N management.

Soil properties such as moisture status and the degree of aeration influence denitrification (Moldrup et al., 2000; Neira et al., 2015), since denitrification occurs under anaerobic conditions. The enzyme N_2O reductase, which reduces N_2O to N_2, is especially sensitive to O_2 and its efficacy declines as O_2 concentrations increase (Firestone, 1982). Understanding different soil physical properties and how they interact to influence N attenuation may play a key role in on farm management of N uptake and loss, retaining valuable nutrients in the system and reducing environmental impact.

Soil type and management affect many soil physical properties that, in turn, influence soil O_2 concentrations, thereby influencing a soils capacity to attenuate NO_3^- (Chamindu-Deepagoda et al., 2019). Total soil porosity, for example, is a function of both soil structure, texture and soil ρ_b which can alter a soil's moisture content or level of aeration (Assouline, 2006; Kay, 2018). Soil pores may be filled with either gas or water, and can thus be delineated as having Ɛ or WFPS, with the latter a function of

soil moisture. Another factor that influences NO_3^- attenuation is soil ρ_b, which varies with soil type, soil depth and soil management. Depth increases compaction due to pressure, while adverse management that allows over-grazing and pugging can also increase soil ρ_b. As soil ρ_b increases, Φ declines due, predominately, to reduced macro-porosity, resulting in decreased Ɛ. Consequently, water inputs result in relatively higher anaerobic conditions which favour denitrification (Beare et al., 2009).

Total porosity and pore size distribution play a key role in how much water a soil holds (Zuraidah et al., 2011). The Φ volume dictates how much water a soil can hold and the pore size distribution, determines how much 'tension' is required to remove water from a soil. The smaller the soil pores are, the more tension there is on water through capillary action and the greater the suction required to remove it, this can be referred to as tortuosity (Moldrup et al., 2001). This means that, all things being equal, the a denser soil has a greater volume of pores that remain water-filled at a more negative matric potential, as well as a decrease in large aerated pores, creating more favourable anaerobic conditions for denitrification (Assouline, 2006; Chamindu-Deepagoda et al., 2019).

Soil moisture, expressed as WFPS has been historically used as a preferred soil moisture parameter for predicting N_2O losses (Beare et al., 2009; Dobbie et al., 1999; Dobbie et al., 2001), with it also used to better understand how microbial activities vary in soils of differing soil ρ_b (Aulakh et al., 1991; Linn et al., 1984b). Peak N_2O emissions are classically reported to occur at between 50 and 70% WFPS (Bateman et al., 2005; Davidson et al., 2000; Dobbie et al., 1999), which is generally an approximation of field capacity for a soil, with N_2 becoming the main end-product once WFPS is greater than 80% (Bowman et al., 1998). However, WFPS alone cannot be used to compare soils of varying soil ρ_b, because soil ρ_b and moisture interact to affect WFPS (Farquharson et al., 2008), as WFPS does not account for the entire fraction of the soil volume for soils with different ρ_b (Figure 2.12).

The main mechanism of gas movement through soil is diffusion (Penman 1940), "diffusion is proportional to the gas concentration gradient" according to Fick's Law. Soil gas diffusion is represented by D_p/D_0, where D_p is the soil-gas diffusion coefficient (cm^3 soil air cm^{-1} soil s^{-1}) and D_0 is the diffusion coefficient of the same gas in free air (cm^2 air s^{-1}) (Moldrup et al., 2000). Many models of soil D_p/D_0 have been developed relating D_p/D_0 to Ɛ and Φ (Buckingham, 1904; Marshall, 1959; Millington et al., 1961; Penman, 1940). Soil diffusivity has generally been modelled, as measuring D_p is more difficult, requiring special equipment and conditions in the laboratory or in situ (Rolston et al., 2002). More recent models also incorporate soil ρ_b (Chamindu Deepagoda et al., 2011b) to account for the large range of ρ_b that exist between soil types.

Anderson and Peterson (2009) suggested that D_p/D_0 could be a better predictor of N_2O emissions from soils than the commonly used WFPS after conducting research using repacked, nutrient amended soil under three soil matric potentials (-1.5 to -10 kPa). Further research by van der Weerden et al. (2012)

went on to also demonstrate a strong relationship between D_p/D_0 and N_2O emissions from soils amended with NO_3^-. More recent research relates urine, urea, or NO_3^- derived N_2O and N_2 emissions to D_p/D_0, as well as examining the interaction between soil ρ_b and soil matric potential (Balaine et al., 2016b; Balaine et al., 2013; Chamindu-Deepagoda et al., 2019; Owens et al., 2016).

Soil moisture conditions that result in a D_p/D_0 value of ≤0.006, were shown by Balaine et al. (2013) to be the threshold for peak N_2O emissions as determined by measuring N_2O fluxes from NO_3^- amended, re-packed soil cores, varying in ρ_b (1.1 to 1.5 g cm^{-3}) and matric potential (-1 to -10 kPa)(Figure 2.13). Furthermore, this study showed the D_p/D_0 threshold was a better indicator of the onset of denitrification than WFPS. This finding was reinforced by the results of Balaine et al. (2016b) when soil cores were treated with urea and both N_2O and N_2 were measured over a 35 day period, and again the same threshold for N_2O production was observed. The cumulative flux data of Balaine et al. (2016b) were modelled by Chamindu-Deepagoda et al. (2019) who found that D_p/D_0 should be $\geq$ 0.038 to limit extensive emission of N_2O and N_2 fluxes.

Previous work by Balaine et al. (2013), using one soil type, found a critical threshold for D_p/D_0 below which denitrification increased as observed by the enhanced production of N_2O. This was further linked to N_2 (Balaine et al., 2016b). This threshold was observed to be independent of soil ρ_b. However, that work examined only one soil type. This current study aims to further refine the concept of the denitrification threshold as it relates to D_p/D_0 in order to better understand if D_p/D_0 can provide an accurate predictor of denitrification occurrence for different soil types. This could potentially allow farmers to optimise soil management (e.g. irrigation, minimising soil compaction, subsoiling, etc.) so that D_p/D_0 remains above given thresholds in order to minimise losses of N as N_2O and N_2. Conversely it could identify areas where the soils might be managed to optimise denitrification to reduce potential NO_3^- leaching. Optimal D_p/D_0 and soil moisture thresholds for N attenuation are hypothesised to be close to those found by Balaine et al. (2013).

This work will investigate the diffusivity thresholds for different soils, with the possibility of extrapolating this out to cover larger areas and predict thresholds for denitrification when combined with real-time moisture/saturation values of soils in the landscape. The data collected from this experiment will permit soil ρ_b and soil moisture effects on D_p/D_0, between different soil types, to be determined.

4.2 Materials & Methods

4.2.1 Soil Collection, Experimental Design & Setup

Soils were collected from two sites in Southland, New Zealand from the 16th to the 18th of November 2016. One site was from the Central Plains area of Southland, New Zealand (E1225681 N4877019) and

one from Five Rivers in northern Southland, New Zealand (E1257349 N4909615). Vegetation at both sites comprised of grazed dairy pasture dominated by perennial ryegrass (*Lolium perenne* L.). The soil at the Central Plains site was classified as a Typic Orthic Gley (Braxton soil type, rolling deep phase) soil, referred to in the text as Central Plains (CP). The soil at the Five Rivers site was classified as a Melanic Orthic Gley (Acton soil type, undulating moderately deep phase) soil (Hewitt, 1998), referred to in the text as Acton Gley (AG). Southland mean annual rainfall and soil temperature (10 cm depth) are 1112 mm and 9.2°C, respectively (Invercargill historical average 1981-2010, NIWA). Soil samples were taken from two depths in the A and B horizons, 0 - 25 cm and 25 - 40 cm, respectively, at each site (Appendix A, Tables A.1 through A.4). See section 3.3.1 for soil sampling methodology.

Soil samples were taken to Lincoln University, sieved to 2 mm then air-dried at 30°C for 4 days. Soil chemical and texture properties were determined by taking representative sub-samples from each soil horizon. Soil particle size analyses were performed at the University of Waikato using a Laser Diffraction Particle Analyser (Mastersizer 3000 v3.50, Malvern Panalytical Ltd.) and soil chemical analyses were performed by Hill Laboratories (Hamilton, New Zealand) (Section 3.3.1). In-situ soil ρ_b was also determined (Section 3.1).

After determining the soil gravimetric water content of the air-dried, sieved soil, stainless steel cylinders (7.3 cm i.d., 4 cm deep) were packed to a constant volume, at soil ρ_b values of 1.0 and 1.2 Mg m^{-3}, representative of the soil A and B horizons, respectively. For soil core repacking methodology refer to Section 3.2.

The factorial experimental design used comprised of: two soil types (central plains (CP) or five rivers (AG)), two soil depths (A or B horizon), and 7 levels of soil moisture (-0.5, -1.0, -2.0, -3.0, -5.0, -7.0 and -10.0 kPa), with each treatment replicated four times, giving a total of 112 repacked soil cores.

Tension tables were used to maintain the soil cores at the desired soil moisture levels (mentioned above) throughout the experiment, they were constructed on the 20th of October 2017. Tension tables were made up according to Romano et al. (2002) using brick-layers' sand and silica flour in trays, with the bottom of the tray connected to the water reservoir bottle by a 1.5 m long tube, that created an adjustable soil water column that enabled soil matric potential to be varied (Section 3.4).

Repacked soil cores were left to soak in a KNO_3 solution (1800 µg mL^{-1} NO_3^--N) for 24 hours, to ensure denitrification was not N-limited during the experiment (Balaine et al., 2013). Soaking in KNO_3 occurred prior to being transferred to the tension tables, where they were then left to equilibrate at their designated matric potentials. Soil cores were left for 3 days to equilibrate to their respective designated matric potentials, as demonstrated by constant mass. Preliminary testing showed 3 days was sufficient for the soil cores to reach the designated soil matric potentials.

4.2.2 Sampling & Analyses

Soil cores were weighed after three days to determine their volumetric water content, and this information was used to develop a soil moisture retention curve. Gas diffusivities were measured on these same soil cores, at each soil matric potential, with diffusivity chambers constructed using the method of Rolston (1986). Soil cores were analysed for their N_2O fluxes (Section 3.5), prior to being destructively sampled for NO_3^-, NH_4^+ and pH. The diffusivity of the cores was modelled using the method of Moldrup et al. (2013) (Section 3.7). The difficulty of measuring precise soil moisture contents at the very wet end of the spectrum (-0.5 to -1 kPa), when cores hold maximum water creates outliers with extreme D_p/D_0 values. This creates calculation problems when determining Ɛ, resulting in negative values. Where this occurred, values were replaced with a minimum Ɛ of 0.0001 when used in modelled calculations (27 out of 112, all for -0.5 to -3 kPa treatments).

After gas sampling was completed the soil cores were destructively sampled for NO_3^--N and NH_4^+-N (two replicates only), pH and soil gravimetric water content (all four replicates). Refer to Chapter 3, Sections 1 and 3 for more detailed descriptions of soil sample chemical and physical analysis.

4.3 Statistical Analyses

Data were analysed using Minitab® (Minitab®18.1.0.0, 2018) with analysis of variance conducted using the General Linear Model to allow for repeated measures. The variables analysed were soil N; NH_4^+, NO_3^-, N_2O emissions and soil diffusivity with factors of soil type, soil horizon, ρ_b and soil matric potential, with differences and interactions between these variables determined. One-way ANOVA and Tukey's Test were used to identify differences between means ($p < 0.05$).

Data were tested for skewness using an Anderson-Darling normality test. The N_2O emission results were transformed to their natural log to improve the normality of the data. Conclusions on transformed data were drawn from the analysis of transformed data. Data presented in tables and figures are untransformed unless stated otherwise.

4.4 Results

4.4.1 Soil Moisture

Measured volumetric water contents of cores after 3 days on the tension tables showed that tension tables were predominantly functioning as desired (Figure 4.1). However, the -3 kPa tension table did not, holding the cores at a lower ψ than required and so further results from this tension table are not reported. Soil volumetric water contents varied from 66 to 55% at -0.5 kPa, to 36 and 35% at -10 kPa average for the A and B horizons, respectively.

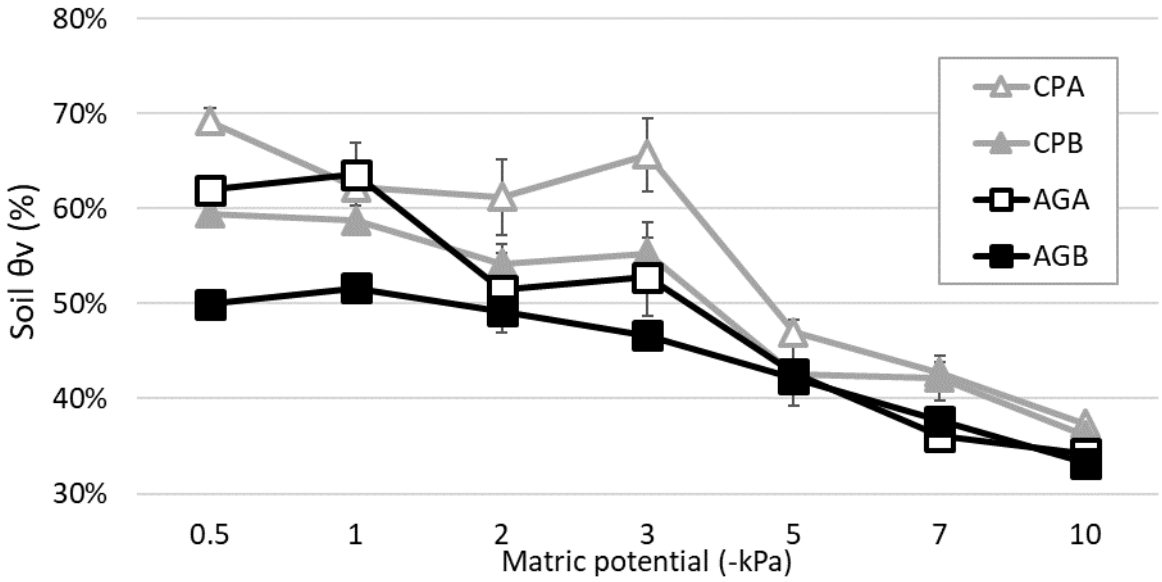

Figure 4.1: Soil volumetric moisture content versus matric potential after 3 days on the tension tables. Error bars = SEM, *n* = 4

4.4.2 Soil Chemistry

Soil NO_3^--N concentrations were not significantly affected by soil type (P = 0.83) or soil ψ (P = 0.31, Figure 4.2a, Table 4.1). Soil NO_3^--N concentrations were significant between soil horizon at a 90% confidence level (P = 0.07). Average NO_3^--N concentrations in the A and B horizons contained, 446 and 384 mg NO_3^--N kg^{-1} soil, respectively. Significant effects may have been found if all four sample replicates had been processed.

Table 4.1: Mean soil NO_3^--N (mg kg^{-1} soil) values ± SEM (*n* = 2). No significant interaction was found using Tukey's pairwise comparisons for a 95% confidence interval for the 'soil type x horizon x matric potential' interaction.

	ψ (-kPa)											
Soil Type	**0.5**		**1.0**		**2.0**		**5.0**		**7.0**		**10.0**	
Central Plains A	302	±74	423	±183	366	±36	584	±21	461	±44	539	±72
Central Plains B	345	±23	456	±60	553	±70	387	±64	306	±170	302	±16
Acton Gley A	310	±10	451	±94	557	±37	524	±50	358	±65	478	±156
Acton Gley B	488	±73	348	±24	394	±12	364	±66	320	±95	340	±44

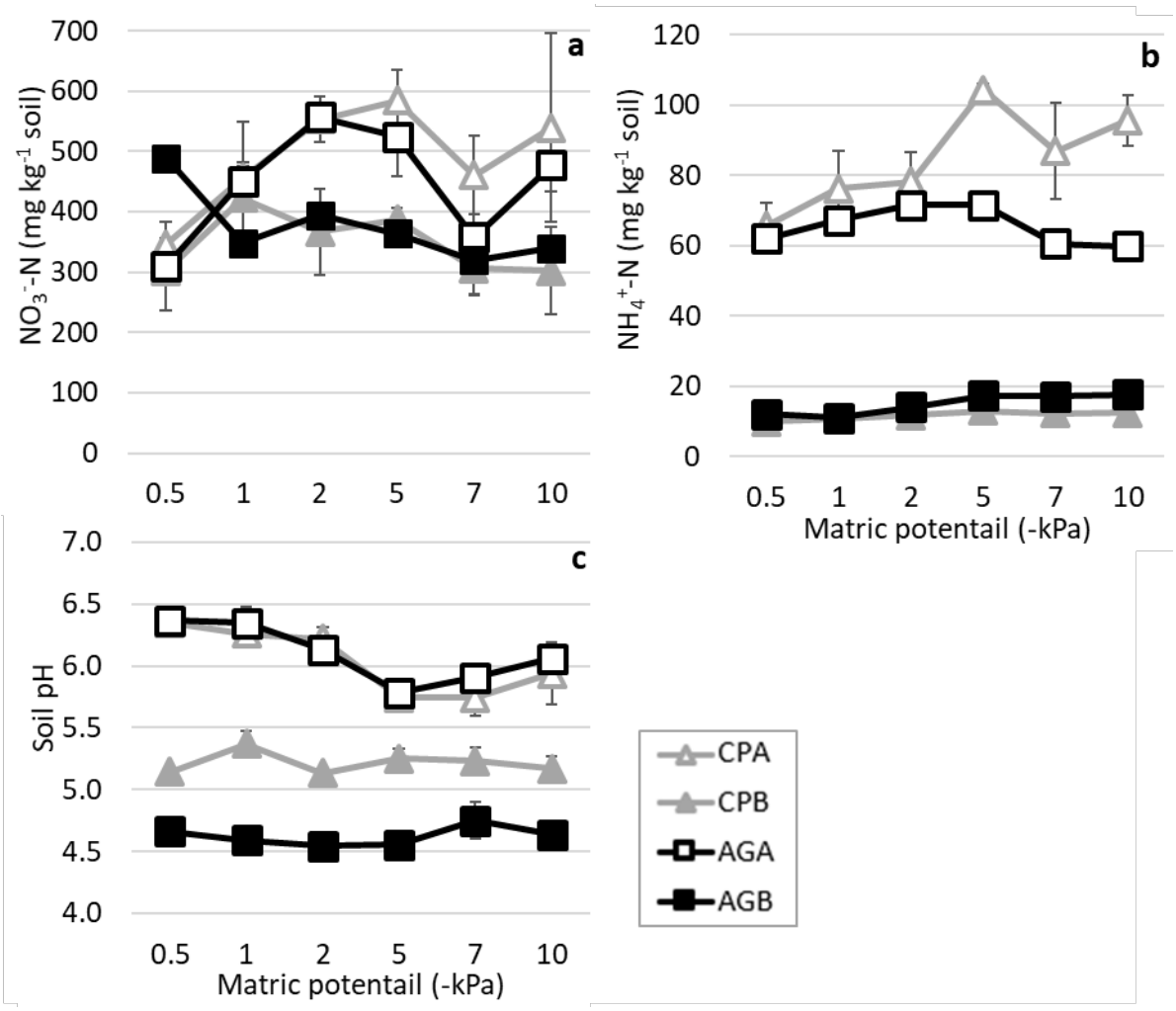

Figure 4.2: Mean soil inorganic N concentrations and soil pH for 6 matric potentials at day 4: (a) NO_3^--N, (b) NH_4^+-N; and (c) soil pH. Letters in legend indicate soil type and horizon; AG - Acton Gley, A and B horizons. CP - Central Plains, A and B horizons. Error bars = SEM, NO_3^--N and NH_4^+-N *n* = 2, pH *n* = 4. Note: Different scale between NO_3^- and NH_4^+-N to show variation.

Soil NH_4^+-N concentrations were higher (P = 0.000) in the A horizon than the B horizon (Figure 4.2b, Table 4.2) with average values in the AG soil of 65 and 15 mg NH_4^+-N kg^{-1} soil, respectively, while in the CP soil the respective concentrations were 84 and 12 mg NH_4^+-N kg^{-1} soil.

Table 4.2: Mean soil NH_4^+-N (mg kg^{-1} soil) values (*n* = 2). Subscripts are Tukey's pairwise comparisons for a 95% confidence interval for the 'soil type x horizon x matric potential' interaction.

	ψ (-kPa)					
Soil Type	**0.5**	**1.0**	**2.0**	**5.0**	**7.0**	**10.0**
Central Plains A	66_{CD}	76_{BCD}	78_{BCD}	104_{A}	87_{ABC}	96_{AB}
Central Plains B	10_{E}	11_{E}	12_{E}	13_{E}	12_{E}	12_{E}
Acton Gley A	62_{CD}	67_{CD}	71_{BCD}	71_{BCD}	61_{D}	60_{D}
Acton Gley B	12_{E}	11_{E}	14_{E}	17_{E}	17_{E}	18_{E}

Soil surface pH values ranged from 4.66 to 6.37 when soil ψ potential was -0.5 kPa, to values of 4.64 to 6.06 at a soil ψ of -10 kPa (Figure 4.2c, Table 4.3). Soils from the A horizon were more alkaline (P =

0.00) than their respective B horizons, with mean pH values of 6.1 and 4.9, respectively (Table 4.3). Soil pH was not affected by an interaction between soil ψ and soil type.

Table 4.3: Mean soil pH values following destructive soil sampling (n = 4) across the seven matric potential treatments, where error bars are ± SEM.

	ψ (-kPa)					
Soil Type	**0.5**	**1.0**	**2.0**	**5.0**	**7.0**	**10.0**
Central Plains A	6.3±0.1	6.3±0.1	6.2±0.1	5.7±0.1	5.7±0.1	5.9±0.3
Central Plains B	5.1±0.02	5.4±0.1	5.1±0.03	5.3±0.1	5.2±0.1	5.2±0.1
Acton Gley A	6.4±0.1	6.3±0.1	6.1±0.1	5.8±0.1	5.9±0.1	6.1±0.1
Acton Gley B	4.7±0.1	4.6±0.04	4.5±0.02	4.6±0.02	4.8±0.1	4.6±0.04

4.4.3 Soil N_2O Fluxes

Soil N_2O-N fluxes varied with soil ψ (P = 0.000), soil type (P = 0.004) and soil horizon (P = 0.022), ranging from a peak of 68.7 mg m^{-2} h^{-1} at -0.5 kPa to fluxes < 0.02 N_2O-N mg m^{-2} h^{-1} at -5 kPa and below (Table 4.4, Figure 4.3). There was significant variation in the N_2O-N fluxes within each level of soil ψ (P < 0.001). Soil N_2O-N fluxes under each soil moisture treatment declined as soils became drier (increasing negative matric potential, Figure 4.3). There were significant interactions between soil type (CP or AG) and soil moisture (P = 0.04), and soil type and soil horizon (P = 0.013)(Table 4.4, Figure 4.3). The CP soil had a greater N_2O flux at all soil moisture levels when compared to the AG soil, declining as soil moisture decreased. Soil A horizons had greater N_2O fluxes than their respective B horizon soils.

Due to the skewness of the data (Anderson-darling P < 0.05) the data were transformed (natural log), data presented are non-transformed but data analysis for significance was performed on natural log transformed data. Analysis was performed for significance on the log transformed data using a Minitab® general linear model ANOVA. Each factor; soil moisture, soil type and soil horizon, was tested for significance as well as testing for significant two and three way interactions between each factor.

Table 4.4: Mean soil N_2O-N fluxes (mg m^{-2} h^{-1}) values for the 'soil type x horizon x matric potential' interaction (*n* = 4). Subscripts are Tukey's pairwise comparisons for a 95% confidence interval on natural log transformed data.

	Matric potential (ψ, -kPa)					
Soil Type	**0.5**	**1.0**	**2.0**	**5.0**	**7.0**	**10.0**
Central Plains A	68.7_{A}	62.8_{A}	28.5_{A}	0.108_{DEFG}	0.063_{EFG}	0.022_{EFG}
Central Plains B	9.54_{ABC}	11.9_{AB}	4.69_{ABCD}	0.077_{EFG}	0.019_{FG}	0.019_{FG}
Acton Gley A	40.8_{A}	46.2_{A}	3.09_{CDEF}	0.011_{G}	0.031_{EFG}	0.015_{FG}
Acton Gley B	8.29_{ABC}	16.9_{AB}	1.87_{BCDE}	0.087_{DEFG}	0.029_{EFG}	0.016_{G}

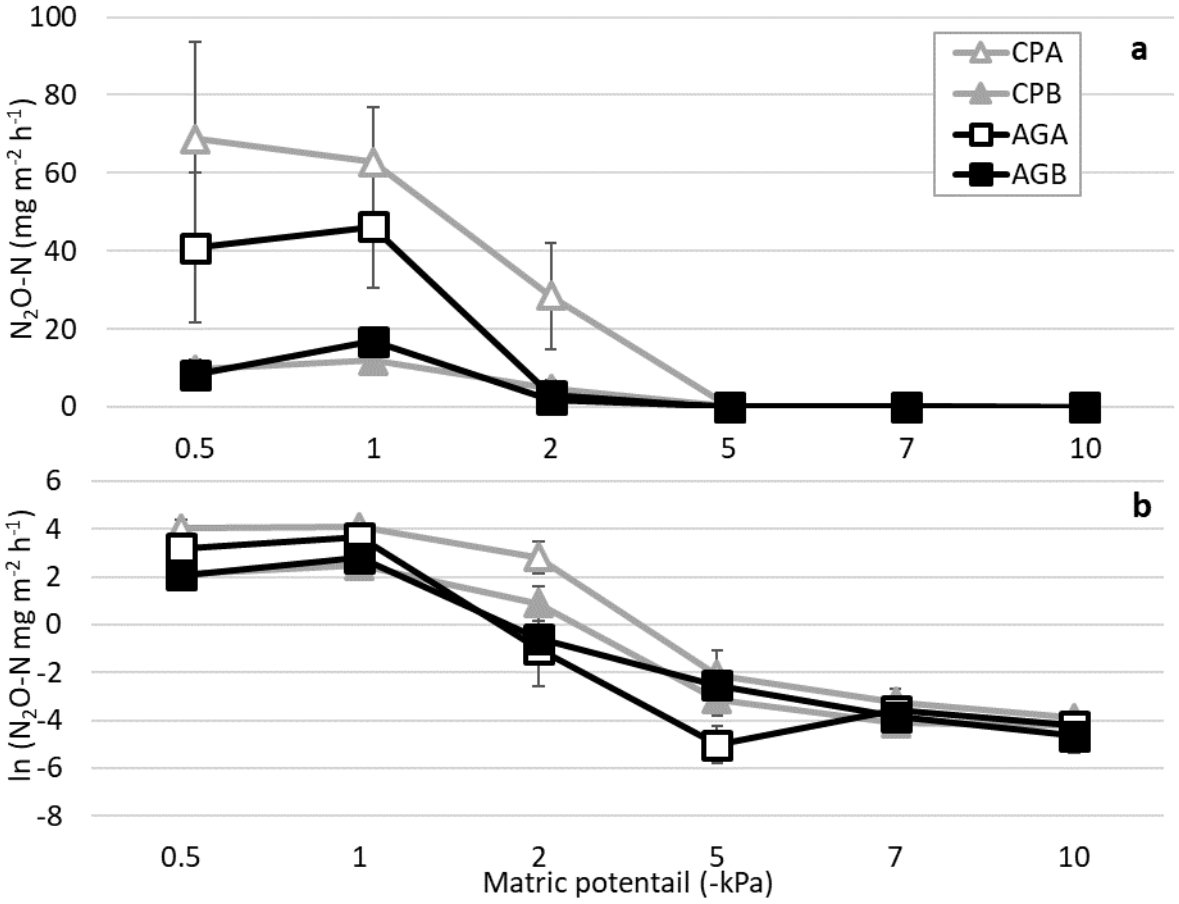

Figure 4.3: Effect of soil type and horizon on mean N_2O-N fluxes for the 6 levels of matric potential (-kPa), untransformed data (a) and natural log transformed data (b). Legend indicates soil type and horizon; AG - Acton Gley, A and B horizons. CP - Central Plains, A and B horizons. Error bars = SEM, *n* = 4.

4.4.4 Relative Gas Diffusivity

There was a significant difference between the modelled D_p/D_0 values due to soil type (AG and CP, P = 0.029) and soil type x soil horizon (P = 0.01), with the A horizon of the AG soil having higher D_p/D_0 values than the B horizon of the CP soil as the matric potential decreased from -0.5 kPa to -10 kPa (Figure 4.4).

Soil type x soil horizon and soil ψ also interacted (P < 0.001), with A horizon of the AG soil and the B horizon of the CP soil having significant differences in D_p/D_0 values across the different soil ψ (Figure 4.4, Table 4.5).

Soil horizon affected D_p/D_0 values (P = 0.02) as a consequence of differing soil ρ_b, the A horizons (soil ρ_b = 1.0) had higher diffusivity than the B horizons (soil ρ_b = 1.2), with mean D_p/D_0 values of 0.0178 and 0.0097 for the A and B horizons, respectively, averaged across soil ψ treatments. Soil ρ_b and ψ interacted to affect diffusivity (P < 0.001), with the difference in diffusivity between the A horizon soils

(ρ_b = 1.0) and B horizon soils (ρ_b = 1.2) becoming greater as the soil ψ became more negative (soils became drier).

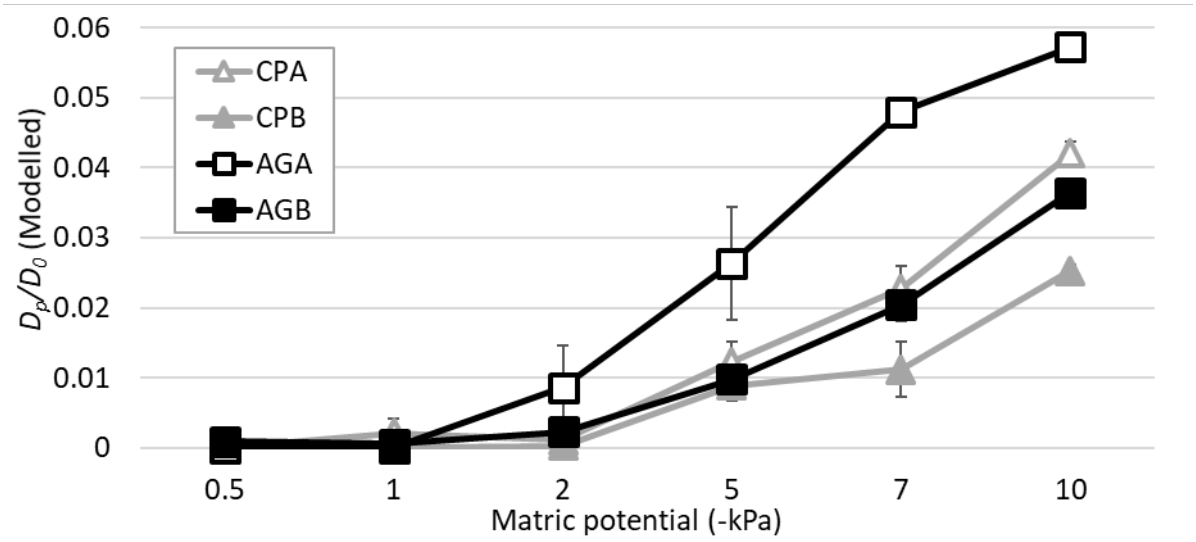

Figure 4.4: Modelled D_p/D_0 values versus matric potential for each soil and horizon. Legend indicates soil type and horizon; CP - Central Plains, A and B horizons. AG - Acton Gley, A and B horizons. Error bars = SEM, *n* = 4

Soil ψ also affected D_p/D_0 (P < 0.001) with D_p/D_0 increasing as the soil became drier (from -0.5 to -10 kPa). The mean D_p/D_0 value across all soil types at -0.5 kPa was 0.0002, and this increased to be 0.0401 at -10 kPa. The wetter soil ψ from -0.5 to -2 kPa showed no significant variation in D_p/D_0, but when the soil was at -5, -7 and -10 kPa values of D_p/D_0 increased for both soils (Table 4.5 and Figure 4.4). Average D_p/D_0 values were significantly (P < 0.001) different when soil ψ was ≥ -5 kPa (Table 4.5, indicated by *values).

Table 4.5: Mean modelled gas diffusivities, D_p/D_0, at each matric potential for the 'soil type x matric potential' interaction with values averaged over reps (*n* = 4). Average (*) D_p/D_0 represent an average across all soils and replicates for each matric potential (n = 16), showing the 'D_p/D_0 x matric potential' interaction. Subscripts are Tukey's pairwise comparisons for a 95% confidence interval. Means that do not share a letter are significantly different. Average (*) subscripts show pairwise comparison between values indicated by * only.

	Modelled D_p/D_0					
	0.5	**1.0**	**2.0**	**5.0**	**7.0**	**10.0**
Soil Type	**(ψ -kPa)**					
Central Plains A	$<0.0000_{H}$	0.0021_{H}	0.0011_{H}	0.0123_{EFGH}	$0.0228C_{DEF}$	0.0420_{AB}
Central Plains B	$<0.0000_{H}$	$<0.0000_{H}$	0.0003_{H}	0.0089_{FGH}	0.0112_{FGH}	0.0253_{CDE}
Acton Gley A	$<0.0000_{H}$	$<0.0001_{H}$	0.0086_{GH}	0.0264_{CD}	0.0480_{AB}	0.0573_{A}
Acton Gley B	0.0009_{H}	0.0006_{H}	0.0023_{H}	0.0099_{FGH}	0.0204_{DEFG}	0.0364_{BC}
Average*	$*0.0002_{D}$	$*0.0007_{D}$	$*0.0031_{D}$	$*0.0144_{C}$	$*0.0256_{B}$	$*0.0401_{A}$

Modelled and measured D_p/D_0 values differed from each other (P = 0.004) with means, across all treatments and soil types, of D_p/D_0 0.038 and 0.018, respectively. Measured values were higher than modelled values for D_p/D_0, but they are strongly correlated (r^2 = 88.2, Figure 4.5). However, measured D_p/D_0 data values were unexplainably outside the commonly accepted ranges that have been previously reported (as seen in Figure 4.6) and therefore are not used from here on.

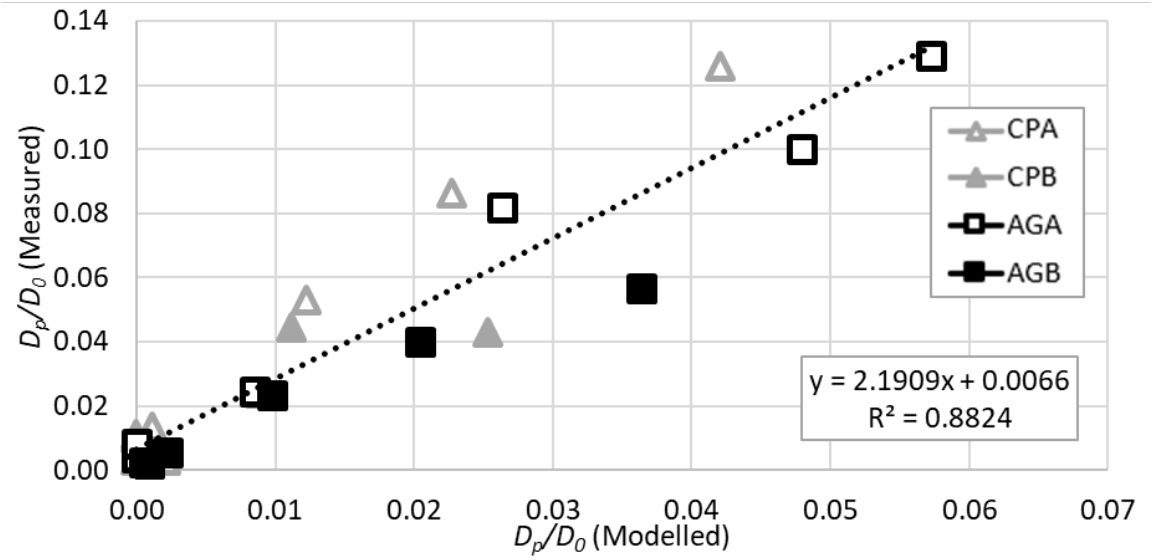

Figure 4.5: Modelled vs. measured D_p/D_0 values for each of the soil types. Legend indicates D_p/D_0 method, soil type and horizon; CP - Central Plains, A and B horizons. AG - Acton Gley, A and B horizons. Error bars = SEM, *n* = 4.

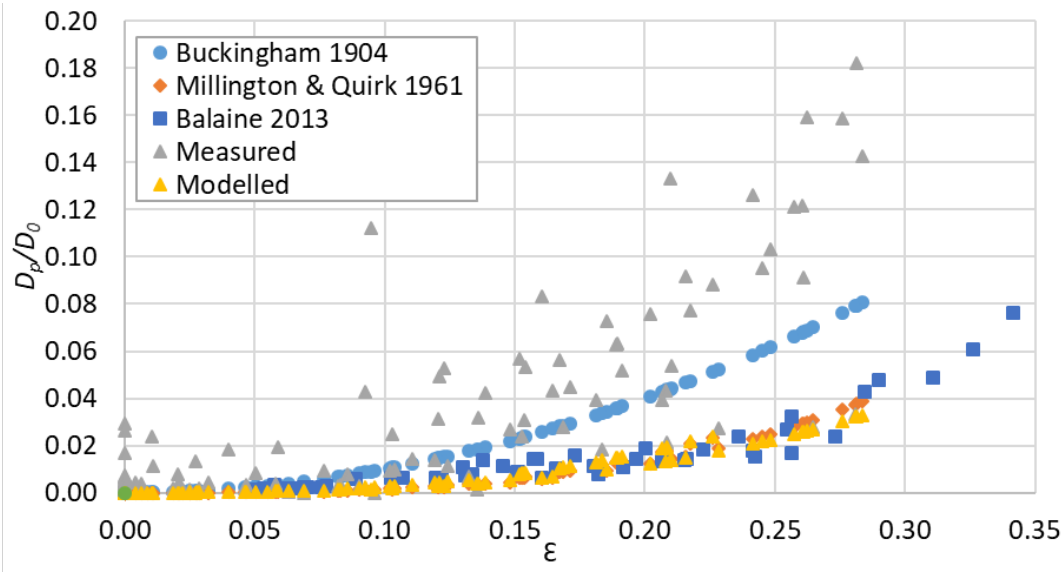

Figure 4.6: Measured and modelled D_p/D_0 vs. air filled porosity (Ɛ). Also plotted are D_p/D_0 values derived from the values of measured Ɛ values but using the classical equations of Buckingham (1904) and Millington et al. (1961). Also plotted are measured D_p/D_0 values from Balaine et al. (2013). Triangle symbols represent data from this trial.

4.4.5 Diffusivity & N_2O Interaction

Net N_2O-N emissions peaks ranged from 12 to 68 mg m^{-2} h^{-1} at modelled D_p/D_0 values of 0 to 0.0006 (Figure 4.7). The N_2O-N emissions began to increase when D_p/D_0 became < 0.006. Peak soil N_2O-N emissions for the CPA (-0.5 kPa), CPB (-1 kPa) and AGA (-1 kPa) soils occurred when soils were saturated (D_p/D_0 = 0) while for the B horizon of the AG soil N_2O-N emissions peaked at a D_p/D_0 value of 0.0003 (-1 kPa).

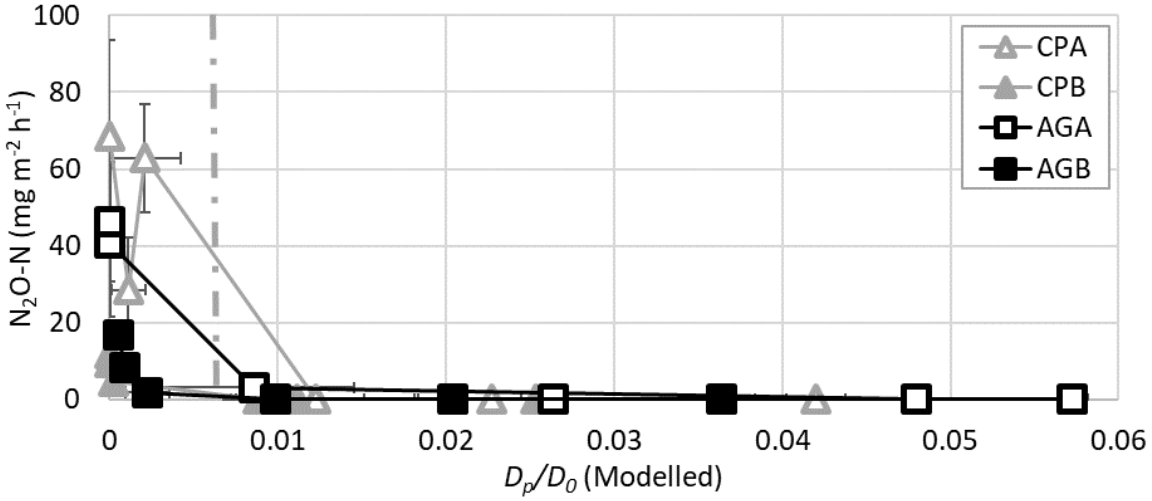

Figure 4.7: Relationship of modelled D_p/D_0 with N_2O-N flux for each of the soil types. Legend indicates soil type and horizon; CP - Central Plains, A and B horizons. AG - Acton Gley, A and B horizons. Error bars = SEM, *n* = 4. Dashed vertical line represents a D_p/D_0 value of 0.006, which was shown by Balaine et al. (2013) to be a threshold for peak N_2O flux occurrence.

The regression of the natural log of the N_2O-N flux and modelled D_p/D_0 resulted in a significant negative linear relationship (P = 0.01, r^2 = 0.47, Figure 4.8).

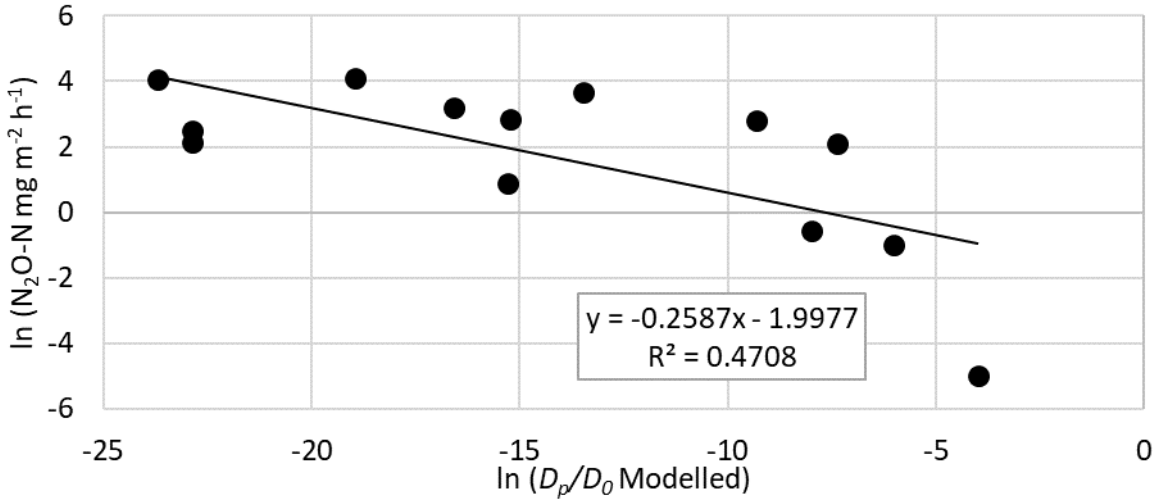

Figure 4.8: Regression plot of natural log of mean N_2O-N fluxes by the natural log of mean modelled D_p/D_0 values >0.006. *n* = 4.

4.5 Discussion

The key result from this study is that the D_p/D_0 values associated with NO_3^- attenuation can be extrapolated to field study sites, to the same soil types in-situ. Giving a general overview of what D_p/D_0 values we expect to see in the field when NO_3^--N attenuation is occurring. Nitrous oxide emissions were stimulated with declining D_p/D_0, as increasing soil moisture and soil ρ_b interacted to affect the movement of O_2 into and out of the soil. Meaning that maximum N_2O fluxes occurred at varying combinations of soil ψ and ρ_b as noted by the interaction of these variables on D_p/D_0. The A horizon soils had higher D_p/D_0 values than the B horizons, at the same soil ψ, due to the greater ρ_b of the B horizon soils changing the relative ε and Φ values of the soil cores, holding less total water but at a higher suction at the same soil ψ. However, this was only true for matric potentials more negative than -1 kPa (Table 4.5). Influence of soil type and horizon on D_p/D_0 becomes insignificant below soil matric potentials of -2 kPa. At ca. -1 kPa the resulting high soil moistures, make precise soil moisture content determination less reliable and therefore this can introduce error in D_p/D_0 calculations.

There are multiple pathways for the production of N_2O which commonly include, but are not limited to; nitrification, nitrifier-denitrification and denitrification, with nitrifiers oxidising NH_4^+ and denitrifiers reducing NO_3^-, NO_2^-, NO or N_2O, and producing N_2 as a final product if denitrification goes through to completion (Wrage et al., 2001). Other pathways of N_2O production include coupled denitrification, DNRA and chemo-denitrification (An et al., 2001; Denk et al., 2017; Robertson et al., 2007). Factors that affect N_2O production pathways include but are not limited to pH (Firestone, 1982), soil moisture and O_2 content (Smith et al., 2003), and C availability (Beauchamp et al., 1980; Weier et al., 1993). The soil in an A horizon generally has a greater capacity to process N than a subsoil as it has all the required components that initiate N cycling: higher microbial biomass, relatively higher C content as an energy source, relatively higher O_2 for nitrification of NH_4^+ to NO_3^-, and then with addition of moisture and the soil becoming anaerobic, denitrification and the reduction of NO_3^- (Jarvis & Hatch, 1994; Murray et al., 2004).

Oxygen is rarely used as an indicator of denitrification (Linn et al., 1984a; Zhu et al., 2013), but it is one of the main controlling factors affecting the onset of denitrification and subsequent denitrification rates and products (Firestone et al., 1989). Soil gas diffusion is the main mechanism of O_2 transport in soil (Neira et al., 2015) and therefore an important trigger for the commencement of N attenuation. Recent research has found soil D_p/D_0 to be a key threshold indicator for denitrification (Balaine et al., 2016b; Balaine et al., 2013; Chamindu-Deepagoda et al., 2019; Owens et al., 2017). Soil D_p/D_0 is the rate at which gas diffuses through soil relative to the rate it diffuses through free air (Moldrup et al., 2000). As O_2 diffusion through soil is limited by water-filled pores blocking gas movement, soil moisture

content plays a key role in influencing soil D_p/D_0 (Farquharson et al., 2008; Moldrup et al., 2013; Moldrup et al., 2001).

Research by Stepniewski (1981) reported that D_p/D_0 values between 0.005 and 0.02 represented the range where soils become anaerobic for plant roots. Soil conditions (ρ_b and WFPS) that resulted in a D_p/D_0 value of 0.006, were shown by Balaine et al. (2013) to be the threshold for peak N_2O flux production during denitrification, with N_2 production occurring as D_p/D_0 decreased further and as the denitrification process went to completion. The same threshold was reported by Balaine et al. (2016b) when soil cores were treated with urea and both N_2O and N_2 were measured over a 35 day period. While Owens et al. (2016) found a similar threshold between ~0.06 and ~0.02 for peak N_2O fluxes under free-draining soils with BU applied with varying irrigation frequencies. The 35 day cumulative flux data of Balaine et al. (2016b) were modelled by Chamindu-Deepagoda et al. (2019) who found that D_p/D_0 should be maintained above ≥ 0.038 to limit extensive emission of N_2O and N_2.

At Ɛ/Φ values < 0.5, D_p/D_0 is predominantly moisture controlled (Chamindu-Deepagoda et al., 2019). All soil moisture states in this study are below an AFP of 0.5, indicating that all reported D_p/D_0 values are predominately soil moisture controlled (Figure 4.9). Soil moisture controlled D_p/D_0 is not influenced by the soil cores being from repacked soil, as the disparity between repacked and intact cores is only thought to become evident in drier soils (Ɛ/Φ >0.5)(Chamindu-Deepagoda et al., 2019).

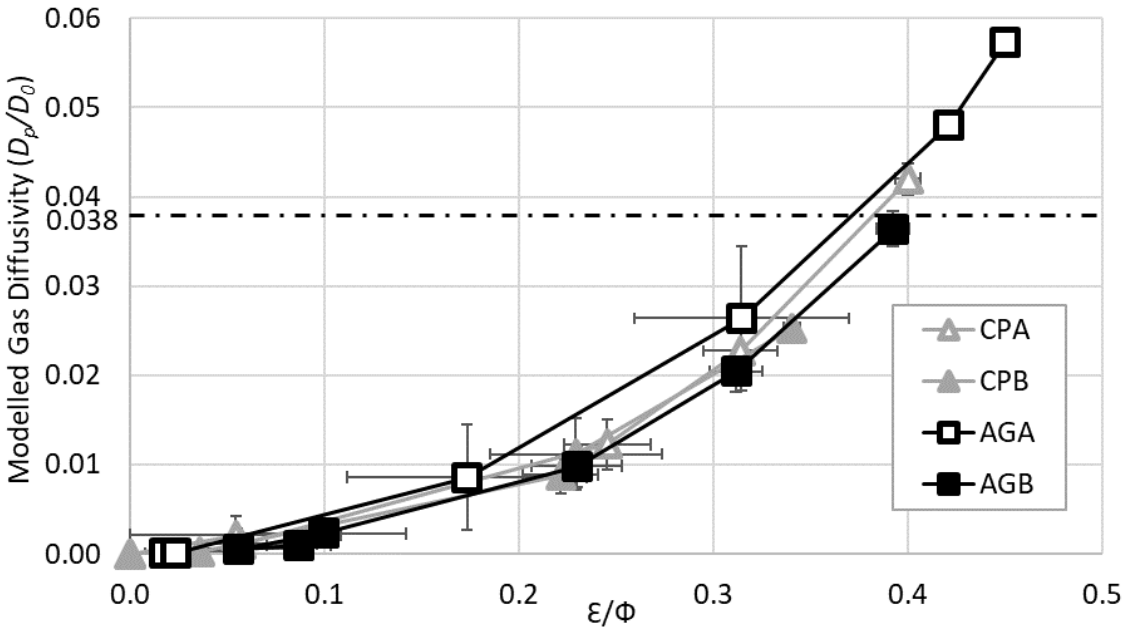

Figure 4.9: Soil relative gas diffusivity (D_p/D_0) as a function of relative air-filled porosity (Ɛ/Φ) for the four pasture soils. Error bars = SEM, *n* = 4. Horizontal dotted line at y = 0.038 represents the D_p/D_0 value derived by Chamindu-Deepagoda et al. (2019), when modelling the cumulative N_2O and N_2 fluxes over 35 days from Balaine et al. (2016b), and who suggested that D_p/D_0 should be ≥ 0.038 to limit extensive emission of gas losses.

Soil moisture significantly affected N_2O-N fluxes, ranging from 68.7 mg to < 0.02 mg m^{-2} h^{-1} for the -0.5 kPa and <-5 kPa treatments, respectively (Table 4.4, Figure 4.3). Soil moisture also significantly influenced D_p/D_0 values, the wetter the soil the smaller the D_p/D_0. The N_2O-N results were significantly related to modelled D_p/D_0 values (r^2 = 0.74, Figure 4.8), as N_2O-N fluxes increased with declining D_p/D_0 values. The magnitude of the N_2O-N fluxes may vary due to soil type, available substrate, microbial community composition and function, which all interact to affect the magnitude of the N_2O flux (Andersen et al., 2009; Chamindu-Deepagoda et al., 2019; Groffman et al., 2009; Kraft et al., 2014; Six et al., 2004).

The A horizon soils were found to have greater N_2O-N fluxes than their respective B horizons (Table 4.4), this is likely to be due to the A horizons containing more labile C (and A.4), as this is an important constraint (Peterson et al., 2013). As the N source was not a limitation due to the addition of KNO_3, the results are indicative that the B horizon was C limited. As found by previous research the addition of C to B horizon soils increases the soils denitrification response (Clough et al., 1998a; Peterson et al., 2013). Significant variation between soil types N_2O-N fluxes was also found, however the variation only occurred between soil types at one soil moisture (-2 kPa), were N_2O-N flux of the A horizon of CP soil was significantly greater than AG A horizon emissions.

Increasing soil ρ_b reduces the amount of gas movement through the soil. Increased ρ_b through compaction has been shown to reduce soil aeration and therefore increase gaseous-N fluxes from soil via microbial denitrification (Menneer et al., 2005; Šimek et al., 2006; Uchida et al., 2008). But there are conflicting reports of compaction increasing D_p/D_0 and therefore not encouraging denitrification, as compaction rearranges air-filled pore space aligning pore pathways and reducing tortuosity (Chamindu-Deepagoda et al., 2019; Deepagoda et al., 2011). However, in this study the differences found in N_2O fluxes between A horizon soils (ρ_b = 1.0) and B horizon soils (ρ_b = 1.2) are more likely to be caused by C limitations than soil ρ_b conditions.

Evidence of denitrification proceeding was provided by the decline in soil NO_3^--N as soil ψ increased (Figure 4.2a), however, the decline in NO_3^--N was not found to be significant by soil ψ or soil type. Greater replication of the soil NO_3^--N measurements may have resulted in a difference. While soil type differences did not occur in this experiment they cannot be ruled out since soils will differ in their ability to supply substrate such as C and their respective microbial communities (Bakken et al., 2012; Bakken et al., 2017). Limited C source may have also played a role in the reduced nitrification of soil-N to NO_3^-, as B horizons contained on average 62 mg NO_3^--N kg^{-1} soil less than A horizon soils. This may be accounted for through additional NO_3^--N from nitrification of soil-N in the A horizons as they were not C limited.

The trend of lower soil NO_3^- concentrations at higher soil moisture contents indicates that there was more NO_3^- attenuation and denitrification occurring when the soil moisture was higher (-0.5 kPa, Table 4.1). Soil moisture (volumetric, θ_v) declined with increasing negative matric potential, as expected, as variation in soil texture and density results in variations in pore size distribution and thus the ability for a soil to retain water. For example, the B horizon of the AG soil had an increase in the percentage of fine sand particles relative to the A horizon. This will have increased the macro-porosity of the repacked AG-B horizon soil and thus, despite the small increase in ρ_b within the B horizon, this soil held less water at -0.5 to -2 kPa (Figure 4.1).

4.6 Conclusions

Soil type and depth (horizon and respective ρ_b) showed an effect on D_p/D_0 values and therefore N attenuation. These effects were significant at matric potentials greater than -5 kPa. No significant effect was found on D_p/D_0 values at the very wet end of the soil moisture spectrum (-0.5 kPa to -2 kPa), this was most likely due to the increased variation in the measurements made as measuring soil moisture contents, and air-filled porosities, becomes more problematic when soil cores reach saturation. Therefore, more research is needed at the very wet end of the soil moisture spectrum to allow for precise soil moisture content measurement, removing variability in results and allowing for further identification of soil type effects on D_p/D_0 values and associated N attenuation.

The D_p/D_0 values associated with NO_3^- attenuation could be extrapolated to field study sites, to the same soil types in-situ through the identification of the onset of anaerobic conditions that trigger denitrification to occur. This study showed a general overview of what D_p/D_0 values we expect to see when NO_3^--N attenuation is occurring. This is important in helping us further our understanding of conditions suitable for NO_3^- attenuation, both temporally and spatially within the landscape.

Peak N_2O emissions for all soil types were found to occur at modelled D_p/D_0 values of <0.006, similar to those previously reported. This further expresses the ability for D_p/D_0 to be used as a key indicator of denitrification thresholds. However, further research on the change in D_p/D_0 values over time, rather than a single point in time, for different soil types may allow for better understanding of D_p/D_0 ability to provide an accurate denitrification predictor for different soil types. Nitrous oxide fluxes were also found to be significantly influenced by soil type, under the conditions of this study soil physical (soil moisture) and chemical (C content) conditions influenced N_2O emissions.

Chapter 5

Lab Experiment - Part Two: Soil Type & Isotope Fractionation.

5.1 Introduction

Nitrogen pollution of freshwater bodies in agricultural areas threatens the environment and sustainable population growth (Nikolenko et al., 2018; Xue et al., 2016). Concentrations of N in freshwater bodies are attributed, but not limited, to: sewage, atmospheric N deposition, fertiliser-N and animal excreta from pasture grazing systems (Anderson et al., 2014; Böhlke, 2002; Malcolm et al., 2014a; Ostrom et al., 1998). New Zealand, with its agricultural base, has experienced increasing NO_3^--N contamination of waterways from fertilisers and animal excreta (Cameron et al., 1986; Close et al., 2016; Stark et al., 2008). Uptake of NO_3^- by biomass such as pasture or its removal through denitrification is desirable, as this can reduce the amount of NO_3^- entering waterways (Clough et al., 1998a; Clough et al., 2005). The key to successful N attenuation is the completion of denitrification to produce N_2, an inert atmospheric gas (Buckthought et al., 2015a; Clague et al., 2015b; Clough et al., 1996; Wells et al., 2016). Partial completion of this pathway, however, leads to the production of N_2O (Figure 5.1), a potent greenhouse gas that also contributes to ozone destruction (IPCC, 2014a; Ravishankara et al., 2009).

Figure 5.1: Denitrification: an outline of the pathway involved and enzymes at each step of the process. Taken from Hochstein et al. (1988).

There are many factors that can affect denitrification and therefore N attenuation (removal of N from the soil system). The main factors are O_2, NO_3^- and C availability (Kraft et al., 2014; Yoon et al., 2015), as well as spatially variable factors such as; soil moisture, soil pH, soil depth, soil gas diffusivity, soil type and landscape position. Climatic temporal variation also occurs; temperature and rainfall. Each

factor can either positively or negatively influence the N_2O/N_2 ratio of the products. For example, when soil moisture increases, denitrification rates increase and therefore so does the amount of N_2O and N_2 produced (Dobbie et al., 1999; Kool et al., 2011a; Ruser et al., 2006).

Different soil types can influence N attenuation through the limitation of controlling factors; O_2/moisture availability, OC and NO_3^- as they vary throughout and between soil profiles (Moldrup et al., 2000; Neira et al., 2015). Soil depth also influences ρ_b, as generally the deeper the soil the greater the ρ_b, reducing soil porosity and therefore its ability to hold O_2 or water (Zuraidah et al., 2011). These differences between soil types make understanding N attenuation at a landscape scale very complex, as they contain so many variables.

Oxygen has been recognised as an important controlling factor of N_2O and NO emissions (Firestone et al., 1989; Wrage et al., 2001). The three main factors influencing O_2 concentration in the soil are; O_2 consumption rate, diffusion rate and the tortuosity of the diffusion pathway (Knowles, 1982). The latter two are a function of the soil's water content. The N_2O reductase enzyme that controls the reduction of N_2O to N_2 is the most sensitive to the presence of O_2 out of the enzymes in the denitrification cascade (Morley et al., 2010).

The main mechanism of gas movement through soil is diffusion (Penman 1940). Soil gas diffusion is represented by D_p/D_0, where D_p is the soil-gas diffusion coefficient (cm^3 soil air cm^{-1} soil s^{-1}) and D_0 is the diffusion coefficient of the same gas in free air (cm^2 air s^{-1}) (Moldrup et al., 2000). Recent research relates urine, urea, or NO_3^- derived N_2O and N_2 emissions to D_p/D_0, as well as examining the interaction between soil ρ_b and soil matric potential (Balaine et al., 2016b; Balaine et al., 2013; Chamindu-Deepagoda et al., 2019; Owens et al., 2016). Recent research into D_p/D_0 identified a threshold (≤ 0.006 D_p/D_0, Balaine et al. (2013), Figure 2.13) for denitrification that was independent of soil ρ_b. Further modelling of cumulative soil N_2O emissions, following urea application, over 35 days showed a D_p/D_0 value of ≥ 0.038 was required to stop denitrification reduction of NO_3^- to N_2O and N_2 (Chamindu-Deepagoda et al., 2019).

Dual NO_3^- isotopes ($\delta^{15}N$ and $\delta^{18}O$) are one tool that can be used to determine the origins of different N sources, as N and O isotopes appear in predictable ratios from different N sources, allowing them to be identified (Liu et al., 2006). Fractionation, the separation of isotopes into two products and then their subsequent mixing, to form a single product once again, can be predicted (Fry, 2007). Recently reported isotope compositions for different NO_3^- sources are: soil organic matter +3‰ to +8‰, mineral fertilisers -8‰ to +7‰ and manure/household waste +5‰ to +35‰ (Nikolenko et al., 2018). The expected $\delta^{15}N\text{-}NO_3^-$ range for a urea or urine source in New Zealand, has been reported to range from -5‰ (Wells et al., 2015) to +1.2‰ (Frank et al., 2004). However, reported ranges vary due to changes

in biochemical processing rates, environmental conditions and other ecosystem variables, such as; soil age, climate and topography (Amundson et al., 2003; Craine et al., 2009; Xue et al., 2009).

As well as source identification, dual NO_3^- isotopes allow us to determine the rate of denitrification by plotting the log of the rate of NO_3^- isotope removal over time using the Rayleigh equation (Kendall et al., 1998):

$$R_t/R_0 = (C_t/C_0)^{1/(\alpha\ denit-1)} \qquad \textbf{Equation 5.1}$$

The Rayleigh model uses the slope of linear regression $\delta^{15}N\text{-}NO_3^-$ at time 't' verses the natural logarithm of the ratio of residual NO_3^- at a time 't' (C_t) relative to time zero (C_0), to estimate microbial denitrification fractionation factors (Figure 5.2). Where α is the fractionation factor for denitrification, defined as the ratio of heavy to light isotope in the product and the substrate, respectively ($\alpha = R_p / R_s$, Kendall et al. (1998)). The residual NO_3^- pool at a given time (R_t) compared to the original (R_0) can be quantified relative to the corresponding change in substrate concentration (C_t/C_0), assuming a constant degree of isotopic discrimination.

Material removed due to copyright compliance

Figure 5.2: Illustration of the linear regression of a Rayleigh calculation used by Warneke et al. (2011) to calculate the $\delta^{15}N\text{-}NO_3^-$ fractionation factor (-19‰). Showing the $\delta^{15}N\text{-}NO_3^-$ verses the log of the ratio of C_t/C_0, where C_t is the NO_3^- concentration at a given time (t) and C_0 is the initial NO_3^- concentration.

The enrichment factor is used to calculate the fraction of substrate remaining, based on the changes in the corresponding isotopic composition. The $\delta^{15}N\text{-}NO_3^-$ value is influenced by fractionation due to denitrification (ε = 5 to 40‰) and nitrification (ε = 5 to 35‰), with the magnitude of fractionation varying depending on temperature, pH, dissolved organic matter, C/NO_3^- ratio, amount of substrate, available electron donors, soil moisture, residence time, land-use and hydrogeology (Nikolenko et al., 2018).

The Southland Region of New Zealand has experienced a rapid decline in sheep numbers due to land being converted to dairying (Ledgard, 2013). The region holds the largest number of dairy herds in the South Island of New Zealand, with 989 herds covering an effective land area of 209,133 ha (SIDDC, 2017). Concerns over the contamination of ground and surface water systems, from agricultural N sources, have led to the introduction of a number of reforms in freshwater management (Close et al., 2016), including but not limited to, a National Policy Statement for Freshwater Management, which

contains a legislative framework for freshwater nutrient limits including NO_3^- (Environment, 2014). Southland's large population of dairy cattle and the considerable increase in the conversion to dairy, with a 513% increase in cow numbers between 1990 and 1999 alone (Hamill et al., 2003), make it an important region to focus on, in terms of understanding NO_3^- attenuation within the landscape.

Soil type variation in the landscape complicates the measurement of N in agricultural soil and freshwater contamination. The use of isotopes to identify when denitrification is occurring and its parallel expression in D_p/D_0 values for different soils may provide a practical tool to help us interpret N contamination across variable landscapes. Building on our understanding of dual NO_3^- isotope signatures and D_p/D_0, the modelling of soil D_p/D_0 in the field using in-situ O_2 sensors may allow for us to calculate where or when N attenuation is occurring and how much N is being removed, through the extrapolation of isotope fractionation data. This tool would allow spatial variation in soil attenuation to be accounted for, in both farming and policy management, providing more accurate data to allow for environmental standards and goals to be meet and a more sustainable agricultural system.

This chapter presents work performed to investigate dual NO_3^- isotope fractionation factors for different soils, with the possibility of extrapolation to cover larger areas and predict denitrification NO_3^- attenuation rates when combined with real-time moisture/saturation values of soils in the landscape and soil diffusivity.

It was hypothesised that the denitrification fractionation factor will vary spatially due to different soils providing different levels of C, NO_3^- and O_2 which are the key factors controlling denitrification. This study attempts to use dual NO_3^- isotope signatures to quantify and identify N attenuation processes alongside measured and modelled D_p/D_0. The data collected from this experiment will permit NO_3^- isotope fractionation factors of different soil types to be determined in order to assess potential spatial variability of Southland soils.

5.2 Materials & Methods

5.2.1 Soil Collection, Experimental Design & Setup

Soils were collected from two sites in Southland, New Zealand between the 16th to the 18th of November 2016. The sites included one from the Central Plains area of Southland, New Zealand (E1225681 N4877019) and one from Five Rivers area in northern Southland, New Zealand (E1257349 N4909615). Both sites had perennial ryegrass (*Lolium perenne* L.) grazed dairy pastures. The soil at the Central Plains site was classified as a Typic Orthic Gley (Braxton rolling deep) soil, and the Five Rivers Gley soil was classified as a Melanic Orthic Gley (Acton undulating moderately deep) soil (Hewitt, 1998). Southland mean annual rainfall and soil temperature (10 cm depth) are 1112 mm and 9.2°C, respectively (Invercargill historical data average 1981-2010, NIWA). Soil samples were taken from two

depths (0 - 25 cm and 25 - 40 cm) at each site (Section 3.3.1). These are the same soil types as used in Chapter 4 (refer to Appendix A for soil physical and chemical characteristics).

Soils were collected, transported back to Lincoln University, sieved to 2 mm then air-dried at 30°C for 4 days. Soil chemical analyses were performed by Hills Laboratories (Hamilton, New Zealand, Section 3.3.1). After determining soil physical parameters (Section 3.1), soils were repacked into stainless steel cylinders (7.3 cm i.d., 4 cm deep) were packed to a constant volume, at soil ρ_b values of 1.0 and 1.2 Mg m^{-3}, representative of the soil A and B horizons, respectively. For soil core repacking methodology refer to Section 3.2.

A factorial experimental design comprised of: two soil types (Central Plains (CP) or Five Rivers (AG), two soil depths (A or B horizon) maintained at one soil moisture (-0.5 kPa), with each treatment replicated four times for six batches, giving a total of 96 repacked soil cores. A soil moisture of -0.5 kPa was used to maintain soil cores in an anaerobic state to encourage denitrification, as identified in Chapter 4. All of the cores were placed onto the tension tables at the same time, with one entire batch (4 soils x 4 reps, batch of 16 cores) used at each sampling point over a time period of 23 days to allow for analyses to be conducted throughout the time period (Six sampling points; 26th, 29th and 31st January, 5th, 9th and 15TH of February 2018). D_p/D_0 was measured at three of the six time points; t_1, t_3 and t_6.

Tension tables were used to hold the repacked soil cores at the desired soil moisture for the length of the experiment. Tension tables were constructed on the 17th - 20th of January 2018. Tension tables were constructed according to Romano et al. (2002)(Section 3.4).

Repacked soil cores were left to soak for 24 hrs in a KNO_3 solution (1800 µg mL^{-1} NO_3^--N, Balaine et al. (2013)), prior to being transferred to the tension tables. Cores were soaked in KNO_3 to ensure there was sufficient N for denitrification. They were then placed onto the tension tables and left to equilibrate at the designated matric potential (-0.5 kPa). Soil cores were left for 3 days to equilibrate, as demonstrated by constant mass. Preliminary testing showed 3 days was sufficient for the soil cores to reach the designated soil matric potential.

5.2.2 Sample Collection & Analyses

Soil cores were maintained on tension tables at a constant soil ψ of -0.5 kPa, using suction from a hanging water column. Soil cores were analysed for their N_2O fluxes (Section 3.5) and D_p/D_0. The diffusivity of the cores was measured using diffusivity chambers that were constructed at Lincoln University following the procedure of Rolston et al. (2002) (Section 3.7). Measurement of D_p/D_0 was only performed on t_1, t_3 and t_6, N_2O flux sampling and destructive sampling for soil chemistry were

performed on each batch. After gas and D_p/D_0 sampling were completed the soil cores were destructively sampled for NO_3^--N, NH_4^+-N, pH and soil gravimetric water content.

Refer to Chapter 3, sections 1 and 3 for a more detailed descriptions of soil sample chemical and physical analyses.

The N_2O flux measurements were taken at each sampling point (using the same batch of 16 cores each time to get comparable results: batch 6) by enclosing them in an airtight chamber (mason jar). Gas samples were taken at time 0, 10 and 20 minutes after the jars were sealed. Sampling time points were shorter for this second laboratory trial as the first showed that concentrations became too high for analysis when sampled at 0, 20 and 40 minute time points (Chapter 4).

The diffusivity of the cores was measured using diffusivity chambers that had been constructed at Lincoln University using a similar set-up to Rolston et al. (2002). This system uses a fully sealed chamber containing O_2 sensors (KE-25, Figaro Engineering Inc., Osaka, Japan) that only allows air to pass through the soil core when it is placed into the lid of the chamber. Diffusivity chamber use and measurements were as per Section 3.7 and 3.8.

For isotope analyses, the samples were sent to Associate Professor Karen Casciotti's Laboratory at Stanford University, USA. Measurements of soil NO_3^- $\delta^{15}N$ and $\delta^{18}O$ were made by the conversion of NO_3^- to N_2O using the "azide method" of McIlvin et al. (2005), using 10 nmol of NO_3^- for samples and standards. The N_2O was purged and trapped cryogenically on a pre-concentration system (Casciotti et al., 2002) before being released to a Delta^{PLUS} XP isotope ratio mass spectrometer. Each sample was analysed in duplicate and reported in delta notation relative to AIR ($\delta^{15}N$) or VSMOW ($\delta^{18}O$) NO_3^- isotopic reference materials that were analysed in parallel (Casciotti & McIlvin, 2007).

Initial soil $\delta^{15}N$ values for the CP soil were 4.55‰ and 7.16‰, for the A and B horizons, respectively. The AG initial soil $\delta^{15}N$ values were 4.94‰ and 7.58‰, for the A and B horizons, respectively. Initial soil $\delta^{15}N$ values were analysed at Lincoln University. The $\delta^{15}N$ composition of the soil was determined on air dried and sieved (<2 mm) soil with visible organic material removed, that had been ground to < 200 μm prior to analyse on a Sercon GSL/20-22 Isotope Ratio Mass Spectrometer.

5.2.3 Statistical Analyses

Data were analysed using Minitab® (Minitab®18.1.0.0, 2018) with analysis of variance conducted using the General Linear Model to allow for repeated measures. The variables analysed were total soil N, NH_4^+, NO_3^-, N_2O fluxes, NO_3^- $\delta^{15}N$ and $\delta^{18}O$ isotopes, soil diffusivity with factors of soil type (CP or AG), soil horizon (A or B), ρ_b, soil moisture and time, with differences and interactions between these

variables determined. One-way ANOVA, followed by Tukey's Test which was used to identify differences between means ($p < 0.05$).

Data were tested for skewness using the Anderson-Darling normality test. The N_2O flux results were transformed to their natural log to improve the normality of the data. Conclusions on transformed data were drawn from the analysis on the transformed scale. Data, presented in tables and figures, is untransformed unless stated otherwise.

5.3 Results

5.3.1 Soil Moisture

Measured volumetric water contents of each soil at each destructive sampling point through the 23-day sampling period are shown in Figure 5.3. The standard error of the means of the volumetric water content of each soil across the entire sampling period varied between 0.5 to 1.5%, demonstrating that the tension tables held the cores at a relatively constant soil moisture content. The WFPS ranged from 85% (AGB - day 18) to 100% (CPA and CPB, Figure 5.3).

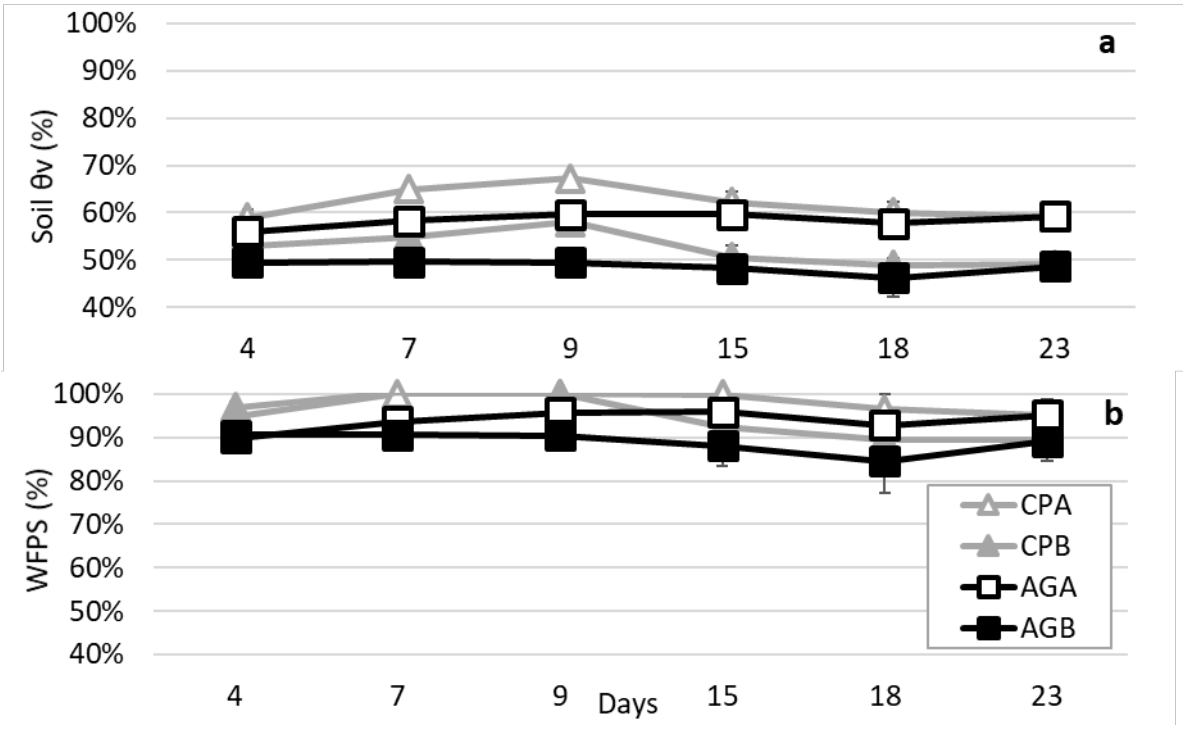

Figure 5.3: The measured (a) volumetric moisture contents (θv %) and (b) water filled pore space (WFPS %) of each soil at each destructive sampling point through the 23 day sampling period. Error bars = SEM, *n* = 4

5.3.2 Soil Chemistry

Soil NO_3^--N concentration was affected by soil horizon (P = 0.000, Figure 5.4a, Table 5.1). On average the B horizons contained more NO_3^--N when compared to the A horizons (CPA 247.3, CPB 333.7, AGA

262.5, AGB 337.1 mg NO_3^--N kg^{-1} soil). Nitrate concentration showed a significant trend of decreasing over time (P=0.001) when averaged across all soil types, starting at an average concentration of 362 mg NO_3^--N kg^{-1} soil when sampled on day 4 and decreasing to an average of 260 mg NO_3^--N kg^{-1} by day 23 (Figure 5.4a). There was no significant interaction between soil type and NO_3^- over time (P = 0.286).

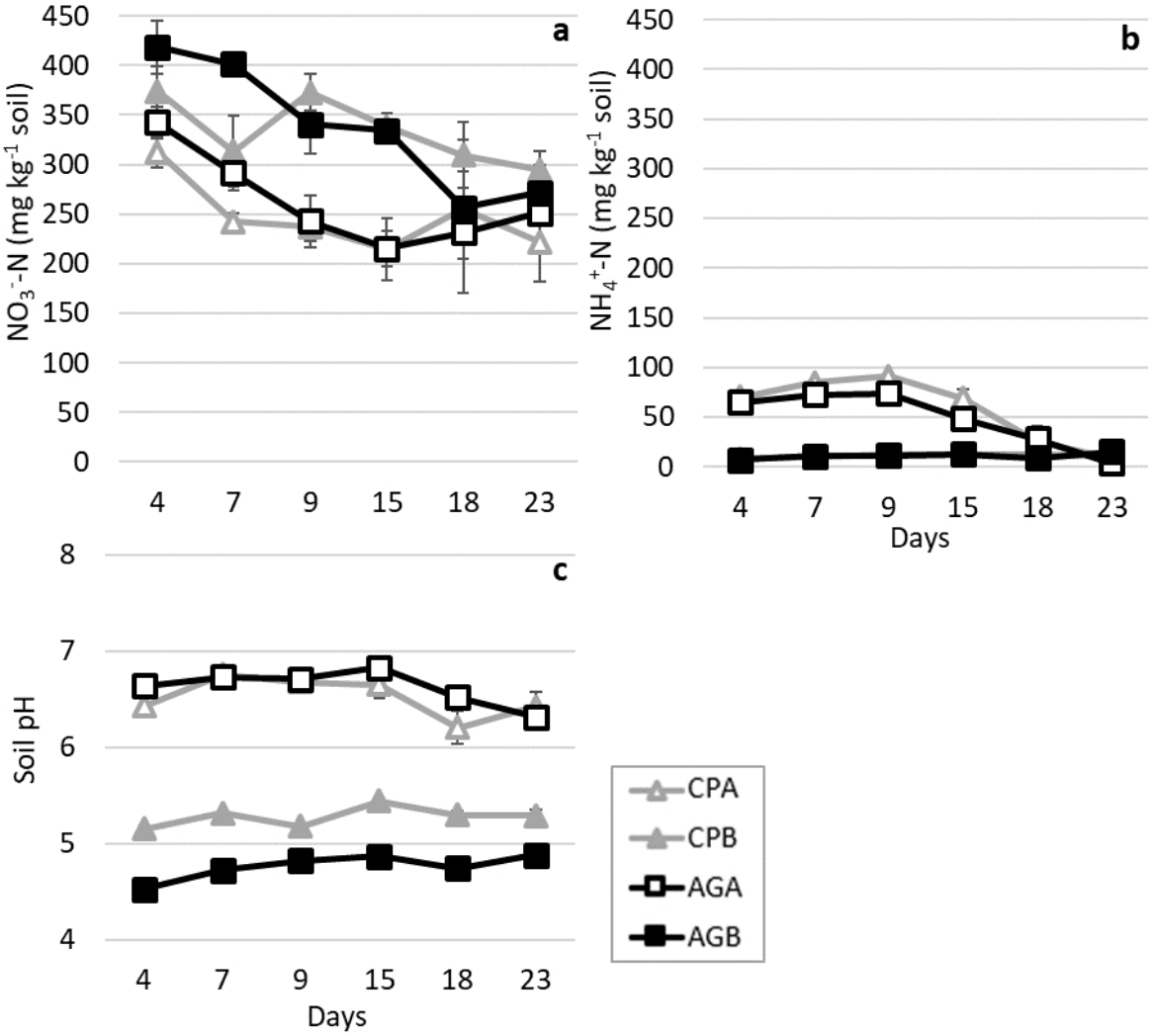

Figure 5.4: Mean inorganic N concentrations across the sampling period at each sampling point; (a) NO_3^--N, (b) NH_4^+-N and (c) soil pH. Letters in legend indicate soil type and horizon; AG - Acton Gley, A and B horizons. CP - Central Plains, A and B horizons. Error bars = SEM. n = 4.

Table 5.1: Mean soil NO_3^--N (mg kg^{-1} soil) values for the 'soil type x time' interaction with values averaged over reps (*n* = 4). Subscripts are Tukey's pairwise comparisons for a 95% confidence interval.

		Time (days)					
Soil Type	**0**	**4**	**7**	**9**	**15**	**18**	**23**
Central Plains A	631	312.5_{ABCD}	242.6_{CD}	237.5_{CD}	214.6_{D}	254.8_{BCD}	221.8_{D}
Central Plains B	568	373.7_{ABC}	313.2_{ABCD}	372.9_{ABC}	338.4_{ABCD}	309.2_{ABCD}	294.6_{ABCD}
Acton Gley A	691	342.8_{ABCD}	291.4_{ABCD}	242.7_{CD}	215.2_{D}	231.5_{CD}	251.3_{BCD}
Acton Gley B	614	418.5_{A}	401.6_{AB}	340.4_{ABCD}	334.0_{ABCD}	256.6_{BCD}	271.4_{ABCD}

Averaged over all the soils the soil NH_4^+-N concentrations were found to be higher at the start of the experiment than the end, declining in concentration from an average of 37.5 mg NH_4^+-N kg^{-1} soil at day 4 to 9.5 mg NH_4^+-N kg^{-1} soil at day 23 (P = 0.000), peaking at day 9 with an average across all soil types of 47 mg NH_4^+-N kg^{-1} soil (Figure 5.4b).

Soil type significantly influenced the NH_4^+ concentration (P = 0.000, Figure 5.4b and Table 5.2). The A horizon soils contained greater concentrations than the B horizon soils, with averages across all treatments of 53.3 and 10.8 mg NH_4^+-N kg^{-1} soil, respectively (P = 0.000). This resulted in a significant interaction between soil horizon and time (P = 0.000), soil type (AG or CP) by horizon (A or B)(P = 0.000) but not soil type by time (P > 0.05)(Table 5.2). By day 23, NH_4^+ concentrations had dropped substantially and were at the same concentrations as B horizon soils.

Table 5.2: Mean soil NH_4^+-N (mg kg^{-1} soil) values for the 'soil type x time' interaction with values averaged over reps (*n* = 4). Subscripts are Tukey's pairwise comparisons for a 95% confidence interval.

	Time (days)					
Soil Type	**4**	**7**	**9**	**15**	**18**	**23**
Central Plains A	70.1_{ABC}	84.7_{AB}	91.1_{A}	68.7_{ABC}	25.6_{DEF}	8.2_{F}
Central Plains B	7.9_{EF}	9.6_{EF}	11.8_{EF}	12.4_{EF}	12.1_{EF}	11.0_{EF}
Acton Gley A	65.2_{BC}	72.8_{AB}	74.0_{AB}	48.4_{CD}	28.1_{DE}	3.4_{EF}
Acton Gley B	7.0_{EF}	10.6_{EF}	11.2_{EF}	12.5_{EF}	8.8_{EF}	15.3_{EF}

The soil surface pH ranged from 4.52 to 6.64 at day 4, to values of 4.88 to 6.32 at day 10 (Table 5.3, Figure 5.4c). There was no significant difference between mean pH values at each sample point. Soil type pH averages were significantly different (P = 0.000). The Central Plains A and B soils had an average pH 6.5 and pH 5.2, respectively, while the Acton Gley A and B averaged pH 6.6 and pH 4.7, respectively. The A horizon soils were more alkaline than the B, with the Acton B horizon the most acidic.

Table 5.3: Mean soil core pH across the sampling period at each sampling point. *n* = 4. Subscripts are Tukey's pairwise comparisons for a 95% confidence interval.

	Time (days)					
Soil Type	**4**	**7**	**9**	**15**	**18**	**23**
Central Plains A	6.4_{BCD}	6.8_{AB}	6.7_{ABC}	6.7_{ABC}	6.2_{D}	6.4_{BCD}
Central Plains B	5.2_{EFG}	5.3_{E}	5.2_{EF}	5.4_{E}	5.3_{E}	5.3_{E}
Acton Gley A	6.6_{ABC}	6.7_{AB}	6.7_{ABC}	6.8_{A}	6.5_{ABCD}	6.3_{CD}
Acton Gley B	4.5_{H}	4.7_{H}	4.8_{FGH}	4.9_{FGH}	4.7_{GH}	4.9_{FGH}

5.3.3 Isotope Signatures of NO_3^-

The soil isotope δ^{15}N-NO_3^- values were influenced by soil horizon (P = 0.000) and time (P = 0.000)(Table 5.4, Figure 5.5). Peak δ^{15}N-NO_3^- values occurred on day 9 of the experiment with a δ^{15}N value of +28‰

for the CPA soil. The A horizon soils had a significantly (P = 0.000) higher mean $\delta^{15}N$ (+24‰) than the B horizon soils (+9‰).

The soil isotope $\delta^{18}O\text{-}NO_3^-$ values were also significantly influenced by soil horizon (P = 0.000) and time (P = 0.000)(Figure 5.5b, Table 5.4). The A horizon soils had significantly (P = 0.005) higher mean $\delta^{18}O$ (+28‰) than the B horizon soils (+27‰). The A horizon soils $\delta^{18}O\text{-}NO_3^-$ values dropped significantly with time, while there was no significant change in the B horizon $\delta^{18}O$ over time (Table 5.4).

Table 5.4: Soil dual isotope values $\delta^{15}N\text{-}NO_3^-$ values (‰ v. AIR) and $\delta^{18}O\text{-}NO_3^-$ (‰ v.VSMOW) for the 'soil type x time' interaction, values are means (n = 4). Subscripts are Tukey's pairwise comparisons for a 95% confidence interval. Means for each soil type, subscripts only comparable between means of given isotope, n = 24.

	Soil Type	Time (days) 4	7	9	15	18	23	Mean
$\delta^{15}N$ (+‰)	**CPA**	20_{D}	24_{ABCD}	28_{A}	25_{ABCD}	20_{D}	22_{BCD}	23.0_{A}
	CPB	9_{E}	8_{E}	9_{E}	11_{E}	9_{E}	9_{E}	9.2_{B}
	AGA	21_{CD}	24_{ABCD}	27_{A}	27_{AB}	26_{ABC}	25_{ABCD}	24.9_{A}
	AGB	7_{E}	8_{E}	9_{E}	9_{E}	10_{E}	10_{E}	8.9_{B}
$\delta^{18}O$ (+‰)	**CPA**	32.6_{ABC}	33.2_{AB}	34.3_{A}	29.9_{BCDE}	24.7_{IJKL}	22.7_{L}	29.6_{A}
	CPB	27.8_{DEFGHI}	27.5_{EFGHIJ}	28.2_{DEFGH}	27.6_{DEFGHI}	27.3_{EFGHIJ}	28.2_{DEFGH}	27.8_{A}
	AGA	29.7_{CDEF}	28.9_{DEFG}	30.9_{BCD}	26.4_{FGHIJK}	25.1_{HIJKL}	23.2_{KL}	27.4_{AB}
	AGB	25.9_{GHIJKL}	24.3_{JKL}	24.9_{HIJKL}	24.5_{IJKL}	25.9_{GHIJKL}	27.3_{EFGHIJ}	25.4_{B}

Mean soil type $\delta^{18}O\text{-}NO_3^-$ values were significantly different (P = 0.000), with the AGB soils having a lower mean $\delta^{18}O$ of 25.4 (Table 5.4). Mean $\delta^{15}N\text{-}NO_3^-$ were significantly different between soil horizons (P = 0.000), with the higher values in the A horizons.

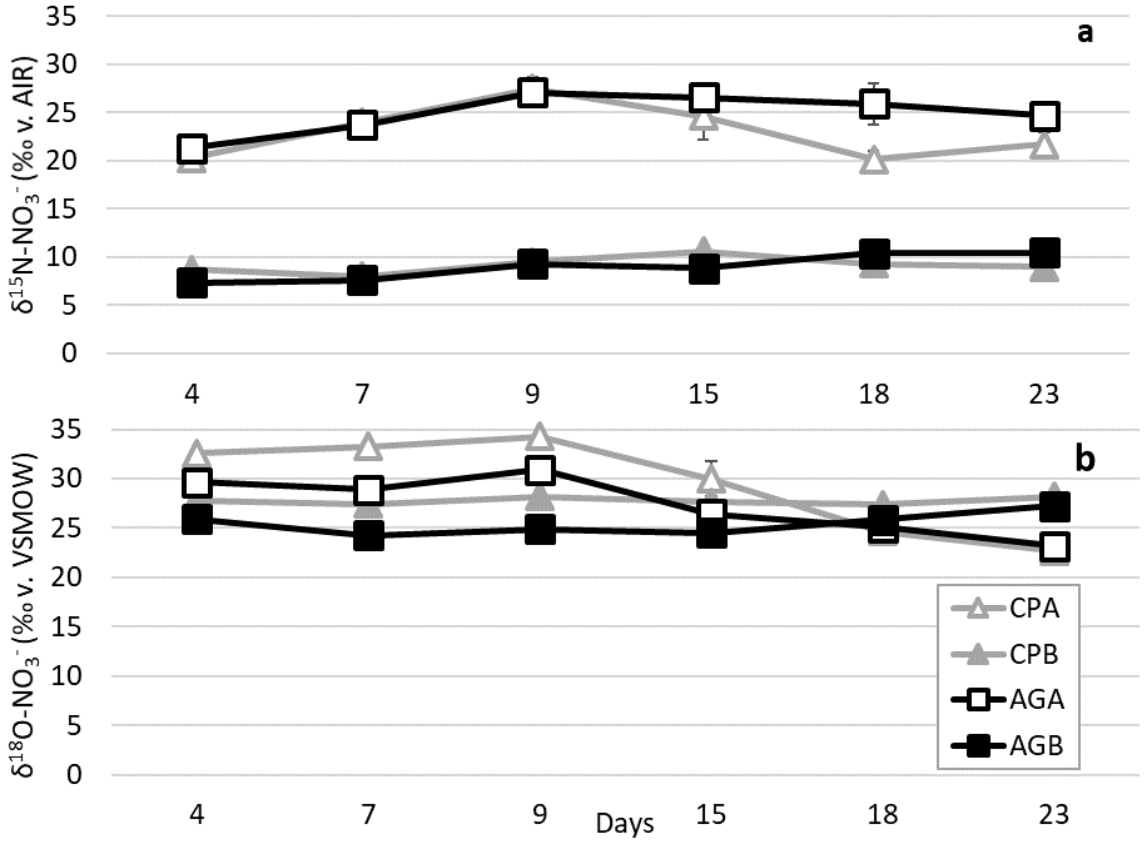

Figure 5.5: Changes in $\delta^{18}O$ (a) and $\delta^{15}N$ (b) composition of soil NO_3^- over the 23 days of the lab trial. Error bars = SEM, n = 4.

Using the isotopic two pool mixing model of Fry (2007), the contribution of nitrification to the change in N between days 15 to 23 was quantified. This time period was used to identify the contribution of soil N to the NO_3^- pool, as NO_3^- concentrations are seen to increase in all soils except CPB (Figure 5.4a). Original soil $\delta^{15}N$ were used for the 'soil N' pool, NO_3^--N concentration (Table 5.1) and its respective $\delta^{15}N$ signature (Table 5.4) were used for days 15 and 23. The soil N contribution was calculated by rearranging the two pool mixing model (Equation 5.2) to obtain the unknown NO_3^--N concentration, as all other values are known. Where the mixture (M), is the combination of two sources (S_1 and S_2):

$$(S_1[NO_3^-]*S_1\delta^{15}N) + (S_2[NO_3^-]*S_2\delta^{15}N) = (M[NO_3^-]*M\delta^{15}N) \qquad \textbf{Equation 5.2}$$

In this study, sources 1 and 2, were 'soil N' and 'day 18 N', and the mixture represents 'day 23 N'. Using this mixing modelled showed that 55 mg kg^{-1} N in the AGA soil, and 20 mg kg^{-1} N in the AGB soil had been nitrified over this 8-day period. The same model for the CPA and CPB soils can show a net decrease in NO_3^--N which has been attenuated (removed), either through denitrification or mixing of other microbial processes, decreasing by -48 and -18 mg kg^{-1} N, respectively.

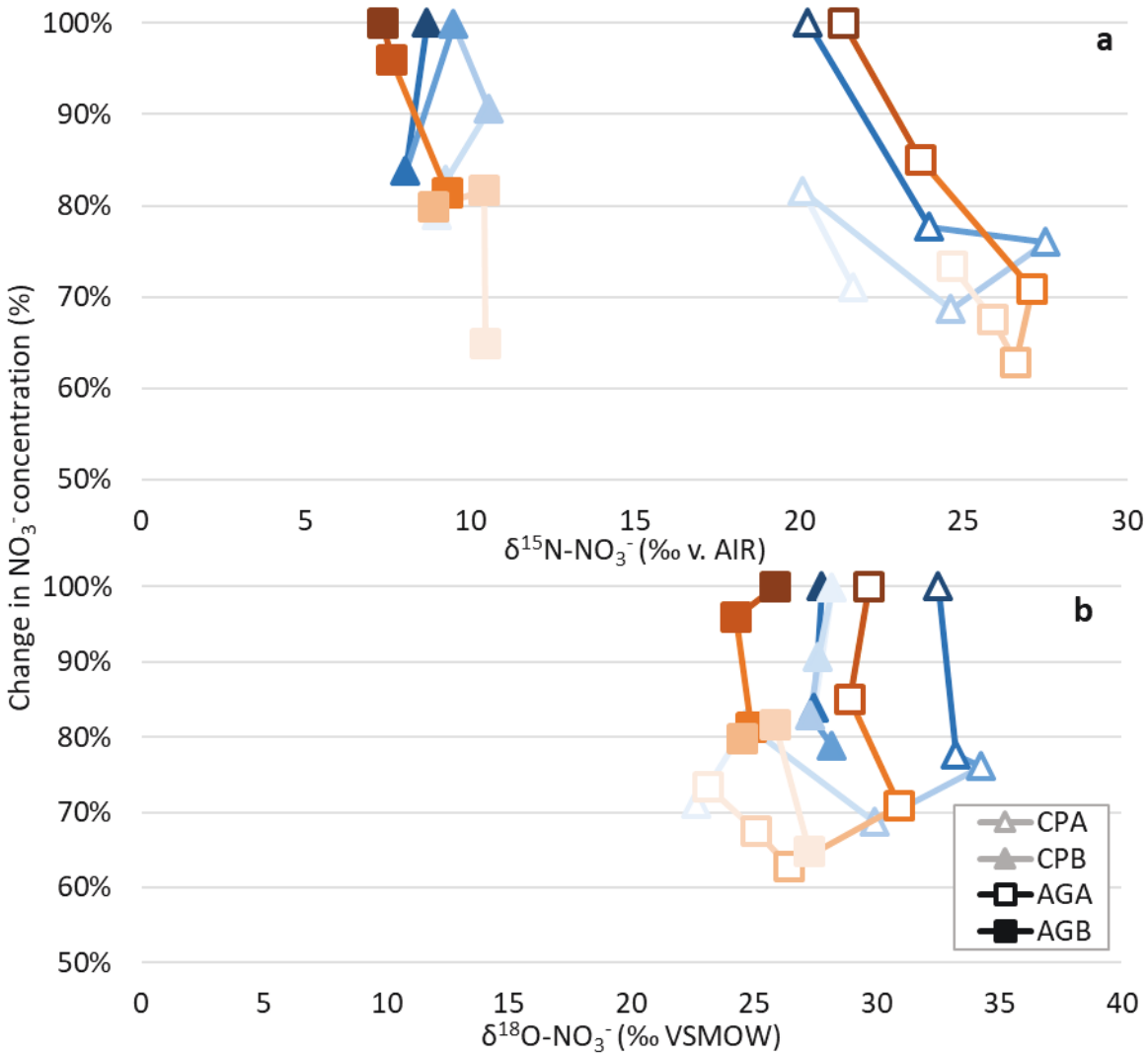

Figure 5.6: Mean changes in (a) δ^{15}N-NO_3^- and (b) δ^{18}O-NO_3^- composition of soil over the 23 days of the study versus the measured NO_3^- concentration expressed as a fraction of the NO_3^- concentration on day 4 (n = 4). Lines connecting points show consecutive sampling points over time with the first sample (day 4), the darkest shade of colour, and the last sample (day 23) the lightest shade of colour.

The soil NO_3^- concentration dropped by 50% for both A horizon soils between when the KNO_3 solution was applied and day 4 (first sampling), with δ^{15}N-NO_3^- increasing in enrichment for the first 3 sampling points, then decreasing in enrichment as NO_3^- concentrations start to increase from day 15 to 23 (Figure 5.6). The B horizon soils dropped by 68% (AGB) and 66% (CPB) between time zero and day 4. The AGA soil showed a steady decline in NO_3^- and corresponding enrichment in δ^{15}N-NO_3^-. The CPB soil did not hold a steady trend in either NO_3^- or δ^{15}N-NO_3^-.

The A horizon soils δ^{15}N-NO_3^- ranged from +20‰ to +28‰, and δ^{18}O-NO_3^- ranged from +23‰ to +34‰. While the B horizon had a lower δ^{15}N-NO_3^- range, from +7‰ to +11‰, and a similar δ^{18}O-NO_3^- range from +24‰ to +28‰ (Table 5.4). The grouping of the A and B horizon values can be seen in Figure 5.7. The average A horizon isotope ratio (δ^{15}N:δ^{18}O) was 0.9 and 0.8 for the AG and CP soils, respectively, compared to the average B horizon ratio of 0.35 and 0.33 for the AG and CP soils, respectively.

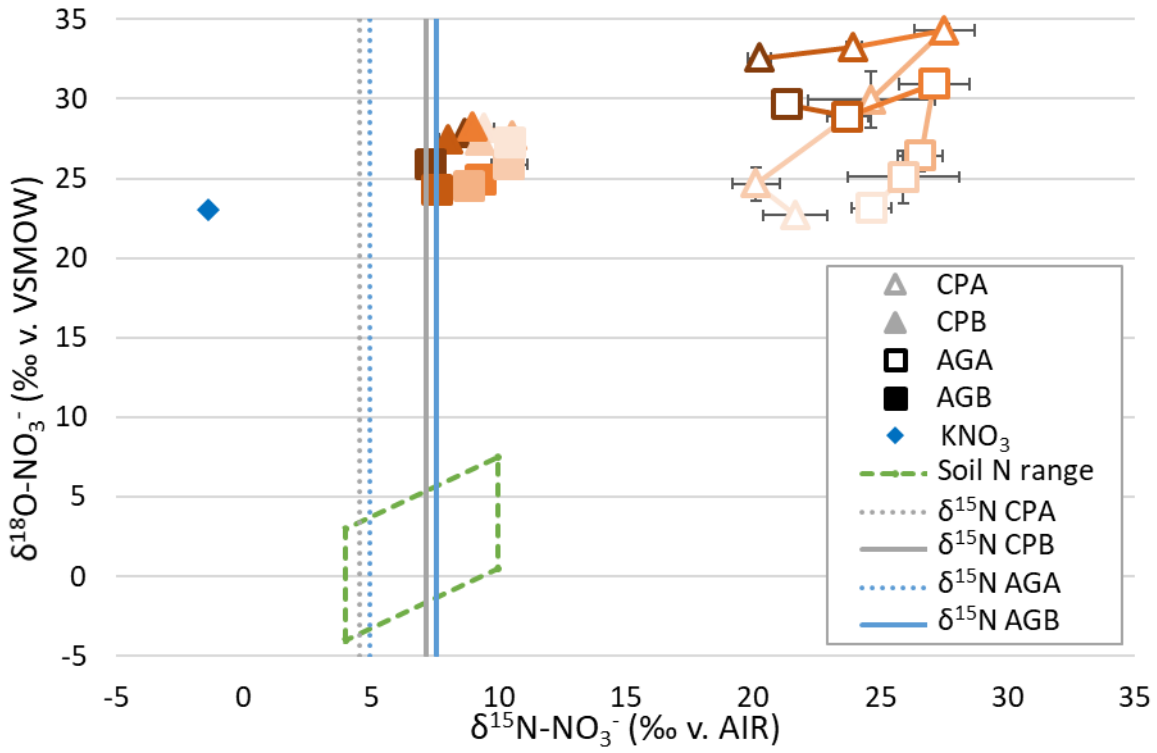

Figure 5.7: The mean isotopic composition of core soils $\delta^{18}O$- NO_3^- (y-axis) and $\delta^{15}N$-NO_3^- (x-axis). Vertical lines represent original soil $\delta^{15}N$, original KNO_3 signal and soil N range are also shown. Legend indicates soil type and horizon; CP - Central Plains, A and B horizons. AG - Acton Gley, A and B horizons. Error bars = SEM, n = 4. Change in colour intensity indicates time, starting at the darkest colour and getting lighter with change in sampling point.

Table 5.5: Linear regression of $\delta^{18}O$ and $\delta^{15}N$ of NO_3^-, used to calculate the slope ratio. Days 4, 7 and 9 were used as t_0, t_1 and t_2 for all soils except CPB, where days 9, 15 and 18 were used in order to align with a period of reducing NO_3^- concentrations (Figure 5.4a, Table 5.1). All $\delta^{18}O$ and $\delta^{15}N$ data across the trial period was used to calculate an overall ratio.

	Linear Regression Equation	r^2
CPA	y = 0.2399x + 27.628	0.9835
CPB	y = -0.0044x + 27.761	0.00006
AGA	y = 0.2426x + 23.997	0.4746
AGB	y = -0.1921x + 26.53	0.0641
All data points	y = 0.1371x + 25.271	0.1216

Between days 4 and 9, when NO_3^- concentrations were decreasing, $\delta^{18}O$ and $\delta^{15}N$ linear regression for the CPA and AGA soils separately, both had slopes of 0.24 (Table 5.5). The average slope of $\delta^{15}N$:$\delta^{18}O$ across the whole trial period was 0.14 (r^2 = 0.12).

Rayleigh calculations were performed using data from days 4, 7 and 9, as t_0, t_1 and t_2, for all soils except CPB, where days 9, 15 and 18 were used in order to align with a period of reducing NO_3^- concentrations (Figure 5.4a, Table 5.1). The Rayleigh fractionation factors for $\delta^{15}N$-NO_3^- ranged from -21.7 ± 9.9‰ (CPA) to +0.94 ± 7.4‰ (CPB, no denitrification) (Figure 5.8). The fractionation factors, the slopes of the regressions were significantly different between soil A and B horizons (P = 0.002) but not between soil types CP and AG (P > 0.05).

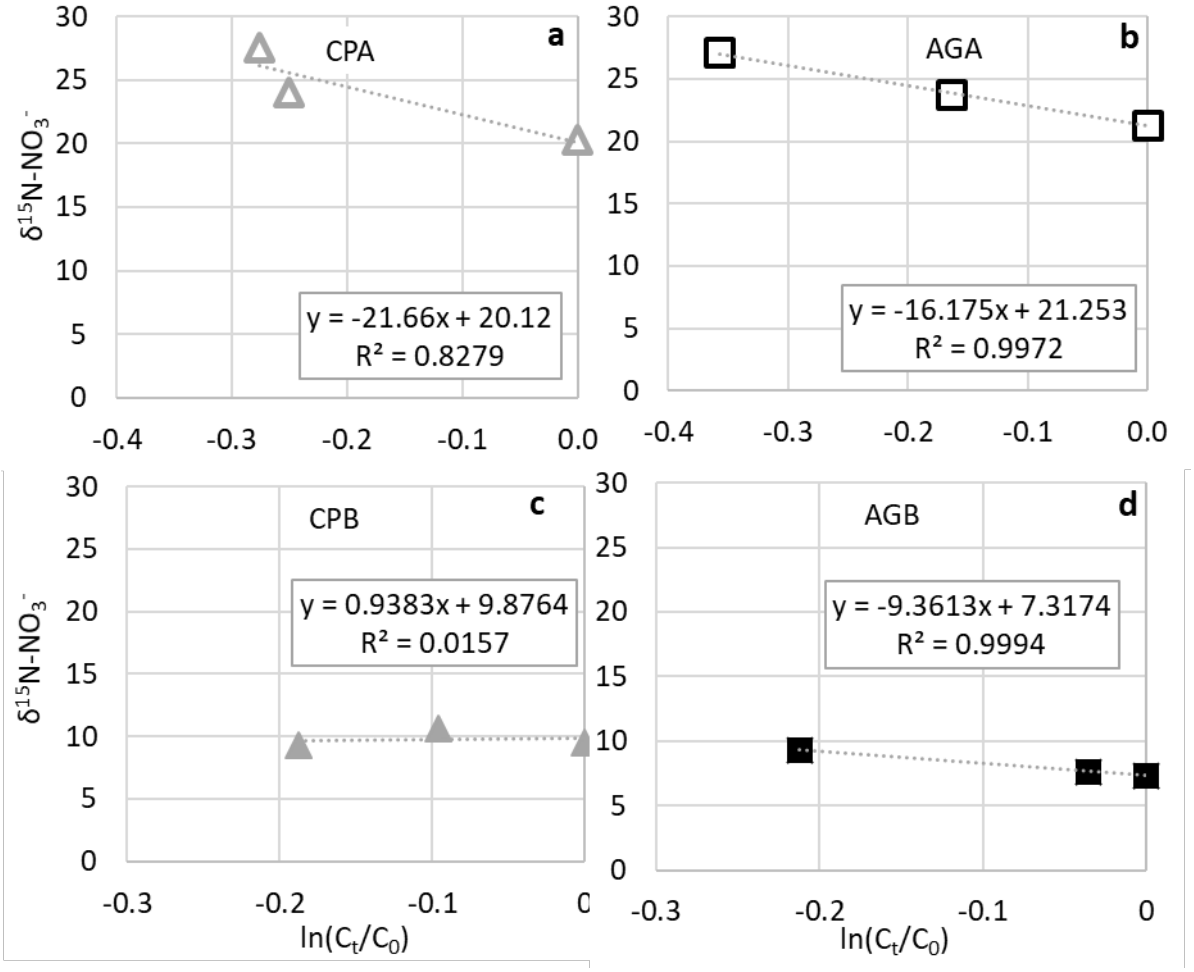

Figure 5.8: Linear regression of a Rayleigh calculation, used to calculate the $\delta^{15}N\text{-}NO_3^-$ fractionation factor for each of the soils; a) CPA -21.7 ± 9.9‰, b) AGA -16.2 ± 0.9‰, c) CPB +0.9 ± 7.4‰, d) AGB -9.4 ± 0.2‰. Showing the $\delta^{15}N\text{-}NO_3^-$ verses the natural log of the ratio of C_t/C_0, where C_t is the NO_3^- concentration at a given time (t) and C_0 is the initial NO_3^- concentration. Days 4, 7 and 9 were used as t_0, t_1 and t_2 for all soils except CPB, where days 9, 15 and 18 were used in order to align with a period of reducing NO_3^- concentrations (Figure 5.4a, Table 5.1).

5.3.4 Soil N_2O Emissions

Due to the skewness of the data (Anderson-darling P < 0.05) the data were transformed (natural log). Data presented are non-transformed, but data analysis for significance was performed on natural log transformed data. Analysis was performed using a Minitab® general linear model ANOVA. Each factor; soil moisture, soil type and soil horizon, was tested for significance as well as testing for significant two and three way interactions between each factor on the log transformed data.

Soil N_2O-N fluxes (mg m^{-2} h^{-1}) varied significantly between soil type (P = 0.000) and sampling date (P = 0.000, Table 5.6, Figure 5.9). Soil horizon influenced N_2O-N gas fluxes (P = 0.015): the mean flux from the A horizon N_2O-N (60.3 mg m^{-2} h^{-1}) was greater than from the B horizon (8.1 mg m^{-2} h^{-1}) across all sampling dates. There was a significant time effect on emissions by soil type (P = 0.000), as they decreased over time, with the AGB soil maintaining higher N_2O-N gas fluxes than the other soils by day 23 (Table 5.6).

Table 5.6: Mean soil N_2O-N flux (mg m^{-2} h^{-1}) values for the 'soil type x horizon x time' interaction (*n* = 4). Subscripts are Tukey's pairwise comparisons for a 95% confidence interval on natural log transformed data.

	Time (days)					
Soil Type	**4**	**7**	**9**	**15**	**18**	**23**
Central Plains A	338_{A}	54_{ABCD}	20_{BCDE}	6.1_{DEFG}	1.3_{EFGH}	0.2_{GHI}
Central Plains B	18_{BCDE}	6.5_{CDEF}	3.5_{DEFG}	0.3_{HIJ}	0.01_{J}	0.02_{IJ}
Acton Gley A	206_{AB}	109_{ABC}	16_{BCDE}	5.7_{DEFG}	2.9_{EFGH}	0.6_{FGHI}
Acton Gley B	14_{BCDE}	23_{ABCDE}	17_{ABCDE}	3.8_{DEFG}	4.0_{EFGH}	7.4_{EFGH}

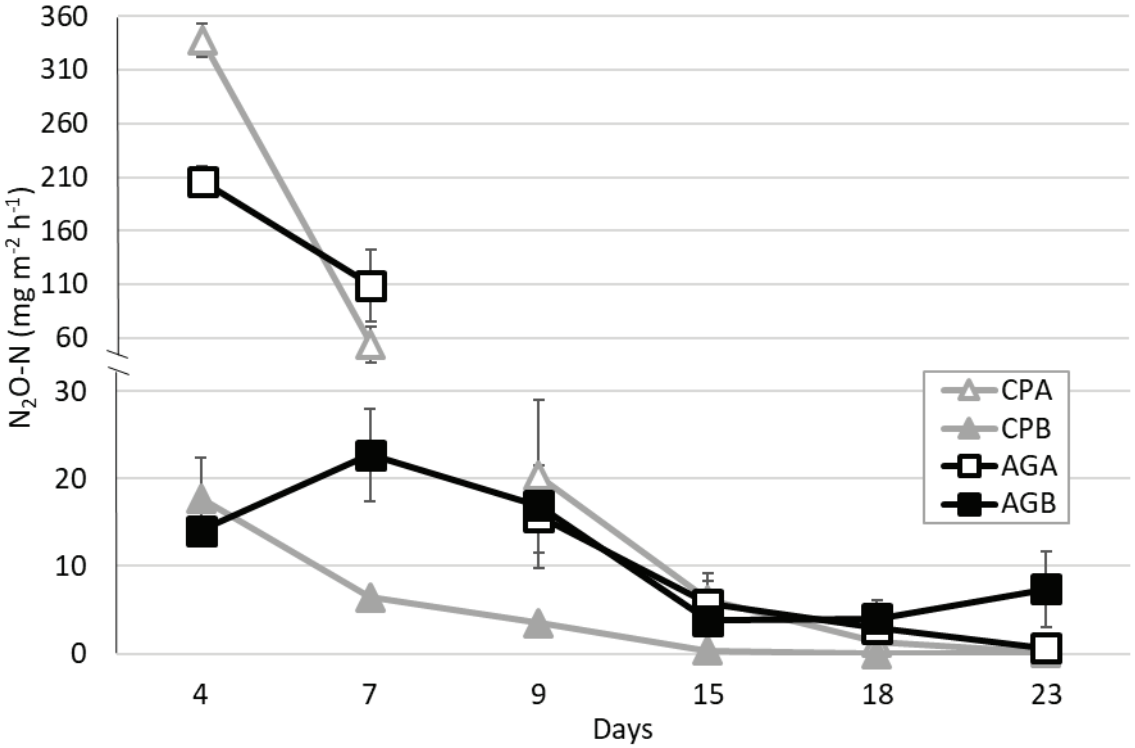

Figure 5.9: Effect of soil type on mean N_2O-N (mg m^{-2} h^{-1}) gas fluxes over the 23 day sampling period. Legend indicates soil type and horizon; AG - Acton Gley, A and B horizons. CP - Central Plains, A and B horizons. Error bars = SEM, *n* = 4. Note break in values on Y axis between days 7 and 9 there is a large decrease in A horizon net N_2O-N gas flux.

5.3.5 Diffusivity

Modelled Diffusivity

There was no significant difference in mean modelled D_p/D_0 across the sampling dates (P = 0.205, Figure 5.10, Table 5.7). However, there was a significant interaction between the modelled D_p/D_0 values soil type x sampling date (P = 0.01), with soil type AGB having higher D_p/D_0 values than the other soils across almost all of the sampling dates (Figure 5.10), also with a significantly greater D_p/D_0 when averaged across sampling dates of 0.0025 (P = 0.000), compared to the other soils; AGA 0.0005, CPA 0.0003 and CPB 0.0008. Modelled values were consistently less than D_p/D_0 of 0.006.

Soil ρ_b affected modelled D_p/D_0 values (P = 0.02), with the A horizons, with a soil ρ_b of 1.0, having lower diffusivity than the B horizons (ρ_b 1.2), with mean D_p/D_0 values of 0.0004 and 0.0017 for A and B horizons, respectively, averaged across sampling dates and soil type (Figure 5.10).

Table 5.7: Mean modelled relative gas diffusivity (D_p/D_0) through soil for the six sampling points of the trial for the 'soil type x soil horizon x time' interaction with values averaged over reps (*n* = 4). Subscripts are Tukey's pairwise comparisons for a 95% confidence interval.

Soil Type	Time (days)					
	4	7	9	15	18	23
CPA	0.000498_{B}	$<0.000001_{B}$	$<0.000001_{B}$	0.000338_{B}	0.000666_{B}	0.000323_{B}
CPB	0.000110_{B}	0.000001_{B}	$<0.000001_{B}$	0.001776_{AB}	0.001283_{AB}	0.001627_{AB}
AGA	0.001238_{AB}	0.000373_{B}	0.000132_{B}	0.000247_{B}	0.000543_{B}	0.000725_{B}
AGB	0.001064_{AB}	0.001736_{AB}	0.001154_{AB}	0.003199_{AB}	0.002232_{A}	0.002822_{AB}

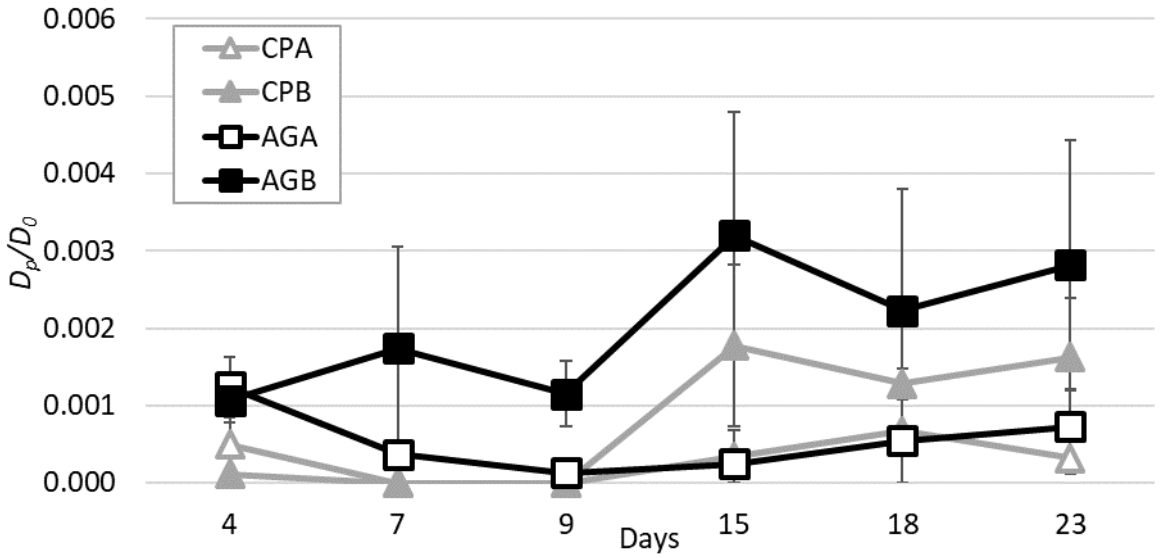

Figure 5.10: Modelled relative gas diffusivity (D_p/D_0) rate through soil for the six sampling dates of the trial for the 'soil type x soil horizon x time'. Legend indicates soil type and horizon; CP - Central Plains, A and B horizons. AG - Acton Gley, A and B horizons. Error bars = SEM, *n* = 4.

Measured Diffusivity

Measured D_p/D_0 values were higher (P = 0.000) than modelled values, mean D_p/D_0 of 0.006 and 0.0005, respectively (Figure 5.11). Measured values were only from two of the six sampling time points (day 4 and 9), to provide a comparison, as measuring D_p/D_0 at high moisture contents is extremely difficult.

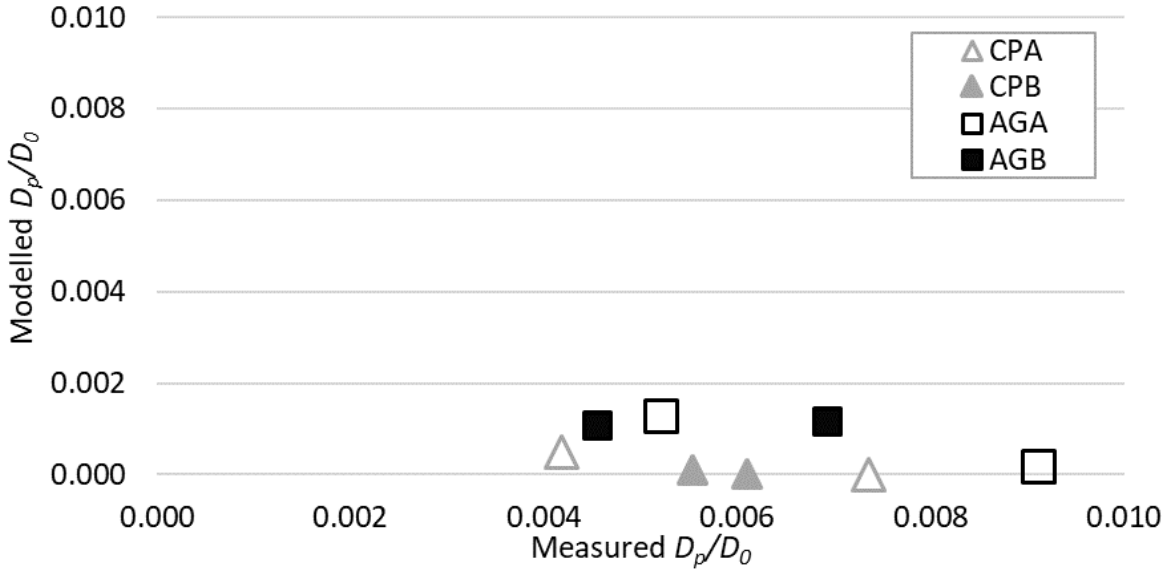

Figure 5.11: Modelled vs. measured D_p/D_0 values for each of the soil types for sampling days 4 and 9. Legend indicates D_p/D_0 method, soil type and horizon; CP - Central Plains, A and B horizons. AG - Acton Gley, A and B horizons.

5.3.6 Diffusivity & N_2O Interaction

At -0.5 kPa, the D_p/D_0 values were effectively zero as the soil was saturated, all below the previously identified D_p/D_0 value of 0.006 for peak denitrification (Balaine et al., 2013). However, there were high SEMs in the modelled D_p/D_0 values, even more so for the AGB soil (Figure 5.12).

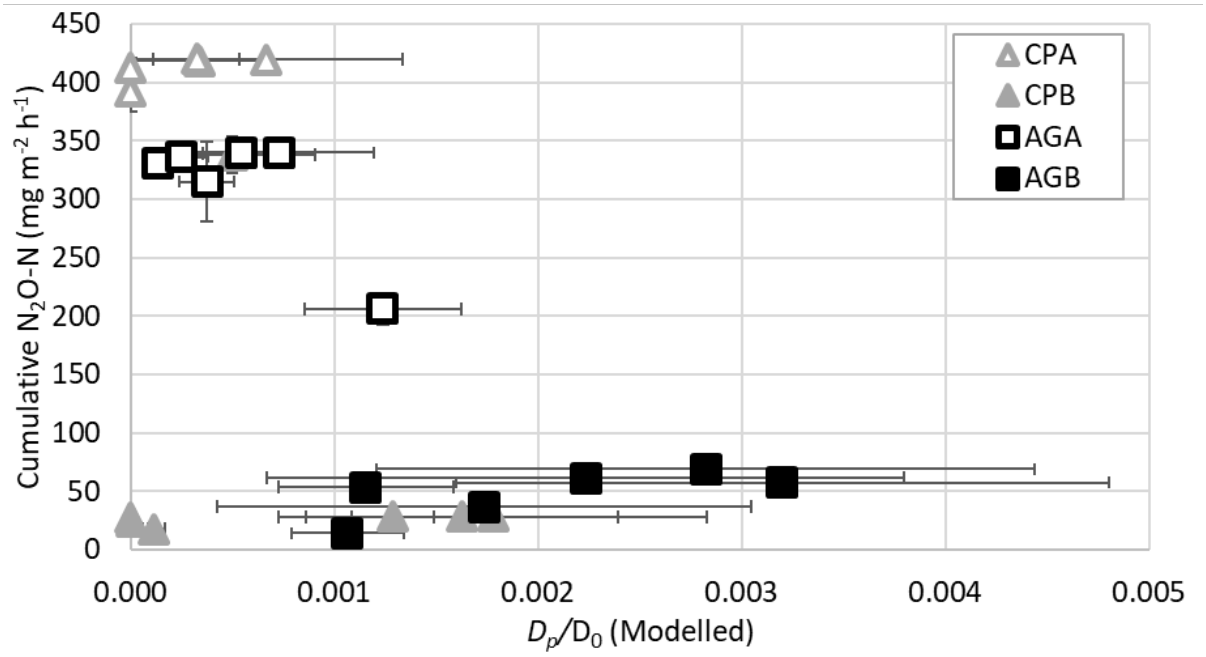

Figure 5.12: Relationship of modelled D_p/D_0 with cumulative N_2O-N flux for each of the soil types. Legend indicates soil type and horizon; CP - Central Plains, A and B horizons. AG - Acton Gley, A and B horizons. Error bars = SEM, *n* = 4.

The regression of the natural log of the N_2O-N flux and modelled D_p/D_0 resulted in a significant relationship for the B horizon soils (P = 0.04, r^2 = 0.42), but not for the A horizon soils (P = 0.2, r^2 = 0.18), shown in Figure 5.13.

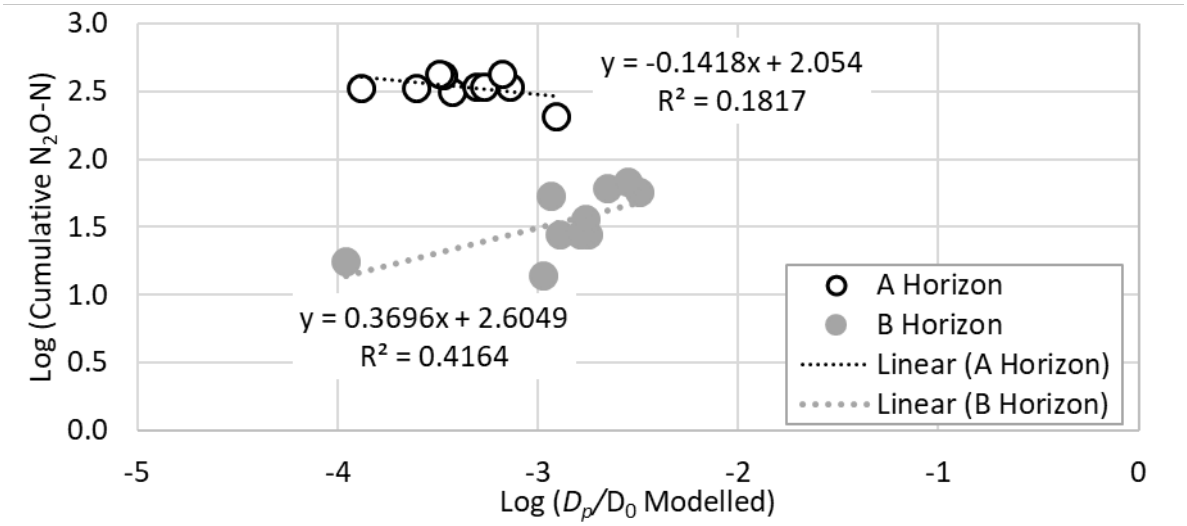

Figure 5.13: Regression of cumulative N_2O-N expressed as log values, vs. log of modelled relative gas diffusivity (D_p/D_0) for A and B horizon soils. Plotted for D_p/D_0 values > 0. Data points are means, n = 4.

5.4 Discussion

5.4.1 Soil NO_3^- Isotopes

Fractionation of NO_3^--N isotopes was higher in the A horizon soils, -22‰ and -16‰ compared to -9‰ and +0.9‰ in the B horizon soils. The CPB soil did not show denitrification fractionation of NO_3^--N isotopes, with a fractionation factor of +0.9‰. Fractionation factors found in the current study were similar to the values of -16.9‰ to -24.8‰ reported by Granger et al. (2008). Where fractionation was thought to be influenced by the degree of external enzymatic (periplasmic NO_3^- reductase, NAP) isotopic expression between different microbial strains.

The isotopic composition of NO_3^- ($\delta^{15}N/^{14}N$‰ and $\delta^{18}O/^{16}O$‰) can potentially provide an indication of either sources or sinks of N in the landscape (Austin et al., 1998; Heaton, 1986), as biogeochemical processes distribute them in predictable unequal ratios across the landscape (Kendall, 1998; Seiler, 2005; Widory et al., 2004). Thus, stable isotopes potentially provide a way to trace natural element cycling, acting as 'natural dyes' that can be followed through natural systems. This experiment showed a shift in the residual NO_3^- pool from being progressively enriched over time, to a situation where the NO_3^- pool becomes progressively depleted. Based on previous studies it is hypothesised that heterotrophic nitrification rates were in excess of denitrification rates and/or denitrification had ceased in order to cause this effect.

Over this same period, from days 4 to 9, the B horizon soils showed traits indicative of reduced rates of denitrification, or nil denitrification, occurring with: slower or nil declines in NO_3^- concentrations, less of an increase or no change to $\delta^{15}N$ and $\delta^{18}O$ enrichment of the NO_3^- pools relative to the A horizons, and much lower enrichment factors. The reasons for these isotopic variations from the A horizon soils are due to reduced denitrification activity which is due to the same factors as noted above for the reduced denitrification rates in the B horizons.

After day 9, in the A horizons, the residual NO_3^- pools, rather than continuing to become progressively enriched, instead began to become progressively depleted relative to their enrichment at day 9 (Figure 5.5, 5.6, 5.7). This switch from enrichment to depletion of the NO_3^- pools in the A horizons coincided with the observed increases in NO_3^- concentration observed after day 9 (Figure 5.4). This trend of continued depletion indicated that another source of NO_3^- was being produced. Given the lack of external inputs this NO_3^- could only have come from the soil-N pool. As discussed above this is likely to have occurred as the result of heterotrophic nitrification given the anaerobic status of the soil. The measured NO_3^- pool represents a net concentration and net isotopic signature, thus, the trend in depletion of the NO_3^-. Based on the change in NO_3^- concentrations and their respective isotopic $\delta^{15}N$ signature, with a soil $\delta^{15}N$ value range of between +4.55 and +7.58‰, the contribution of soil-N to the NO_3^- pool was calculated to be 55 mg kg^{-1} d^{-1} (AGA soil) which is comparable in magnitude to the highest heterotrophic rates presented by (Friedl et al., 2018) of > 20 mg kg^{-1} d^{-1} from clay and loam soils at ≥ 80% WFPS.

The original soil $\delta^{15}N$ values of the CP and AG soils, ranged from +4.55‰ to +7.58‰, which fit within the reported range of +0.3‰ to +12.9‰ Rogers et al. (2017) for Southland soils. However, saturation of the soil cores with KNO_3 provided a NO_3^- pool with a $\delta^{15}N$-NO_3^-, $\delta^{18}O$-NO_3^- signature ($\delta^{15}N$ -1.4, $\delta^{18}O$ +23) typical of that found in fertiliser (Figure 5.7), typically, fertilisers have been reported to have a low $\delta^{15}N$ ranging from -8‰ to +7‰ and $\delta^{18}O$ of ~+40‰ (Fischer, 2014; Nikolenko et al., 2018). The saturation with KNO_3 created an environment that was not NO_3^- limited, and one that allowed for denitrification if sufficient C was present and available.

The A horizon soil $\delta^{15}N$-NO_3^- values at day 4, average +20.5‰, demonstrate enrichment of the residual $\delta^{15}N$-NO_3^- pool relative to the starting KNO_3 and/or soil-N, indicating that denitrification had already commenced, as further evidenced by the decline in NO_3^- and the release of N_2O. Similar results have previously been reported, for example, Clague et al. (2015b) observed seasonal denitrification $\delta^{15}N$-NO_3^- values reaching +28.5‰, which is similar to the peak ^{15}N of +28‰ for the CPA soil on day 9, AGA soil peaking at +27‰.

From days 4 to 9, in the A horizon soils (which had original soil $\delta^{15}N$ values of +4.55‰ and +4.94‰ for the CP and AG soils, respectively) there were within the NO_3^- pools: declining NO_3^- concentrations, increases in both ^{15}N enrichment (~ 7‰) and ^{18}O enrichment (~ 2‰) of the residual NO_3^- pools, and positive fractionation factors for $\delta^{15}N\text{-}NO_3^-$ as shown by the Rayleigh plots. Taken together these results conclusively indicate that denitrification was occurring from days 4 to 9 in the A horizon soils (Figure 5.7). Enrichment in $\delta^{15}N\text{-}NO_3^-$ during denitrification has previously reported to range from +2 to +30‰ over a range of denitrifiers and experimental conditions (Granger et al., 2008). Low ranges (+2 to +12‰)(Wada & Hattori, 1978), similar to those in this experiment, have been reported for freshwater samples, while soil based denitrification experiments where at the high end (+14 to +29‰)(Blackmer & Bremner, 1977; Mariotti et al., 1981). Enrichment in this study may not have been as strong as those previously reported due to mixing of isotope signals from other N processes occurring at the same time. Nitrification for example, creates a lighter NO_3^- pool depleted in $\delta^{15}N$, which can mask denitrification enrichment (Casciotti et al., 2003; Mariotti et al., 1981).

Nitrate that has been partially denitrified plots along a slope of 2:1 or 1:1 enriching in parallel as time progresses, with both N and O isotopes increasing in value (Fischer, 2014; Granger et al., 2008; Granger et al., 2004; Sigman et al., 2001). Granger and Wankel (2016) reported ratios varying from 0.6 to 1.02 for different laboratory cultures of denitrifying bacteria. However, the slopes of data from this experiment between days 4 to 9, when denitrification is thought to have occurred indicated by a decrease in NO_3^- concentrations, do not fit this 1:1 or 2:1 line, with A horizon slopes of 0.24. This suggests that disparity in slopes found in this study and those previously reported may be due to differing microbial communities.

Nitrate isotopic enrichment in O_2-defiecient waters has been reported to be enriched in $\delta^{18}O\text{-}NO_3^-$ by 3‰ more than $\delta^{15}N\text{-}NO_3^-$, rather than the more commonly reported ratio of 1:1 (Sigman et al., 2005). This anomaly was reportedly due to either; remineralization of newly fixed N (unlikely in this experiment), or active cycling between NO_3^- and NO_2^- (coupled NO_3^- reduction and NO_2^- oxidation). Another study by Granger et al. (2016), also points out discrepancies between these ratios, with ratios < 1 suggested to be due to concurrent NO_3^- production by anaerobic NH_4^+ oxidation under O_2 limited conditions. Further analysis for microbial community structure, activity and C substrate supply is needed to better understand these results but is outside the scope of this experiment.

At the microbial level heterotrophic denitrification fractionation is thought to depend on isotopic fractionation during enzymatic NO_3^- reduction inside the cell (Granger et al., 2004; Kritee et al., 2012). With the discrimination of heavy N and O isotopes dependant on cellular ratio of NO_3^- efflux relative to uptake (Granger et al., 2008; Kritee et al., 2012). Expression of fractionation in soil (or external substrate), greater when efflux (NO_3^- moving out of the cell) is more important (Needoba et al., 2004).

However, as denitrification is highly regulated by environmental conditions, understanding its effects on the cellular level processes that control efflux and uptake are difficult and lead to large variation in fractionation between different microbes.

It should be remembered that the isotope signatures and the measured NO_3^- concentrations are net values and thus they indicate that the NO_3^- inputs exceeded NO_3^- removal via denitrification or other processes such as DNRA. It cannot be assumed that NO_3^- attenuation ceased.

After day 9 in the B horizons the evidence for depletion of the $\delta^{15}N$ of the NO_3^- pool was less clear, with little observed depletion in the AGB but some depletion in the CPB soils. The depletion of the NO_3^--$\delta^{15}N$ is again presumed to be the result of heterotrophic nitrification but at lower rates due to the lower organic matter contents in the soil.

5.4.2 Soil NO_3^- Concentrations

At the end of the experiment, although starting at a high concentration, the A horizon soils in this study had, on average, less soil NO_3^--N than the B horizons. The lack of an available C source in the B horizon may explain the NO_3^--N concentrations not being reduced by denitrification, as C becomes less available as you move down through the soil profile, therefore C is limiting at depth (Jahangir et al., 2012). It is also commonly noted that B horizon soils have lower microbial biomass (Spohn et al., 2016). Thus, an A horizon soil generally has a greater capacity to attenuate N than a subsoil as it has all the required components that initiate N cycling: higher microbial biomass, relatively higher C content as an energy source, relatively higher O_2 for nitrification of NH_4^+ to produce NO_3^-, and then with addition of moisture and the soil becoming anaerobic, a higher denitrification rate with the reduction of NO_3^- ensuing (Jarvis et al., 1994; Murray et al., 2004). This explains why the N_2O-N emissions were higher in the A horizon soils (60.3 mg m^{-2} h^{-1}) than the B horizon soils (8.1 mg m^{-2} h^{-1}), when averaged across all sampling dates. The soil A horizons showed much more significant variation in NO_3^- concentrations over time than the B horizons, highlighting the role A horizons play in N attenuation and associated processes.

The underlying microbial processes responsible for N attenuation are influenced by C and N substrate availability (Andersen et al., 2009). Carbon is used as the electron donor during denitrification, and N-oxides as the electron acceptor during energy production (Morley et al., 2010). At low concentrations NO_3^- controls the rate of denitrification (Knowles, 1982). Thus, in the current study where cores were pre-soaked in KNO_3 to make sure N was not a limitation for denitrifiers, it is more likely that C limitation would influence potential denitrification. Where a significant decrease in NO_3^--N concentrations over time occurred, it indicates that microbial denitrification was readily occurring: (Figure 5.4a). Soil microbial community composition may have also driven the observed differences in the rate of NO_3^-

depletion (Kraft et al., 2014; Yoon et al., 2015). The microbial community composition influences attenuation, as different communities process N at different rates and can behave differently in changing environments and in response to prior soil management (Zhu et al., 2013).

Losses of N_2O and N_2 are tightly linked to NO_3^- availability and denitrification with elevated NO_3^- concentrations shifting the N_2O/N_2 ratio towards N_2O, as NO_3^- is preferred to N_2O as an electron acceptor during denitrification (Chen et al., 2015; Dendooven et al., 1995). The fact soil N_2O fluxes reached a low at day 15, may indicate a shift in the N_2O/N_2 ratio, as available NO_3^- is consumed and with a shift to using N_2O as the electron acceptor and an increase in N_2 production. Alternatively, it may signal that C was limiting and the denitrification rate had slowed accordingly.

The moment of peak denitrification may have been missed in the sampling as δ^{15}N-NO_3^- isotope signatures demonstrate that the soil NO_3^- pools were already ^{15}N enriched at the first sampling point (day 4) in the A horizon soils and the amount of NO_3^- removed compared to the theoretical time zero NO_3^- concentration was only 50% in the A horizon soils (Figure 5.6). This indicates that the 3-day time period for soil moisture equilibration of the tension tables is in the same time window as peak denitrification and in future studies sampling should commence earlier.

5.4.3 Soil NH_4^+ Concentrations

The A horizons initially had higher concentrations of NH_4^+-N than the B horizons. The A horizons contain more organic matter, by sieving and then and repacking these soils, there may have been mineralization of this organic material to create the enhanced NH_4^+-N concentrations observed in the A horizons. Intriguingly these NH_4^+-N concentrations decreased after day 9 (Figure 5.4b) despite the soils being near saturation with poor O_2 supply as indicated by the D_p/D_0 values.

In temperate soils both ammonia oxidising Archaea (AOA) and autotrophic ammonia oxidising bacteria (AOB) are widespread (Pett-Ridge et al., 2013). While AOA may be numerically dominant in an ecosystem the AOB may still be the functionally dominant nitrifying organisms (Pett-Ridge et al., 2013). For example, Di et al. (2009) found AOB were the dominant nitrifier's following BU deposition. Both AOA and AOB require O_2 in order to perform nitrification where they gain energy following the oxidation of inorganic-N, which they use as an energy source to fix CO_2 and for growth (De Boer & Kowalchuk, 2001; Stein, 2019). In a study to examine nitrification potentials in wet tropical soils Pett-Ridge et al. (2013) did not find AOB activity and assumed AOA were responsible for the observed nitrification although heterotrophic nitrification was also measured and considered as a possible mechanism responsible for the observed nitrification. Pett-Ridge et al. (2013) measured heterotrophic nitrification potential using acetylene inhibition, which blocks autotrophic nitrification, and found it to be substantial in several soil types.

Heterotrophic nitrifying organisms can have similar or distinctly different enzymology compared with AOB that allows them to nitrify inorganic or organic N sources under anaerobic conditions to produce NO_2^- and/or NO_3^- (Stein, 2011). As soils were continually saturated in this experiment, increase in NO_3^- concentrations through nitrification of NH_4^+, will have been under anaerobic conditions. Recently, Friedl et al. (2018), using a ^{15}N tracing model, found that heterotrophic nitrification dominated NO_3^- production in a loam soil across all WFPS levels (40 - 95%) and that it dominated at 95% WFPS in both a clay and a sandy soil, where soils came from subtropical pastures. In the same study autotrophic nitrification peaked at 60% WFPS. Given these results it is likely that heterotrophic nitrification was responsible for the reduction in the A horizon NH_4^+ concentrations under the highly saturated conditions seen occurring after day 9 (Figure 5.4b).

5.4.4 Soil pH

In this study soil type specific variation in pH ranges were found to be significant, A horizon soils maintained a more alkaline pH than the B horizons (Figure 5.4c), however, pH did not drop below 4, with a low of 4.5 (AGB). Regardless, the low pH in the B horizons could have been a cause of the lower denitrification rates, along with general soil fertility and OM, due to the influence of pH on microbial community structure and function. Denitrification reportedly has an optimum pH range of 7 to 8 (Delwiche et al., 1976; Knowles, 1982; Müller et al., 1980; Nömmik, 1956; Van Cleemput et al., 1974; Wijler et al., 1954). At low pH (< 4) N_2O-reductase was previously reported to be repressed, causing a decrease in the overall rate of denitrification but increases in the fraction of N_2O produced, and with N_2O as the major product at a pH < 4 (Nömmik, 1956; Wijler et al., 1954). More recently it was shown that low pH does not stop N_2O reductase from working, but instead that low pH interferes with assembly of the N_2O reductase enzyme (Bakken et al., 2012).

5.4.5 Soil N_2O Flux

The peak N_2O emissions occurred in the first 7 to 9 days, with a rapid decline in emissions after this point. Emissions of N_2O, along with observed declines in the NO_3^- concentrations are indicative of NO_3^- attenuation via denitrification. An average decline of 88 mg NO_3^--N kg^{-1} soil across the A horizon soils between days 4 to 9 (Table 5.1). Soil type, available substrate, microbial community composition and function, all interact to affect the magnitude of the N_2O flux (Andersen et al., 2009; Chamindu-Deepagoda et al., 2019; Groffman et al., 2009; Kraft et al., 2014; Six et al., 2004). Treatment of the soil cores with KNO_3 removed the N constraint on denitrification, allowing for large N_2O fluxes to occur, assuming C was available. When there is an increase in available soil C, it generally increases the production of N_2 as the final product of denitrification (Mathieu et al., 2006). Higher available C and soil moisture levels cause denitrification to progress to completion with a greater N_2/N_2O ratio seen under these conditions. Changes in pH, NO_3^- and O_2 levels also change the ratios of N_2O/N_2 as end

products of denitrification, with increased NO_3^- and O_2 availability having a negative effect on N_2 as the end product (Knowles, 1982; Tiedje et al., 1983). The significant variation in N_2O emission between soil horizons is likely due to limited C availability in the B horizon soils, and therefore the A horizons had a greater potential to denitrify available NO_3^-. The soil A horizons contained on average 3% more total carbon than the B horizons used in this study (and A.4). a While N_2 emissions were not measured the results are indicative of the A horizon soils producing higher N_2 emissions that the B horizons. Microbial community composition and size will have likely varied between the A and B horizons due to the differing original soil physical and chemical factors and these may have also played a role in the significant variation in the N_2O fluxes that occurred between horizons.

5.4.6 Relative Gas Diffusivity

There was no significant change in D_p/D_0 values over time, and this was expected as the soil cores were being maintained at -0.5 kPa to induce denitrification. As was found in Chapter 4, influence of soil type and horizon on D_p/D_0 becomes insignificant when soil matric potentials range from 0 to -2 kPa, when D_p/D_0 was measured across six different soil moistures, with D_p/D_0 variation between soil types.

Soil gas diffusion is the main mechanism of O_2 transport in soil (Neira et al., 2015) and therefore an important trigger for the commencement of N attenuation. The reported D_p/D_0 threshold for peak N_2O flux production during denitrification has been reported to be 0.006, with N_2 production becoming dominant as D_p/D_0 decreased below this value (Balaine et al., 2013). Examining cumulative fluxes over 35 days following urea application, Chamindu-Deepagoda et al. (2019) found that D_p/D_0 should be maintained above ≥ 0.038 to limit extensive cumulative emission of N_2O and N_2.

Previous studies looking at the relationship between D_p/D_0 values and N_2O-flux found significant linear relationships of log transformed data, with slopes of -2.68 (Balaine et al., 2013), -1.44 (Balaine et al., 2016b) and -0.744 (Owens et al., 2016). The A horizon soils had a linear relationship of -0.14 but it was not significant, while the B horizon soils had a linear relationship of 0.37 (P = 0.02, Figure 5.13). Only 18% of the variation N_2O fluxes were explained by D_p/D_0 for the A horizon and 42% for the B horizon. This study did not show a significant relationship between N_2O fluxes and D_p/D_0 values, due to the use of a single low soil moisture content (-0.5 kPa) to maintain soils at a D_p/D_0 that encouraged denitrification. Therefore, due to the low D_p/D_0 there is a lack of relationship between D_p/D_0 and N_2O, as N_2O is consumed and N_2 production is increased (Balaine et al., 2016b).

Soil moisture conditions that result in a D_p/D_0 value of ≤0.006, were shown by Balaine et al. (2013) to be the threshold for peak N_2O emissions as determined by measuring N_2O fluxes from NO_3^- amended, re-packed soil cores, varying in ρ_b (1.1 to 1.5 g cm^{-3}) and matric potential (-1 to -10 kPa). As all soils were maintained at -0.5 kPa, D_p/D_0 values did not go above this N_2O emission threshold, with the

highest modelled D_p/D_0 value of 0.003 occurring on day 15 for the AGB soil. The results suggest that all soils were maintained below denitrification thresholds, potentially allowing for maximum N attenuation to occur, with other variables controlling rates. A factor influencing the variability of D_p/D_0 results are the high soil moistures, potentially at saturation, when soil cores hold maximum water, making precise soil moisture content determination more problematic and therefore this introduces error in D_p/D_0 calculations.

5.5 Conclusions & Implications

A key finding of this experiment is the shift in the residual NO_3^- pool from being progressively enriched over time to a situation where the NO_3^- pool becomes progressively depleted. Based on previous studies it is hypothesised that heterotrophic nitrification rates were in excess of denitrification rates and/or denitrification had ceased in order to cause this effect.

This effect has practical implications for the NO_3^- isotopic signature of any NO_3^- that leaches into water ways. Ignoring dilution effects, such an effect could lead to erroneous conclusions (underestimates) as to the magnitude of the soil's denitrification capacity. Thus, in order to better interpret the spatial and temporal variation in NO_3^- isotopic signatures the antecedent soil moisture regime also needs to be considered. For example, it should be considered if the winter season was sufficiently wet to cause prolonged waterlogging of soils. The control of other physical and environmental parameters such as barometric pressure, wind, soil and air temperature over diffusion should also be considered and are relevant to future research.

Fractionation of $\delta^{15}N$ did not vary between different soil types, however, it was significantly different between soil horizons because the A horizon generally contains a larger denitrifying microbial population, with access to more available C substrate. Based on these results, where the soil diffusivity was at a value conducive to denitrification, it may be concluded that, given the same NO_3^- substrate concentration, the $\delta^{15}N$ and $\delta^{18}O$ of NO_3^- will not vary significantly between soil types when denitrifying conditions exist. However, the effects of C availability and quality, untested in this experiment, might still generate soil type differences with respect to NO_3^- isotope signatures. Measurements of soil C, during destructive sampling over time are needed in order to further examine the potential for soil type driven spatial variation in NO_3^- isotope signatures.

This study demonstrated higher NO_3^- attenuation and stronger fractionation of NO_3^- in the A horizon soil and thus it shows the importance and dominance of the A horizon in determining NO_3^- isotopic signatures in the landscape.

The practical outcomes of this study show that:

(i) there is spatial variability in NO_3^- isotope signatures with soil horizon with the A horizon playing a dominant role,

(ii) prolonged saturation of the A horizon may drive a shift in the isotopic signature of denitrification resulting in depletion of NO_3^- isotope signatures, thus confusing the expression of NO_3^- attenuation.

Chapter 6

Lysimeter Study - Can Ruminant Urine-N Rate & Plants Affect NO_3^- Leaching & its Isotopic Composition?

6.1 Abstract

Worldwide there is an increasing awareness of the potential risks that pasture grazing systems pose to freshwater. Excess nutrient levels, predominately NO_3^-, result in reduced water quality. This study focused on further understanding how the presence or absence of perennial ryegrass (*Lolium perenne* L) and bovine urine (BU: 0, 300 or 700 kg N ha^{-1}) influenced both the NO_3^- isotopic signature and the amount of NO_3^- leached. Plant presence resulted in lower NO_3^--N concentrations and reduced NO_3^--N leaching ($P < 0.001$) over the nine-month trial period. A total of 15, 79 and 234 kg N ha^{-1} was leached from the 0, 300 and 700 BU treatments, respectively. Drainage volumes varied with season and plant treatments (plants 420 ± 47 mm, no-plants 539 ± 29 mm total drainage). Nitrate isotope signatures, ($\delta^{15}N\text{-}NO_3^-$ and $\delta^{18}O\text{-}NO_3^-$) varied temporally, with evidence of denitrification occurring. The $\delta^{15}N\text{-}NO_3^-$ and $\delta^{18}O\text{-}NO_3^-$ values were found to be most influenced by plant treatment in the absence of BU. Under BU these isotopic signatures varied temporally due to denitrification. The $\delta^{15}N\text{-}NO_3^-$ and $\delta^{18}O\text{-}NO_3^-$ values may be influenced by plant treatment in the absence of BU but this does not confound interpretation of isotope data when BU is applied. The $\delta^{15}N\text{-}NO_3^-$ and $\delta^{18}O\text{-}NO_3^-$ show potential for identifying NO_3^- sources and soil processes forming and removing NO_3^-. Further datasets are required to improve our understanding of BU rate effects on the temporal dynamics.

Keywords: Nitrate; attenuation; isotopes; $\delta^{15}N$; $\delta^{18}O$; plant effect; temporal variation

This thesis chapter has been published by the New Zealand Journal of Agricultural Research (30th July 2019).

Can ruminant urine-N rate and plants affect nitrate leaching and its isotopic composition?

Sephrah Rayner, Tim Clough, Troy Baisden and Jim Moir.

6.2 Introduction

Worldwide there is an increasing awareness of the potential risks that pasture grazing systems pose to freshwater, including increased nutrient loadings and faecal contamination (Stark et al., 2008). Excess nutrient concentrations, predominately NO_3^-, result in reduced water quality for recreation, and freshwater ecosystems, due to eutrophication of surface waters (Galloway et al., 2015; McLaren et al., 1996; Parfitt et al., 2012). Nitrate contamination of potable waters is also a potential problem with respect to human health and is controversial: the often-cited effect of NO_3^- contamination causing methemoglobinemia is now generally seen as low risk (Cooke, 2014) although other health effects are still debated (Schullehner et al., 2018). Sewage and atmospheric deposition of N compounds can also contribute to NO_3^- in waterways, alongside fertiliser and animal excreta from pasture grazing systems (Malcolm et al., 2014b).

The main contaminant in New Zealand groundwater is NO_3^- (Close et al., 2016), which is becoming increasingly problematic in areas of intensively grazed pasture (Cameron et al., 2013; Stark et al., 2008). Under pasture, N application rates within dairy cow urine patches are typically 700 to 1000 kg ha^{-1} (Moir et al., 2011). Urine patches have been identified as the main source of N leached under grazed pastures (Di & Cameron, 2002). Measuring the stable isotopic compositions of the N and O atoms in NO_3^- enables contributions to an N pool in the environment to be determined (Kendall, 1998; Seiler, 2005; Widory et al., 2004). Nitrogen fertilisers, atmospheric deposition, manure and sewage are NO_3^- sources that have well documented NO_3^- isotopic compositions, for example, the $\delta^{15}N$ of NO_3^- for these sources range from -6‰ to +6‰, -13‰ to +13‰, +5‰ to +25‰ and +4‰ to +19‰, respectively (Xue et al., 2009). Reported isotope ranges for $\delta^{18}O$ differ significantly between atmospheric (from +52.5‰ to +60.9‰) and soil derived (from +0.8‰ to +5.8‰) NO_3^- sources (Durka et al., 1994). These high atmospheric derived ^{18}O values are not as relevant to New Zealand pasture systems, due to negligible inputs from atmospheric deposition, industrial and urban N inputs (Stevenson et al., 2010).

Fractionation of isotopes occurs when the lighter isotopes react faster, creating differentially weighted product and reactant pools (Kendall, 1998). This has been defined as "the extent to which the isotopes of an element are separated between substrate and a product during a reaction" (Robinson, 2001). Nitrification, for example, decreases the $\delta^{15}N$ of NO_3^- as lighter NH_4^+ is preferentially oxidised, leading to the formation of lighter NO_3^- (Mariotti et al., 1981; Ostrom et al., 1998). Subsequently, however, during most biological NO_3^- reactions the light NO_3^- molecule is preferentially converted into reaction products, leaving behind an isotopically heavier NO_3^- pool with a higher $\delta^{15}N$ value (Kendall et al., 2007).

Dual isotope analysis potentially enables both the sources of NO_3^- to be identified and the potential for NO_3^- to be denitrified within the landscape, otherwise referred to as the attenuation of NO_3^- (Denk

et al., 2017; Kendall, 1998; Robinson, 2001). However, there is limited knowledge on the capacity of land forms to attenuate NO_3^- concentrations in agricultural landscapes, especially within New Zealand (Clague et al., 2015b; Stenger et al., 2012; Woodward et al., 2013). But the utilisation of NO_3^- by pasture or its removal via denitrification is desirable, as this can reduce the quantity leached into waterways (Clough et al., 1998a; Seitzinger et al., 2006). Denitrification has been reported to enrich both N and O stable isotopes at commonly expected ratios of 1:1 or 1:2 due to denitrification and assimilation (Granger et al., 2008; Granger et al., 2004). Clague et al. (2015b) found an enrichment of 1.4:1 when looking at shallow ground water in the Waikato region of New Zealand, concluding that denitrification rates varied spatially, but noting that the interpretation of the results was confounded by insufficient knowledge of flow-paths and very low NO_3^- concentrations. Identifying sources of NO_3^- in grazed pasture systems within New Zealand catchments is hampered by a lack of knowledge about how N cycling processes affect fractionation of NO_3^-, particularly attenuation, and variability in source appointment (Xue et al., 2009). As pasture based agricultural systems come under further scrutiny with respect to their environmental impact, especially the dairy industry, there is an increased need to identify both the source(s) of leached N and the potential removal of leached NO_3^- within the landscape. Reduced NO_3^- leaching will result in greater N use efficiency, which potentially could result in reduced N fertiliser requirements, and lower indirect emissions of N_2O, a potent greenhouse gas.

Internationally, the $\delta^{15}N$ signature of NO_3^- leached from pasture soils has been reported to sit between +0.3‰ to +6.6‰ (Minet et al., 2012; Oelmann et al., 2007; Rock et al., 2011) and pasture soil leachate in New Zealand has been found to sit within this range (Mudge et al., 2013; Stevenson et al., 2010). Isotope analyses of two long-term New Zealand pasture trials gave ranges of +2.8‰ to +4.6‰ across all irrigation and fertiliser treatments from soils between 1958 and 2009 (Mudge et al., 2013), while another study of 210 soils across different land uses within New Zealand found $\delta^{15}N$ values ranged from +3.8‰ to +5.4‰ for dry-stock and dairy cattle, respectively (Stevenson et al., 2010). A wider range of $\delta^{15}N\text{-}NO_3^-$ values, from -3.38‰ to +19.2‰, was reported in a trial based in Canterbury, New Zealand, where pasture soils were subjected to different rates of bovine BU or urea-N (Wells et al., 2015). The expected $\delta^{15}N\text{-}NO_3^-$ range for a urea or urine source has been reported to range from -5‰ (Wells et al., 2015) to +1.2‰ (Frank et al., 2004). However, Wells et al. (2015) concluded that this range of $\delta^{15}N\text{-}NO_3^-$ previously assigned to livestock sources should be expanded to -10‰ to account for the influence of post-deposition soil N cycling on $\delta^{15}N$ values.

The potential of pasture plants to influence the soil N-isotope signature, and the $\delta^{15}N$ of NO_3^- that may be subsequently leached, has not been widely researched. It also remains to be seen if temporal variation occurs in the isotopic signature of urine-NO_3^- leached from a pasture system. Temporal $\delta^{15}N\text{-}NO_3^-$ variation may confound the interpretation of such data when modelling N attenuation in the landscape. While previous research has found pasture production to correlate positively ($r^2 = 0.77$, P =

0.02) with the rate of $\delta^{15}N\text{-}NO_3^-$ enrichment, this was due to the influence of fertilizer and irrigation on production and their respective effects on $\delta^{15}N$ rather than the pasture growth (Mudge et al., 2013). Rock et al. (2011) found an average $\delta^{15}N$ shift of~ +5‰ $\delta^{15}N$, between the range of +0.3 and +8‰, when comparing soils under legume (Lucerne, (*Medicago sativ*a L.)) and non-legume treatments, with the legume having lower $\delta^{15}N$ but greater $\delta^{18}O$ (up to +7‰) due to fixation of atmospheric N_2. Ranges of $\delta^{15}N\text{-}NO_3^-$ from 0‰ to +19‰ and +9‰ to +18‰ for plant N assimilation of NO_3^- and NH_4^+ into organic N, respectively, were previously reported (Högberg, 1997; Robinson, 2001).

The objectives of this study were to (i) determine if pasture plants influenced the isotope signature of leached NO_3^- following deposition of ruminant urine onto pasture, (ii) determine if such an effect was N rate dependent, and (iii) determine if the isotope signature of leached NO_3^- exhibited any temporal variability.

6.3 Materials & Methods

6.4 Lysimeter Collection, Installation & Experimental Design

Lysimeters, intact soil cores (18 cm diameter by 50 cm deep), were collected from the 16th to the 18th of November 2017, from the Central Plains of Southland, New Zealand (E1225681 N4877019 NZTM). The site was a perennial ryegrass (*Lolium perenne* L.) grazed dairy pasture. Mean annual rainfall and soil temperature (10 cm depth) are 1112 mm and 9.2°C, respectively (Invercargill historical data average 1981 - 2010, NIWA (n.d)). The soil at the site was classified as a moderately deep Braxton soil, Typic Orthic Gley (New Zealand Soil Classification, Hewitt (2010)) and had a heavy silt loam to silty clay texture, with topsoil clay reported to range from 22 to 30%, with some gravels at 45 to 90 cm (CropsSouthland, 2002).

Soil chemical and textural properties were determined by taking representative soil samples from each soil horizon (Appendix A, Tables A.1 and A.2). Soil from both horizons (A horizon 0 – 25 cm, B horizon 25 – 40 cm) was collected over a 5 cm by 5 cm area from the top of the horizon to the bottom. Soil was then sieved to 2 mm, air dried, then sampled to allow for a representative analysis of the horizons chemical and physical properties. The A horizon contains a higher proportion of finer particles, with higher percentages of clay and silt (25 and 35%, respectively) than found in the B horizon (17 and 28%, respectively), which is dominated by sand (54%).

Sections of PVC pipe, fitted with an annular cutting ring, were placed on the soil surface and then the surrounding soil was methodically cut away as the PVC pipe was slowly lowered around the intact soil profile to create the lysimeters (Cameron et al., 1992; Woods et al., 2016). Molten Vaseline was then carefully injected into the annular gap between the soil and the PVC pipe to prevent bypass flow. The

lysimeters were then transported to Lincoln University and placed into a lysimeter trench where they were positioned flush with the soil surface. The bottom 2 cm of soil was removed and replaced with gravel. Then PVC caps were fitted with a drainage outlet and connected to the lysimeter bases. Drainage was collected in 5 L containers.

A factorial experimental design comprised of two levels of plants (present (P) or absent (no-plants, NP)) and three levels of BU (0, 300 and 700 kg N ha^{-1}), with each treatment replicated four times, giving a total of 24 lysimeters.

Irrigation was applied to the lysimeters at a maintenance rate of 21.3 mm every 3 days, from December 2016 to 23rd January 2017, where after they received simulated rainfall from an automated irrigation system using a spray nozzle (Tee Jet FL-5VC) mounted directly over the lysimeters until the 2nd of November 2017. Irrigation simulation was equal to the 75th percentile of rainfall received at Drummond in the Central Plains area, Southland. This was calculated using historical weather data from New Zealand's National Institute of Water and Atmospheric Research (NIWA) for the last 10 years.

To establish uniform plant treatments in the lysimeters the existing herbage was first sprayed off with glyphosate (2 L ha^{-1}) on 1st of February 2017. Then, in all lysimeters, the senesced plant material was removed. On the 1st of March, perennial ryegrass (cultivar: Base AR37) was sown into those lysimeters designated to have plants present. Urea fertiliser (20 kg N ha^{-1}; 140 g N $lysimeter^{-1}$) was applied to all lysimeters on the 3rd of April to stimulate plant establishment. Bovine urine was collected from Friesian-Jersey-cross cows grazing perennial ryegrass pasture, during the Lincoln University Research Dairy Farm's afternoon milking. First, the BU-N content was measured (6 g N L^{-1}) using a Sercon (Crewe, UK) GSL elemental analyser while the $\delta^{15}N$ value was determined (-0.81‰$_{N2AIR}$) using a Sercon 20-20 continuous flow isotope ratio mass spectrometer (CF-IRMS) and normalised to the international reference IAEA-N1. Bovine urine treatments were applied to the lysimeters on the 28th of April. The volume of BU required was determined based on the N concentration and was applied directly to the corresponding lysimeters. The 700 kg N ha^{-1} equivalent treatments received 30 mL of BU-N (1781 mg N) and the 300 kg N ha^{-1} equivalent treatments received 13 mL of BU-N (763 mg N).

6.5 Leachate Sample Collection & Chemical Analyses

Leachate from the lysimeters was collected at approximately fortnightly intervals from the 29th of March until the 2nd of November, more frequently if a heavy rainfall had occurred, and sampling for $\delta^{15}N\text{-}NO_3^-$ and $\delta^{18}O\text{-}NO_3^-$ commenced on the 20th of April. Total leachate volumes from the lysimeters were measured and then collected in 50 mL sample bottles, two bottles were collected at each sampling date whenever possible. Sample bottles were rinsed three times with leachate and then

filled. Leachate sub-samples for isotope analysis had 0.5 mL of 11.6 M HCl and 1 mM of sulfanilic acid added per 50 mL of sample and these were then frozen until analysis.

Analysis of leachate mineral N (NO_3^-, NH_4^+ and NO_2^- concentrations) were measured on an Alpkem FS3000 twin channel Flow Injection Analyser. Total C (organic and inorganic) concentrations in the leachate were analysed on a Shimadzu TOC-5000A fitted with an ASI-5000A auto sampler.

Measurements of leachate NO_3^- $\delta^{15}N$ and $\delta^{18}O$ were performed at the National Isotope Laboratory, Geological and Nuclear Science, Wellington, New Zealand, using the cadmium-azide method (McIlvin et al., 2005). Isotope values were analysed using a GVI Isoprime coupled with an AquaPrep for water samples. The reference standard used for $\delta^{18}O$ analyses was VSMOW for waters (Vienna Standard Mean Ocean Water, absolute isotope ratio (2005.20 ± 0.45) x 10^{-6} (Baertschi, 1976), with a measurement precision of 0.1‰. The reference standard used for $\delta^{15}N$ analyses was Air (atmospheric N gas, absolute isotope ratio (3676 ± 4) x 10^{-6} (Coplen et al., 1992; Junk et al., 1958), with precision of 0.3‰. All isotope results are reported in δ‰.

The $\delta^{15}N$ composition of the BU treatment input was determined by pipetting two replicate 5 mL aliquots into tin capsules filled with Chromosorb W (Supelco, Bellefonte, PA; Cheng et al. (2011)). The $\delta^{15}N$ composition of the soil was determined on air dried and sieved (< 2 mm) soil with visible organic material removed on the CF-IRMS. To determine the effect of urine-affected and non-urine affected soil on the isotopic signature of NO_3^- a standard two-pool isotope mixing model was used (Fry, 2007).

6.5.1 Statistical Analyses

Data were analysed using Minitab® (Minitab®18.1.0.0 2018) with analysis of variance conducted using the General Linear Model to allow for repeated measures. Date, plant treatment, and BU rate were fixed factors while date, BU rate, plant treatment, date x BU rate, date x plant treatment, and BU rate x plant treatment comprised the terms in the model. Variables analysed included drainage volumes, total N leached; NH_4^+, NO_2^- and NO_3^-, total inorganic and organic C leached, NO_3^- isotopes composition; $\delta^{15}N$ and $\delta^{18}O$.

6.6 Results

6.6.1 Climate Overview

Daily air temperature averaged over the experimental period (1.3.2017 to 2.11.2017) was 9.3°C, with a maximum of 19.9°C in March and a minimum of 1.4°C in July (Figure 6.1). Mean daily soil temperature (10 cm depth) ranged from 20.5°C to 4.2°C (Figure 6.1). Cumulative water input for the experimental period was 916 mm, comprising 244 mm from irrigation and 673 mm from rainfall (Figure 6.2).

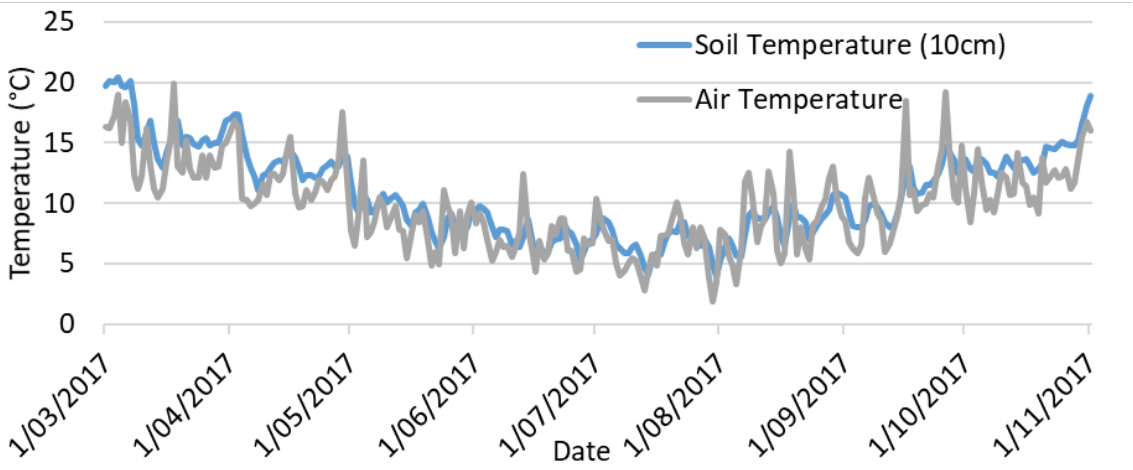

Figure 6.1**: Average daily air temperature and soil temperature (10 cm depth) at the lysimeter site in Lincoln, New Zealand.**

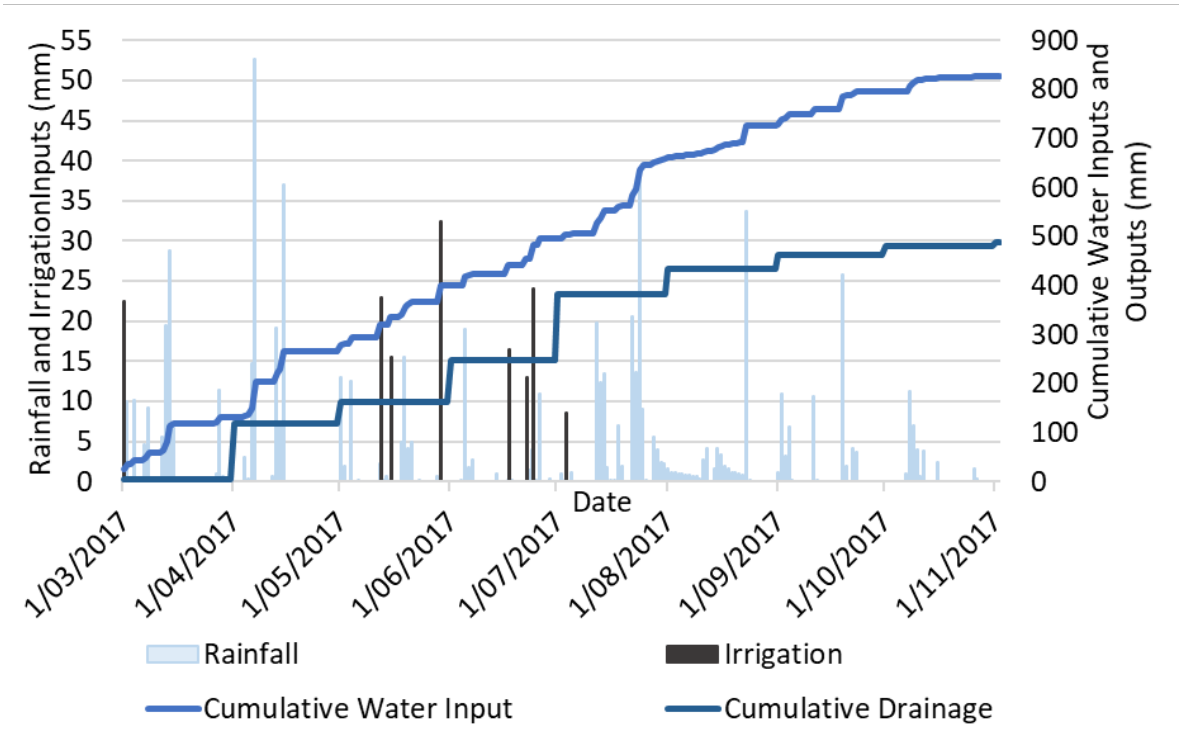

Figure 6.2: Cumulative and daily rainfall and irrigation inputs at the lysimeter site, Lincoln, New Zealand.

6.6.2 Lysimeter Leachate Volumes

Season had a significant effect on drainage volumes when averaged across treatments (Figure 6.3a) with higher drainage volumes ($P < 0.001$) in winter 270 ± 21 mm (June - August), and lower drainage volumes ($P < 0.001$) in spring 47 ± 6 mm (September - November). The NP treatment resulted in greater cumulative ($P < 0.05$) drainage than when plants were present: 539 ± 29 mm and 420 ± 47 mm, respectively (Figure 6.3b). Cumulative drainage was not affected by BU rate.

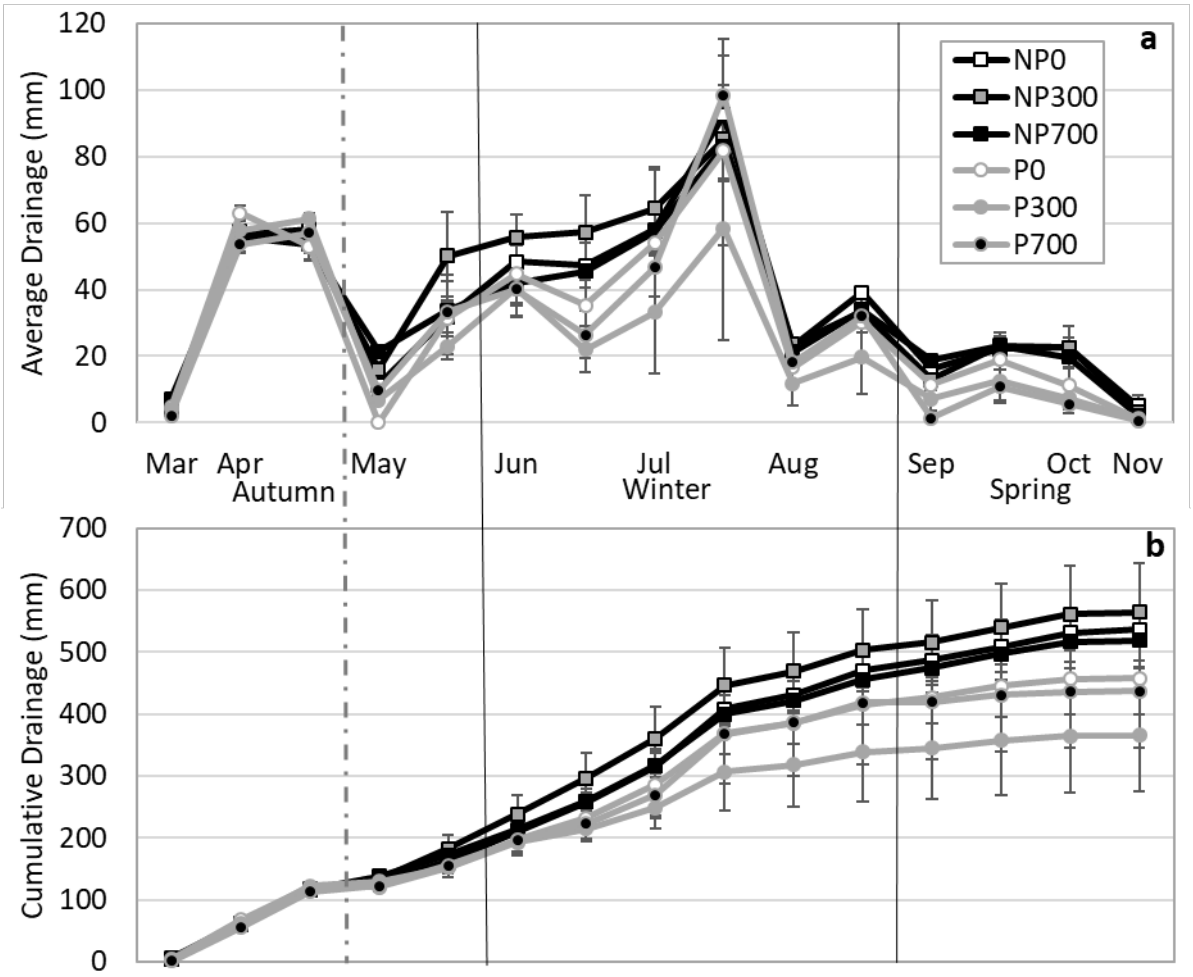

Figure 6.3: Sampling drainage (a) and cumulative drainage averages (b) of the lysimeters from the 29/3/2017 until 2/11/2017. Points represent the mean ± SEM (n = 4) drainage volumes (mm). Dotted line indicates time of BU treatment application.

6.6.3 Leachate Chemistry

Ammonium concentrations ranged from 0.1 to 1.81 mg L^{-1}, with an average of 0.17 mg L^{-1} across all treatments for the trial period. Nitrite concentrations peaked at 1.5 mg L^{-1} and averaged 0.07 mg L^{-1}.

Peak NO_3^--N leachate concentrations occurred over the winter season (Figure 6.4a). As the BU rate of N applied increased, the peak NO_3^--N concentrations in the leachate increased accordingly, peaking at concentrations of 13.6, 81.0 and 192.0 mg L^{-1} for the 0, 300 and 700 BU treatments, respectively, when averaged across the NP treatments (Figure 6.4a). Thus, more NO_3^--N was leached in winter ($P < 0.001$) with totals, averaged over all treatments, for winter, autumn (March - May) and spring of 93.3, 10.4 and 5.5 kg ha^{-1}, respectively (Figure 6.4b). Less NO_3^--N ($P < 0.001$) was leached with plants present, compared to NP, with cumulative NO_3^--N losses equal to 33 kg N ha^{-1} and 186 kg N ha^{-1}, respectively, when averaged across all BU treatments (Figure 6.4b). Within individual BU treatments, the 700-BU treatment leached more N ($P < 0.001$) than the BU-0 treatment in both winter and spring, when averaged across plant treatment. There was a significant interaction ($P < 0.01$) between the BU and

plant treatments, with leaching of N increasing at a greater rate in the NP as the BU-N rate increased, ranging from 28 to 375 kg N ha^{-1} under the NP-0 to NP-700 treatments, respectively, and from 2 to 93 kg N ha^{-1} under the P-0 to P-700 treatments, respectively (Figure 6.4b).

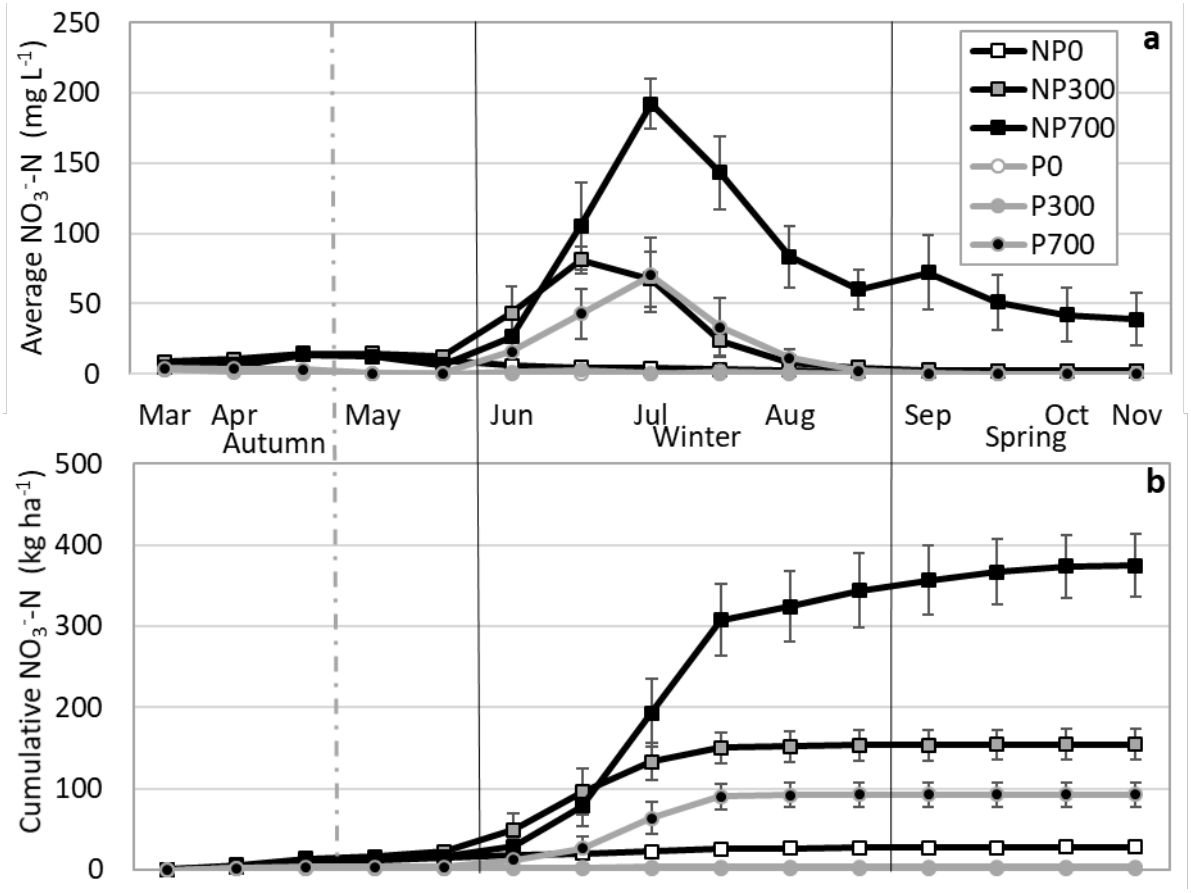

Figure 6.4: (a) Average NO_3^--N concentration (mg L^{-1}) in leachate from lysimeters from March to November 2017, (b) cumulative NO_3^--N (kg ha^{-1}) over trial period. Treatment codes in key; NP: No Plants. P: Plants. Three rates of BU kg N ha^{-1} equivalent; 0, 300 and 700. Data points are means ± SEM (n = 4). Dotted line indicates time of BU treatment application.

Total C (organic and inorganic) concentrations ranged from 11 to 39 mg L^{-1}, and averaged 20 mg L^{-1} across all treatments for the trial period with, on average, 75% as inorganic C and 25% as organic C. Total C concentrations in leachate peaked in spring (Figure 6.5). There were no significant treatment effects on total organic C found over the trial period.

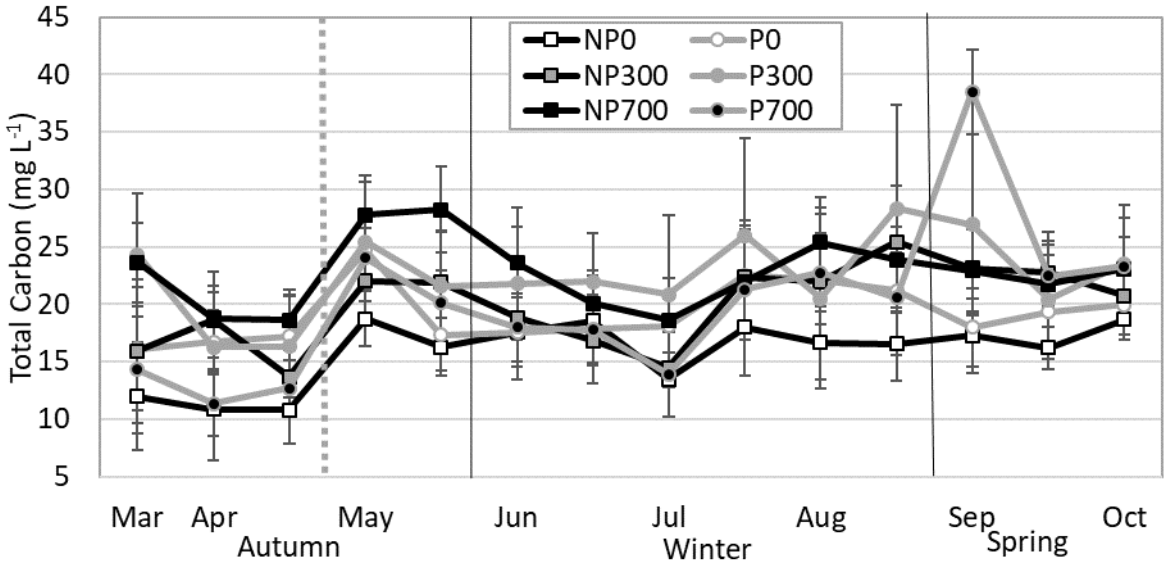

Figure 6.5: Total carbon (mg L^{-1}) in leachate from lysimeters from March to November 2017. Data points shown are sampling averages for each treatment at a collection event. Treatment codes in key; NP: No Plants. P: Plants. Three rates of kg N ha^{-1} equivalent, 0, 300 and 700 kg N ha^{-1}. Dotted line indicates time of BU treatment application.

6.6.4 Isotope Signatures of NO_3^-

Mean soil $\delta^{15}N$ (‰ v. AIR) values prior to treatment application were +4.55‰ ± 0.04‰ and +7.16‰ ± 0.28‰ for the A and B horizons, respectively (mean value ± SE, n = 6). The BU applied had a mean $\delta^{15}N$ value (‰ v. AIR) of -0.81‰ ± 0.06‰ (n = 6). Nitrate isotope composition of leachate, prior to treatment application, ranged from +2.80‰ to +6.54‰ for $\delta^{15}N\text{-}NO_3^-$ (mean: +5.09 ± 0.60‰) and from -1.84‰ to +3.63‰ for $\delta^{18}O\text{-}NO_3^-$ (mean: -0.2 ± 0.89‰).

The leachate $\delta^{18}O\text{-}NO_3^-$ values did not differ over time due to sampling date or plant treatments (Figure 6.6a). However, $\delta^{18}O\text{-}NO_3^-$ values were affected by BU rate, and when averaged over the plant treatments and time the $\delta^{18}O\text{-}NO_3^-$ values in the 300 and 700 kg N ha^{-1} rates (+4.02, and +4.13‰, respectively) were higher ($P < 0.001$) than in the 0 kg N ha^{-1} rate (0.02‰). An interaction ($P = 0.05$) between sampling date and BU rate ($P = 0.05$) also occurred, with a lower $\delta^{18}O\text{-}NO_3^-$ value on the 22nd June under the 0 kg N ha^{-1} treatment (-3.83‰) than on either the 22nd June, 10th July or 24th July under the 300 kg N ha^{-1} treatment, or the 24th July and 28th August under the 700 kg N ha^{-1} treatment, where $\delta^{18}O\text{-}NO_3^-$ values on these dates ranged from +0.28 to +6.07‰ when averaged across plant treatments (Figure 6.6a, Table 6.1).

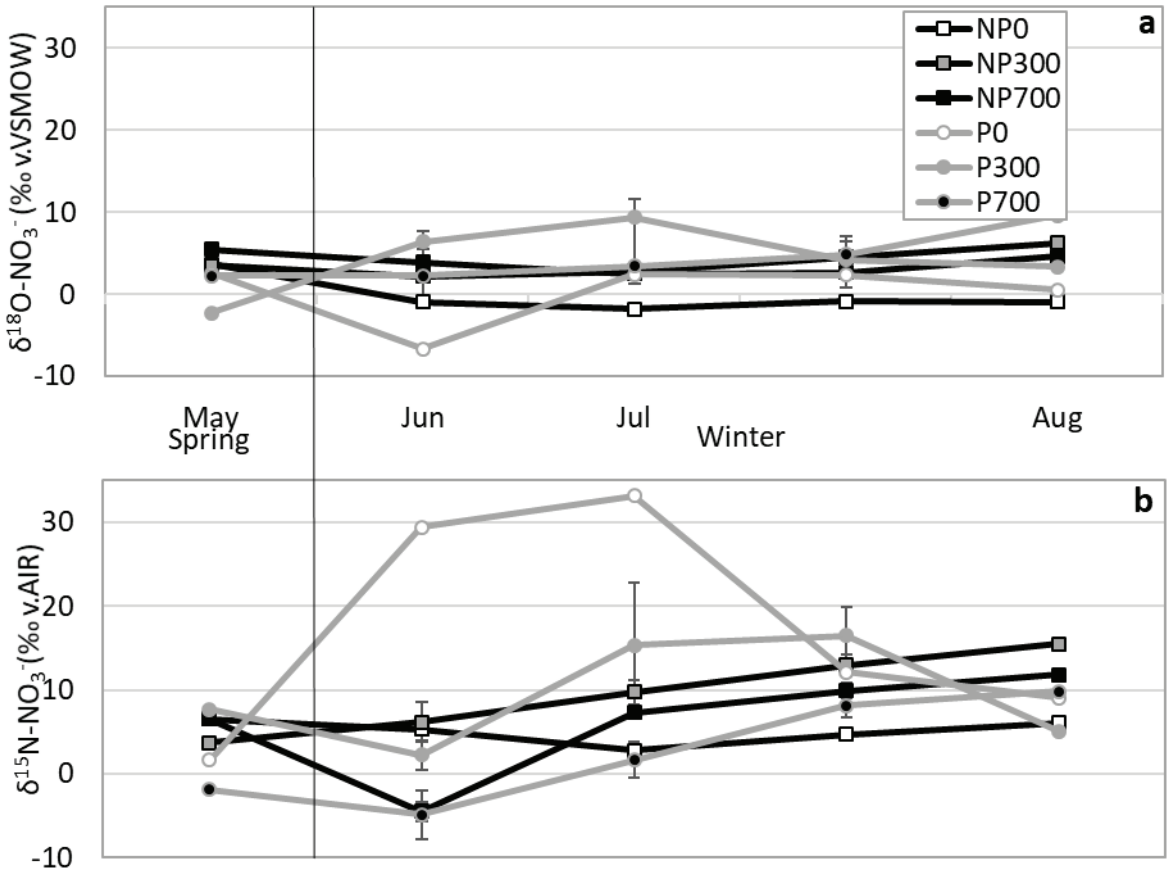

Figure 6.6: Mean NO_3^- isotopic composition $\delta^{18}O\text{-}NO_3^-$ (a) and $\delta^{18}O\text{-}NO_3^-$ (b) in leachate from lysimeters containing the Braxton soil from the Central Plains area in Southland, New Zealand. Points represent the mean (± SEM) isotope values (‰). *n* = 4 when error bars are present, when SEM is absent, points represent bulked sample average of 4 replicates. Leachate were sampled in 2017 winter season (date range shown: 17.5.17, 22.6.17, 10.7.17, 24.7.17, 28.8.17). Treatment codes in key; NP: No Plants. P: Plants. Three BU rates of kg N ha^{-1} equivalent, 0, 300 and 700 kg N ha^{-1}. Bovine urine was applied on the 28th of April 2017.

Table 6.1: Leachate $\delta^{18}O\text{-}NO_3^-$ values (‰ v.VSMOW) for the 'BU rate x time' interaction with values averaged over plant treatment. Subscripts are Tukey's pairwise comparisons for a 95% confidence interval.

Date (2017)	Bovine Urine N Rate		
	0 kg N ha^{-1}	300 kg N ha^{-1}	700 kg N ha^{-1}
17th May	$+3.10_{AB}$	$+0.62_{AB}$	$+3.83_{AB}$
22nd June	-3.83_{B}	$+4.28_{A}$	$+3.06_{AB}$
10th July	$+0.28_{A}$	$+6.07_{A}$	$+2.96_{AB}$
24th July	$+0.75_{AB}$	$+4.37_{A}$	$+3.72_{A}$
28th August	-0.21_{AB}	$+4.78_{AB}$	$+7.06_{A}$

In the presence of plants $\delta^{15}N\text{-}NO_3^-$ equalled +9.93‰, when averaged across BU treatments and over time, and this was higher (P = 0.04) than NP, where $\delta^{15}N\text{-}NO_3^-$ equalled +6.56‰ (Figure 6.6b, Figure 6.7). With BU rates of 0, 300, and 700 the $\delta^{15}N\text{-}NO_3^-$ values, when averaged across plant treatments and over time, equalled +11.08, +9.45, +4.20‰, respectively, with the value at BU-700 lower that in the BU-0 (P = 0.012) and the BU-300 treatment (P = 0.027), which did not differ from each other (P =

0.75). When averaged across all treatments the date of leachate sampling had no effect on $\delta^{15}N\text{-}NO_3^-$ values. When averaged over time there was a plant treatment x BU rate interaction (P = 0.024): at the BU rate of 700 kg N ha^{-1}, with or without plants, the $\delta^{15}N\text{-}NO_3^-$ values were lower than in the plant treatment at 0 kg N ha^{-1} ($P \leq 0.01$); while in the absence of plants $\delta^{15}N\text{-}NO_3^-$ values were also lower (P = 0.02) than NP at 0 kg N ha^{-1} (Figure 6.6b, Table 6.2). There was also an interaction (P = 0.024) between date of sampling and the BU rate applied (Table 6.3) with $\delta^{15}N\text{-}NO_3^-$ values, averaged over plant treatments, recorded on: 22nd June and 10th July in the BU-0 treatment (+17.35 and +17.96‰, respectively), 10th July and 24th July in the BU-300 treatment (+12.53 and +14.51‰, respectively), and 24th July in the BU-700 treatment (+9.01‰), all higher than the value measured on the 22nd June in the BU-700 treatment (-4.67‰).

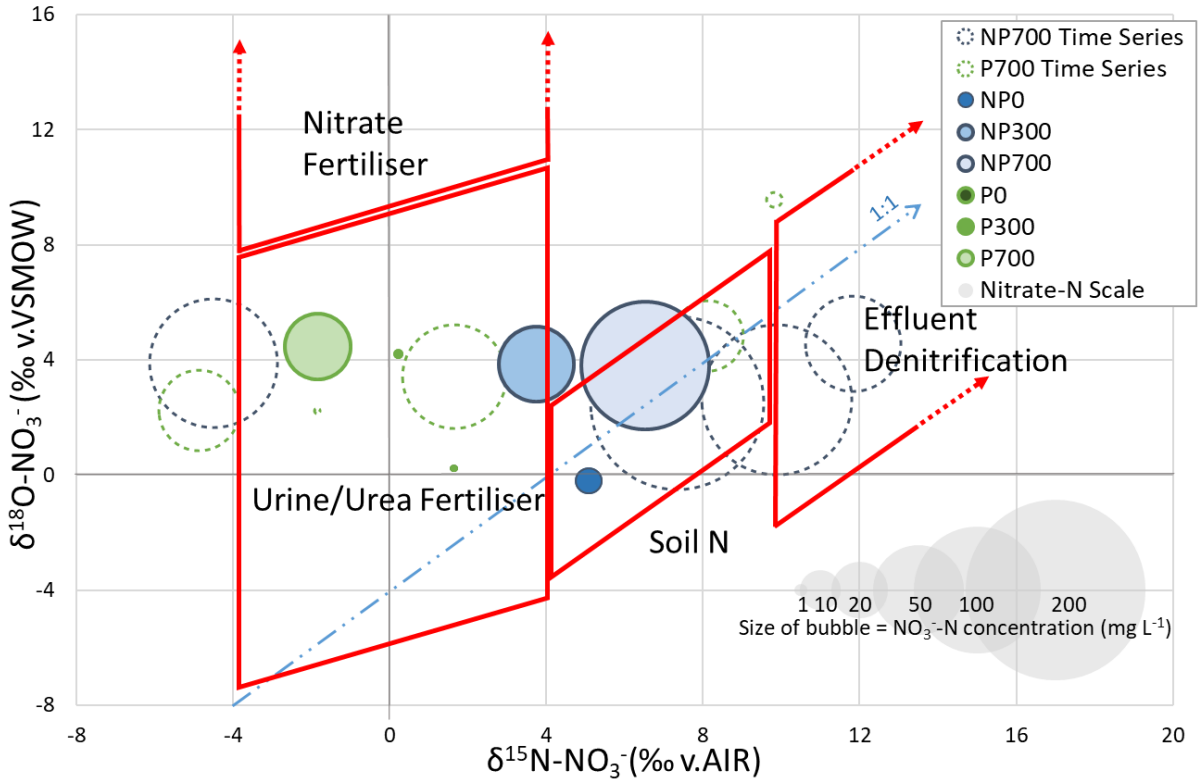

Figure 6.7: The isotopic composition of lysimeter leachate $\delta^{18}O\text{-}NO_3^-$ (y-axis) and $\delta^{18}O\text{-}NO_3^-$ (x-axis): weighted $\delta^{15}N\text{-}NO_3^-$ average of the six experimental treatments; no plants (NP) and plants (P), by three rates of cow urine 0, 300, 700 kg N ha^{-1}, weighted by NO_3^- mass. Dashed circles indicate time scale of NP700 and P700 timescale over 5 sampling points from the 17th of May to the 28th of August 2017. Size of circle indicates the corresponding NO_3^- (mg L^{-1}) concentration, scale bottom right corner. Red parallelograms represent ranges presented by Baisden et al. (2016a) based on a board range of research across New Zealand agricultural systems.

Table 6.2: Leachate $\delta^{15}N\text{-}NO_3^-$ values (‰ v. AIR) for the 'plant x BU rate' interaction with values averages over time. Subscripts are Tukey's pairwise comparisons for 95% confidence interval. *n* = sample size.

Plant Treatment	Bovine Urine N Rate		
	0 kg N ha^{-1}	300 kg N ha^{-1}	700 kg N ha^{-1}

Plants	$+17.08_{A}$ $n = 5$	$+9.71_{AB}$ $n = 12$	$+3.00_{B}$ $n = 14$
No Plants	$+5.09_{B}$ $n = 5$	$+9.19_{AB}$ $n = 13$	$+5.41_{B}$ $n = 11$

Table 6.3: Leachate $\delta^{15}N\text{-}NO_3^-$ values (‰ v.AIR) for the 'BU rate x time' interaction with values averaged over plant treatment. Subscripts are Tukey's pairwise comparisons for a 95% confidence interval.

Date (2017)	Bovine Urine N Rate		
	0 kg N ha^{-1}	**300 kg N ha^{-1}**	**700 kg N ha^{-1}**
17th May	$+4.10_{AB}$	$+5.71_{AB}$	$+2.35_{AB}$
22nd June	$+17.35_{A}$	$+4.22_{AB}$	-4.67_{B}
10th July	$+17.96_{A}$	$+12.53_{A}$	$+3.51_{AB}$
24th July	$+8.43_{AB}$	$+14.51_{A}$	$+9.01_{A}$
28th August	$+7.58_{AB}$	$+10.26_{AB}$	$+10.83_{AB}$

There was no correlation between $\delta^{15}N\text{-}NO_3^-$ and $\delta^{18}O\text{-}NO_3^-$ ($r = 0.12$, $P = 0.36$) if all data were pooled over time. However, on the 24th of July, there was a correlation between $\delta^{15}N\text{-}NO_3^-$ and $\delta^{18}O\text{-}NO_3^-$ ($r = 0.63$, $P = 0.007$) but this relationship was not significant by 28th August ($r = 0.52$, $P = 0.29$). Values of $\delta^{15}N\text{-}NO_3^-$ aligned with those previously reported for pasture soils (-10 to +10‰ $\delta^{15}N\text{-}NO_3^-$, Granger et al., 2008; Rock et al., 2011) and manures (0 to +25‰ $\delta^{15}N\text{-}NO_3^-$, Kendall et al., 2007).

6.7 Discussion

6.7.1 Leachate NO_3^- Concentrations & N Loss

The low NO_3^- concentrations (< 25 mg N L^{-1}) observed in April and May are likely derived from mineralised organic matter (Cameron et al., 2013). Subsequent increases in leachate NO_3^- concentration resulted from BU application. Typically, leachate NO_3^- concentrations peak 1 – 3 months after urine application (Buckthought et al., 2015b; Cameron et al., 2013; Clough et al., 1996; Di & Cameron, 2007) with time differences due to varying rates of nitrification and drainage. Typically, autumn urine deposition results in winter NO_3^- leaching (Buckthought et al., 2015b). Consistent with this, peak NO_3^- concentrations in the current study occurred 2 – 3 months after BU application, or soon after one pore volume of drainage had occurred (ca. 250 mm of drainage).

The leachate NO_3^- concentrations were lower when plants were present due to plant N uptake which reduced the pool of soil NO_3^- available for leaching (Moir et al., 2007; Moir et al., 2016). However, BU deposition rates typically exceed a pasture's ability to take up N and so NO_3^- leaching increases as BU-N rates increase, as observed in the current study. However, this effect was exacerbated in the NP: NO_3^- leaching losses were negligible with plants present at a BU rate ≤ 300 kg N ha^{-1}, but without plants present, N losses were significant at all rates of urine. The average recorded N leaching losses (33 - 186 kg NO_3^--N ha^{-1}) for treatments with and without plants are within ranges previously reported for grazed pastures: urine N application rates of 0 – 750 kg N ha^{-1} resulted in NO_3^- leaching losses of 11 - 162 kg N

ha^{-1} (Cameron et al., 2013) and 1 - 183 kg N ha^{-1} (Moir et al., 2013), with losses dependent on both N rate, stocking rate, feed quality, pasture type and soil texture effects.

Thus, pastoral grazing systems with BU-N loading rates of ~300 kg N ha^{-1} (Di et al., 2007) have minimal N leaching losses even in areas without plants present (< 50 kg N ha^{-1}). However, under higher BU loading rates, e.g. 700 to 1000 kg N ha^{-1} (Moir et al., 2011), leaching losses of N will be substantially higher. Thus, in addition to isotopic signatures a knowledge of stock type, stocking rate and management practices within a catchment could provide an initial basis for identifying potential NO_3^- leaching sources.

6.7.2 Nitrate Isotopes

Ruminant urine-N exists predominately as urea (Selbie et al., 2015). Urea deposited onto a pasture soil surface is rapidly hydrolysed to NH_4^+ and bicarbonate ions (HCO_3^-), and the ensuing hydrolysis of HCO_3^- results in an elevated soil pH which drives the equilibrium between NH_4^+ and NH_3 in favour of NH_3 (Sherlock & Goh, 1984). The ^{15}N fractionation associated with NH_3 volatilisation was previously thought to strongly determine the resulting isotopic signature of the leached NO_3^- (Frank et al., 2004; Heaton, 1986). However, Wells et al. (2015) showed this not to be the case: despite NH_3 volatilisation removing 5 - 40% of ruminant urine (80 - 600 kg N ha^{-1}) or urea (80 kg N ha^{-1}) N inputs the predicted ^{15}N enrichment of the soil inorganic N pool, at 0 - 10 cm depth, did not occur due to the greater influence of ongoing soil mineralisation and nitrification processes. In the current study there was a period of rainfall (> 20 mm) commencing 3 days after BU deposition which, along with the relatively cool soil temperatures, would have reduced any NH_3 volatilisation that may have been occurring (Sherlock et al., 1984). Hence, in the current study, NH_3 volatilisation did not significantly predicate the isotopic composition of the NO_3^- subsequently leached.

In a laboratory study using 38 non-legume plant species and nutrient solutions (Mariotti et al., 1980b) found that the discrimination against ^{15}N, due to the uptake of NO_3^-, was low ranging from -2.2 to +0.6‰. While Mariotti et al. (1982) found evidence for plant ^{15}N fractionation at the NO_3^- reductase step, with increasing variation in plant tissue $\delta^{15}N$ values as the ratio of substrate supply (NO_3^-) to plant enzyme (NO_3^- reductase) increased (Högberg, 1997; Mariotti et al., 1982). Most of these prior studies examined the potential for ^{15}N fractionation based upon N assimilation dynamics, without measuring the soil $\delta^{15}N$-NO_3^- pools. It is generally thought that plant root uptake of soil NO_3^- and returned root exudates do not discriminate against plant ^{15}N composition (Cernusak et al., 2009; Comstock, 2001) and thus presumably the soil $\delta^{15}N$- NO_3^- signal. In the current study, the observed effect of plants on leached $\delta^{15}N$-NO_3^- values, averaged over time and BU rate, was to elevate $\delta^{15}N$-NO_3^-. However, closer inspection reveals that this effect was the result of significant $\delta^{15}N$-NO_3^- enrichment in the planted BU-0 treatment (Fig. 6.6b) which had extremely low NO_3^- concentrations (< 1 mg L^{-1}), on two sampling

dates. Interestingly, this was not observed in the NP treatment. This suggests that denitrification may have been driven by a plant derived C supply, such as root exudation, that made a significant impact on $\delta^{15}N\text{-}NO_3^-$ at very low soil NO_3^- concentrations. The absence of elevated $\delta^{15}N\text{-}NO_3^-$ values following BU application in the 'plant' and NP treatments leads us to conclude that plants have a negligible effect on leachate $\delta^{15}N\text{-}NO_3^-$ values.

Thus, given the assumptions above, the $\delta^{15}N\text{-}NO_3^-$ signature of the leached NO_3^- should reflect either (i) the original BU-N, (ii) the soil-N or (iii) be a composite of the N source and the subsequent N fractionating pathways such as nitrification and denitrification, or a combination of these.

Leachate $\delta^{15}N\text{-}NO_3^-$ values ranged from -4.9‰ to +33.1‰ with the higher values occurring in the BU-0 plant treatment as discussed above. On the 17th of May, the leachate $\delta^{15}N\text{-}NO_3^-$ values (+2.35 to +5.71‰) align well with the soil $\delta^{15}N\text{-}NO_3^-$ values (+5.55 to +7.16‰) which, in conjunction with the relatively low concentration of NO_3^- in the leachate at this time, strongly indicates that regardless of the BU treatment leached NO_3^- was predominantly derived from the soil-N pool with BU derived N yet to be leached. By early winter (June 22nd) approximately one pore volume of drainage had eluted resulting in the release of the highly enriched NO_3^- in the BU-0 treatment, albeit at a very low concentration, while higher NO_3^- concentrations occurred under the BU-300 and BU-700 treatments. Under the BU-300 treatment the $\delta^{15}N\text{-}NO_3^-$ values remained unchanged from the 17th May, while under the BU-700 rate there was a shift to a negative $\delta^{15}N\text{-}NO_3^-$, a value more depleted than in the BU applied. This may have been the result of nitrification being incomplete prior to leaching occurring. Nitrification causes fractionation as the substrate (NH_4^+) is nitrified to NO_2^- and NO_3^-. The oxidation of NH_4^+ to NO_2^- creates a depleted product pool (Mariotti et al., 1981) while the oxidation of NO_2^- to NO_3^- may result in an inverse kinetic isotopic fractionation (Casciotti, 2009). In a closed system (no product removal) the product pool ultimately attains a $\delta^{15}N\text{-}NO_3^-$ value consistent with that of the initial NH_4^+ pool. If NO_3^- is progressively removed by leaching prior to complete nitrification occurring, then depleted $\delta^{15}N\text{-}NO_3^-$ values may be observed in the leachate. An in-situ study, with a similar rate of BU-N (865 kg N ha^{-1}) and pasture soil temperatures, found that NO_3^- formation took approximately one week to commence and that complete nitrification of the NH_4^+ pool took ca. 30 days (Clough et al., 2009). Thus, while not statistically different from the May result, the shift to a negative $\delta^{15}N\text{-}NO_3^-$ value in the leachate under the BU-700 rate indicates that, under the higher N loading rate, movement of the nitrification product (NO_3^-) down the soil profile had commenced prior to complete nitrification of the substrate (NH_4^+). This was likely due to the rainfall events that occurred within the first two weeks of the study. Such an effect was most likely not seen under the BU-300 treatment due to both a greater proportion of the BU-N being taken up by plants and because the ammonia oxidising bacteria, which dominate nitrification within ruminant urine patches (Di et al., 2009), were less likely to be inhibited by NH_3 at the lower BU rate applied (Venterea et al., 2015).

The BU-300 and BU-700 leachate $\delta^{15}N\text{-}NO_3^-$ values peaked on the 24th of July and 28th August, respectively, coinciding with peak NO_3^- concentrations in the case of the BU-300 treatment. While these temporal changes in the leachate $\delta^{15}N\text{-}NO_3^-$ values were only statistically different for a few of the possible 'treatment x time' comparisons (Table 6.2) the trend of increasing values indicates that the $\delta^{15}N\text{-}NO_3^-$ values were not simply the product of direct contributions from the BU-N and soil-N pools, which would have resulted in lower $\delta^{15}N\text{-}NO_3^-$ values. Instead $\delta^{15}N\text{-}NO_3^-$ values demonstrate that $\delta^{15}N\text{-}NO_3^-$ enrichment had occurred, and that the likely cause was denitrification.

Denitrification occurs in anoxic zones within the soil profile. It is well recognized that kinetic fractionation results in the substrate (NO_3^-) becoming enriched in ^{15}N as the denitrification products (N_2O and/or N_2) are evolved (Granger et al., 2008; Granger et al., 2004). However, the displacement of NO_3^- via leaching potentially provides another mechanism for further fractionation. Following BU deposition the soil NO_3^- pool evolved does not follow classical 'piston flow' when leached, instead it is dispersed vertically within the soil profile during leaching, predominantly due to convection and diffusion (Cameron et al., 1986). Despite soil microbial populations being higher in the surface soil (Fierer et al., 2003b), the high soil NO_3^- concentrations that occur under BU deposition will initially saturate the microbial denitrifier community. Thus, a BU derived soil NO_3^- pool is likely to leach prior to being fully denitrified. When leaching down the profile occurs the rates of denitrification will also be less due to both; microbial biomass declining exponentially with depth (Fierer et al., 2003b) and declining microbial C availability with depth (Kelliher et al., 2015). If the NO_3^- pool is progressively denitrified as it leaches down the soil profile it will become increasingly enriched. Thus, it might be expected that the leachate $\delta^{15}N\text{-}NO_3^-$ values become progressively enriched with increasing depth. Such an effect explains the high leachate $\delta^{15}N\text{-}NO_3^-$ values observed in the BU-0 treatment, discussed above, and where the NO_3^- source is thought to have come from mineralised soil-N. In this instance the initial substrate concentration was able to be almost completely denitrified by the microbial pool over the depth of the soil profile leached. The positive correlation between the $\delta^{15}N\text{-}NO_3^-$ and $\delta^{18}O\text{-}NO_3^-$ values on 24th July, the period of peak leaching, provides further evidence for denitrification occurring in the BU treatments since both $\delta^{15}N\text{-}NO_3^-$ and $\delta^{18}O\text{-}NO_3^-$ are enriched in parallel during denitrification (Granger et al., 2008).

The influence of the observed temporal variation to affect catchment $\delta^{15}N\text{-}NO_3^-$ and $\delta^{18}O\text{-}NO_3^-$ values will depend on many factors such as stocking rate (area of pasture covered by BU), N excretion rate (stock class and feed type), and water inputs. But if it is assumed, as in the current study, that 420 mm of drainage occurs and 5% of the pasture is affected by urine, and that BU-affected leachate has an average NO_3^--N loading of 25 mg L^{-1} and non-BU-affected leachate has an average NO_3^--N loading of 1 mg L^{-1}, with $\delta^{15}N$ values of +15 and +5‰, respectively, then, using a two pool mixing model (Fry, 2007), the average $\delta^{15}N$ of the mixed drainage water would be +10.7‰. This value clearly increases as the

area of pasture covered by urine varies: 3 or 7% urine coverage results in $\delta^{15}N$ values of +9.3 and +11.5‰, respectively. Using the same mixing model but with the most depleted $\delta^{15}N$ value for BU-affected leachate of -4.67, and +5‰ for non-affected leachate results in a mixed $\delta^{15}N$ values in the drainage of -1.3‰. However, such a $\delta^{15}N$ value was not sustained in the BU-affected leachate. Antecedent soil N contributions may also be seasonally variable and could in the winter season be close to zero if cool soil conditions reduce mineralisation or if plant N uptake occurs. Thus, the results highlight the need to understand the relative timing of the leaching event with respect to prior grazing event(s) and the leachate/drainage sample time.

6.8 Conclusions

An objective of this study was to assess the impact of plants and BU rate on potential temporal variability in $\delta^{15}N\text{-}NO_3^-$ and $\delta^{18}O^{-}NO_3^-$ values. Plants only altered $\delta^{15}N\text{-}NO_3^-$ when BU was not applied, and then only under very low NO_3^- concentrations. We conclude that plants have a negligible influence on leached $\delta^{15}N\text{-}NO_3^-$ values. Temporal variability in $\delta^{15}N\text{-}NO_3^-$ and $\delta^{18}O^{-}NO_3^-$ values occurred as a result of the interaction between N loading, drainage and time with (i) relatively depleted $\delta^{15}N\text{-}NO_3^-$ prior to complete nitrification of the NH_4^+ pool, as observed in the BU-700 treatment, (ii) pasture inducing strong isotopic shifts in $\delta^{15}N\text{-}NO_3^-$ for antecedent NO_3^- in the absence of any BU loading (BU-0 with plants), and (iii) an increase in $\delta^{15}N\text{-}NO_3^-$ over time due to denitrification of NO_3^- (both BU-300 and BU-700 treatments). There is the potential for BU rate to influence temporal $\delta^{15}N\text{-}NO_3^-$ dynamics as rate increases since NO_3^- leaching prior to complete nitrification or denitrification occurring is more likely. This study shows that with associated information on catchment grazing management and history to assist in interpreting data, that there is potential for $\delta^{15}N\text{-}NO_3^-$ and $\delta^{18}O^{-}NO_3^-$ signatures to be used to identify NO_3^- sources and soil processes forming and removing NO_3^-. However, further datasets are required to better understand the observed BU rate effects on the temporal dynamics of NO_3^- isotope composition. Ultimately, such information will assist in better understanding of N cycling in grazed pasture systems and allow agricultural practices to comply with best environmental guidelines.

Chapter 7

Field Trial - Spatial & Temporal Variation in N Attenuation

7.1 Introduction

Since the invention of the Haber-Bosh process in 1913, human intervention in the N cycle has had an increasing global impact (Bakken et al., 2017). Boosted N loadings have altered terrestrial and aquatic biogeochemical processes, and increased N_2O emissions to the atmosphere (Bobbink et al., 2010; Elser et al., 2009; Galloway et al., 2004; Ravishankara et al., 2009). Anthropogenic emissions of N_2O, a greenhouse gas, are associated with pasture-based agricultural systems and the deposition of ruminant urine (Selbie et al., 2015). Ruminant urine deposition also causes NO_3^- leaching, which can contaminate waterways, reducing water quality for recreation and freshwater ecosystems (Daughney et al., 2009; Galloway et al., 2015; McLaren et al., 1996; Parfitt et al., 2012). Nitrate is the main contaminant in New Zealand groundwater (Close et al., 2016). Sources of NO_3^- in groundwater can also potentially include sewage, atmospheric N deposition and fertiliser-N (Malcolm et al., 2014a). Uptake of NO_3^- by biomass such as pasture or its removal through denitrification, hereafter termed 'attenuation', is desirable, as this can reduce the amount of NO_3^- entering waterways (Clough et al., 1998a; Clough et al., 2005).

Spatial variation in N attenuation throughout the landscape makes it a difficult process to measure and model (Groffman et al., 2009). Spatial and temporal variation are difficult to measure as small areas (hot spots) and brief periods (hot moments) often account for a large proportion of the denitrification that occurs. Spatial denitrification variation is influenced by the soil's three-dimensional matrix comprised of solid, liquid and gaseous phases that receive pulsed inputs of water (and therefore changes in O_2 supply) via rainfall or irrigation, and N via fertilisers, ruminant excreta, N-fixation, and C via plant residues, excreta and root exudation (Firestone, 1982; Knowles, 1982). The main factors controlling 'hotspots' of denitrification are O_2, NO_3^- and C availability (Kraft et al., 2014; Yoon et al., 2015).

Temporal variation, or 'hot moments' of attenuation are generally associated with seasonal variation in rainfall and temperature (wetting and drying cycles), which influence the rate and quantity of soil N attenuation by promoting nitrification, followed by denitrification (Knowles, 1982; Robertson et al., 2007). For example, frequent simulated rainfall events (5 day intervals), were found to cause consistent anaerobic conditions that limited nitrification and therefore NO_3^- production and denitrification (Gu et al., 2010), whereas under prolonged dry periods (15 day intervals) nitrification was facilitated, increasing soil NO_3^- concentrations but denitrification became limited by aerobic conditions. Seasonal

variation was also found in the Waikato region of New Zealand, where higher soil solution NO_3^- concentrations were found in early winter (June and July), due to a build-up of NO_3^- in the top soil over summer, and the subsequent flush of autumn rain with the seasonal wetting up of soils (Clague et al., 2015b).

Research into the removal of NO_3^- from agricultural ecosystems is important for New Zealand agriculture as pasture systems are dominated by year-round grazing of live-stock (De Klein et al., 2006), which can detrimentally affect water quality if NO_3^- leaches (Parfitt et al., 2012; Smith et al., 1993). Southland's increased number of dairy cows and the land area associated (36% of the region is pastoral land, 8% of the national total, Ledgard (2013)) make it an important region to focus on, in terms of understanding NO_3^- attenuation within the landscape.

The Southland region experiences annual rainfall averages anywhere from 750 mm up to 7000 mm (Ledgard, 2013). However, these high rainfall areas (4000 - 7000 mm) are found on the West Coast, in the Fiordland Region, which is predominantly conservation land. Low land and coastal areas along the Southern coast experience annual rainfall from 1000 to 1250 mm year, with rainfall volumes steadily declining further inland and eastwards from Fiordland, with the Waimea basin averaging 750 mm of rainfall a year. Temperature may also limit denitrification in the Southland region which experiences temperatures below freezing in winter (June - August), especially in inland basins where frosts and snowfall are a regular occurrence during winter (Ledgard, 2013). Temperature readily effects microbial activity (Braker et al., 2010), thereby influencing the rate of N attenuation. Denitrification rate and temperature are positively correlated, with shifts in denitrifier community composition also occurring at different temperatures. Nitrous oxide production is greater at higher temperatures (Nömmik, 1956), while NO is also dominant at low temperatures (Bailey, 1976). Denitrification slows at lower temperatures but is still measurable at temperatures of 0 to 5°C (Bailey et al., 1973; Bremner et al., 1958; Ryden, 1986; Smid et al., 1976).

The Five Rivers region in Southland used in this study, is a recognised NO_3^- 'hot spot' area, displaying elevated aquifer NO_3^- concentrations (Figure 7.1). These areas generally have a greater thickness of alluvial gravels, with strongly oxidising groundwaters showing little evidence of reducing conditions (Rissmann, 2011). This indicates that the region is sensitive to NO_3^- leaching with land-use intensification a risk to groundwater quality, reinforcing the requirement for a better understanding of the spatial coverage of these sensitive areas to assess their management and to increase the understanding of how these areas might reduce the impact of NO_3^- on groundwaters.

Figure 7.1: Contoured median NO_3^--N concentrations for the northern Southland Region. Where the white/blue lines delimit regional groundwater zones. Red circle indicates study area. Maximum NO_3^--N threshold is set at 8.4 mg L^{-1} (75% of the Maximum Allowable Value (MAV) of 11.2 mg L^{-1} NO_3^--N. Taken from Rissmann (2011).

The role of O_2 in the regulation of NO and N_2O production has been difficult to explain (Bollmann et al., 1998; Khalil et al., 2004; Venterea, 2007). Oxygen is rarely measured and used as an indicator of denitrification (Linn et al., 1984a; Zhu et al., 2013). However, O_2 is one of the main controlling factors affecting the onset of denitrification and subsequent denitrification rates and products (Firestone et al., 1989). Soil gas diffusion is the main mechanism of O_2 transport in soil (Neira et al., 2015) and therefore an important influence on the potential for NO_3^- attenuation. Soil gas diffusion is influenced by soil physical properties such as soil ρ_b, texture, structure, pore size distribution and pore connectivity (Moldrup et al., 2000; Neira et al., 2015).

When comparing soils of varying ρ_b Balaine et al. (2016b) found that a soil's D_p/D_0 was better than WFPS at explaining peak fluxes in both N_2O and N_2. This was because D_p/D_0 accounted for the interactive effect of soil ρ_b and soil water content on functional pore space within the soil, that the commonly used measurement of WFPS does not account for (Farquharson et al., 2008). A study by Balaine et al. (2013) found that D_p/D_0 was a key indicator of soil N_2O emission potential, with N_2O emissions commencing as D_p/D_0 declined to ~0.02 and with maximum N_2O emissions occurring at a D_p/D_0 value of 0.006 (Figure 2.13). The N_2O fluxes were found to increase rapidly as D_p/D_0 decreased to a value of 0.006, before declining rapidly due to complete denitrification, expressed as an increase in N_2. Owens et al. (2017) also showed declining D_p/D_0 linked to enhanced N_2O emissions in a field study in Canterbury, New Zealand. Modelled D_p/D_0 has also been shown to link N_2O emissions with low D_p/D_0 values (Friedl et al., 2017). Thus, denitrification can be expected to be occurring when D_p/D_0 values are below ~0.02 and peaking at around 0.006.

Changes in NO_3^- source can influence N attenuation, changing available substrate, as well as becoming a problem for policy and management. Stable isotopes potentially provide a way to trace natural element cycling, acting as 'natural dyes' that can be followed through natural systems (Fry, 2007). The isotopic composition of NO_3^- ($\delta^{15}N/^{14}N‰$ and $\delta^{18}O/^{16}O‰$) can provide an indication of either sources or sinks of N in the landscape (Austin et al., 1998; Heaton, 1986), as biogeochemical processes distribute them in predictable unequal ratios across the landscape (Kendall, 1998; Seiler, 2005; Widory et al., 2004). Kinetic fractionation of isotopes during biogeochemical processing causes this unequal distribution, as heavy isotopes have a slower reaction rate than light isotopes (Kendall et al., 1998).

Distinguishable ratios of the dominant N isotopes potentially allow for the identification of the NO_3^- source (Liu et al., 2006). Precipitation (atmospheric deposition), fertilisers, soil N, sewage and manures are the major NO_3^- sources that have been well documented in terms of their NO_3^- isotopic compositions and respective ranges (Figure 2.14, Fischer (2014)). Synthetic N fertilisers have a low $\delta^{15}N$ (~0‰) and a high $\delta^{18}O$ (~+20‰), sitting to the left on the $\delta^{15}N$ and $\delta^{18}O$-NO_3^- cross plot, while NO_3^- that has been partially denitrified sits to the right, increasing in the enrichment of N and O isotopes along a slope of 2:1 or 1:1. Nitrate leached from under pastoral agriculture originates from a mixture of urea fertilisers and BU (Buckthought et al., 2015b; Romera et al., 2012) which have been reported to be normalised to a range of between -10‰ to +10‰ for both $\delta^{15}N$ and $\delta^{18}O$ during transport through agricultural soil (Granger et al., 2008; Oelmann et al., 2007; Rock et al., 2011). Stable isotope signatures in the landscape, when moving down through the soil profile, will be increasingly biologically processed (Chapter 5). Thus, isotope signatures should reflect the progressive changes from the dominance of the urine-N source in the surface horizons, to a microbially produced and transformed NO_3^- molecule at depth (Curtis et al., 2011; Kendall et al., 2007; Wells et al., 2015).

A better understanding of the hydro-geochemical system and its effect on denitrification is needed to better predict and manage the impact of agricultural practices on NO_3^- contamination of ground and surface waters (Böhlke et al., 2007) and the impact on N_2O emissions (van der Weerden et al., 2012). Attenuation of N in the soil under grazing systems in Southland is poorly understood, with previous research focusing on ground and surface water N concentrations, with modelled estimations of a soils ability to remove N and limited physical quantification. This is highly important in terms of management and implementation of new regional and national laws to improve the state of New Zealand's environment. Soil properties and models used are generic and do not account for temporal change, while also being spatially broad in their approach.

Gas diffusivity could provide a useful tool in farm and policy management as it could provide real time data showing N attenuation through the measurement of soil O_2 using sensors placed in soils where

in-situ soil ρ_b measurements have been taken. Alternatively, the modelling of D_p/D_0 and identification of attenuation moments showing when and where NO_3^- attenuation could potentially occur.

The key aims of this field trial were (i) to identify in situ temporal and spatial change in soil conditions (e.g. D_p/D_0) that would align with potential N attenuation conditions, and (ii) to assess if changes in NO_3^- isotopes occurred under these soil conditions that theoretically trigger attenuation. It was anticipated that field data would show 'hot moments' (duration) and 'hot spots' (location) within the soil profile. Sensors and ceramic cup samplers will measure different variables in the landscape over time. This allows for a comparison of isotopes with total NO_3^- concentrations over time. While soil moisture, O_2 and ρ_b will allow for the D_p/D_0 of the soil to be both calculated and modelled in order to identify 'hot moments'.

7.2 Materials & Methods

7.2.1 Field Sites, Installation & Experimental Design

Experimental Sites

Two field trial sites were installed from the 1st to the 6th of March 2017, in the Five Rivers Area of Southland, New Zealand. Site one (E1241567 N4939016 NZTM, 273 m a.s.l, Plate 7.1) is in an oxidising physiographic zone (free draining). The soil is classified as an Acidic Orthic Brown (Gore undulating shallow)(Hewitt, 2010) and is referred to in the text as the 'GM Site'. The GM soil is stony in both the top and the subsoil and is situated in an area that receives centre pivot irrigation through the summer months. A dense iron pan layer was found in the soil profile at the GM experimental site, at a depth of 18 – 20 cm (Plate A.6 a). The paddock was of improved pasture, so assumed to have been cultivated, however there was no visual evidence of mechanical ripping of the iron pan.

Site two (E1257349 N4909615 NZTM, 262 m a.s.l, Plate 7.2) is in a gleyed physiographic zone (poorly drained). Site two was classified as a Melanic Orthic Gley soil (Acton undulating moderately deep)(Hewitt, 2010) and is referred to in the text as 'DH Site'. On excavation of the DH site, redoximorphic features were visually apparent, iron mottles were evident throughout the B horizon as well as reduced 'gley' pigmentation. The gley soil site was near a tile drain that the farmer had installed at approximately 1 m depth, a single drain ran the length of the paddocks situated in line with the field trial location, draining into a nearby open man-made culvert.

Plate 7.1: The GM Site - Gore Oxidising, location on farm represented by red dot (a). Google map images ©2019 DigitalGlobal, MapData Sciences pty Ltd, PSMA. The site during installation (b).

Plate 7.2: The DH site - Acton Gleyed, location on farm represented by red dot (a). Google map images ©2013 DigitalGlobal MapData Sciences pty Ltd, PSMA. The site (b).

Figure 7.2: Monthly temperature records for the Invercargill and Lumsden weather stations, from all available data, NIWA, 2012. (Macara, 2014).

The Five Rivers area has an average daily summer air temperature (December - February) of between 18 to 19°C, while the winter daily average (June - August) drops to between 0 to -2°C, with a yearly average of between 8 to 10°C (Figure 7.2, NIWA, 2012)(Macara, 2014). Lumsden (~16 km SE from experimental sites), has 62 days on average where the air temperature drops below freezing (0°C).

The Five Rivers area annual rainfall is within the 1000 to 1100 mm yr^{-1} range, based on data over a 30 year period (1981 - 2010)(NIWA, n.d). Mean annual rainfall in Kingston is recorded as 944 mm yr^{-1} (~40 km NE from experimental sites), with rainfall evenly distributed throughout the year, 7 to 10% of the annual rain falls each month of the year (Macara, 2014). Inland, Northern Southland receives less rainfall than coastal areas, Kingston (~38 km NE from experimental sites), receives 205 mm less per year than Invercargill (1149 mm yr^{-1})(Macara, 2014).

Soils were sampled and taken back to Lincoln University, air-dried and sieved to 2 mm (Section 3.3.1). Soil chemical and texture properties were determined by taking representative sub-samples from each soil horizon (Appendix A, Tables A.5 through A.8). Soils from both sites were collected from 0 to 80 cm depth, in 5 cm increments to 80 cm, which was approximately a soil volume of 50 cm^3, air dried and sieved to 2 mm, then sub-sampled to allow for a representative analysis of each horizon's chemical and physical properties. In addition to soil sampling over depth a 50 m transect was sampled, every meter, with a 7.5 cm deep corer, cores were bulked, air dried and sieved to 2 mm before being sent for analysis. Soil particle size analyses were performed at the University of Waikato using a Laser Diffraction Particle Analyser (Mastersizer 3000 v3.50, Malvern Panalytical Ltd.). Soil chemical analyses were performed by Hill Laboratories (Hamilton, New Zealand) (Section 3.3.1). In-situ soil ρ_b cores were also taken (Section 3.1, Equation 3.1).

The factorial experimental design was comprised of two sites (GM and DH) and four soil depths (10, 20, 50 and 80 cm), with each treatment replicated four times (Table 7.1). Giving a total of 16 ceramic suction cups at each site. Three soil depths at each site (20, 50 and 80 cm) were monitored with sensors, with each sensor replicated two times. Giving a total of 6 sensors at each site: two O_2 and two moisture/temperature sensors at each depth for each site. Each site also had a rain gauge and a barometric pressure sensor. All equipment and sensors were installed between the 1st and the 6th of March 2017.

Table 7.1: Experimental design of trial. Quantity of ceramic suction cups and sensors at each site. An 'x' indicates placement at the designated depth.

	Soil Depths (cm)				Reps	Total
Site 1 & 2	**10**	**20**	**50**	**80**		
Ceramic Suction Cups	x	x	X	x	4	16
Oxygen Sensors		x	X	x	2	6
Moisture & Temperature Sensors		x	X	x	2	6

Ceramic Cup Sampler Installation

Ceramic suction cups (CSC) are advantageous as they allow for sampling of the soil solution by applying a suction (Linden, 1977). As the soil solution is closer to the source of water and N, it removes the problem of dilution of the soil solution that occurs when sampling surface or groundwater. The porous ceramic head allows for soil solution to move from the soil into the CSC (Plate 7.3). The CSC are comprised of a sealed length of pipe connected to a porous ceramic head which is inserted into the soil. When suction is applied it allows for the sampling of soil solution through a tube which runs the length of the pipe and into the ceramic head.

Plate 7.3: Cut away view of ceramic cup sampler showing soil water interaction between ceramic cup wall and soil particles. Taken from Linden (1977).

Ceramic suction cups were installed in sets of four replicates at four depths at the two contrasting soil sites at Five Rivers. The installation was similar to that described by Linden (1977) for the DH site,

except petroleum jelly was used in place of tampered soil. The CSCs were inserted into a pre-formed hole that held approximately 20 mL of silica flour slurry (Plate 7.4a and b). This slurry fills the void between the ceramic suction cup and the soil to ensure good contact between the soil and the ceramic wall. The rest of the hole was then back filled with petroleum jelly to avoid bypass flow down the walls of the tubing from the soil surface. A silica flour slurry inserted around the head of the CSC also helps to ensure a longer sampling life as it reduces the amount of soil particles, organic matter and microbial growth that can block the ceramic head over time (Linden, 1977).

Plate 7.4: Installation of the ceramic suction cups (CSC) at the DH site. (a) steel rod was used to pre-form a hole for the CSC, (b) silica flour slurry was inserted into the pre-formed hole for the head of the CSC to sit in once inserted, (c) top of the CSC as seen from the soil surface, showing stopcock and syringe heads for sampling and suction application to CSC chamber, (d) view of all the CSC installed at the DH site.

At the DH site the pre-formed hole was made using a motorised hammer which pushed a steel rod into the ground to form the space for the CSC. The rod was then pulled out and the CSC inserted using the described method (Plate 7.4d). However, this method did not work for the GM site due to the high stone content of the soil. At this site an alternative method was used where angled hollows were dug into the side of a soil pit at the desired depths (Plate 7.5). The CSC were then placed in the hollows with silica flour slurry around the head and back filled using fines collected from that horizon (Plate 7.5b). Tubes were then run from the ends of the tubes to the soil surface before it was back filled, allowing soil solution collection from the CSC at different depths within the soil profile.

Plate 7.5: Ceramic suction cup (CSC) installation at the GM site, where the stone content did not permit for regular installation of equipment. (a) holes were dug into the wall of the soil pit at appropriate depths for CSC, (b) CSC were inserted into holes with silica flour slurry around the ceramic heads, then back filled with fines collected when constructing holes, (c) all sensors and CSC exposed on the soil pit wall before back filling.

A plastic stopcock was inserted into the top of the tube with two syringe needles passing through it into the chamber with a piece of tube and a small tap at the end of each (Plate 7.6). One of the syringe needles allowed for a syringe to be applied so that air could be drawn out of the chamber, creating suction. This suction resulted in soil solution surrounding the CSC to pass through the CSC. Then, at sampling, a syringe was attached to the stopcock and the soil solution sample removed. A total of 32 CSC were installed (16 per site), with four replicates at each soil depth monitored (10, 20, 50 and 80 cm).

Plate 7.6: Soil solution sample collect from the ceramic suction cups. (a) syringe connected to the sampling tube running from the head of the CSC in the soil to the surface to allow for soil solution sampling, (b) stopcock and tubes connected to the top of the CSC where suction is applied to collect soil solution samples, with taps to hold pressure in CSC.

7.2.2 Sensor Installation & Data Collection

All sensors were installed between the 1st and the 6th of March 2017 (Plate 7.7). Data from the O_2 and moisture sensors were collected from time of installation. However, sensor data were not continuous due to technical failures, human error and environmental disruption of equipment.

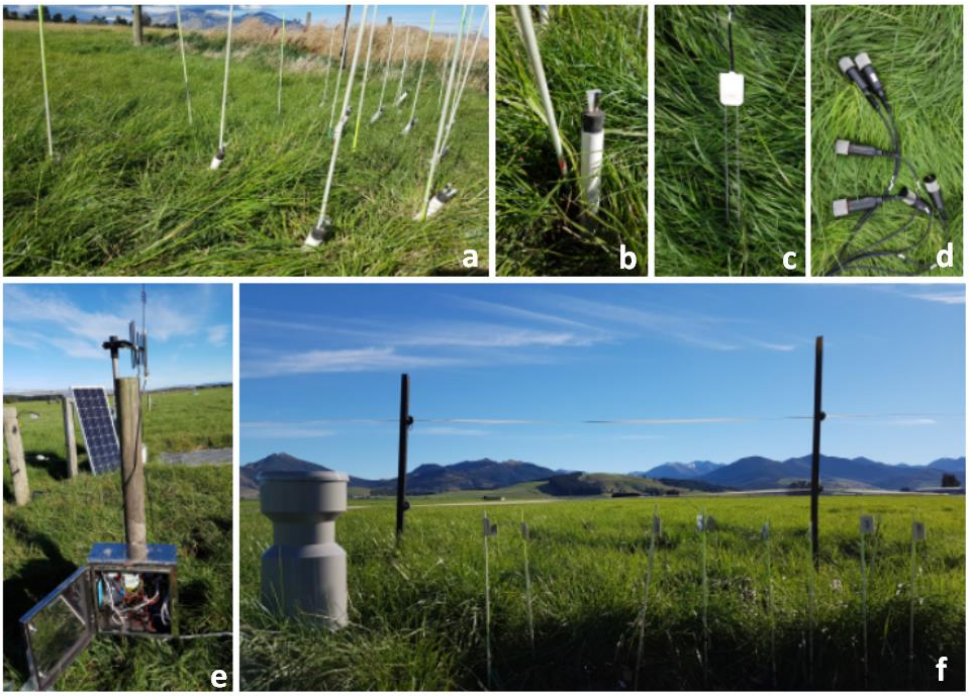

Plate 7.7: Equipment at sites. (a) DH site CSC, (b) top of CSC showing sampling and pressure syringes, (c) moisture sensor, (d) oxygen sensors, (e) data logger connected to sensor equipment, solar panel and aerial for 3G cell network communication, (f) tipping bucket rainfall gauge and CSC markers at the GM site.

A CR1000 data logger (Campbell Sci. Logan, UT, Plate 7.8c) was installed at each site to allow for the collection of sensor data and for it to be sent back to the Lincoln University network via the 3G mobile network. All equipment was calibrated before installation according to instructions provided by the sensor manufactures. Data loggers were run off solar panels set up on-site. A CRbasic Program was used to run the collection of data through the data loggers.

A barometric pressure sensor (Apogee SB-100 BPS), six soil moisture sensors (CS650-UL20 TDR Water Content Reflectometer, Plate 7.8a), six O_2 sensors (Apogee Soil O^2 Sensor SO-411 SDI-12 with Apogee AO-001 diffusion heads, Plate 7.8b) as well as a tipping bucket rain gauge (Plate 7.7f), were installed at each site and connected to the CR1000 data logger (Plate 7.8c). A total of two barometric pressure sensors, 12 O_2 sensors, 12 moisture sensors, two data-loggers each with its own battery and solar panel set-up were installed.

Plate 7.8: The moisture sensor (a), oxygen sensor (b) and datalogger set-up (c). Moisture and oxygen sensor installed at the two sites varied with soil type, DH (d) and GM (e). At the DH site the soil allowed for moisture sensors to be pushed into intact soil, the GM site was too stony for this technique and therefore it was installed in dug out hollows and back filled with fines from the same horizon.

Installation of O_2 sensors at the DH site (Plate 7.8d) was performed with small hollows dug into the side of the soil pit at required depths, with the sensor placed in and then back filled. The soil moisture sensors were pushed into the intact soil profile at appropriate depths next to the O_2 sensors (Plate 7.8d). Installation of the O_2 and moisture sensors at the GM was different to the DH site due to the high gravel content of the soil (Plate A.6). Oxygen sensor, moisture sensor and CSC were all put into one hollow at each of the required depths then back filled with fines (Plate 7.8e). Soil pits were back-filled after installation of equipment.

Analog O_2 sensors were installed to replace SDI-12 O_2 sensors that were not preforming. The first were replaced on the 29th of June 2017, one at each site at the 50 cm depth. The second set of sensors were replaced on the 28th of May 2018, one at the GM site at 50 cm, two at the DH site at 20 and 50 cm depths. The two deepest O_2 sensors at the DH site (80 cm depth), failed to work successfully but as these were in a saturated soil zone, they were not replaced as the assumption was made that at such high soil moistures the O_2 readings would generally be very low.

Bovine urine was collected from Friesian-Jersey-cross cows during the Lincoln University Research Dairy Farm's afternoon milking in April 2017 and again in April 2018, which was then frozen at -20^{o}C until use (Plate 7.9a). Nitrogen content was measured (0.06%) measured on six replicate sub-samples via combustion (Elementar EA-TCD, Lincoln University, NZ). Bovine urine was applied to the pasture above the ceramic suction cups and sensors on the 23rd of May 2017 (396 kg N ha^{-1}) and again the following year on the 23rd of May 2018 (396 kg N ha^{-1}), using a watering can for even application (Plate 7.9b). This was to simulate dairy pasture conditions under a urine patch, and this ensured there was sufficient N to undertake leaching through the soil profile. The BU was applied at a rate of 2.2 L 0.2 m^{-2}, slightly higher than the average cow urination volume of 2.0 L 0.2 m^{-2} reported by Moir et al. (2011). Bromide tracer was also added to the BU before it was applied (4.5 g Br L^{-1} BU, 2017, 10 g Br L^{-1} BU, 2018).

Plate 7.9: Bovine urine collection at the Lincoln University Dairy Farm (a). Application of BU to site on the 23rd of May 2017 using a watering can (b).

7.2.3 Sampling & Analyses

Leachate from the ceramic suction cups was collected at approximately 3-4 day intervals over a two-month period in both 2017 and 2018 (Table 7.2). The first sampling period was from the 15th of May until the 30th of June 2017 with 14 sampling points, the second period was from the 10th of May until the 29th June 2018 with 13 sampling points. These sampling periods aimed to collect soil solution samples over the period of the winter when soil wet-up occurred, thus, allowing the initial leaching of NO_3^- through the soil profile to be captured.

Samples were collected from a CSC by evacuating the air to create suction within the sampling tube using a 30 mL plastic syringe, waiting for 15 minutes, before drawing the sample out of the CSC. Once the sample was collected in the 30 mL syringe it was passed through a 0.2 µm filter into a 30 mL collection vial before being frozen. Samples were then sent back to Lincoln University for analyses (Section 3.3.2).

Measurements of leachate NO_3^- $\delta^{15}N$ and $\delta^{18}O$ were performed at the National Isotope Lab, Geological and Nuclear Science, Wellington, New Zealand, using the cadmium-azide method (McIlvin et al., 2005), refer to Section 3.6.

Table 7.2: Sampling dates for ceramic cup samplers 2017 and 2018, with associated date of BU application and cumulative rainfall over the sampling period. (-) No data due to technical failure GM site: 1 - 31.5.2017, 25 - 28.5.2018, 12-13.6.2018, 27-30.6.2018, DH site 20 - 29.6.2017.

Sample #	2017 Sample Dates	Bovine Urine Applied	Cumulative Rainfall (mm)		2018 Sample Dates	Bovine Urine Applied	Cumulative Rainfall (mm)	
			GM	DH			GM	DH
1	15.5.2017		-	0	10.5.2018		0	1
2	19.5.2017		-	7	17.5.2018		11	8
3	22.5.2017	23.5.2017	-	26	21.5.2018	23.5.2018	35	30
4	26.5.2017		-	28	25.5.2018		-	71
5	30.5.2017		-	32	28.5.2018		-	77
6	2.6.2017		1	33	30.5.2018		68	77
7	6.6.2017		3	35	5.6.2018		68	78
8	9.6.2017		3	36	11.6.2018		82	90
9	14.6.2017		30	62	15.6.2018		82	91
10	16.6.2017		43	69	20.6.2018		85	93
11	21.6.2017		48	-	22.6.2018		85	93
12	23.6.2017		58	-	26.6.2018		101	106
13	26.6.2017		65	-	29.6.2018		-	112
14	30.6.2017		66	-	.	.	.	.

Ceramic suction cups at the GM site were mistakenly destroyed by local council staff using a weed-eater in early 2018. The four replicates at the 10 cm depth were not recoverable, but the 20, 50 and 80 cm CSC were able to be re-connected and sampling conducted.

Modelled Diffusivity Calculation

Modelled D_p/D_0 was calculated using the Moldrup et al. (2000) model, based on the original WLR (water-induced linear reduction) concept. See Section 3.8.

7.2.4 Statistical Analyses

The following variables were reviewed and summarised below; total soil solution NO_3^- concentration, soil moisture, soil temperature, soil O_2, soil diffusivity and rainfall, with factors of site, soil depth and time, with differences and interactions between these variables determined.

Statistical analyses of data were not possible for all variables due to fluctuation of sample numbers limiting analysis of multiple replicates. Results summarise raw data means and trends.

7.3 Results

7.3.1 Rainfall & Irrigation Inputs

Seasonal rainfall varied between the two sites (P = 0.00), with the GM site receiving 270 mm more rainfall than the DH site over the trial period from March 2017 to February 2019 (Figure 7.3, Table 7.3). Total measured rainfall over the two-year period for the GM site was 1462 mm and 1193 for the DH site. The GM site peaked at 408 mm in the summer of 2018 - 2019. This is more than double what the

DH site received in the same season (183 mm, summer of 2018 - 2019) (Table 7.3). This indicates that the majority of water input for the GM site, for that season, was from centre pivot irrigation. The DH site's peak rainfall was in spring 2018, with a total of 255 mm received.

Table 7.3: Seasonal rainfall (mm) for the DH site, and rainfall + irrigation (mm) for the GM trial site, from Autumn 2017 to Summer 2019. Seasonal totals are the sum of total daily rainfall of each month within that season. NOTE: April - May 2017 for the GM site and July for the DH site did not have complete rainfall data due to technical issue, so these totals were removed so as not to show false trends.

Year	Season	Months	GM Site	DH Site
2017	Autumn	Mar-May	-	142.6
2017	Winter	Jun-Aug	201.5	-
2017	Spring	Sep-Nov	257.0	137.2
2017/18	Summer	Dec-Feb	65.0	156.0
2018	Autumn	Mar-May	68.0	142.8
2018	Winter	Jun-Aug	101.5	123.2
2018	Spring	Sep-Nov	297.0	255.4
2018/19	Summer	Dec-Feb	407.5	182.6
Total			1462	1193

The GM site varied from a low of 0 mm combined rainfall and irrigation inputs a month, to a high of 159 mm (November 2018) (Figure 7.3, Table B.1). The DH site monthly rainfall varied from a low of 4.4 mm (March 2018) to a high of 124 mm (November 2018) (Figure 7.3, Table B.1). Data gaps at GM site for April - May 2017 were due to equipment issues, while the February to May 2018 were due to accidental weed-eating of equipment at site by local council staff.

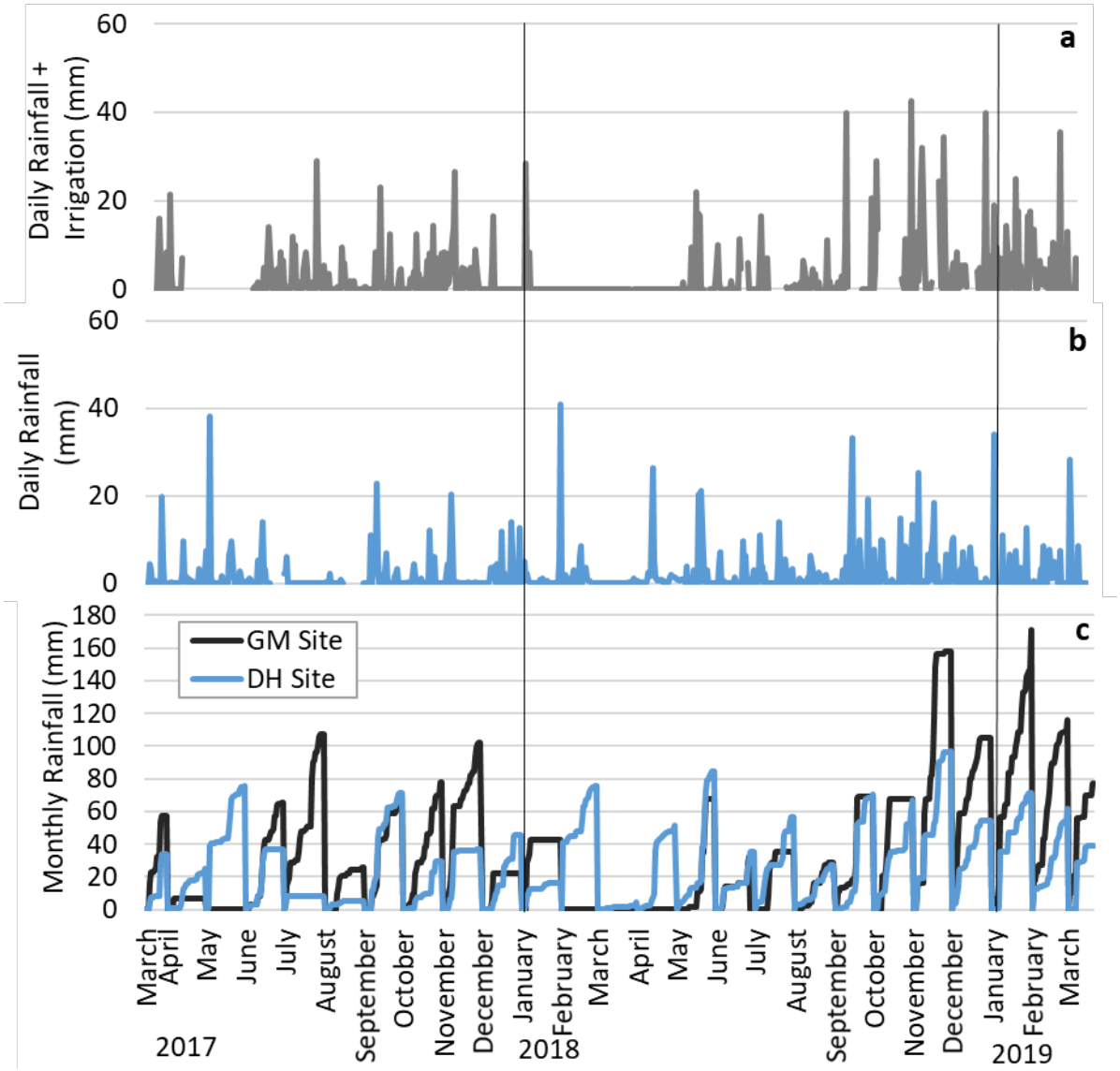

Figure 7.3: Site daily and monthly cumulative water input data for the GM site (grey) and the DH site (blue) over the trial period between March 2017 - March 2019. Daily rainfall (a & b) and cumulative monthly rainfall (c) collected using an automated tipping bucket on site. Note: GM site missing data April to June 2017 and February - May 2018, thus not 0 mm rainfall.

Barometric pressure ranged from a low of 96 kPa (September 2017) to a high of 101 kPa (March 2019) over the trial period (Figure 7.4).

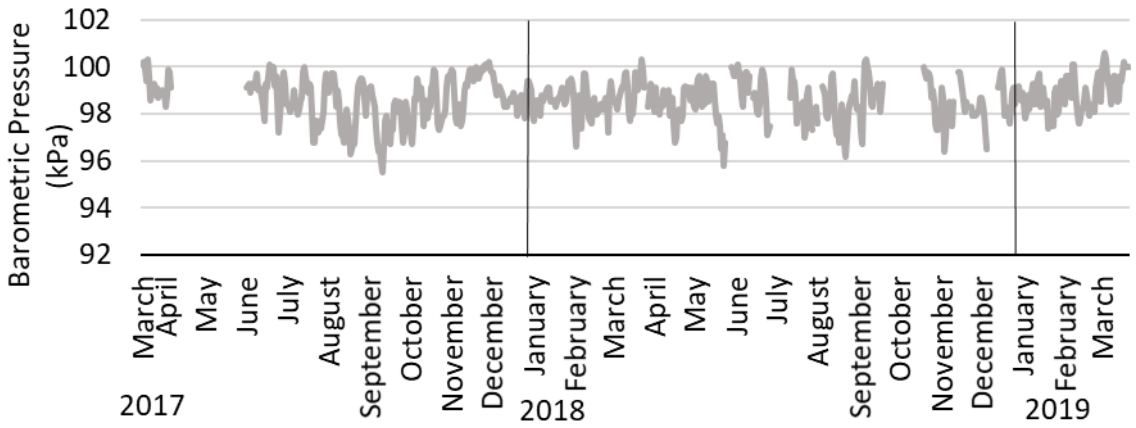

Figure 7.4: Barometric pressure for the DH and GM sites over the trial period.

7.3.2 Temporal Soil Data

The DH site average daily soil temperature ranged from a low of 3.0°C (20 cm depth) to a high of 20.3°C (20 cm)(Figure 7.5a), with peak temperatures in December to January (summer), and lows in June, July or August (winter) each year. Monthly maximum temperatures ranged from a peak of 17.4°C (January 2018) to a minimum of 2.9°C (July 2017) at the DH site (Table 7.4). The GM site also experienced its most extreme average daily soil temperature fluctuations at the 20 cm depth, ranging from an average daily low of 2.0°C, to a high of 19.7°C (Figure 7.6a), with an average monthly maximum of 18.3°C (January 2018) and minimum of 3.4°C (July 2017)(Table 7.4). July 2017 and January 2018 were, respectively, the coldest and hottest months over the trial period.

The GM site was, on average, 0.3°C warmer than the DH site at each soil depth. The GM site experienced the greatest temperature fluctuations, with a 14.6°C temperature range at the 20 cm depth, and an 11.2°C range at the 80 cm depth. The DH site in comparison had a similar range at 20 cm (14.3°C), but at 80 cm only had a temperature variation of 7.6°C. By season, the GM site had the warmest monthly averages in the summer months, up to 1.7°C warmer than the DH site (January 2018) and down to -1.8°C colder in winter (July 2017).

Table 7.4: Average monthly maximum and minimum soil temperatures each year, for each site's different soil depths. All temperatures are in degrees Celsius (°C). Data values are the average across two sensors at each depth for that month, n = (number of days in month)*2.

Site	Depth	2017		2018		2019
	cm	Max	Min	Max	Min	Max
DH	20	17.2 Dec	**2.9 Jul**	**17.4 Jan**	4.8 Jun	14.4 Jan
	50	14.7 Dec	5.9 Jul	15.6 Feb	6.3 Jul	13.7 Jan
	80	14.4 Dec	6.8 Jul	15.5 Feb	6.6 Aug	13.9 Feb
GM	20	18.0 Dec	**3.4 Jul**	**18.3 Jan**	3.8 Jun	15.7 Jan
	50	16.3 Dec	4.9 Jul	16.8 Jan	5.8 Jun	15.1 Jan
	80	16.1 Dec	5.0 Jul	16.7 Jan	5.9 Jun	15.1 Feb

DH site O_2 concentrations at the 50 cm depth varied from an average daily high of 20.8% (March 2017) to a low of 4.7% (December 2018)(Figure 7.5b). The GM site O_2 concentrations at the 50 cm depth varied from an average daily high of 20.5% (March 2017) to a low of 12.8% (June 2017)(Figure 7.6b). Data gaps at DH site July to August 2017 were due to malfunction of equipment after a lightning strike.

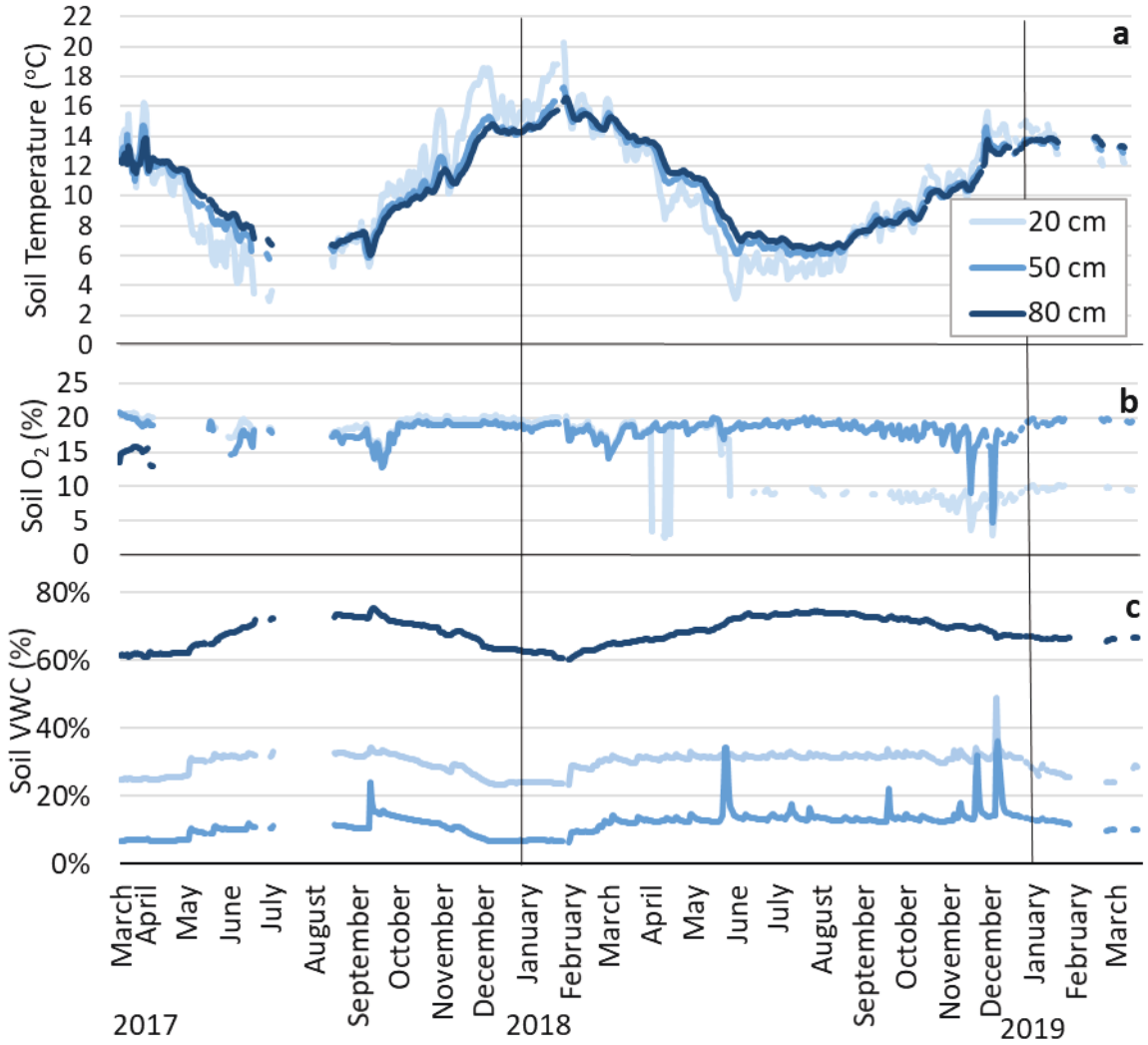

Figure 7.5: DH site average daily soil temperature (a), oxygen (b) and volumetric water content (VWC, θ_v)(c) at the three sensor depths of 20, 50 and 80 cm. Each value represents an average of two sensors at each depth. Note: the 20 cm O^2 appears to have failed from March 2018, so data is dubious from this point (b).

Soil O_2 concentrations at both sites experienced technical issues which lead to disrupted data sets, as seen with areas of missing data (Figure 7.5b and Figure 7.6b). The DH site O_2 sensors failed at 80 cm by May 2017, these were not replaced as they sat in a saturated soil zone and therefore continual saturation with water was assumed. Only the DH O_2 sensor at 50 cm depth remained reliable, as the 20 cm depth sensor started giving erratic results from April 2018 (Figure 7.5b). The GM site O_2 sensors at all depths had periods of technical failure (periods with no data, Figure 7.6b).

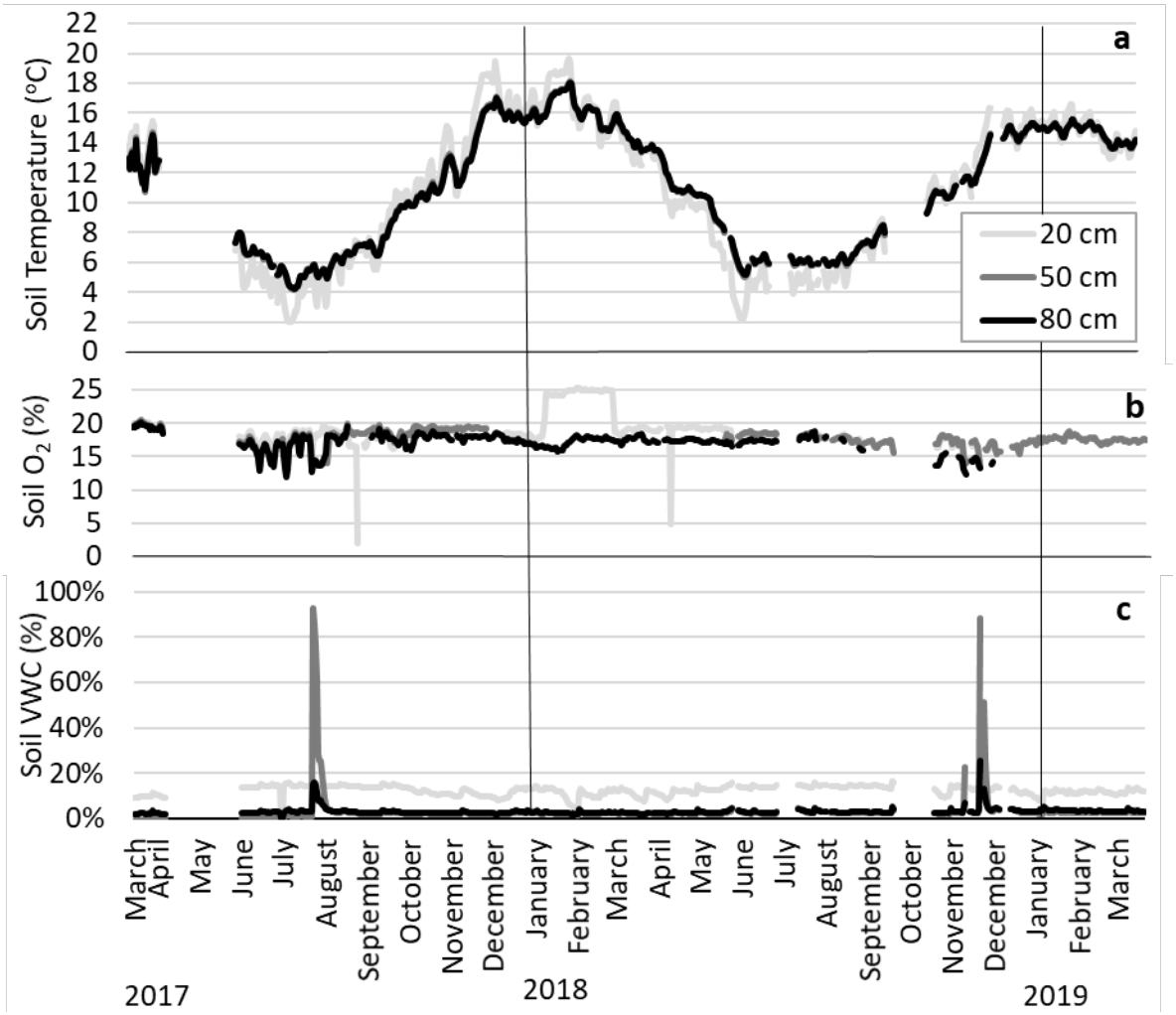

Figure 7.6: GM site average daily soil temperature (a), oxygen (b) and volumetric water content (VWC, θ_v)(c) at the three sensor depths of 20, 50 and 80 cm. Each value represents an average of two sensors at each depth.

Average daily soil VWC (θ_v) ranged from a peak of 76% (80 cm, September 2017) to a low of 0.06% (50 cm, February 2018) at the DH site (Figure 7.5c), and from a peak of 93% (50 cm, July 2017) to a low of 0.3% (50 cm, June 2017) at the GM site (Figure 7.6c). However, the aforementioned low is unlikely in June and therefore thought to be due to technical error with sensor, with all VWC data for GM site used with caution to illustrate trends. The DH site experienced continually high moisture saturation at 80 cm (68% θ_v average) and lowest at 50 cm (12% θ_v average), while at the GM site the 20 cm depth was the most saturated out of the measured depths and experienced the greatest fluctuation in θ_v (ranging from 17% to 3%).

Plate 7.10: Both sites experienced freezing temperatures. (a) The GM site covered in snow and (b) frost at the DH site on the 6th of July 2018.

Field trial sites dropped below freezing on multiple occasions (Plate 7.10). The week of 23.5.2018, snowfall, rain and frosts, with exceptional levels of ice were noted at the DH site on the 25.5.2018.

7.3.3 Soil Temporal Diffusivity Dynamics

Modelled D_p/D_0 dropped below the trigger point of N_2O and N_2 emission of 0.038 described by Chamindu-Deepagoda et al. (2019) at multiple time points throughout the field trial when modelled using maximum sensor derived θ_v (Figure 7.7). The DH site had very low diffusivity at 80 cm depth for the duration of the experiment, with the other depths dropping below a D_p/D_0 of 0.05 each winter as well as in the summer of 2018/19 (Figure 7.7b). The DH 50 cm also dropped to a low of 0.06 on the 11/09/2017, which corresponded with a rainfall of 23 mm at both sites. In 2018 the DH 50 cm depth dropped below a D_p/D_0 of 0.05 at three points, hitting a low of 0.014 on the 7/12/2018. The DH 20 cm dropped to a low of 0.002, the day before (6/12/2018).

The GM maintained higher modelled D_p/D_0 values than the DH site, with the 50 cm depth only dropping below 0.05 at two points and the 80 cm at one point (Figure 7.7a). GM 20 cm dropped to a low of 0.036 D_p/D_0 on the 27/07/2017, after receiving a daily rainfall total of 29 mm over 5 days and 10.5 mm 4 days before. Dropping to a low of 0.004 at 50 cm and 0.048 at 80 cm in November 2018.

Rainfall events triggered a noticeable decrease in D_p/D_0 at both sites. But rainfall events during summer of 2017/18 did not seem to have as much of an affect as the summer of 2018/19, however, the rainfall intensity was greater in the summer of 18/19.

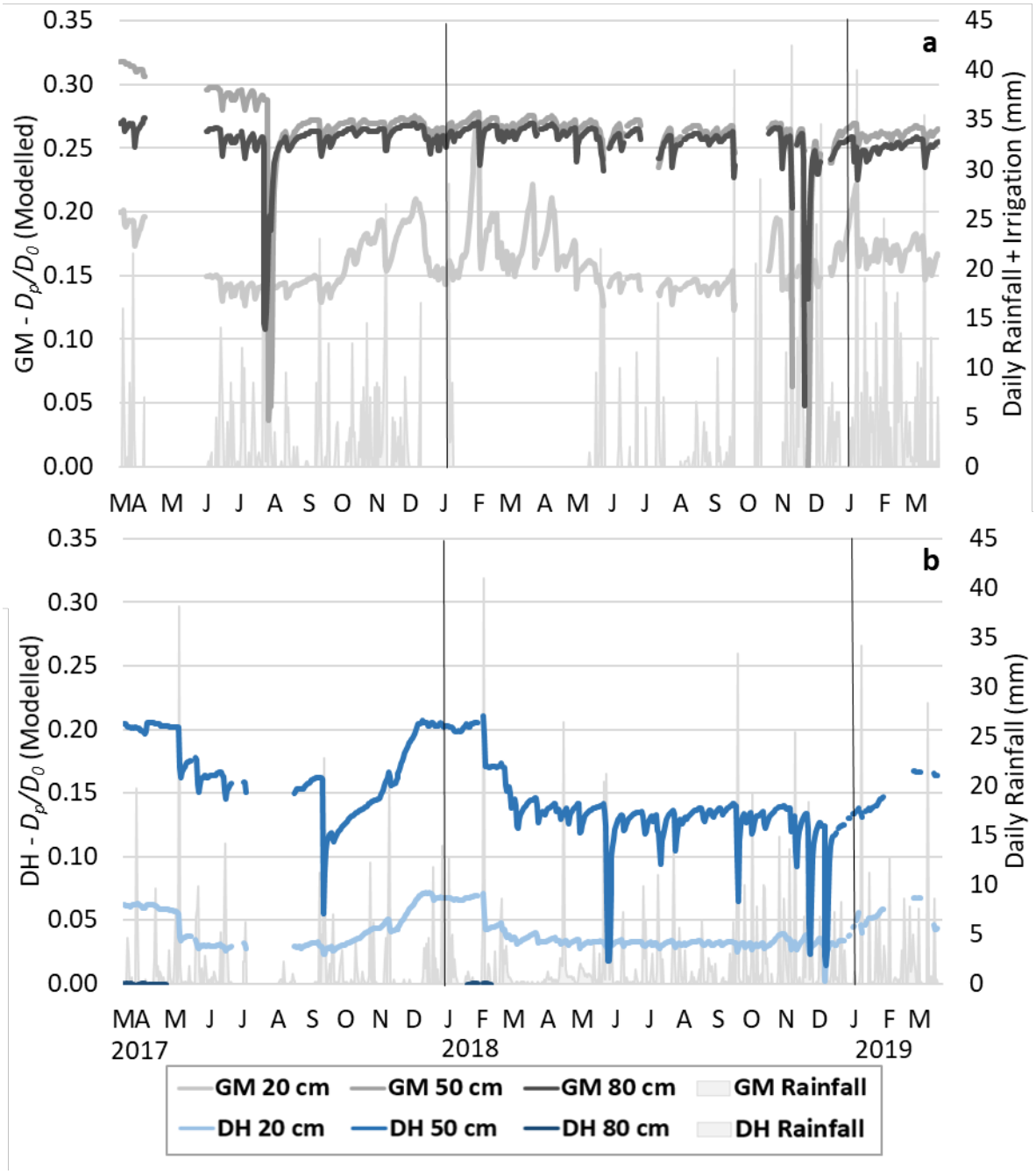

Figure 7.7: Modelled soil relative gas diffusivity (D_p/D_0) for each site at the three depths. GM site (grey - a) and DH site (blue - b), colour gets darker with depth. Modelled D_p/D_0 used sensor measured volumetric water contents (VWC, θ_v) and measured soil bulk densities to calculate air filled porosity (AFP, Ɛ) and total porosity (TP, Φ) throughout the field trial. Calculation from Moldrup et al. (2013), with a C_m value of 2.1. Mean θ_v was the daily maximum between two sensors at the specific depth, *n* = 2. Black vertical lines indicate calendar year boundary.

Hourly D_p/D_0 data shows that moments of low D_p/D_0 (< 0.02) lasted for up to 104 hours (GM 50 cm, 20th - 24th Nov 2018) after a prolonged rainfall (+ irrigation) event of 33 mm over 21 hours (Figure 7.8a). A second rainfall event of 67 mm in 13 hours also caused a drop in D_p/D_0 (4th - 7th Dec), but sensor data was sporadic at this time. The DH 50 cm depth shows that extended rainfall periods influenced D_p/D_0

to drop below 0.02, for a period of 16 hours (21st Nov) and again for a period of 50 hours (5th - 7th Dec) after a cumulative rainfall volume of 18.6 (21 hrs) and 17.6 mm (19 hrs), respectively (Figure 7.8b). The D_p/D_0 of GM 80 cm (6 hrs < 0.038) and DH 20 cm (25 hrs < 0.02) also dropped after rainfall events.

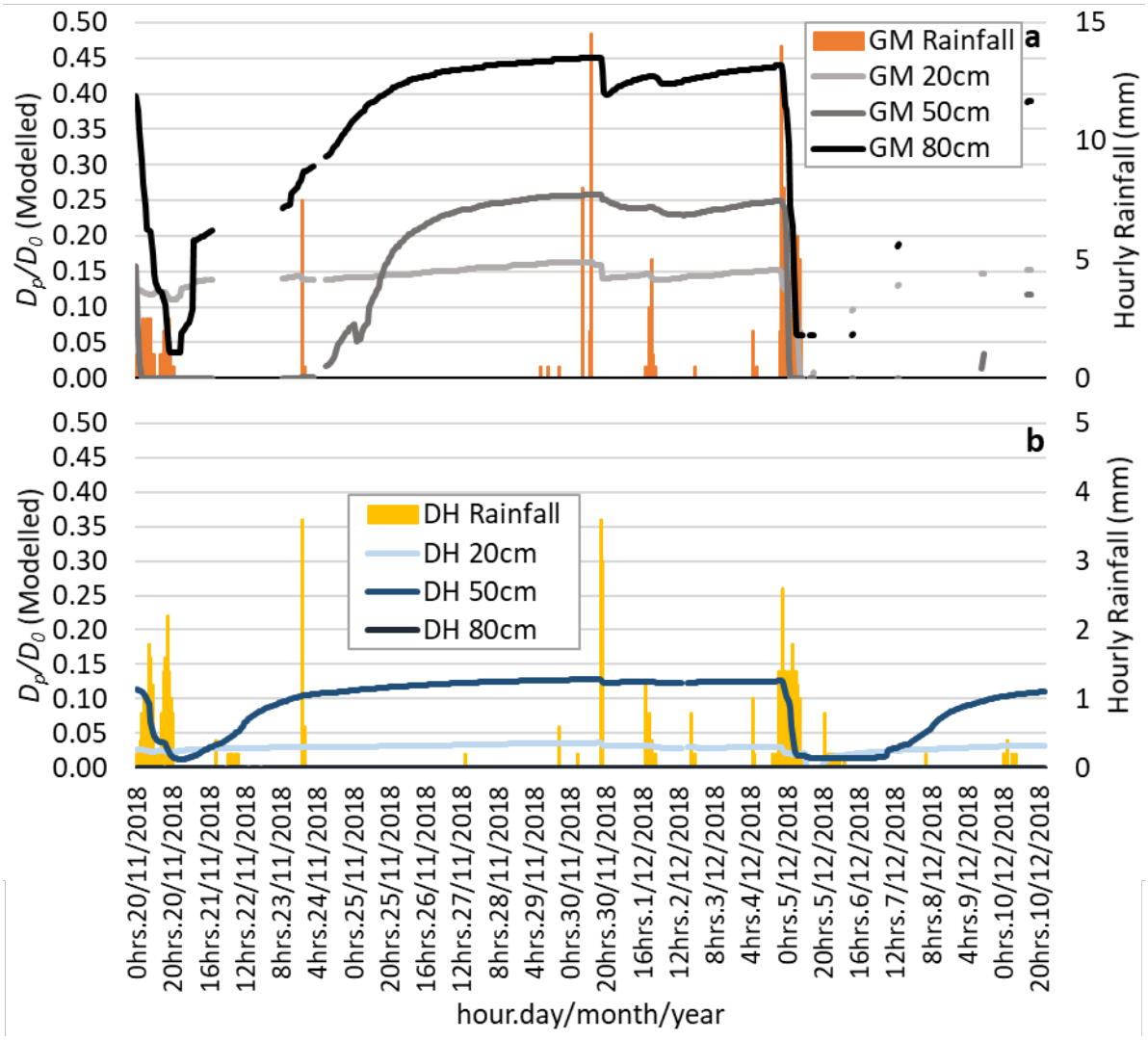

Figure 7.8: Hourly modelled soil relative gas diffusivity (D_p/D_0) for each site at the three depths from November 20th to the December 10th, 2018. GM site (grey - a) and DH site (blue - b), colour gets darker with depth. Modelled D_p/D_0 used sensor measured volumetric water contents (VWC, θ_v) and measured soil bulk densities to calculate air filled porosity (AFP, Ɛ) and total porosity (TP, Φ) throughout the field trial. Calculation from Moldrup et al. (2013), with a C_m value of 2.1. Mean θ_v was the daily max between two sensors at the specific depth, n = 2. Note: Different hourly rainfall y-axis scales between sites to show data detail.

7.3.4 Soil Solution Chemistry

Nitrate

The NO_3^--N concentrations increased after the application of BU on the 23rd of May each year (2017 and 2018, Figure 7.9). The GM site showed higher variation and greater concentrations at 10 cm depth, while the other three sampling depths had little variation (Figure 7.9, Table B.2). Interestingly the 80 cm depth had greater concentrations of NO_3^--N than the 20 and 50 cm depths at the GM site. Rather

than seeing the NO_3^--N move down through the depths there was the potential for the NO_3^--N to be held up at an iron pan above the 20 cm sampling point and subsequently being moved laterally. Thus, the NO_3^--N seen at the 80 cm depth may be an expression of NO_3^--N potentially moving through the top of the saturated zone in winter from another area. However, there was a weak Br^- signal seen in the 80 cm depth at the DH site (Figure 7.10). The contrasting expression of NO_3^--N at the 10 cm depth could not be monitored in the sampling period of 2018 as the sampling equipment was destroyed by a council-operated weed-eater!

There was more evidence of the NO_3^--N from the BU applied passing down through the DH soil, with both the 10 and 20 cm depths increasing noticeably in concentration after the application of urine on the 23rd of May (Figure 7.9, Table B.3).

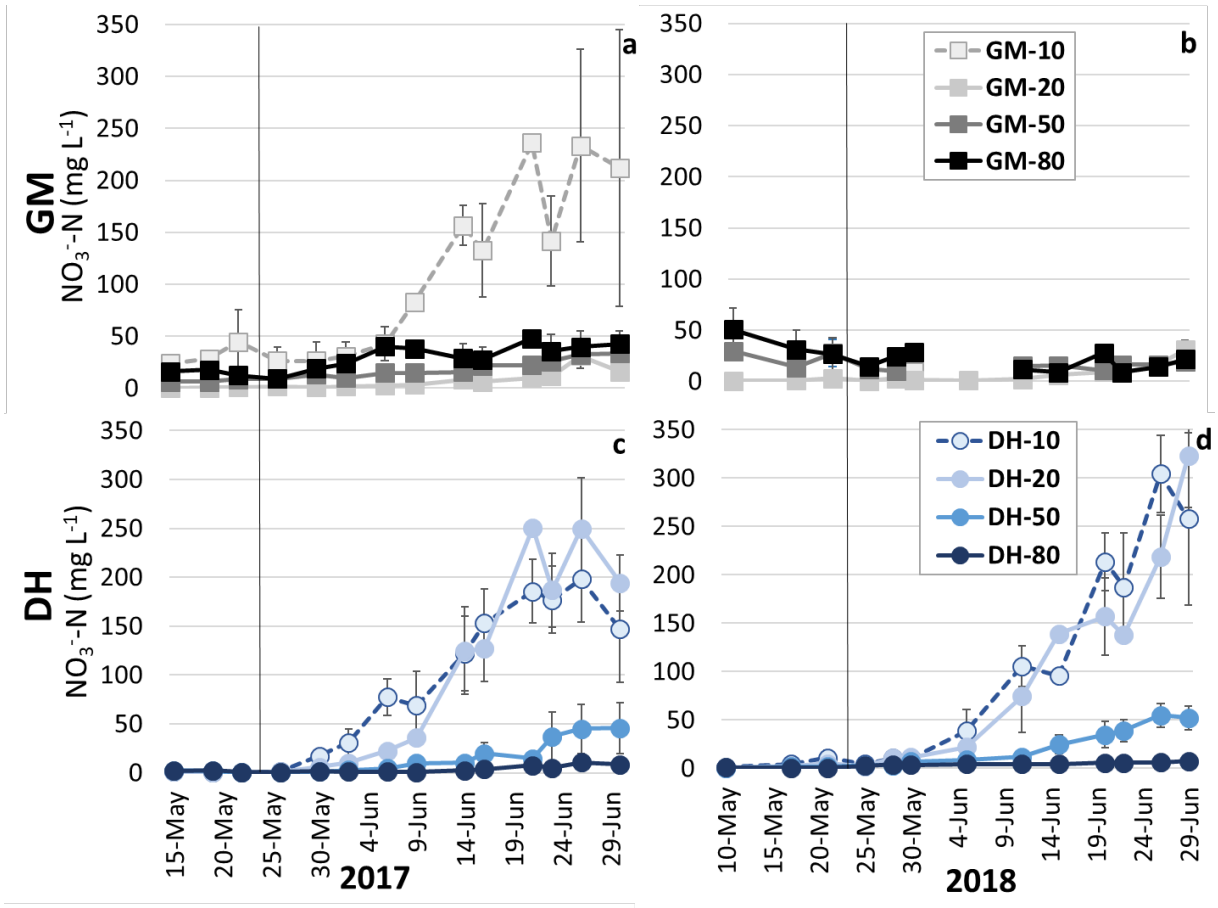

Figure 7.9: Concentration of NO_3^--N in soil solution collected from suction cups for the two soils for each year, GM 2017 (a), GM 2018 (b, no 10 cm) and DH 2017 (c), DH 2018 (d). Error bars = SEM, n = 1 where no error bars are present, n = 2, 3, or 4 where error bars are present. Replication of samples was limited by collected volumes due to environmental conditions. Vertical line represents BU application on the 23rd of May each year.

Bromide

Expression of Br^- in the samples analysed for NO_3^--N was found throughout every sampling depth each year (Figure 7.10). However, the 80 cm depth at the GM site had very low concentrations of Br^- (Table B.5), as well as the 80 cm depth in 2018 at the DH site (Table B.4).

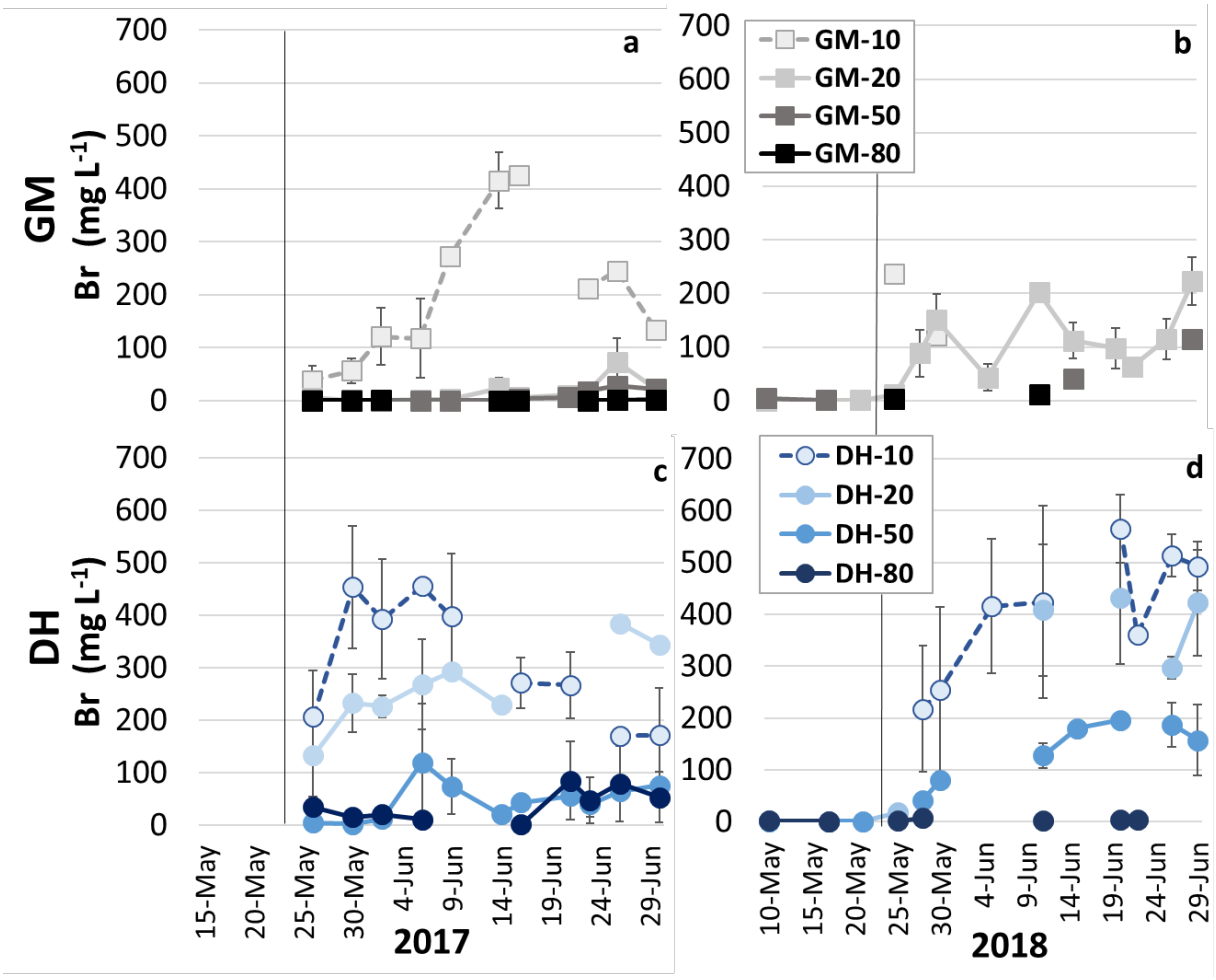

Figure 7.10: Concentration of bromide (Br^- mg L^{-1}) in soil solution collected from suction cups for the two soils for each year, GM 2017 (a), GM 2018 (b) and DH 2017 (c), DH 2018 (d). Black vertical line represents BU application on the 23rd of May each year. Error bars = SEM, n = 1 where no error bars are present, n = 2, 3, or 4 where error bars are present. Replication of samples was limited by collected volumes due to environmental conditions.

7.3.5 Nitrate Isotopes

The cow urine applied had a mean $\delta^{15}N$ value (‰ v. AIR) of -0.81‰ ± 0.06‰ (*n* = 6) and was applied on the 23rd of May 2017 and on the 23rd of May 2018. Mean soil $\delta^{15}N$ was +4.75‰ for the A horizon soils and +7.37‰ for the B horizon soils. Samples were analysed for isotopes every second sampling date in 2017 for both sites and every sampling date after BU application in 2018 but only for the DH site.

At the DH site in 2017 (Figure 7.11, Table B.6), $\delta^{15}N\text{-}NO_3^-$ values were initially stable, but decreased (becoming more negative) after BU application for all depths except the 80 cm. After 29th May there was a steady increase in $\delta^{15}N\text{-}NO_3^-$ values, which was also mimicked by the $\delta^{18}O\text{-}NO_3^-$ values, until 26th June.

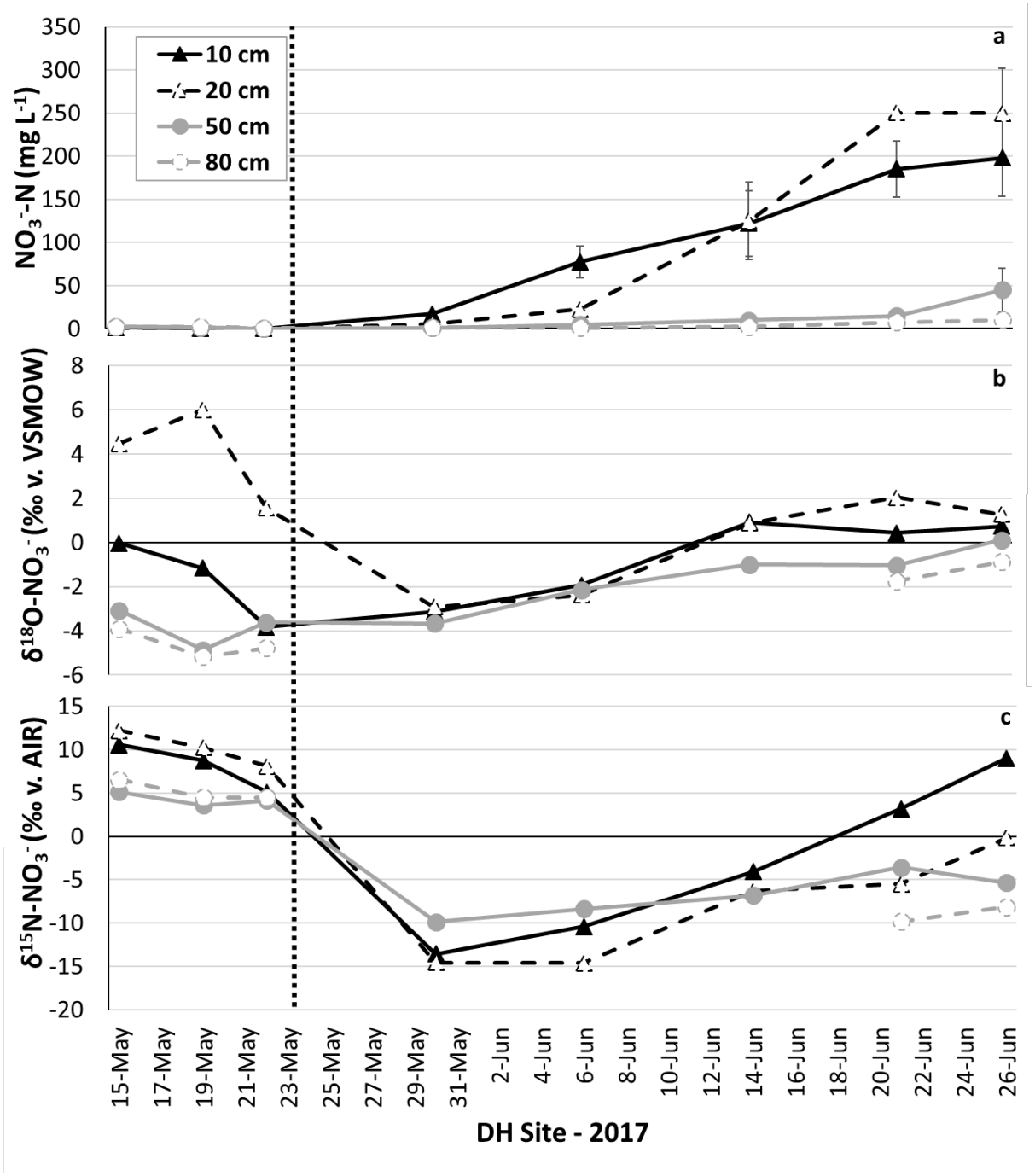

Figure 7.11: DH site 2017 sampling period NO_3^--N concentration (a) and dual isotope values, NO_3^--$\delta^{18}O$ (b) and $\delta^{15}N$ (c). Vertical dotted line represents BU application on the 23rd of May 2017. Points represent the four different soil depths that were sampled for soil solution from ceramic suction cups. Error bars = SEM.

At the DH site in 2018 (Figure 7.12, Table B.6) $\delta^{15}N\text{-}NO_3^-$ values again declined until the 15th of June, with the 10 cm sampling depth being the first depth where $\delta^{15}N\text{-}NO_3^-$ values began to increase. Missing

data points in the 10 cm and 20 cm depths for the 30th of May and 5th of June, make it difficult to define if there is an increase in $\delta^{15}N\text{-}NO_3^-$ values at these depths before the deeper 50 and 80 cm. However, after 15th of June there was a general increase in $\delta^{15}N\text{-}NO_3^-$ values which was, again, also seen in $\delta^{18}O\text{-}NO_3^-$.

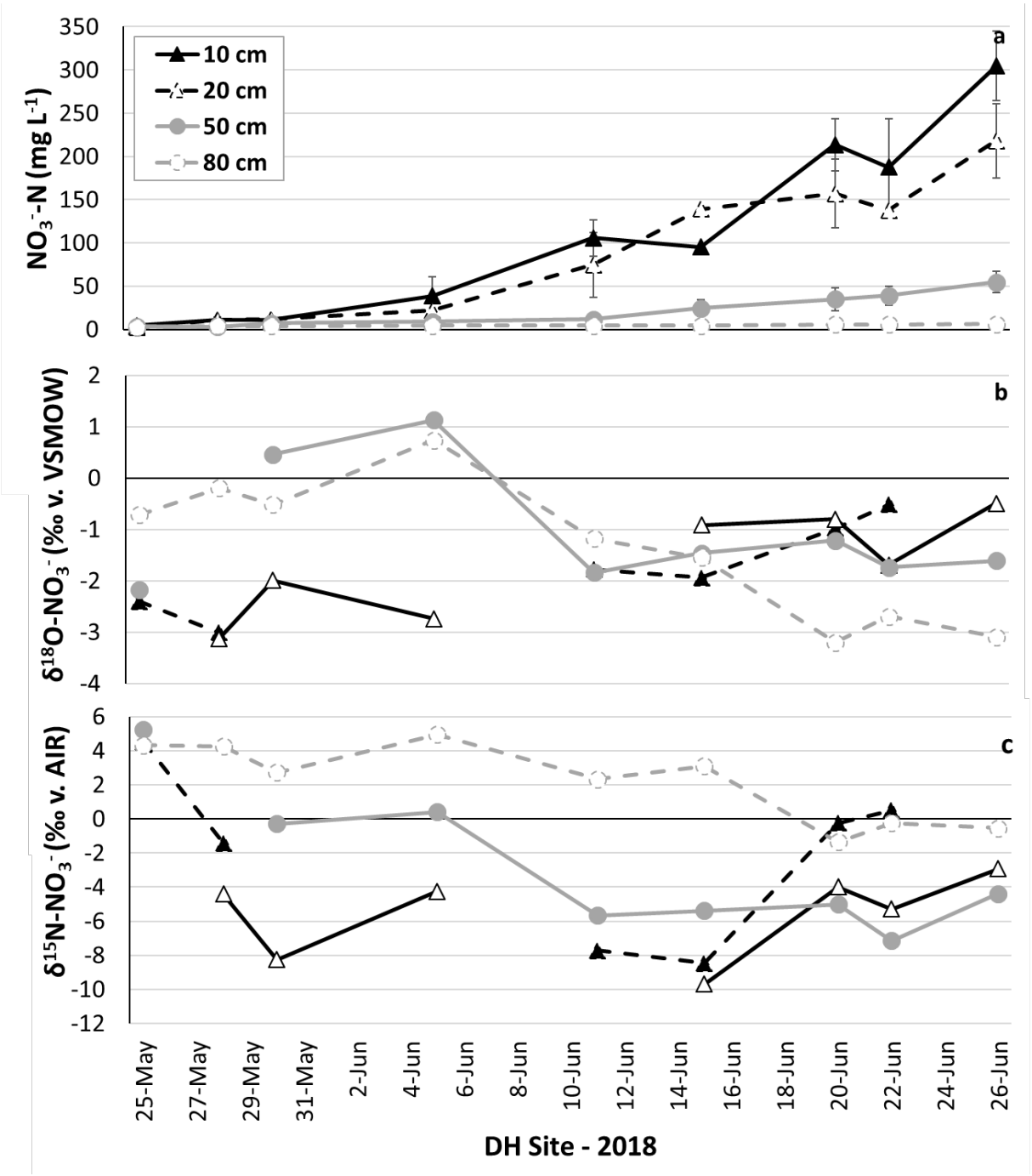

Figure 7.12: DH site 2018 sampling period NO_3^--N concentration (a) and dual isotope values, NO_3^--$\delta^{18}O$ (b) and $\delta^{15}N$ (c). Bovine urine was applied on the 23rd of May 2018. Points represent the four different soil depths that were sampled for soil solution from ceramic suction cups. Error bars = SEM.

The GM site in 2017 (Figure 7.13, Table B.6) had a decrease in $\delta^{15}N\text{-}NO_3^-$ values after BU application until 14th of June where this was a minimal increase in values. Both $\delta^{18}O$ and $\delta^{15}N$ at the 10 cm depth

show a period of enrichment from the 15th to the 29th of May 2017 (Figure 7.13), before the NO_3^- concentrations are seen to increase (6th to the 24th of June). Both the 10 cm and 20 cm depths show a peak in $\delta^{15}N$ on the 30th of May before starting to be depleted until the 14th of June.

The 50 cm depth shows a drop in $\delta^{15}N$ of +8‰ from the 15th to the 22nd of May 2017 at the GM site. The 50 and 80 cm depths do not have sufficient isotope data to show clear trends. Isotope analysis of samples from the GM site were not performed in 2018 due to destruction of the ceramic cup samplers at the 10 cm depth, which was the depth with most NO_3^- expression.

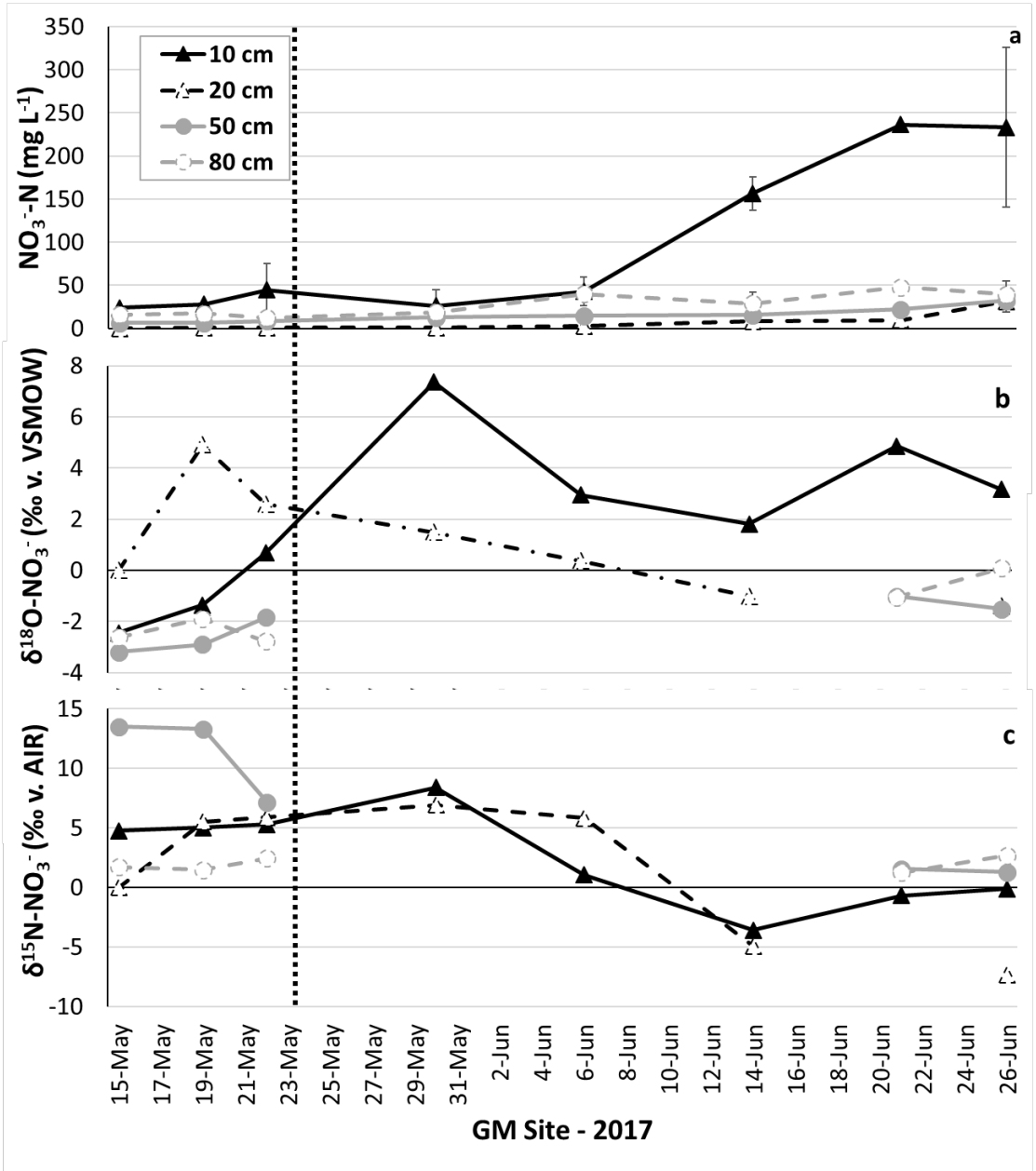

Figure 7.13: GM site 2017 sampling period NO_3^--N concentration (a) and dual isotope values, NO_3^--$\delta^{18}O$ (b) and $\delta^{15}N$ (c). Vertical dotted line represents BU application on the 23rd of May 2017. Points represent the four different soil depths that were sampled for soil solution from ceramic suction cups. Error bars = SEM.

The greatest range in $\delta^{15}N$ was seen at the DH site in 2017 (Figure 7.14a), with the greatest range in $\delta^{18}O$ at the GM site (Figure 7.14c). Maximum variation in NO_3^--N concentration and dual NO_3^- isotope signatures occurred at the 10 and 20 cm depths at both sites.

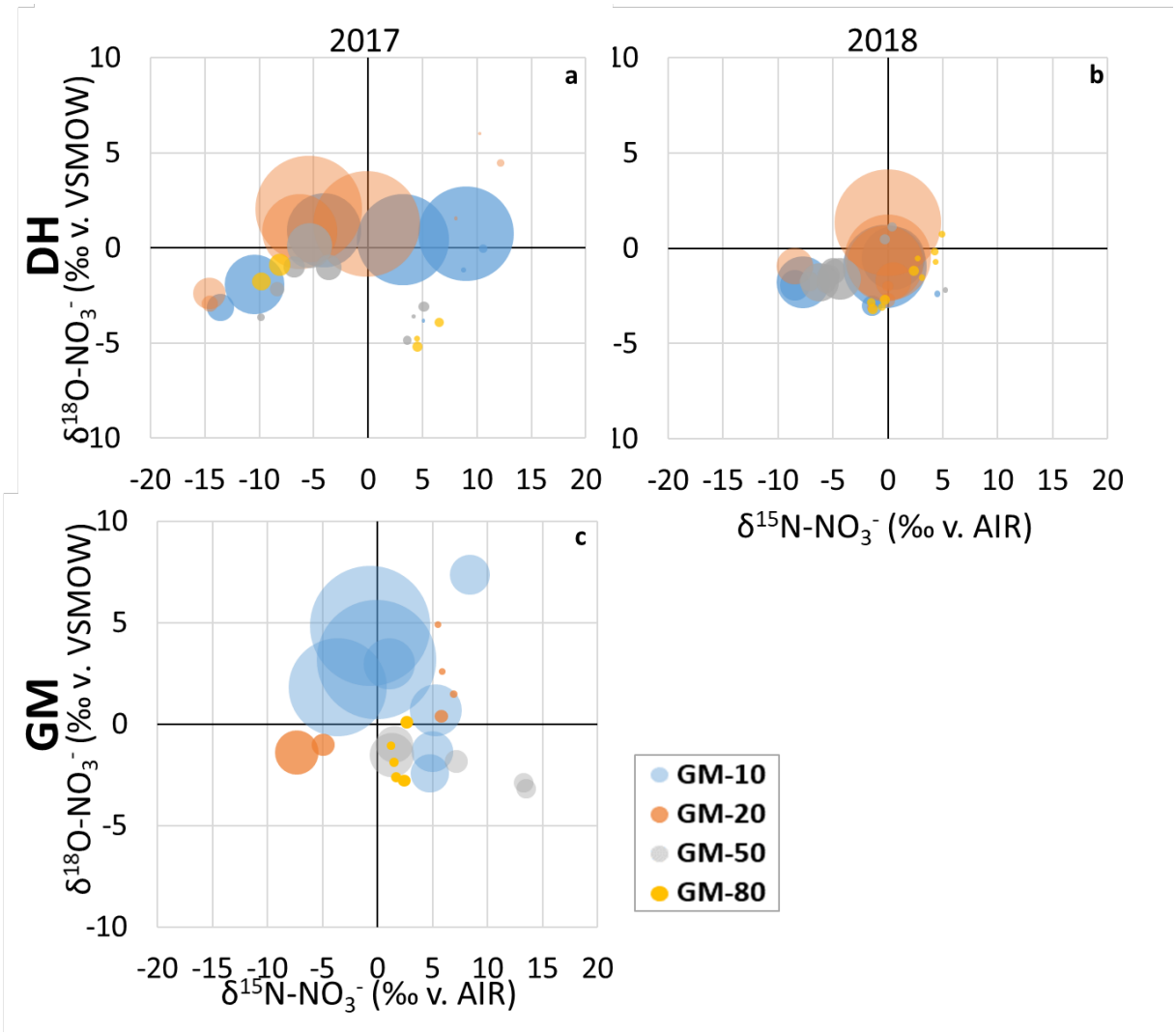

Figure 7.14: Isotope ratio of $\delta^{18}O$ and $\delta^{15}N$-NO_3^- with NO_3^--N concentration represented by the size of the bubble. The two soils, DH (a, b) and GM (c), isotope ratios over the May - June sampling period in 2017 and 2018, with different colours representing the soil solution depth (10, 20, 50 and 80cm below the soil surface).

7.3.6 Rayleigh Fractionation

At the DH site in 2017, $\delta^{15}N$-NO_3^- showed enrichment from the 30th of May until the 26th of June 2017 as NO_3^--N concentrations increased at the 10, 20 and 50 cm depths. The fractionation rates of this period were 8.0‰, 3.5‰ and 2.3‰, with $\delta^{15}N$ enrichment of +22.6‰, +14.4‰ and +4.5‰, respectively for the 10, 20 and 50 cm depths (Figure 7.15). The fractionation rate of the 10 cm depth was significantly greater than the 20 and 50 cm depths (LINEST confidence interval, Figure 7.15). Over this time period NO_3^--N concentrations increased by 181, 244 and 44 mg N L^{-1} at the 10, 20 and 50 cm

depths respectively. The 80 cm depth was not modelled as there were only two isotope values after BU application, not allowing for a reliable regression.

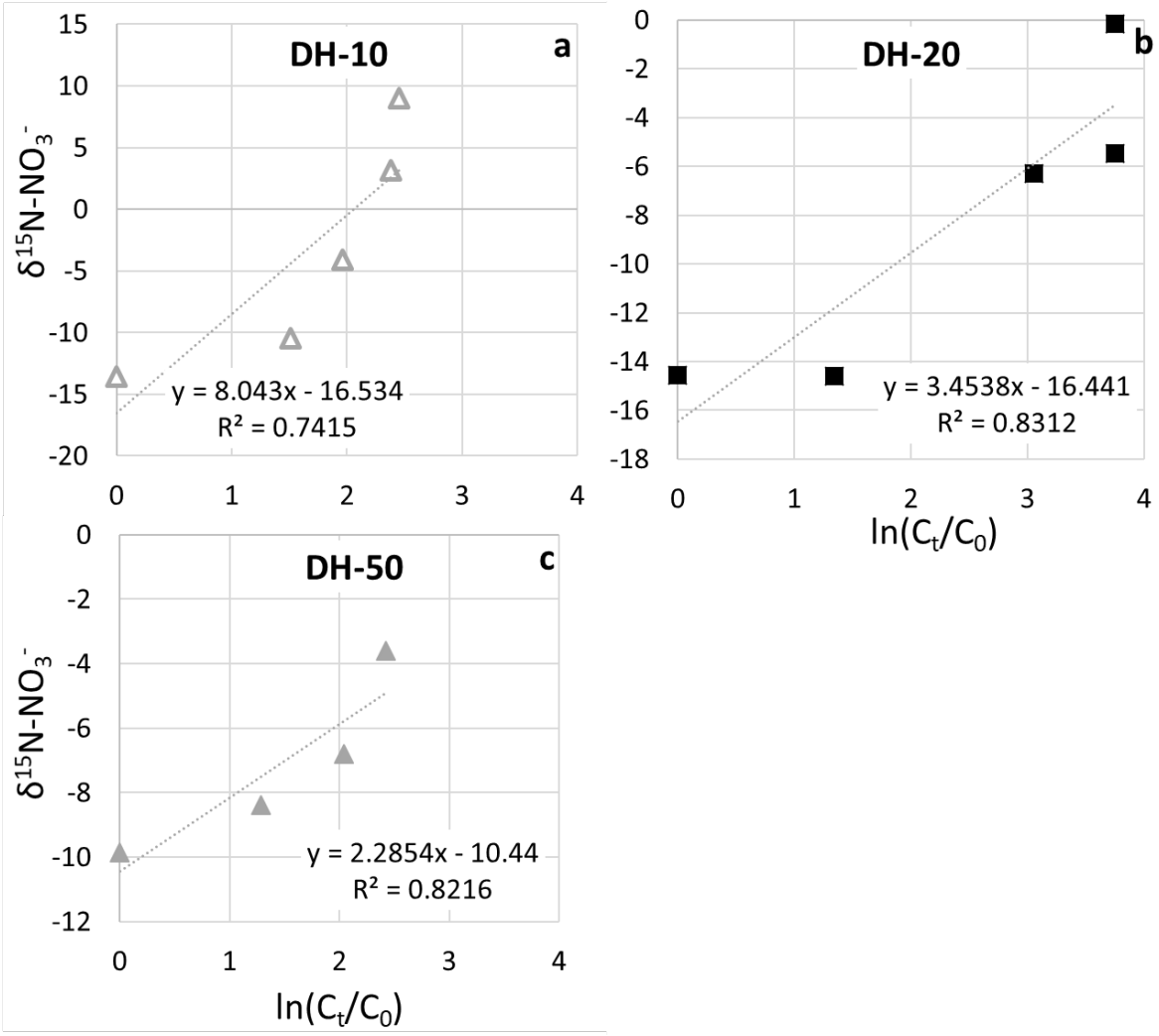

Figure 7.15: Linear regression of a Rayleigh calculation, used to calculate the $\delta^{15}N\text{-}NO_3^-$ fractionation factor for the 2017 DH soil depths; a) 10 cm +8.0 ± 2.7‰, b) 20 cm +3.5 ± 0.9‰, c) 50 cm +2.3 ± 0.8‰. Showing the $\delta^{15}N\text{-}NO_3^-$ verses the natural log of the ratio of C_t/C_0, where C_t is the NO_3^- concentration at a given time (t) and C_0 is the initial NO_3^- concentration. Sampling dates between the 30th of May and 26th of June were used as t_0 to t_4 for the 10 and 20 cm depths, the 50 cm depth used one less sampling date, until the 21st of June for t_0 to t_3 were used in order to align with a period of a constant trend in NO_3^- concentrations (Figure 7.11).

At the GM site in 2017, $\delta^{15}N\text{-}NO_3^-$ showed a depleting trend from the 30th of May until the 14th of June at 10 cm and until the 26th of June at 20 cm, while NO_3^--N concentrations increased. The isotope fractionation rates for this period were -6.0‰ and -4.7‰, with depletion of -12.0‰ and -14.3‰ for the 10 and 20 cm depths, respectively (Figure 7.16). While the NO_3^--N concentrations increased by 130 mg N L^{-1} at the 10 cm depth and by 30 mg N L^{-1} at the 20 cm depth. The 50 cm depth was not modelled due to limited isotope samples, but also showed depletion of $\delta^{15}N$ by -5.9‰ from the 22nd of May to the 26th of June with an increase of 24 mg NO_3^--N L^{-1}, however, isotope value t_0 was before BU application. The 80 cm depth was also limited by only two isotope samples post BU application, but

showed a $\delta^{15}N$ enrichment of +1.4‰ with a decrease of 8 mg NO_3^--N L^{-1} between the 21st and 26th of June.

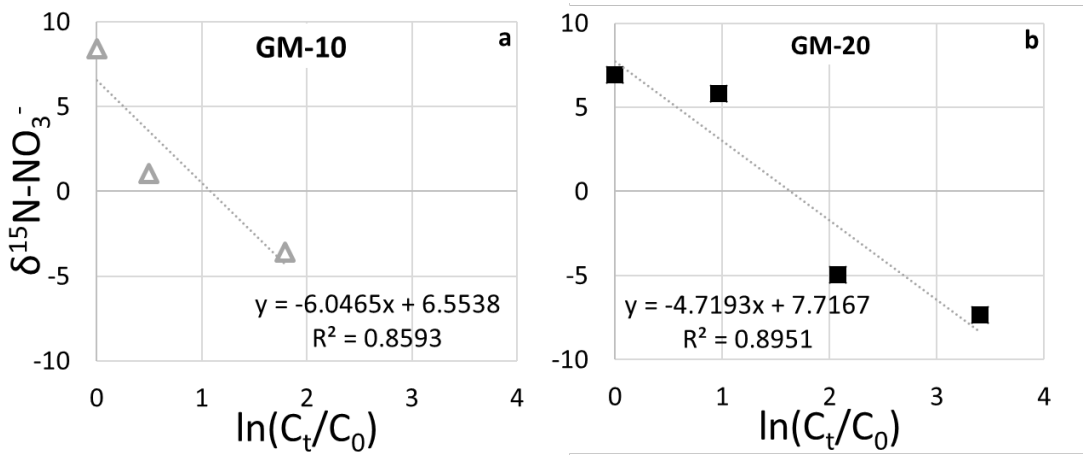

Figure 7.16: Linear regression of a Rayleigh calculation, used to calculate the $\delta^{15}N$-NO_3^- fractionation factor for the 2017 GM soil depths; a) 10 cm -6.0 ± 2.4‰, b) 20 cm -4.7 ± 1.1‰. Showing the $\delta^{15}N$-NO_3^- verses the natural log of the ratio of C_t/C_0, where C_t is the NO_3^- concentration at a given time (t) and C_0 is the initial NO_3^- concentration. Sampling dates between the 30th of May and 26th of June were used as t_0 to t_3 for the 20 cm depth, the 10 cm depth only used 3 sample points from the 30th of May until the 14st of June for t_0 to t_2 were used in order to align with a period of a constant trend in NO_3^- concentrations (Figure 7.13).

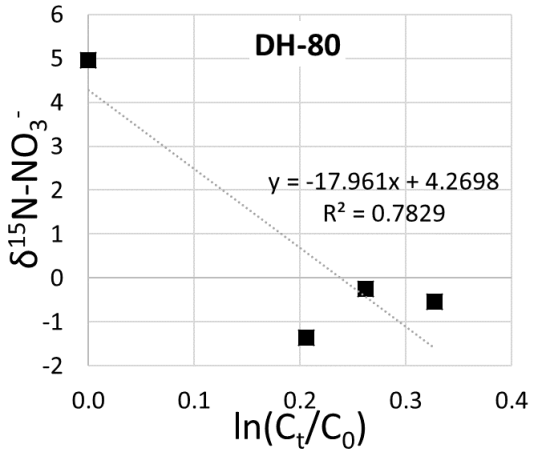

Figure 7.17: Linear regression of a Rayleigh calculation, used to calculate the $\delta^{15}N$-NO_3^- fractionation factor for the 2018 DH soil depths of 80 cm -18 ± 6.7‰. Showing the $\delta^{15}N$-NO_3^- verses the natural log of the ratio of C_t/C_0, where C_t is the NO_3^- concentration at a given time (t) and C_0 is the initial NO_3^- concentration. Sampling dates between the 5th and 26th of June were used as t_0 to t_3 in order to align with a period of a constant trend in NO_3^- concentrations (Figure 7.12).

The DH site in 2018 did not show sufficiently constant isotope trends with either increasing or decreasing NO_3^--N concentrations to allow for Rayleigh regression except for at the 80 cm depth (Figure 7.17). Depletion of $\delta^{15}N$-NO_3^- (-5.5‰) occurred over a 21 day period from the 5th to the 26th of June, with a fractionation rate of -18‰ while NO_3^--N concentrations increased (+1.8 mg NO_3^--N L^{-1})(Figure 7.17). The DH 10 cm depth showed a period of $\delta^{15}N$ enrichment by +9‰ over 7 days between the 15th

and 22nd of June, with fluctuating NO_3^--N concentrations. The 20 cm depth showed consistent increases in NO_3^--N concentrations, with an increase of 146 mg NO_3^--N L^{-1} between the 28th of May and 20th of June, but with fluctuating isotope values. The 50 cm depth also showed fluctuating isotope values, with an increase of 27 mg NO_3^--N L^{-1} between the 11th and 22nd of June.

7.3.7 Soil Diffusivity & Isotopes

In 2018 at the DH site during the two month soil solution sampling period, the 50 cm depth was initially below the denitrification D_p/D_0 threshold of 0.02, with the 80 cm depth maintaining D_p/D_0 values well below this throughout the whole sampling period (Figure 7.18).

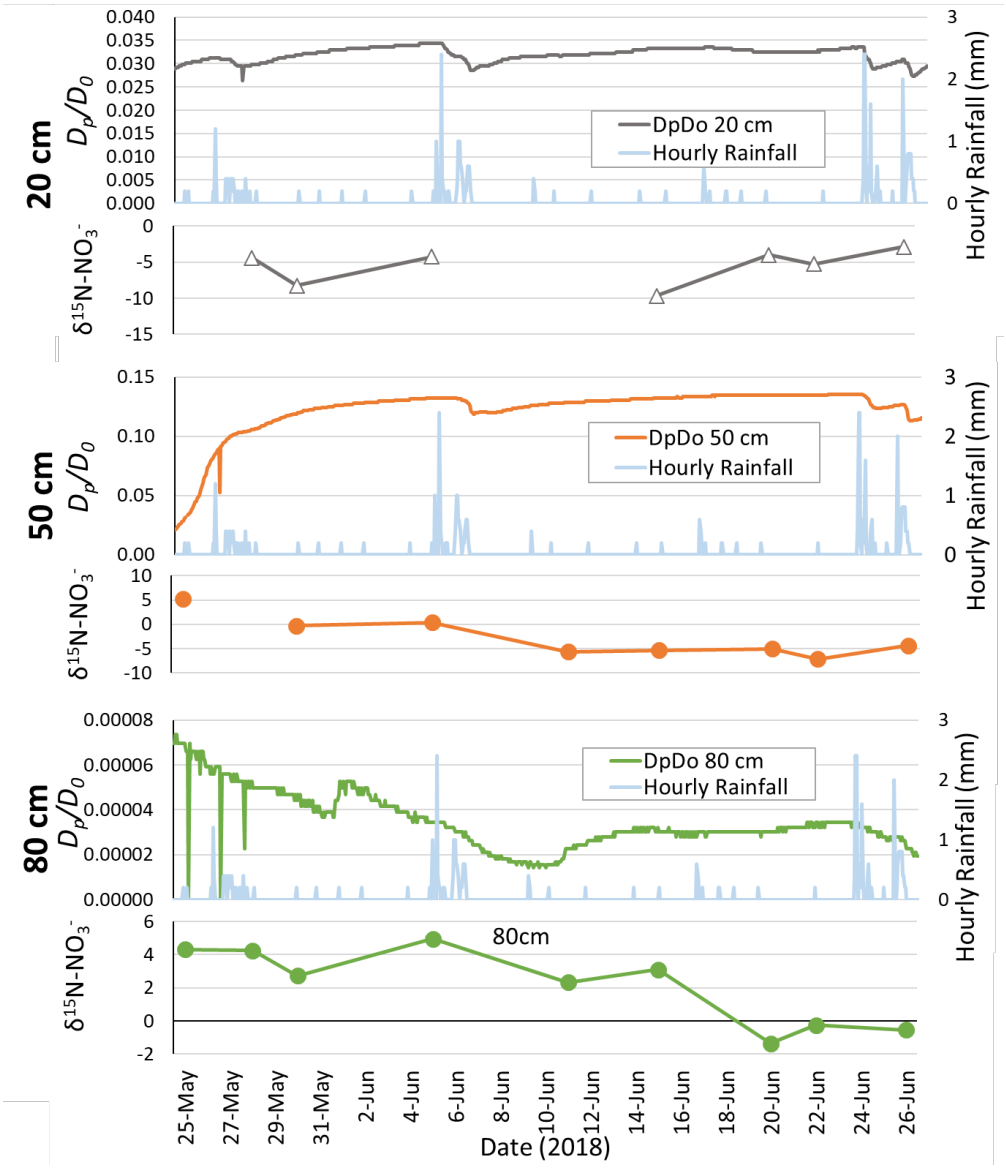

Figure 7.18: Hourly modelled soil diffusivity (using max VWC data) and rainfall (mm) for the DH site over the 2018 two month sampling period, plotted with the corresponding $\delta^{15}N\text{-}NO_3^-$ (‰ v. AIR) values for the 20, 50 and 80 cm sampling depths. 20 cm = grey, 50 cm = orange, 80 cm = green. Note: change in D_p/D_0 and $\delta^{15}N$ scales with each depth.

There was a linear relationship between D_p/D_0 and $\delta^{15}N$ isotope values for the DH site over the 2018 sampling period, with r^2 values of 17, 65 and 31% for the 20, 50 and 80 cm depths, respectively (Figure 7.19).

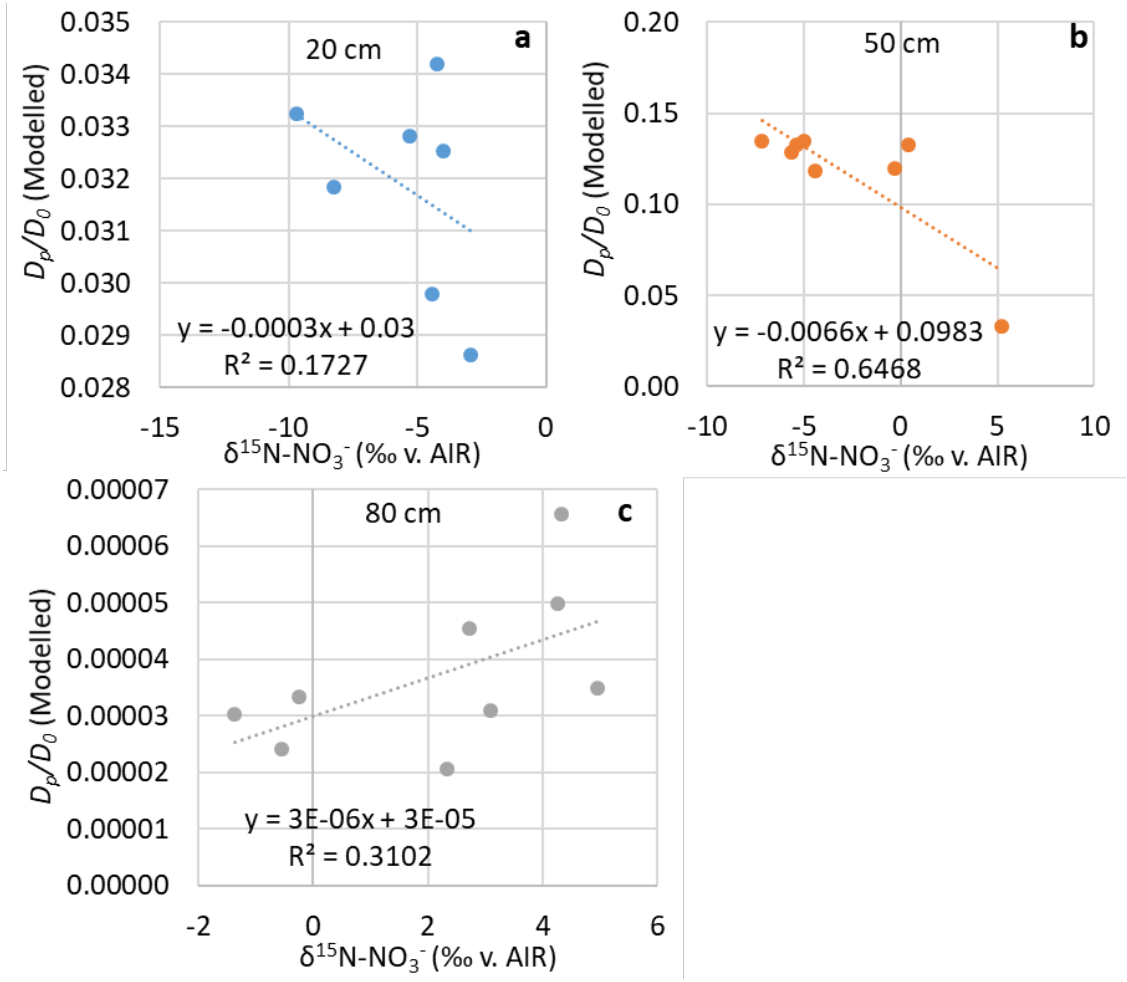

Figure 7.19: Linear regression of modelled D_p/D_0 and $\delta^{15}N\text{-}NO_3^-$ at the DH site for the 2018 sampling period (May - June) at soil depths; (a) 20 cm, (b) 50 cm and (c) 80 cm. Note: change in D_p/D_0 and $\delta^{15}N$ scales with each depth.

7.4 Discussion

7.4.1 Isotope Fractionation

Initially NO_3^- isotope signatures overlapped with those of the soil $\delta^{15}N$ signal, before becoming depleted after the addition of BU. Measured site soil samples had mean $\delta^{15}N$ values of +4.75‰ and +7.37‰ for the A and B horizons, respectively, with soil solution isotope values ranging from $\delta^{15}N\text{-}NO_3^-$ of 0‰ to +13.5‰ at the GM site and between +3.6‰ and +12.2‰ at the DH site before BU application. Previous research in Southland also reported soil $\delta^{15}N$ values ranging from +0.3‰ to +12.9‰ across a regional transect (Rogers et al., 2017). The depletion of the $\delta^{15}N$ signal following BU application is explained by the applied BU having a relatively depleted $\delta^{15}N$ signal compared to the soil, of -0.81‰. As the BU-N was transformed via urea hydrolysis and nitrification it would have created a relatively

depleted $\delta^{15}N$ signal, compared to the soil-N, and which increased as NO_3^- concentrations increased due to (i) the completion of nitrification, (ii) mineralisation and nitrification of antecedent soil-N, and/or (iii) denitrification occurring. Previous data (Chapter 5) indicates that soil derived N may have contributed to this increase in $\delta^{15}N$ signal.

The majority of isotope values measured during this field trial correspond with the reported -10 to +10‰ range for $\delta^{15}N$ and $\delta^{18}O$, which encompasses the range of NO_3^- leached under pastoral agriculture and that originates from a mixture of urea fertiliser and BU, and which is normalised as it moves through agricultural soil (Buckthought et al., 2015c; Granger et al., 2008; Oelmann et al., 2007; Rock et al., 2011). Wells et al. (2015), in a study in Canterbury, New Zealand, stated that this wider range accounts for the effect of post-deposition soil N cycling on $\delta^{15}N$ signatures. The current isotope values generally cluster within reported ranges for urine-N, fertiliser-N and soil-N (Figure 7.20)(Baisden et al., 2016a).

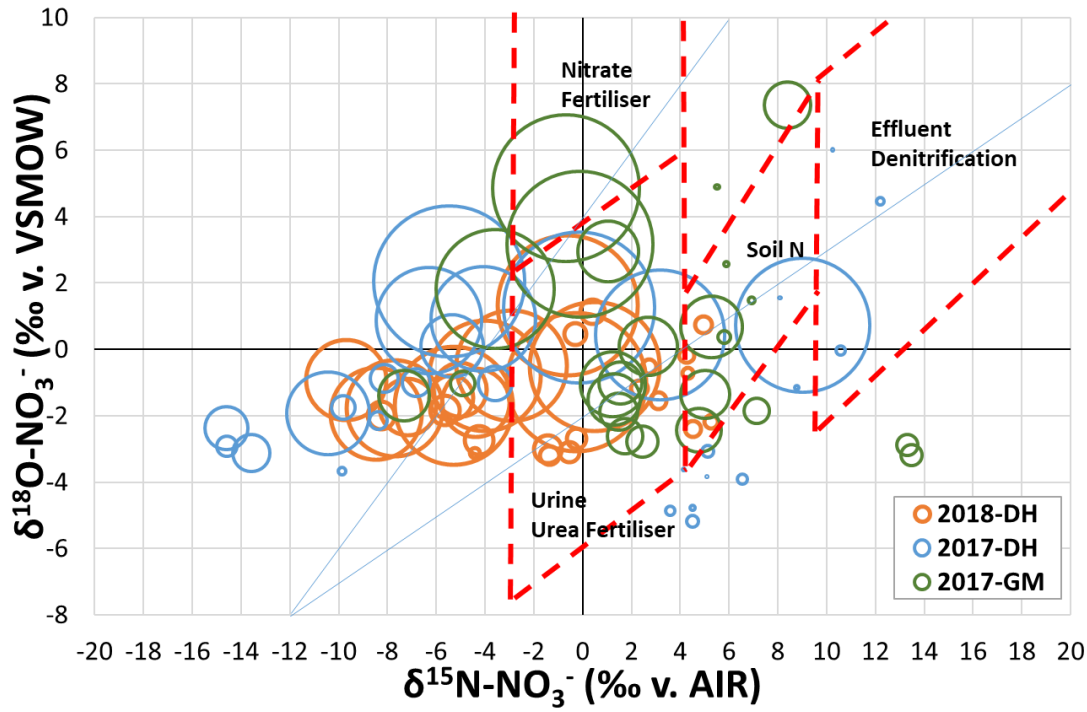

Figure 7.20: Isotope ratio of $\delta^{18}O$ and $\delta^{15}N$-NO_3^- with NO_3^--N concentration represented by the size of the circle. The two soils isotope ratios over the sampling period are shown; DH - 2017 and 2018, GM only 2017. Dashed red boxes represent recognised isotope ratios for specific N sources (Baisden et al., 2016a).

The gley site (DH) shows an initial period of depletion in both $\delta^{18}O$ and $\delta^{15}N$ in 2017 until the end of May, after which parallel enrichment of both NO_3^- isotopes occur as NO_3^- concentrations start to rise. This indicates, that as the BU derived NO_3^- moves down into the soil profile, predominantly evident in the 10 and 20 cm samples, denitrification of BU derived NO_3^- is occurring, as evidenced by the parallel enrichment of the dual NO_3^- isotopes (slope of 0.43 between 30th of May and 14th of June, Figure 7.11). Presence of Br^- at all depths of sampling further supports the presence of BU derived NO_3^-.

In 2017 the $\delta^{18}O$ and $\delta^{15}N$ follow a similar trend at each site, a peak in enrichment, followed by depletion then enrichment again. The difference between sites being that at the oxidising GM site there was enrichment after the application of BU (23rd of May), peaking at a $\delta^{15}N$ of +8.4‰ on the 30th of May at 10 cm. Consequent depletion occurs, dropping to $\delta^{15}N$ -3.6‰ on the 14th of June, before starting to become enriched again. While at the gley DH site the peak in $\delta^{15}N$ of +10.6‰ occurs before BU application on the 15th of May, then it becomes depleted after BU application to -13.6‰ on the 30th of May, with consequent enrichment occurring thereafter. By comparing the two sites after BU application, it seems that the GM site shows a denitrified BU signature after application, before mineralisation causes depletion while the signal of denitrified BU becomes masked straight away at the DH site with a rapid drop to a mineralised signal.

Faster leaching of NO_3^- through the oxidising GM soil indicates that there was less time for microbial denitrification, as shown by the $\delta^{15}N$ signature getting lighter as the NO_3^- concentration increases over time with the BU derived NO_3^- moving through the soil. Whereas the gleyed DH soil shows that as the BU derived NO_3^- moves through the soil, there is some microbial processing of NO_3^- occurring as the $\delta^{15}N$ signal is getting heavier, increasing from -13.6‰ $\delta^{15}N$ at 10 cm on the 30th May 2017 to +9‰ on the 26th of June 2017. The oxidising GM site shows dominance of nitrification as $\delta^{15}N$ gets depleted, with fractionation rates ranging from -14‰ to -46‰ (Casciotti et al., 2003; Mariotti et al., 1981; Shearer et al., 1988). The gley GM site also shows depletion, but this is followed by enrichment, indicating that BU derived NO_3^- was being denitrified.

The DH site, in 2017, shows a denitrification signal with $\delta^{15}N$ enrichment occurring at 10, 20 and 50 cm depths (Figure 7.15) while NO_3^- concentrations increase, indicating that some of the BU derived NO_3^- applied is being denitrified, or that antecedent soil-N has been mineralized and nitrified, but the parallel increase in $\delta^{18}O$ and $\delta^{15}N$ suggests denitrification. However, the GM site, in 2017, only shows depletion in $\delta^{15}N$ as NO_3^- concentrations increase after BU application. The high gravel content and free-draining nature of the GM site in conjunction with the isotopic signal show that denitrification has not occurred, as hypothesised due to soil conditions not being conducive for denitrification processes. Neither does the data show that a contribution from soil organic matter has occurred, but this may not be evident due to the relative magnitude of the BU derived NO_3^- pool.

A study by Wells et al. (2015) found the expected enrichment of soil N as a consequence of NH_3 volatilisation did not occur following urine application to soil, with urine induced mineralisation and subsequent nitrification diluting the $\delta^{15}N$ signal of the urine-N pool. Therefore, the fewer the urine patches (proportional to stocking rate) the bigger the soil influence in overriding urine patch isotope signatures in drainage waters, in addition to the seasonal dilution of the signal through wetting and drying cycles, as aerobic periods trigger mineralisation and nitrification of soil-N (Gu et al., 2010;

Knowles, 1982; Robertson et al., 2007). Nitrification of NH_4^+, through NO_2^- to NO_3^- initially creates a lighter NO_3^- $\delta^{15}N$ signal as the lighter isotopes have a faster rate of reaction (Casciotti et al., 2003), masking NO_3^- $\delta^{15}N$ enrichment. Thus, using ceramic cup samplers, the results show that following BU application the isotopic signature of the leached NO_3^- is in fact highly dynamic over time. The NO_3^- isotopic values obtained in the current study are a net measure of several potentially concurrent effects: soil mineralization and subsequent nitrification; NH_3 volatilisation from BU; nitrification of BU; immobilisation; and denitrification.

In this in situ study NO_3^--N concentrations were higher, but with lower enrichment of $\delta^{15}N$, indicating that less denitrification had occurred compared to the lysimeter trial (Chapter 6). The lysimeter trial and field trial showed peak $\delta^{15}N$ enrichment of +33‰ and +12.2‰, with peak NO_3^--N concentrations of 222 and 323 mg L^{-1}, respectively. Temporal variation in plant N uptake, soil temperatures and soil moisture conditions between the two locations of the trials may have played a role in influencing the presence and activity of the microbial community and therefore the NO_3^--N and $\delta^{15}N$ coming through the soils. The lysimeter study was conducted in Canterbury, where soil temperatures reached a low of 1.4°C (Figure 6.1), compared to the field trials low of 2°C in Southland. The key difference between the two locations being that the lysimeter site in Canterbury also received irrigation to maintain high soil moisture, with total water inputs of 916 mm over the 9 month period from Autumn to the end of Spring, compared to the sites in Southland which received totals of 466 and 520 mm (GM and DH sites, respectively) over the same length of time (Table 7.3). Denitrification occurs under anaerobic conditions, as seen in Chapter 5, the laboratory trial, with the expression of enriched $\delta^{15}N$ peaking at +28‰ corresponding with a decline in NO_3^--N. The high NO_3^--N and low enrichment of $\delta^{15}N$ in the field trial may be due soil conditions not reaching the desired soil moisture level for sufficiently prolonged anaerobic periods that permit denitrification to occur.

7.4.2 Temporal & Spatial Variation

The spatial variation between sites was evident for D_p/D_0: the DH site maintained lower D_p/D_0 values (< 0.2) than the GM site which predominantly ranged between 0.27 and 0.15. Both the 20 and 80 cm depths at the DH site maintained D_p/D_0 < 0.02 for extended periods, a previously reported threshold for denitrification to commence (Balaine et al., 2013). This variation in D_p/D_0 between sites could affect variability in microbial community and activity. Despite receiving similar water inputs, the GM site did not maintain anaerobic soil conditions suitable for denitrifiers as shown by the modelled D_p/D_0 (Figure 7.7). Differences in anaerobic conditions might also be expected to result in differences in substrate supply or conditions for nitrification. For example, Friedl et al. (2018) showed that as WFPS increased heterotrophic nitrification became the dominant source of NO_3^-, a condition which would lead to variation in BU-derived isotope signatures. Similarly, as redox drops under prolonged saturation (< 100

hours) of soils the increasing soil pH can lead to the release of organic matter from mineral surfaces as shown by Grybos et al. (2009), where DOC concentrations increased under saturation of soils, a process that would potentially enhance denitrification.

The two sampling periods over the length of the field trial were intended to test the idea that soil moisture values and subsequent modelled D_p/D_0 could pinpoint temporal shifts in NO_3^- attenuation. Daily and hourly data from the sites allowed for D_p/D_0 to be modelled throughout the trial period, with hourly data showing periods of D_p/D_0, suitable for denitrification, lasting as long as 106 hours (Figure 7.8). However, the periods of low D_p/D_0 did not align with the intensive soil solution sampling periods due to low rainfall intensity over winter months when intensive sampling occurred, and this was intended to ground truth shifts in NO_3^- attenuation occurring with low D_p/D_0 (< 0.02).

Rainfall events were the greatest trigger for the formation of anaerobic conditions as expressed by D_p/D_0 modelling (Figure 7.7 and Figure 7.8). Rainfall events were seen to cause a drop in D_p/D_0 at the 50 and 80 cm depths at both sites, but only if rainfall occurred over an extended period. As seen in this trial, rainfall events of 3 hours or less cause minimal impact to D_p/D_0 values at all depths (Figure 7.9). The occurrence of denitrification is likely after these rainfall events, indicated by D_p/D_0 values less than 0.02 (Balaine et al., 2013). Denitrification has been commonly reported after rainfall events, due to the reduction in available O_2 (Robertson et al., 2007), with 93% of N attenuation shown to occur after rainfall in a pasture based catchment study (Wells et al., 2016). More thorough investigation into ground truthing of attenuation occurring in align with D_p/D_0 is needed to confirm attenuation occurrence in situ. This clearly requires more intensive sampling of NO_3^- and its associated isotopes at time scales conducive to the dynamics of the change in anaerobicity, i.e. D_p/D_0. Modelling of D_p/D_0 is potentially more reliable than using the current O_2 sensors which did not have the resolution to measure subtle changes in O_2 and which also failed on numerous occasions. More intensive sampling within lysimeter studies, on large scale lysimeters is required, as one component of future research, in order to better understand the NO_3^- isotope dynamics.

The two month intensive sampling periods in this trial show an increase in NO_3^--N concentration after the application of BU, and the presence of Br at the same sampling points after indicates that the NO_3^--N source is from applied BU (Figure 7.9 and Figure 7.10). But this two-month sampling period, defined by financial and human resource limitations, did not capture the entire BU breakthrough curve, as the decrease in NO_3^--N concentration back to base level was not observed. As seen in the lysimeter study in Chapter 6, the BU-300 kg N ha^{-1} treatment breakthrough curve started approximately 1 month after application and continued for 3 months, from mid-May to mid-August. However, there was less water input in this field trial and to capture the whole breakthrough curve, intensive sampling would need to have been carried out until one pore volume of drainage had occurred after the BU application. At the

GM site this equated to 6 months (ca. 390 mm of drainage) and 11 months at the DH site (ca. 475 mm of drainage), based on how long it took after BU application in May 2017, for one pore volume (to 80 cm depth) of rainfall and/or irrigation to fall at each site. Sampling for this length of time at the field trial site was inhibited due to lack of resources, but the length of time that it took for NO_3^- to pass through the soil would have had implications in terms of the proportion of NO_3^- denitrified.

This study demonstrates that the NO_3^- isotopic composition, at the study sites, is highly dynamic. The hypothesised temporal trends in denitrification will occur as evidenced by modelled D_p/D_0 under high soil moisture, and 'hot moments' can be triggered by rainfall events and generally appear to be limited to a duration of hours rather than days.

7.5 Conclusions

- D_p/D_0 values and therefore N attenuation hotspots were strongly influenced by spatial variation (soil type) and extended rainfall events. More intense sampling across other soils and other times of the year could be performed to further support this finding.

- Extended sampling to capture the full BU derived NO_3^- breakthrough curve is needed, as denitrification isotope signatures may change further after the soil has had more time to processes N.

- Dilution of denitrification isotope signal by mineralisation of soil N and/or nitrification is evident. Thus, future work looking at nitrification rates and mechanisms at different depths and soil horizons under varying soil moisture contents is warranted.

- Stoney oxidising soils demonstrated movement of BU derived NO_3^- and the dominance of nitrification through the depletion of $\delta^{15}N$. In contrast, the heavier gley soil showed microbial processing of NO_3^- occurring as it moved down through the soil profile, indicated by $\delta^{15}N$ enrichment.

- Further attempts of ground-truthing in situ NO_3^- attenuation, as determined by modelled D_p/D_0 values < 0.02 is warranted, as this would provide a valuable, economic way for farmers and policy makers to both recognise and even engineer 'hot moments' and 'hot spots' of N attenuation occurring in the landscape.

Chapter 8

Summary

8.1 Introduction

This chapter synthesizes all the experimental findings of this study, which were described in detail in previous chapters. The main conclusions for this study are listed along with recommendations for future research and implications for managing spatial and temporal variation in N attenuation in the landscape.

8.2 Why Relative Gas Diffusivity, NO_3^- Isotopes & N Attenuation?

New Zealand agriculture is based on grazed-pasture systems, where urine deposition has become a significant environmental concern (Cameron et al., 2013; Clough et al., 2005). Intensive grazing of pasture results in high soil NO_3^- concentrations resulting from animal excreta, leading to leaching of NO_3^- and N_2O emissions (Close et al., 2016; Galloway et al., 2015; Ravishankara et al., 2009; Selbie et al., 2015). Intensification of the dairy industry has increased stocking rates and fertiliser applications, largely due to farm conversions from sheep and beef systems to dairy (Clark, 2011), putting even more pressure on the environment through excess N loading. Ways of managing this excess N in the landscape are needed if we are to maintain a balance between environmental and economical sustainability. Understanding of key soil parameters, such as soil D_p/D_0, and measurement tools such as natural isotope abundance, may allow for quantification and identification of N attenuation 'hot-spots' and 'hot-moments' in the landscape.

Recent research has outlined the relationship between D_p/D_0 and soil N attenuation thresholds (Balaine et al., 2016b; Balaine et al., 2013; Chamindu-Deepagoda et al., 2019; Deepagoda et al., 2011; Owens et al., 2017; Owens et al., 2016), identifying that it relates strongly with N_2O flux from soils. Measurement of soil moisture and ρ_b in the landscape permit D_p/D_0 to be modelled, from which moments of N attenuation can potentially be pin pointed. Dual NO_3^- isotopes allow for the identification of N processes and sources, a tool which could potentially be used in line with D_p/D_0 modelling to quantify attenuation. Dual NO_3^- isotopes allow for the validation of N processes and sources found in a landscape, as they hold the key signatures of origin and environmental cycles (Baisden et al., 2016b; Mudge et al., 2013; Stevenson et al., 2010; Wells et al., 2015; Wells et al., 2016). Understanding of the variation in isotope signatures in different landscapes and conditions is key to understanding what N processes are occurring, therefore research looking at isotope signature expression under varying spatial and temporal conditions is needed for this tool to be reliably applied.

The use of these two tools will allow for NO_3^- transfers and transformations from grazed pastures to be better understood at a landscape scale.

8.3 Summary & Conclusions

- The main focus of this study was to identify spatial and temporal changes in isotope signatures and D_p/D_0 to help quantify and identify "hot moments" and "hot spots" of N attenuation occurring in the soil, to improve our understanding of soil impacts on NO_3^- dynamics moving through New Zealand's freshwater systems.

- In Chapter 4, a controlled laboratory study was conducted using repacked soil cores to assess spatial change in D_p/D_0, using different soil types, maintained at varying levels of soil moisture. Soil type was found to significantly effect D_p/D_0 at soils moistures of -5 kPa and greater, however, for soil moistures at the wet end of the spectrum (-0.5 kPa to -2 kPa) when peak N_2O emissions occurred, no significance between soil type was found. It was found that peak emissions for all soil types occurred at D_p/D_0 values of <0.006, similar to those previously reported (Balaine et al., 2016a; Balaine et al., 2013; Chamindu-Deepagoda et al., 2019), when the soil was at the wet end of the moisture spectrum. This indicates that D_p/D_0 values associated with NO_3^- attenuation can be extrapolated to field study sites, to the same soil types in-situ. Giving a general overview of what D_p/D_0 values we expect to see in the field when NO_3^--N attenuation is occurring, thus identifying key soil moisture conditions for the occurrence of denitrification.

- In Chapter 5, another laboratory study was conducted with repacked soil cores to assess temporal and spatial change in dual NO_3^- isotope signatures, using the same group of soil types over a three-week period. The aim was to identify the shift in $\delta^{15}N$ and $\delta^{18}O$ for a given decrease in NO_3^- across different soil types. This laboratory experiment took the soil moisture findings from Chapter 4, running all cores at -0.5 kPa to ensure peak denitrification. The key findings from this laboratory study were, (i) there is spatial variation in NO_3^- isotope signatures between A horizons, which play a key role in N processing as seen by much greater fractionation rates than in the B horizons, averaging -19‰ and +4.95‰, respectively for the A and B horizons, (ii) prolonged saturation of the A horizon may drive a shift in the isotopic signature, changing from enrichment to depletion of the NO_3^- isotope signatures, confusing the expression of NO_3^- attenuation. The process of organic-N release under prolonged saturation requires further investigation.

- In Chapter 6, a Lysimeter study was conducted to identify if there was variation in NO_3^- isotope fractionation between intact soil columns with and without plants under varying BU-N

application rates. The role of plant N uptake was evident in this study, as significantly less N was leached under lysimeters that contained plants than those without. Increased BU application shows enrichment of $\delta^{15}N\text{-}NO_3^-$ over time due to denitrification of NO_3^-. However, influence of the presence or absence of plants/plant growth on the isotope signature of NO_3^- was only evident under plant treatments that did not receive any BU. Concluding that denitrification may have been driven by a plant derived C supply, such as root exudation, that made a significant impact on $\delta^{15}N\text{-}NO_3^-$ at very low soil NO_3^- concentrations. But the contribution of such low NO_3^- concentrations to the proportion of N leached under a grazed pastural soil will be minimal compared to the high levels of N leached under a BU patch, indicating that the effect of plants on dual NO_3^- isotope signatures will generally have a negligible influence on interpreting drainage $\delta^{15}N$ values, and that associated information on catchment grazing management and history should be used to interpret data.

- In Chapter 7, two sites in Five Rivers, Southland, New Zealand with contrasting soils were used to run a two-year field trial. The aim of the field trial was to identify spatial and temporal influences on N attenuation and N isotope signatures. Sensors installed at each site were used to look at insitu temporal and spatial change in soil conditions to identify their alignment with potential N attenuation conditions, while soil solution samples were used to assess changes in NO_3^- isotopes. Nitrate attenuation 'hot moments' (duration) and 'hot spots' (location) within the soil profile were analysed by comparing NO_3^- isotope signatures with total NO_3^- concentrations over time, while O_2 sensor data, soil moisture, and soil ρ_b, allowed for the D_p/D_0 of the soil to be both calculated and modelled in order to identify 'hot moments'. Spatial soil variation and temporal events of extended rainfall were found to strongly influence modelled D_p/D_0 values, and therefore N attenuation. Dilution of the denitrification isotope signal by mineralisation and/or nitrification was evident, demonstrating that NO_3^- isotopic composition, over the study period, was highly dynamic. Further ground-truthing of in situ NO_3^- attenuation as determined by modelled D_p/D_0 values (< 0.02) is warranted, with an extended period of sampling needed to capture the full BU breakthrough curve, to provide a more complete picture of soil N processes influence on NO_3^- isotope signatures over time and space (soil depth).

8.4 Future Research Recommendations

- Measurement of soil C during destructive sampling of repacked soil cores may allow for better understanding of NO_3^- isotopic shifts between soil types, as C availability holds the key to variation between soil types. Redox status and measurement of other N-gas products emitted from different soil types over time. This should focus on A horizons, where the significant N

cycling and signature effects occur may allow for the identification of what N processes are occurring to shift NO_3^- isotopes from enrichment to depletion at a time of NH_4^+ concentration reduction. Molecular analyses of the microbial community using DNA and RNA methods (who's there and who's active) would also be desirable in understanding microbial community structure and function in relation to N cycling.

- To further understand spatial and temporal variation in dual NO_3^- isotopic signatures; consideration of the relevant soil moisture regime and its dilution effects on dual NO_3^- isotopic signatures due to prolonged water logging and heterotrophic denitrification is required.

- The $\delta^{15}N\text{-}NO_3^-$ and $\delta^{18}O\text{-}NO_3^-$ show potential for identifying NO_3^- sources and soil processes forming and removing NO_3^-. Further datasets are required to better understand the observed BU rate effects on the temporal dynamics of NO_3^- isotope composition. Such information will assist in better understanding of N cycling in grazed pasture systems and allow agricultural practices to comply with best environmental guidelines. Such data would be best gathered using controlled conditions in lysimeters.

- Continued research into understanding N cycling in New Zealand landscape is vital if we are to continue agricultural production in the future. Finding ways to reduce the impact of our farming systems in a sustainable, financially viable way will allow farming to be continued by future generations.

Appendix A

Soil Information

A.1 Lab & Lysimeter Trials, Braxton Soil, Central Plains

Classified as a Typic Orthic Gley soil (Braxton rolling deep)(Hewitt, 2010). This site was situated in the Central Plains Area of Southland, New Zealand (E1225681 N4877019). Found on the Central Plains physiographic zone, referred to in the text as 'CP'. The soil profile had a 25 cm deep Ap horizon (10YR 4/3), over a Bw to 40cm deep (10YR 5/6). Worm mixing between the Ap and Bw was visible between 25 to 30 cm in the soil profile (Plate A.1). This site was on a Dairy farm, under a rotationally grazed ryegrass pasture.

Plate A.1: Soil profile at location of soil collection for 'Braxton' soil, used in laboratory and lysimeter trials.

This soil was used in the lab trials (Chapters 4 and 5) and the lysimeter trial (Chapter 6). Soil physical and chemical parameters are outlined in Tables A.1 and A.2, below.

Table A.1: Soil texture of the A and B horizons of the Braxton soil used in the laboratory studies. Particle size percentage analysed at University of Waikato (Malvern Matersizer - v3.50). Soil bulk density (Section 3.1, Eq. 3.1).

			Particle size classes (% Volume)				
Soil	Depth cm	Horizon	Clay 0.05 µm	Silt 2 µm	Fine Sand 63 µm	Sand 2000 µm	Bulk Density
Braxton	0 - 25	A	25.1	35.5	39.4	0	0.9
	25 - 40	B	17.2	28.8	54.1	0	1.1

Table A.2: Chemical data for the Braxton soil, Central Plains, Southland.

	Horizon	Depth cm		pH	Olsen P mg/L	Total C %	Total N %	C/N Ratio	CEC me/100g	Total BS %
CP	A	0	25	5.8	30	3.6	0.3	11.2	17	60
	B	25	40	5.5	4	0.9	0.1	10.8	12	46

Plate A.2: The lysimeter collection of Braxton soil from Central Plains, Southland. a) digging the PVC lysimeters down over the intact soil columns. b) some of the completed intact soil columns in their PVC casing. c) Friesian Dairy cows on ryegrass pasture at site. d) pouring heated petroleum jelly down the sides of the columns before removal from site.

Plate A.3: The lysimeter construction and installation at Lincoln University, Canterbury. a) digging out the bottom 5 cm of soil to replace with gravel. b) gravel in the bottom of the PVC lysimeter casing. c) attaching the base cap and drainage bung, silicon sealed. d) lysimeters in place with irrigation system set up.

A.2 Lab Trial Acton Soil, Five Rivers

Classified as a Melanic Orthic Gley (Acton undulating moderately deep)(Hewitt, 2010). This site was in the Five Rivers area of northern Southland (E1257349 N4909615 NZTM, 262 m a.s.l.). Referenced in text as 'AG' (Acton Gleyed) is on a gleyed physiographic zone. This soil was used in the lab trials, Chapters 4 and 5. Soil physical and chemical parameters are outlined in Tables A.3 and A.4, below.

Table A.3: Soil texture of the A and B horizons of the Acton soil used in the laboratory studies. Particle size analysed at University of Waikato (Malvern Matersizer - v3.50). Soil bulk density (Section 3.1, Eq. 3.1).

			Particle size classes (% Volume)				
Soil	Depth cm	Horizon	Clay 0.05 µm	Silt 2 µm	Fine Sand 63 µm	Sand 2000 µm	Bulk Density
Acton Gley	0 - 25	A	16.6	29.1	52.9	1.4	1.0
	25 - 40	B	21.4	35.5	43.1	0	1.3

Table A.4: Chemical data for the Acton soil, Five Rivers, Southland. This soil was used in the laboratory studies.

	Horizon	Depth cm		pH	Olsen P mg/L	Total C %	Total N %	C/N Ratio	CEC me/100g	Total BS %
AG	Ap	0	25	6.1	20	4.6	0.4	10.8	22	73
	Bw	25	40	5.4	3	1.2	0.1	10.2	14	44

Plate A.4: Soil profile at location of soil collection for gley 'Acton' soil for lab trials. Smaller image of B horizon bulk density core sample, showing grey gley colours and rusty mottles.

Plate A.5: The laboratory trial soils (CP and AG), at Lincoln University, Canterbury. a) repacked soil cores ready to go onto tensions tables, from back: AG-B, AG-A, CP-B, CP-A. b) soils after drying in the oven to check moisture contents. Note A and B horizon colour contrast.

A.3 Field Trial Gore Soil (GM - Oxidising), Five Rivers

Classified as an Acidic Orthic Brown (Gore undulating shallow)(Hewitt, 2010), used to represent a well-drained, oxidising site. This site was in the Five Rivers area of northern Southland (E1241567 N4939016 NZTM, 273 m a.s.l.). Referenced in text as 'GM' is in an oxidising physiographic zone. This soil was used in the field trial, Chapter 7. Soil physical and chemical parameters are outlined in Tables A.5 and A.6, below.

Table A.5: Soil texture of the A, B and C horizons of the Gore soil at the field trial site. Particle size analysed at University of Waikato (Malvern Matersizer - v3.50).

			Particle size classes (% Volume)			
Soil	Horizon	Depth cm	Clay 0.05 µm	Silt 2 µm	Fine Sand 63 µm	Sand 2000 µm
GM Site (Oxidising)	A	0 - 15	24.44	45.53	28.85	1.14
	B	15 - 30	18.69	37.46	42.35	1.47
	C	30+	2.84	8.67	78.51	9.7

Table A.6: Chemical data for the Gore soil, Five Rivers, Southland. This soil was one of the field trial sites.

	Horizon	Depth Range cm		pH	Olsen P mg/L	Total C %	Total N %	C/N Ratio	CEC me/100g	Total BS %
GM - Gore Oxidising	Ap	0	5	5.7	47	9.2	0.75	12.2	30	63
	Ap	5	10	5.6	33	7	0.57	12.4	26	52
	Ap	10	15	5.7	34	7.6	0.62	12.3	28	55
	Bw	15	20	5.7	31	6.9	0.57	12.3	25	56
	Bw	20	25	5.6	23	4.9	0.36	13.5	17	36
	Bw2	25	30	5.4	19	2.8	0.19	14.4	11	18
	C	30	80	5.3	11	1	0.07	14.9	5	9
	transect	0	7.5	5.6	29	8.1	0.64	12.7	29	54

Plate A.6: The oxidising field trial site 'GM', Gore Soil, Five Rivers, Southland. a) soil profile, taken while excavating a pocket for the sensors in the side of the profile face. White marker indicating hard iron pan type layer. b) the site during equipment installation, view Northwest. c) Beacon snapshot photo of an Acton Soil Profile, taken in 1999, retrieved from EnvironmentSouthland (2017). d) in the GM soil pit during installation.

Plate A.7: The oxidising field trial site 'GM', Five Rivers, Southland. a) datalogger box, aerial and solar panel at site. b) tipping bucket rain-gauge and tops of ceramic suction cup markers, view North. c) view West.

A.4 Field Trial Acton Soil (DH - Gley), Five Rivers

Classified as a Melanic Orthic Gley soil (Acton undulating moderately deep)(Hewitt, 2010) This site was in the Five Rivers area of northern Southland (E1235143 N4935467 NZTM, 262 m a.s.l.). Referenced in text as 'DH' and is in a gleyed physiographic zone (poorly drained). This soil was used in the field trial (Chapter 7). Soil physical and chemical parameters are outlined in Tables A.7 and A.8, below.

Table A.7: Soil texture of the A, B and C horizons of the Acton soil at the field trial site. Particle size analysed at University of Waikato (Malvern Matersizer - v3.50).

			Particle size classes (% Volume)			
	Horizon	Depth	Clay	Silt	Fine Sand	Sand
Soil		cm	0.05 µm	2 µm	63 µm	2000 µm
DH Site (Gley)	A	0 - 25	21.72	58.36	18.24	1.63
	B	25 - 50	15.46	51.32	33.22	0
	C	50+	7.73	31.79	58.76	1.66

Table A.8: Chemical data for the Acton soil, Five Rivers, Southland. This soil was one of the field trial sites.

	Horizon	Depth Range cm		pH	Olsen P mg/L	Total C %	Total N %	C/N Ratio	CEC me/100g	Total BS %
DH - Acton Gley	Ap	0	5	6.9	62	5.1	0.46	11.2	26	94
	Ap	5	10	6.9	73	5.7	0.5	11.2	27	91
	Ap	10	15	6.5	53	4	0.38	10.5	25	82
	AB	15	20	6.4	31	3	0.3	10.1	22	77
	AB	20	25	6.2	19	2.4	0.24	10.4	21	77
	AB	25	30	6.2	14	2.4	0.22	10.8	20	75
	Bg	30	35	6.2	7	2.1	0.19	11.3	18	71
	Bg	35	40	6.2	4	1.3	0.11	12	16	70
	Bg	40	45	6.2	3	1.2	0.09	13.2	15	69
	Bs	45	50	6.1	4	1.3	0.1	12.9	14	68
	BC	50	80	6.3	5	0.7	0.06	11.1	12	71
	transect	0	7.5	6.4	22	4.5	0.43	10.7	29	77

Plate A.8: The gley field trial site 'DH', Acton Soil, Five Rivers, Southland. a) View North at the DH site before installation. b) Beacon snapshot photo of an Acton Soil Profile, taken in 1999, retrieved from EnvironmentSouthland (2017). c) soil profile, taken while excavating a pocket for the sensors in profile face. Colour discrepancy as profile face has dried. d) a handful of the waterlogged gley subsoil in the DH soil pit during installation.

Plate A.9: Gley field trial site, 'GM', Five Rivers, Southland. a) Solar panel and aerial, above datalogger box, with ceramic suction cup markers visible. b) the internal workings of the datalogger. c) view on site farm looking East, toward Mid-dome.

A.5 Site Locations

Figure A.1: Site locations in Southland, New Zealand; Five Rivers and Central Plains areas where soil samples were taken for laboratory experiments and lysimeters. The field trial sites were in Five Rivers. Underlying reference zone map (Rissmann, 2011).

Appendix B

Field Trial Data

B.1 Rainfall & Irrigation Data

Table B.1: Monthly total water inputs (mm) over the trial period at the two field trial sites. GM = rainfall + centre pivot irrigation. DH = rainfall only.

Year		Month	GM Site	DH Site
2017	Autumn	Mar	57.5	34.2
		Apr	7.0	25.4
		May		83.0
	Winter	Jun	65.5	37.2
		Jul	107.0	10.6
		Aug	29.0	5.2
	Spring	Sep	68.5	71.2
		Oct	78.0	29.4
		Nov	110.5	36.6
	Summer	Dec	22.5	45.6
2018		Jan	42.5	29.4
		Feb		81.0
	Autumn	Mar		4.4
		Apr		52.0
		May	68.0	86.4
	Winter	Jun	28.0	16.6
		July	46.0	67.2
		Aug	27.5	31.6
	Spring	Sep	70.5	58.8
		Oct	67.5	72.4
		Nov	159.0	124.2
	Summer	Dec	131.0	66.6
2019		Jan	127.5	64.4
		Feb	149.0	51.6
	Autumn	Mar	84.5	57.2

B.2 Nitrate Concentrations

Table B.2 Mean NO_3^--N concentrations (mg L^{-1}) for the GM soil, at each of the sampling depths over the May - June sampling points in 2017 and 2018 in Southland, New Zealand. Values are replicate means, SEM and sample size shown (n).

2017	10 cm	SEM	*n*	20 cm	SEM	*n*	50 cm	SEM	*n*	80 cm	SEM	*n*
15-May	24.0		*1*	0.0		*1*	6.2		*1*	15.9		*1*
19-May	28.2		*1*	0.7		*1*	6.3		*1*	17.7		*1*
22-May	44.6	± 30.9	*3*	0.7		*1*	8.7	± 1.3	*4*	12.4	± 5.5	*3*
26-May	26.2	± 13.7	*3*	1.8		*1*	9.2	± 1.3	*4*	9.0	± 1.3	*3*
30-May	26.1	± 18.5	*3*	1.0		*1*	13.0	± 3.7	*4*	19.0	± 8.4	*3*
2-Jun	30.9	± 13.8	*3*	1.7	± 0.6	*2*	9.9	± 2.3	*4*	23.7	± 9.1	*3*
6-Jun	42.7	± 16.6	*3*	2.7	± 0.5	*2*	14.9	± 3.2	*4*	40.1		*1*
9-Jun	82.6		*1*	3.4	0.4	*2*	15.0	± 2.8	*4*	38.2		*1*
14-Jun	156.5	± 19.4	*2*	8.3	± 4.3	*2*	15.7	± 2.3	*4*	28.8	± 13.6	*2*
16-Jun	132.6	± 44.8	*2*	6.3		*1*	21.6	± 3.9	*4*	27.6	± 11.6	*3*
21-Jun	236.2		*1*	9.9		*1*	22.3	± 4.9	*4*	48.0		*1*
23-Jun	141.7	± 43.1	*2*	11.6		*1*	25.8	± 3.4	*3*	35.7	± 16.0	*2*
26-Jun	233.4	± 92.7	*2*	31.1	± 11.8	*2*	32.2	± 4.3	*3*	39.7	± 15.3	*2*
30-Jun	212.1	± 133.2	*2*	16.1		*1*	33.5	± 3.4	*4*	42.4	± 12.6	*2*
2018	**10 cm**	**SEM**	***n***	**20 cm**	**SEM**	***n***	**50 cm**	**SEM**	***n***	**80 cm**	**SEM**	***n***
10-May				0.6	± 0.3	*2*	29.6		*1*	50.6	± 20.75	*2*
17-May				0.9	± 0.8	*3*	14.0	± 8.5	*2*	31.1	± 19.05	*2*
21-May				2.8	± 2.2	*4*	27.6	± 13.5	*4*	26.8	± 15.82	*2*
25-May	2.0		*1*	0.7	± 0.5	*3*	12.3		*1*	14.5	± 4.94	*2*
28-May				3.0	± 1.7	*4*	10.3	± 7.5	*2*	24.6	± 7.246	*3*
30-May	9.8		*1*	1.4	± 1.1	*2*				28.4		*1*
5-Jun				0.7	± 0.2	*2*						
11-Jun				2.4	± 0.7	*3*	14.9	± 6.5	*4*	11.6	± 5.726	*3*
15-Jun				6.5	± 2.0	*3*	15.5	± 5.4	*4*	9.0		*1*
20-Jun				9.2	± 3.2	*3*	11.0	± 4.2	*3*	27.9		*1*
22-Jun				8.4	± 3.8	*2*	16.4	± 5.2	*4*	8.7		*1*
26-Jun				16.3	± 5.9	*3*	16.2	± 5.1	*4*	14.3	± 7.002	*2*
29-Jun				30.8	± 9.3	*4*	19.3	± 7.1	*4*	21.5		*1*

Table B.3: Nitrate-N concentrations (mg L^{-1}) for the DH soil, at each of the sampling depths over the May - June sampling points in 2017 and 2018 in Southland, New Zealand. Values are replicate means, SEM and sample size shown (n).

2017	10 cm	SEM	*n*	20 cm	SEM	*n*	50 cm	SEM	*n*	80 cm	SEM	*n*
15-May	1.7	± 0.9	*2*	1.2	± 0.8	*2*	2.4	± 0.4	*4*	1.8	± 1.0	*3*
19-May	0.6		*1*	0.3	± 0.1	*4*	1.8	± 0.7	*4*	2.3	± 1.3	*3*
22-May	0.3	± 0.1	*2*	0.3	± 0.2	*3*	0.4	± 0.1	*4*	0.8	± 0.2	*4*
26-May	1.5	± 0.5	*3*	1.1	± 0.2	*3*	0.4	± 0.1	*4*	0.9	± 0.4	*4*
30-May	17.1	± 3.5	*4*	5.9	± 1.4	*4*	1.3	± 1.1	*4*	1.6	± 0.7	*4*
2-Jun	31.2	± 13.6	*4*	10.1	± 3.7	*4*	2.7	± 2.4	*4*	1.0	± 0.1	*4*
6-Jun	77.4	± 18.4	*4*	22.5	± 2.2	*4*	4.7	± 4.3	*4*	0.9	± 0.2	*3*
9-Jun	68.6	± 35.0	*4*	35.8	± 6.9	*4*	9.9	± 7.0	*4*	0.7	± 0.1	*2*
14-Jun	122.0	± 37.9	*4*	124.8	± 44.8	*4*	10.0	± 5.3	*4*	2.4	± 1.5	*4*
16-Jun	152.9	± 34.7	*4*	126.9	± 33.1	*4*	20.0	± 11.0	*4*	3.8	± 2.3	*4*
21-Jun	185.5	± 32.5	*4*	250.5		*1*	14.7	± 7.8	*3*	7.6	± 5.0	*3*
23-Jun	176.9	± 34.4	*4*	186.7	± 37.6	*3*	37.0	± 24.7	*4*	4.9	± 2.9	*4*
26-Jun	198.0	± 44.2	*4*	249.9	± 51.9	*4*	45.0	± 25.3	*4*	10.5	± 7.0	*4*
30-Jun	147.1	± 54.4	*4*	194.1	± 28.5	*4*	46.0	± 26.1	*4*	8.4	± 5.8	*4*
2018	**10 cm**	**SEM**	***n***	**20 cm**	**SEM**	***n***	**50 cm**	**SEM**	***n***	**80 cm**	**SEM**	***n***
10-May	1.5	± 0.9	*4*	0.6	± 0.3	*4*	0.6	± 0.6	*4*	1.0	± 0.5	*4*
17-May	4.4	± 1.7	*4*	2.3	± 0.9	*3*	1.9	± 1.3	*3*	0.5	± 0.1	*4*
21-May	10.8	± 7.5	*2*	5.0	± 1.4	*3*	1.9	± 0.7	*4*	0.4	± 0.2	*4*
25-May	4.4		*1*	2.2		*1*	3.3		*1*	2.5	± 1.4	*4*
28-May	10.6	± 2.3	*4*	10.6	± 3.3	*2*	3.0	± 1.3	*4*	3.9	± 1.5	*4*
30-May	10.7	± 4.2	*4*	11.6	± 2.4	*3*	7.0	± 1.1	*4*	3.8	± 0.4	*4*
5-Jun	38.6	± 22.4	*4*	22.0		*1*	8.9		*1*	4.6		*1*
11-Jun	105.6	± 20.9	*4*	74.7	± 37.3	*3*	11.7	± 0.4	*3*	4.6	± 0.5	*4*
15-Jun	95.5		*1*	139.2		*1*	24.7	± 9.5	*2*	4.4	± 1.0	*3*
20-Jun	213.6	± 30.0	*3*	156.9	± 39.7	*3*	34.8	± 13.5	*2*	5.6	± 1.2	*4*
22-Jun	187.4	± 56.0	*2*	137.7		*1*	39.0	± 11.2	*2*	5.9	± 1.1	*4*
26-Jun	304.5	± 40.0	*3*	218.3	± 43.0	*3*	54.8	± 12.2	*4*	6.3	± 1.3	*4*
29-Jun	257.9	± 89.2	*4*	323.1	± 53.1	*3*	52.2	± 12.6	*4*	7.4	± 2.8	*4*

B.3 Bromide Concentrations

Table B.4: Mean bromide concentrations (mg L^{-1}) for the GM soil, at each of the sampling depths over the May - June sampling points in 2017 and 2018 in Southland, New Zealand. Values are replicate means, SEM and sample size shown (n).

2017	10 cm	SEM	*n*	20 cm	SEM	*n*	50 cm	SEM	*n*	80 cm	SEM	*n*
15-May												
19-May												
22-May												
26-May	38.2	± 26.8	*3*	5.2		*1*	0.6	± 0.5	*4*	0.0	± 0.0	*2*
30-May	56.1	± 23.4	*3*	0.0		*1*	1.0	± 0.7	*2*	0.2	± 0.1	*2*
2-Jun	121.2	± 53.1	*3*	0.8	± 0.7	*2*	0.0	± 0.0	*3*	0.6	± 0.1	*2*
6-Jun	117.8	± 74.2	*2*	1.9	± 0.8	*2*	0.2	± 0.2	*3*			
9-Jun	271.9		*1*	2.3	± 0.3	*2*	0.0	± 0.0	*3*			
14-Jun	415.7	± 52.7	*2*	23.4	± 19.5	*2*	0.3	± 0.0	*2*	0.1	± 0.1	*2*
16-Jun	426.1		*1*	6.1		*1*	3.4	± 2.6	*3*	0.1	± 0.1	*2*
21-Jun				10.5		*1*	6.1	± 2.3	*4*			
23-Jun	212.2		*1*	16.2		*1*	17.1	± 10.7	*3*	0.3	±	*1*
26-Jun	245.5		*1*	73.1	± 45.4	*2*	27.9	± 15.2	*3*	0.8	±	*1*
30-Jun	133.0		*1*	22.1		*1*	21.4	± 6.4	*3*	1.7	±	*1*
2018	**10 cm**	**SEM**	***n***	**20 cm**	**SEM**	***n***	**50 cm**	**SEM**	***n***	**80 cm**	**SEM**	***n***
10-May				0.4	± 0.1	*2*	4.5		*1*			
17-May				1.1		*1*	1.1		*1*			
21-May				1.0	± 0.7	*4*						
25-May	236.2		*1*	10.8	± 4.3	*3*				2.7		*1*
28-May				88.2	± 43.1	*2*						
30-May	121.3		*1*	150.7	± 48.3	*2*						
5-Jun				42.9	± 24.9	*2*						
11-Jun				202.1	± 14.2	*2*				11.1		*1*
15-Jun				111.6	± 33.6	*2*	41.5	± 16.6	*4*			
20-Jun				97.6	± 38.6	*3*						
22-Jun				63.9	± 7.3	*2*						
26-Jun				115.1	± 37.5	*3*						
29-Jun				222.9	± 44.2	*3*	114.8		*1*			

Table B.5: Mean bromide concentrations (mg L^{-1}) for the DH soil, at each of the sampling depths over the May - June sampling points in 2017 and 2018 in Southland, New Zealand. Values are replicate means, SEM and sample size shown (n).

2017	10 cm	SEM	*n*	20 cm	SEM	*n*	50 cm	SEM	*n*	80 cm	SEM	*n*
15-May												
19-May												
22-May												
26-May	206.1	± 88.6	*3*	132.9	± 78.0	*2*	4.6	± 3.4	*3*	34.3		*1*
30-May	453.3	± 116.1	*2*	233.0	± 55.3	*2*	1.7		*1*	15.4	± 11.7	*4*
2-Jun	392.4	± 113.9	*4*	226.9	± 21.0	*2*	11.6	± 7.9	*2*	20.4	± 12.3	*4*
6-Jun	455.5	±	*1*	267.5	± 86.0	*2*	120.0	± 112.2	*2*	11.1		*1*
9-Jun	397.4	± 119.3	*4*	292.4		*1*	73.6	± 53.4	*4*			
14-Jun				229.5		*1*	20.4		*1*			
16-Jun	271.0	± 48.4	*2*				43.3		*1*	1.3		*1*
21-Jun	267.0	± 63.4	*3*				55.6	± 13.6	*3*	84.8	± 74.3	*2*
23-Jun							39.7	± 23.8	*2*	47.5	± 43.3	*2*
26-Jun	170.2		*1*	384.0		*1*	64.7	± 13.8	*3*	79.5	± 72.0	*2*
30-Jun	171.4	± 90.7	*2*	344.0		*1*	76.1		*1*	53.4	± 48.1	*2*
2018	**10 cm**	**SEM**	***n***	**20 cm**	**SEM**	***n***	**50 cm**	**SEM**	***n***	**80 cm**	**SEM**	***n***
10-May	1.2	± 0.2	*4*	1.6	± 0.4	*3*	1.0	± 0.1	*2*	1.5	± 1.0	*3*
17-May	0.6	± 0.3	*2*	0.2	± 0.1	*2*	0.3	± 0.2	*2*	0.8	± 0.1	*2*
21-May				0.3		*1*	0.4	± 0.2	*2*			
25-May				17.3		*1*				1.8		*1*
28-May	217.9	± 122.5	*3*				41.3	± 8.1	*3*	7.0		*1*
30-May	255.1	± 158.5	*3*				80.8		*1*			
5-Jun	415.7	± 129.8	*2*									
11-Jun	423.7	± 184.9	*2*	408.4	± 126.6	*2*	127.5	± 24.0	*2*	2.6	± 1.0	*2*
15-Jun							179.8		*1*			
20-Jun	565.4	± 66.0	*2*	431.5	± 127.2	*2*	196.4		*1*	3.8		*1*
22-Jun	360.6		*1*							4.0		*1*
26-Jun	513.3	± 40.7	*3*	296.8	± 21.6	*2*	186.9	± 42.1	*3*			
29-Jun	493.0	± 47.6	*3*	422.8	± 102.1	*2*	157.3	± 67.8	*2*			

B.4 Dual NO_3^- Isotopes

Table B.6: Nitrate-$\delta^{15}N$ isotope values (‰ v. AIR) for both the GM (2017) and DH (2017 and 2018) field trial sites, at each of the sampling depths, Southland, New Zealand. GM not analysed for isotope values in 2018. SEM and sample size shown (*n*).

GM 2017	10 cm	SEM	*n*	20 cm	SEM	*n*	50 cm	SEM	*n*	80 cm	SEM	*n*
15-May	4.8		1	0.0		1	13.5		1	1.7		1
19-May	5.0		1	5.5		1	13.3		1	1.5		1
22-May	5.3	± 0.4	3	5.9		1	7.1	± 1.7	4	2.4	± 1.4	3
26-May												
30-May	8.4		1	6.9		1						
2-Jun												
6-Jun	1.0		1	5.8		1						
9-Jun												
14-Jun	-3.6	± 3.7	2	-4.9		1						
16-Jun												
21-Jun	-0.7		1				1.6		1	1.2		1
23-Jun												
26-Jun	-0.1	± 1.1	2	-7.3		1	1.3		1	2.7		1
30-Jun												
DH 2017	**10 cm**	**SEM**	***n***	**20 cm**	**SEM**	***n***	**50 cm**	**SEM**	***n***	**80 cm**	**SEM**	***n***
15-May	10.6	± 0.1	2	12.2	± 1.1	2	5.1	± 1.2	4	6.5	± 1.4	3
19-May	8.8		1	10.2	± 2.4	4	3.6	± 1.2	4	4.5	± 1.6	3
22-May	5.1	± 0.9	2	8.1	± 1.3	3	4.2	± 1.2	4	4.5	± 0.6	4
26-May												
30-May	-13.6		1	-14.6		1	-9.9		1			
2-Jun												
6-Jun	-10.4		1	-14.6		1	-8.4		1			
9-Jun												
14-Jun	-4.1		1	-6.3		1	-6.8		1			
16-Jun												
21-Jun	3.2	± 2.3	4	-5.5		1	-3.6		1	-9.8		1
23-Jun												
26-Jun	9.0	± 2.7	4	-0.2	± 0.4	4	-5.4		1	-8.1		1
30-Jun												
DH 2018	**10 cm**	**SEM**	***n***	**20 cm**	**SEM**	***n***	**50 cm**	**SEM**	***n***	**80 cm**	**SEM**	***n***
10-May												
17-May												
21-May												
25-May	4.5		1				5.3		1	4.3		1
28-May	-1.4		1	-4.4	± 4.4	2				4.3		1
30-May				-8.3	± 4.2	3	-0.3	± 2.3	3	2.7		1
5-Jun				-4.3		1	0.4		1	5.0		1
11-Jun	-7.7	± 1.9	2				-5.7		1	2.3		1
15-Jun	-8.5		1	-9.7		1	-5.4		1	3.1		1
20-Jun	-0.3		1	-4.0		1	-5.0		1	-1.4		1
22-Jun	0.5		1	-5.3		1	-7.2	± 2.3	2	-0.3		1
26-Jun				-2.9		1	-4.4		1	-0.5		1
29-Jun												

Table B.7: Nitrate-$\delta^{18}O$ isotope values (‰ v. VSMOW) for both the GM (2017) and DH (2017 and 2018) field trial sites, at each of the sampling depths, Southland, New Zealand. GM not analysed for isotope values in 2018. SEM and sample size shown (*n*).

GM 2017	10 cm	SEM	*n*	20 cm	SEM	*n*	50 cm	SEM	*n*	80 cm	SEM	*n*
15-May	-2.4		*1*	0.0		*1*	-3.2		*1*	-2.6		*1*
19-May	-1.4		*1*	4.9		*1*	-2.9		*1*	-1.9		*1*
22-May	0.7	± 2.5	*3*	2.6		*1*	-1.8	± 0.3	*4*	-2.8	± 0.4	*3*
26-May												
30-May	7.4		*1*	1.5		*1*						
2-Jun												
6-Jun	3.0		*1*	0.4		*1*						
9-Jun												
14-Jun	1.8	± 1.5	*2*	-1.0		*1*						
16-Jun												
21-Jun	4.9		*1*				-1.0		*1*	-1.1		*1*
23-Jun												
26-Jun	3.2	± 2.9	*2*	-1.4		*1*	-1.5		*1*	0.1		*1*
30-Jun												
DH 2017	**10 cm**	**SEM**	***n***	**20 cm**	**SEM**	***n***	**50 cm**	**SEM**	***n***	**80 cm**	**SEM**	***n***
15-May	0.0	± 0.5	*2*	4.5	± 3.2	*2*	-3.1	± 1.3	*4*	-3.9	± 1.8	*3*
19-May	-1.2		*1*	6.0	± 5.6	*4*	-4.9	± 1.5	*4*	-5.2	± 1.8	*3*
22-May	-3.8	± 1.0	*2*	1.6	± 1.1	*3*	-3.6	± 1.4	*4*	-4.8	± 0.3	*4*
26-May												
30-May	-3.1		*1*	-2.9		*1*	-3.7		*1*			
2-Jun												
6-Jun	-1.9		*1*	-2.4		*1*	-2.2		*1*			
9-Jun												
14-Jun	0.9		*1*	0.9		*1*	-1.0		*1*			
16-Jun												
21-Jun	0.4	± 0.3	*4*	2.0		*1*	-1.0		*1*	-1.8		*1*
23-Jun												
26-Jun	0.7	± 0.4	*4*	1.3	± 0.5	*4*	0.1		*1*	-0.9		*1*
30-Jun												
DH 2018	**10 cm**	**SEM**	***n***	**20 cm**	**SEM**	***n***	**50 cm**	**SEM**	***n***	**80 cm**	**SEM**	***n***
10-May												
17-May												
21-May												
25-May	-2.4		*1*				-2.2		*1*	-0.7		*1*
28-May	-3.0		*1*	-3.1	± 0.5	*2*				-0.2		*1*
30-May				-2.0	± 0.4	*3*	0.5	± 0.9	*3*	-0.5		*1*
5-Jun				-2.7		*1*	1.1		*1*	0.7		*1*
11-Jun	-1.8	± 0.04	*2*				-1.8		*1*	-1.2		*1*
15-Jun	-1.9		*1*	-0.9		*1*	-1.5		*1*	-1.6		*1*
20-Jun	-1.0		*1*	-0.8		*1*	-1.2		*1*	-3.2		*1*
22-Jun	-0.5		*1*	-1.7		*1*	-1.7	± 0.5	*2*	-2.7		*1*
26-Jun				-0.5		*1*	-1.6		*1*	-3.1		*1*
29-Jun												

References

Abbasi, M. K., & Adams, W. A. (2000). Gaseous N emission during simultaneous nitrification–denitrification associated with mineral N fertilization to a grassland soil under field conditions. *Soil Biology & Biochemistry, 32*, 1251-1259.

Abe, Y., & Hunkeler, D. (2006). Does the Rayleigh equation apply to evaluate field isotope data in contaminant hydrogeology? *Environmental Science & Technology, 40*, 1588-1596.

Addiscott, T. M., & Benjamin, N. (2004). Nitrate and human health. *Soil Use & Management, 20*, 98-104.

Aeppli, C., Berg, M., Cirpka, O. A., Holliger, C., Schwarzenbach, R. P., & Hofstetter, T. B. (2009). Influence of mass-transfer limitations on carbon isotope fractionation during microbial dechlorination of trichloroethene. *Environmental Science & Technology, 43*, 8813-8820.

Alexander, R. B., Elliott, A. H., Shankar, U., & McBride, G. B. (2002). Estimating the sources and transport of nutrients in the Waikato River Basin, New Zealand. *Water resources research, 38*, 4-1-4-23.

Alexander, R. B., Smith, R. A., & Schwarz, G. E. (2000). Effect of stream channel size on the delivery of nitrogen to the Gulf of Mexico. *Nature, 403*, 758-761.

Amberger, A., & Schmidt, H.-L. (1987). Natürliche isotopengehalte von Nitrat als Indikatoren für dessen Herkunft. *Geochimica et Cosmochimica Acta, 51*, 2699-2705.

Amundson, R., Austin, A. T., Schuur, E. A. G., Yoo, K., Matzek, V., Kendall, C., Uebersax, A., Brenner, D., & Baisden, T. W. (2003). Global patterns of the isotopic composition of soil and plant nitrogen. *Global Biogeochemical Cycles, 17*, 1031.

An, S., & Joye, S. B. (2001). Enhancement of coupled nitrification-denitrification by benthic photosynthesis in shallow estuarine sediments. *Limnology & Oceanography, 46*, 62-74.

Andersen, A. J., & Petersen, S. O. (2009). Effects of C and N availability and soil-water potential interactions on N_2O evolution and PLFA composition. *Soil Biology & Biochemistry, 41*, 1726-1733.

Anderson, T. R., Groffman, P. M., Kaushal, S. S., & Walter, M. T. (2014). Shallow groundwater denitrification in riparian zones of a headwater agricultural landscape. *Journal of Environmental Quality, 43*, 732-744.

Assouline, S. (2006). Modeling the Relationship between Soil Bulk Density and the Water Retention Curve,. *Vadose Zone Journal, 5*, 554-563.

Aulakh, M. S., Doran, J. W., Walters, D. T., & Power, J. F. (1991). Legume residue and soil water effects on denitrification in soils of different textures. *Soil Biology & Biochemistry, 23*, 1161-1167.

Austin, A. T., & Vitousek, P. M. (1998). Nutrient dynamics on a precipitation gradient in Hawai'i. *Oecologia, 113*, 519-529.

Baertschi, P. (1976). Absolute ^{18}O content of standard mean ocean water. *Earth and Planetary Science Letters, 31*, 341-344.

Bahn, M., Schmitt, M., Siegwolf, R., Richter, A., & Brüggemann, N. (2009). Does photosynthesis affect grassland soil-respired CO_2 and its carbon isotope composition on a diurnal timescale? *New Phytologist, 182*, 451-460.

Bailey, L. D. (1976). Effects of temperature and root on denitrification in a soil. *Canadian Journal of Soil Science, 56*, 79-87.

Bailey, L. D., & Beauchamp, E. G. (1973). Effects of temperature on NO_3^- and NO_2^- reduction, nitrogenous gas production, and redox potential in a saturated soil. *Canadian Journal of Soil Science, 53*, 213-218.

Baily, A., Rock, L., Watson, C. J., & Fenton, O. (2011). Spatial and temporal variations in groundwater nitrate at an intensive dairy farm in south-east Ireland: Insights from stable isotope data. *Agriculture, ecosystems & environment, 144*, 308-318.

Baisden, T. W., Rissman, C., Ellis, T., Rayner, S., Clough, T. J., Moore, C., Killick, M., Rodway, E., Horton, T. W., & Clark, M. (2016a). Informing Policy and Management in New Zealand Agricultural

Regions Using Nitrogen and Oxygen Isotopes to Quantify Hot Spots and Hot Moments of Nitrate Loss Symposium conducted at the meeting of the American Geophysical Union

Baisden, W. T., Rissman, C., Ellis, T., Rayner, S., Clough, T. J., Moore, C., Killick, M., Rodway, E., Horton, T. W., & Clark, M. (2016b). Informing Policy and Management in New Zealand Agricultural Regions Using Nitrogen and Oxygen Isotopes to Quantify Hot Spots and Hot Moments of Nitrate Loss Symposium conducted at the meeting of the AGU Fall Meeting Abstracts

Bakken, L. R., Bergaust, L., Liu, B., & Frostegård, Å. (2012). Regulation of denitrification at the cellular level: a clue to the understanding of N_2O emissions from soils. *Philosophical Transactions of the Royal Society B: Biological Sciences, 367*, 1226-1234.

Bakken, L. R., & Frostegård, Å. (2017). Sources and sinks for N_2O, can microbiologist help to mitigate N_2O emissions? *Environmental Microbiology, 19*, 4801-4805.

Balaine, N., Clough, T. J., Beare, M. H., Thomas, S. M., & Meenken, E. D. (2016a). Soil Gas Diffusivity Controls N_2O and N_2 Emissions and their Ratio. *Soil Science Society of America Journal, 80*, 529-540.

Balaine, N., Clough, T. J., Beare, M. H., Thomas, S. M., & Meenken, E. D. (2016b). Soil Gas Diffusivity Controls N_2O and N_2 Emissions and their Ratio. *Soil Science Society of America Journal*.

Balaine, N., Clough, T. J., Beare, M. H., Thomas, S. M., Meenken, E. D., & Ross, J. G. (2013). Changes in relative gas diffusivity explain soil nitrous oxide flux dynamics. *Soil Science Society of America Journal, 77*, 1496-1505.

Baldwin, D. S., & Mitchell, A. M. (2000). The effects of drying and re-flooding on the sediment and soil nutrient dynamics of lowland river–floodplain systems: a synthesis. *Regulated Rivers: Research & Management, 16*, 457-467.

Balogh, J., Pintér, K., Fóti, S., Cserhalmi, D., Papp, M., & Nagy, Z. (2011). Dependence of soil respiration on soil moisture, clay content, soil organic matter, and CO_2 uptake in dry grasslands. *Soil Biology and Biochemistry, 43*, 1006-1013.

Bateman, E. J., & Baggs, E. M. (2005). Contributions of nitrification and denitrification to N_2O emissions from soils at different water-filled pore space. *Biology and Fertility of Soils, 41*, 379-388.

Bates, H. K., & Spalding, R. F. (1998). Aquifer denitrification as interpreted from in situ microcosm experiments. *Journal of Environmental Quality, 27*, 174-182.

Beare, M. H., Gregorich, E. G., & St-Georges, P. (2009). Compaction effects on CO_2 and N_2O production during drying and rewetting of soil. *Soil Biology & Biochemistry, 41*, 611-621.

Beauchamp, E. G., Gale, C., & Yeomans, J. C. (1980). *Organic Matter Availability for Denitrification in Soils of Different Textures and Drainage Classes* (Vol. 11). doi:10.1080/00103628009367119

Becker, J. C., Rodibaugh, K. J., Labay, B. J., Bonner, T. H., Zhang, Y., & Nowlin, W. H. (2014). Physiographic gradients determine nutrient concentrations more than land use in a Gulf Slope (USA) river system. *Freshwater Science, 33*, 731-744.

Blackmer, A. M., & Bremner, J. M. (1977). Nitrogen isotope discrimination in denitrification of nitrate in soils. *Soil Biology & Biochemistry, 9*, 73-77.

Blackmore, L. C., Searle, P. L., & Daly, B. K., &. (1987). *Methods for Chemical Analysis of Soils. New Zealand Soil Bureau Scientific Report No. 80*: Wellington, New Zealand: Department of Scientific and Industrial Research.

Blackmore, L. C., Serle, P. L., & Daly, B. K. (1972). Methods for chemical analsysis of soils. In *Scientific Report, New Zealand Soil Bureau.*

Bobbink, R., Hicks, K., Galloway, J., Spranger, T., Alkemade, R., Ashmore, M., Bustamante, M., Cinderby, S., Davidson, E., & Dentener, F. (2010). Global assessment of nitrogen deposition effects on terrestrial plant diversity: a synthesis. *Ecological applications, 20*, 30-59.

Böhlke, J. K. (2002). Groundwater recharge and agricultural contamination. *Hydrogeology Journal, 10*, 153-179.

Böhlke, J. K., O'Connell, M. E., & Prestegaard, K. L. (2007). Ground water stratification and delivery of nitrate to an incised stream under varying flow conditions. *Journal of Environmental Quality, 36*, 664-680.

Bolinder, M. A., Angers, D. A., Bélanger, G., Michaud, R., & Laverdière, M. R. (2002). Root biomass and shoot to root ratios of perennial forage crops in eastern Canada. *Canadian Journal of Plant Science, 82*, 731-737.

Bollmann, A., & Conrad, R. (1998). Influence of O_2 availability on NO and N_2O release by nitrification and denitrification in soils. *Global Change Biology, 4*, 387-396.

Bowman, W. D., & Steltzer, H. (1998). Positive feedbacks to anthropogenic nitrogen deposition in Rocky Mountain alpine tundra. *Ambio*, 514-517.

Braker, G., Schwarz, J., & Conrad, R. (2010). Influence of temperature on the composition and activity of denitrifying soil communities. *FEMS Microbiology Ecology, 73*, 134-148.

Bremner, J., & Shaw, K. (1958). Denitrification in soil. II. Factors affecting denitrification. *The Journal of Agricultural Science, 51*, 40-52.

Bryan, B. A., Shearer, G., Skeeters, J. L., & Kohl, D. H. (1983). Variable expression of the nitrogen isotope effect associated with denitrification of nitrite. *Journal of Biological Chemistry, 258*, 8613-8617.

Buckingham, E. (1904). Contributions to our knowledge of the aeration of soils. *United States Department of Agriculture, Bureau of Soil Bulletin, Washington, DC, 25*.

Buckthought, L., Clough, T., Cameron, K., Di, H., & Shepherd, M. (2015a). Fertiliser and seasonal urine effects on N_2O emissions from the urine-fertiliser interface of a grazed pasture. *New Zealand journal of agricultural research, 58*, 311-324.

Buckthought, L., Clough, T., Cameron, K., Di, H., & Shepherd, M. (2015b). Urine patch and fertiliser N interaction: Effects of fertiliser rate and season of urine application on nitrate leaching and pasture N uptake. *Agriculture, Ecosystems & Environment, 203*, 19-28.

Buckthought, L. E., Clough, T. J., Cameron, K. C., Di, H. J., & Shepherd, M. A. (2015c). Urine patch and fertiliser N interaction: Effects of fertiliser rate and season of urine application on nitrate leaching and pasture N uptake. *Agriculture, Ecosystems & Environment, 203*, 19-28.

Bullen, T. D., & Kendall, C. (1998). Tracing of weathering reactions and water flowpaths: a multi-isotope approach. In *Isotope Tracers in Catchment Hydrology* (pp. 611-646): Elsevier.

Burns, D. A., Boyer, E. W., Elliott, E. M., & Kendall, C. (2009). Sources and transformations of nitrate from streams draining varying land uses: evidence from dual isotope analysis. *Journal of Environmental Quality, 38*, 1149-1159.

Burns, D. A., & Kendall, C. (2002). Analysis of $\delta^{15}N$ and $\delta^{18}O$ to differentiate NO_3^- sources in runoff at two watersheds in the Catskill Mountains of New York. *Water Resources Research, 38*.

Cameron, K. C. (1992). Nitrogen in Soil. *Encyclopaedia of Earth System Science*, 307-317.

Cameron, K. C., Di, H. J., & Moir, J. L. (2013). Nitrogen losses from the soil/plant system: a review. *Annals of Applied Biology, 162*, 145-173.

Cameron, K. C., & Haynes, R. J. (1986). Retention and movement of nitrogen in soils. *Mineral nitrogen in the plant-soil system.*, 166-241.

Cameron, K. C., Smith, N. P., McLay, C., Fraser, P. M., McPherson, R., Harrison, D., & Harbottle, P. (1992). Lysimeters without edge flow: an improved design and sampling procedure. *Soil Science Society of America Journal, 56*, 1625-1628.

Cannavo, P., Richaume, A., & Lafolie, F. (2004). Fate of nitrogen and carbon in the vadose zone: in situ and laboratory measurements of seasonal variations in aerobic respiratory and denitrifying activities. *Soil Biology & Biochemistry, 36*, 463-478.

Caranto, J. D., & Lancaster, K. M. (2017). Nitric oxide is an obligate bacterial nitrification intermediate produced by hydroxylamine oxidoreductase. *Proceedings of the National Academy of Sciences, 114*, 8217-8222.

Casciotti, K. L. (2009). Inverse kinetic isotope fractionation during bacterial nitrite oxidation. *Geochimica et Cosmochimica Acta, 73*, 2061-2076.

Casciotti, K. L., & McIlvin, M. R. (2007). Isotopic analyses of nitrate and nitrite from reference mixtures and application to Eastern Tropical North Pacific waters. *Marine Chemistry, 107*, 184-201.

Casciotti, K. L., Sigman, D. M., Hastings, M. G., Böhlke, J. K., & Hilkert, A. (2002). Measurement of the oxygen isotopic composition of nitrate in seawater and freshwater using the denitrifier method. *Analytical Chemistry, 74*, 4905-4912.

Casciotti, K. L., Sigman, D. M., & Ward, B. B. (2003). Linking diversity and stable isotope fractionation in ammonia-oxidizing bacteria. *Geomicrobiology Journal, 20*, 335-353.

Cernusak, L. A., Winter, K., & Turner, B. L. (2009). Plant $\delta^{15}N$ correlates with the transpiration efficiency of nitrogen acquisition in tropical trees. *Plant Physiology, 151*, 1667-1676.

Chamindu-Deepagoda, T. K. K., Clough, T. J., Thomas, S. M., Balaine, N., & Elberling, B. (2019). Density Effects on Soil-Water Characteristics, Soil-Gas Diffusivity, and Emissions of N_2O and N_2 from a Re-packed Pasture Soil. *Soil Science Society of America Journal, 83*, 118-125.

Chen, Z., Wang, C., Gschwendtner, S., Willibald, G., Unteregelsbacher, S., Lu, H., Kolar, A., Schloter, M., Butterbach-Bahl, K., & Dannenmann, M. (2015). Relationships between denitrification gene expression, dissimilatory nitrate reduction to ammonium and nitrous oxide and dinitrogen production in montane grassland soils. *Soil Biology & Biochemistry, 87*, 67-77.

Cheng, L., Kim, E., Merry, R., & Dewhurst, R. (2011). Nitrogen partitioning and isotopic fractionation in dairy cows consuming diets based on a range of contrasting forages. *Journal of Dairy Science, 94*, 2031-2041.

Cirmo, C. P., & McDonnell, J. J. (1997). Linking the hydrologic and biogeochemical controls of nitrogen transport in near-stream zones of temperate-forested catchments: a review. *Journal of Hydrology, 199*, 88-120.

Clague, J. C., Stenger, R., & Clough, T. J. (2015a). Denitrification in the shallow groundwater system of a lowland catchment: A laboratory study. *Catena, 131*, 109-118.

Clague, J. C., Stenger, R., & Clough, T. J. (2015b). Evaluation of the stable isotope signatures of nitrate to detect denitrification in a shallow groundwater system in New Zealand. *Agriculture, Ecosystems & Environment, 202*, 188-197.

Clark, D. (2011). Changes in pastoral farming practices and pasture persistence–a review Symposium conducted at the meeting of the Pasture persistence symposium. Grassland research and practice series

Clark, F. E. (1962). Losses of nitrogen accompanying nitrification. *Trans. Int. Soc. Soil Sci*, 173-176.

Clément, J., Aquilina, L., Bour, O., Plaine, K., Burt, T. P., & Pinay, G. (2003). Hydrological flowpaths and nitrate removal rates within a riparian floodplain along a fourth-order stream in Brittany (France). *Hydrological Processes, 17*, 1177-1195.

Close, M. E., Abraham, P., Humphries, B., Lilburne, L., Cuthill, T., & Wilson, S. (2016). Predicting groundwater redox status on a regional scale using linear discriminant analysis. *Journal of contaminant hydrology, 191*, 19-32.

Clothier, B. E., Mackay, A. D., Carran, A., Gray, R., Parfitt, R. L., Francis, G., & Green, S., &. (2007). *Farm strategies for contaminant management. A report by SLURI, the sustainable Land Use Research Initiative for Horizons Regional Council.,(June)*: Palmerston North, New Zealand. Retrieved from http://www.horizons.govt.nz/assets/horizons/Images/one_plan/Farm.

Clough, T., Kelliher, F., Wang, Y., & Sherlock, R. (2006). Diffusion of ^{15}N-labelled N_2O into soil columns: a promising method to examine the fate of N_2O in subsoils. *Soil Biology and Biochemistry, 38*, 1462-1468.

Clough, T. J., Jarvis, S. C., Dixon, E. R., Stevens, R. J., Laughlin, R. J., & Hatch, D. J. (1998a). Carbon induced subsoil denitrification of ^{15}N-labelled nitrate in 1 m deep soil columns. *Soil Biology and Biochemistry, 31*, 31-41.

Clough, T. J., Ledgard, S. F., Sprosen, M. S., & Kear, M. J. (1998b). Fate of ^{15}N labelled urine on four soil types. *Plant and Soil, 199*, 195-203.

Clough, T. J., Ray, J. L., Buckthought, L. E., Calder, J., Baird, D. B., O'Callaghan, M., Sherlock, R. R., & Condron, L. M. (2009). The mitigation potential of hippuric acid on N_2O emissions from urine patches: An in situ determination of its effect. *Soil Biology and Biochemistry, 41*, 2222-2229.

Clough, T. J., Sherlock, R. R., Cameron, K. C., & Ledgard, S. F. (1996). Fate of urine nitrogen on mineral and peat soils in New Zealand. *Plant & Soil, 178*, 141-152.

Clough, T. J., Sherlock, R. R., & Rolston, D. E. (2005). A review of the movement and fate of N_2O in the subsoil. *Nutrient Cycling in Agroecosystems, 72*, 3-11.

Comstock, J. (2001). Steady-state isotopic fractionation in branched pathways using plant uptake of NO3–as an example. *Planta, 214*, 220-234.

Condron, L. M., Hopkins, D. W., Gregorich, E. G., Black, A., & Wakelin, S. A. (2014). Long-term irrigation effects on soil organic matter under temperate grazed pasture. *European Journal of Soil Science, 65*, 741-750.

Conley, D. J., Paerl, H. W., Howarth, R. W., Boesch, D. F., Seitzinger, S. P., Havens, K. E., Lancelot, C., & Likens, G. E., &. (2009). *Controlling eutrophication: nitrogen and phosphorus*: American Association for the Advancement of Science.

Cooke, J. (2014). Are Rising Nitrate Levels in Rural Groundwater a public health concern? *Water, 183*, 63-65.

Coplen, T. B., Krouse, H., & Böhlke, J. K. (1992). Reporting of nitrogen-isotope abundances (Technical Report). *Pure and Applied Chemistry, 64*, 907-908.

Craine, J. M., Elmore, A. J., Aidar, M. P. M., Bustamante, M., Dawson, T. E., Hobbie, E. A., Kahmen, A., Mack, M. C., McLauchlan, K. K., & Michelsen, A. (2009). Global patterns of foliar nitrogen isotopes and their relationships with climate, mycorrhizal fungi, foliar nutrient concentrations, and nitrogen availability. *New Phytologist, 183*, 980-992.

CropsSouthland. (2002). Topoclimate Southland Soil Information Sheet. (31). Retrieved 2/11/18, from www.cropssouthland.co.nz gis.es.govt.nz/apps/topoclimate/sheets/

Crush, J. R., Waller, J. E., & Care, D. A. (2005). Root distribution and nitrate interception in eleven temperate forage grasses. *Grass and Forage Science, 60*, 385-392.

Currie, J. A. (1960). *Gaseous Diffusion in Porous Media .1. A Non-Steady State Method* (Vol. 11). doi:10.1088/0508-3443/11/8/302

Curtis, C. J., Evans, C. D., Goodale, C. L., & Heaton, T. H. (2011). What have stable isotope studies revealed about the nature and mechanisms of N saturation and nitrate leaching from semi-natural catchments? *Ecosystems, 14*, 1021-1037.

Daughney, C., & Randall, M. (2009). National groundwater quality indicators update: state and trends 1995–2008. *GNS Science Consultancy Report, 145*, 60.

Davidson, E. A., Keller, M., Erickson, H. E., Verchot, L. V., & Veldkamp, E. (2000). Testing a conceptual model of soil emissions of nitrous and nitric oxides: using two functions based on soil nitrogen availability and soil water content, the hole-in-the-pipe model characterizes a large fraction of the observed variation of nitric oxide and nitrous oxide emissions from soils. *Bioscience, 50*, 667-680.

Davies, H., & Neal, C. (2007). Estimating nutrient concentrations from catchment characteristics across the UK. *Hydrology & Earth System Sciences Discussions, 11*, 550-558.

De Boer, W., & Kowalchuk, G. A. (2001). Nitrification in acid soils: micro-organisms and mechanisms. *Soil Biology & Biochemistry, 33*, 853-866.

De Klein, C., Smith, L., & Monaghan, R. (2006). Restricted autumn grazing to reduce nitrous oxide emissions from dairy pastures in Southland, New Zealand. *Agriculture, ecosystems & environment, 112*, 192-199.

Deepagoda, T. K. K., Moldrup, P., Schjønning, P., de Jonge, L. W., Kawamoto, K., & Komatsu, T. (2011). Density-corrected models for gas diffusivity and air permeability in unsaturated soil. *Vadose Zone Journal, 10*, 226-238.

Delwiche, C., & Bryan, B. A. (1976). Denitrification. *Annual Reviews in microbiology, 30*, 241-262.

Dendooven, L., & Anderson, J. M. (1995). Use of a “least square” optimization procedure to estimate enzyme characteristics and substrate affinities in the denitrification reactions in soil. *Soil Biology & Biochemistry, 27*, 1261-1270.

Denk, T. R., Mohn, J., Decock, C., Lewicka-Szczebak, D., Harris, E., Butterbach-Bahl, K., Kiese, R., & Wolf, B. (2017). The nitrogen cycle: A review of isotope effects and isotope modeling approaches. *Soil Biology and Biochemistry, 105*, 121-137.

Di, H., & Cameron, K. (2002). Nitrate leaching in temperate agroecosystems: sources, factors and mitigating strategies. *Nutrient cycling in agroecosystems, 64*, 237-256.

Di, H. J., & Cameron, K. C. (2007). Nitrate leaching losses and pasture yields as affected by different rates of animal urine nitrogen returns and application of a nitrification inhibitor—a lysimeter study. *Nutrient Cycling in Agroecosystems, 79*, 281-290.

Di, H. J., Cameron, K. C., Shen, J. P., Winefield, C. S., O’callaghan, M., Bowatte, S., & He, J. Z. (2009). Nitrification driven by bacteria and not archaea in nitrogen-rich grassland soils. *Nature Geoscience, 2*, 621.

Dias, A. T. C., Van Ruijven, J., & Berendse, F. (2010). Plant species richness regulates soil respiration through changes in productivity. *Oecologia, 163*, 805-813.

Dobbie, K. E., McTaggart, I. P., & Smith, K. A. (1999). Nitrous oxide emissions from intensive agricultural systems: variations between crops and seasons, key driving variables, and mean emission factors. *Journal of Geophysical Research: Atmospheres, 104*, 26891-26899.

Dobbie, K. E., & Smith, K. A. (2001). The effects of temperature, water-filled pore space and land use on N_2O emissions from an imperfectly drained gleysol. *European Journal of Soil Science, 52*, 667-673.

Dodds, W. K., & Smith, V. H. (2016). Nitrogen, phosphorus, and eutrophication in streams. *Inland Waters, 6*, 155-164.

Drewry, J., & Paton, R. (2000). Effects of cattle treading and natural amelioration on soil physical properties and pasture under dairy farming in Southland, New Zealand. *New Zealand Journal of Agricultural Research, 43*, 377-386.

Durka, W., Schulze, E.-D., Gebauer, G., & Voerkeliust, S. (1994). Effects of forest decline on uptake and leaching of deposited nitrate determined from ^{15}N and ^{18}O measurements. *Nature, 372*, 765.

Elliott, E., Kendall, C., Wankel, S. D., Burns, D., Boyer, E., Harlin, K., Bain, D., & Butler, T. (2007). Nitrogen isotopes as indicators of NO x source contributions to atmospheric nitrate deposition across the midwestern and northeastern United States. *Environmental Science & Technology, 41*, 7661-7667.

Elser, J. J., Andersen, T., Baron, J. S., Bergström, A.-K., Jansson, M., Kyle, M., Nydick, K. R., Steger, L., & Hessen, D. O. (2009). Shifts in lake N: P stoichiometry and nutrient limitation driven by atmospheric nitrogen deposition. *science, 326*, 835-837.

Engler, R., Antie, D., & Patrick, W. (1976). Effect of dissolved oxygen on redox potential and nitrate removal in flooded swamp and marsh soils. *Journal of Environmental Quality, 5*, 230-235.

Environment, M. f. t. (2014). *National Policy Statement for Freshwater Management 2014*. Wellington: Ministry for the Environment.

Environment Southland. (2017). Beacon (Online Database). Retrieved 5/06/2019, from Environment Southland Regional Council http://gis.es.govt.nz/index.aspx?app=topoclimate&ext=1161738,4854869,1359710,4948887

Farquharson, R., & Baldock, J. A. (2008). Concepts in modelling N_2O emissions from land use. *Plant & Soil, 309*, 147-167.

Farquharson, R., & Baldock, J. A. (2009). Erratum to: Concepts in modelling N_2O emissions from land use. *Plant & Soil, 325*, 353-353.

Fierer, N., & Schimel, J. P. (2003a). A proposed mechanism for the pulse in carbon dioxide production commonly observed following the rapid rewetting of a dry soil. *Soil Science Society of America Journal, 67*, 798-805.

Fierer, N., Schimel, J. P., & Holden, P. A. (2003b). Variations in microbial community composition through two soil depth profiles. *Soil Biology and Biochemistry, 35*, 167-176.

Firestone, M. (1982). Biological denitrification. *Nitrogen in agricultural soils*, 289-326.

Firestone, M. K., & Davidson, E. A. (1989). Microbiological basis of NO and N_2O production and consumption in soil. *Exchange of trace gases between terrestrial ecosystems and the atmosphere, 47*, 7-21.

Fischer, S. J. L. (2014). *Seasonal patterns of $\delta^{15}N$ and $\delta^{18}O$-NO_3^- in the Murderkill River Watershed and Estuary, DE*. University of Delaware.

Fleming, P. H., &. (2003). *Lincoln University farm technical manual* [Pasture Grasses]. The Caxton Press, Christchurch.

Frank, D. A., Evans, R. D., & Tracy, B. F. (2004). The role of ammonia volatilization in controlling the natural 15 N abundance of a grazed grassland. *Biogeochemistry, 68*, 169-178.

Franzluebbers, A. J., Haney, R. L., Honeycutt, C. W., Schomberg, H., & Hons, F. M. (2000). Flush of carbon dioxide following rewetting of dried soil relates to active organic pools. *Soil Science Society of America Journal, 64*, 613-623.

Friedl, J., De Rosa, D., Rowlings, D., Grace, P., Müller, C., & Scheer, C. (2018). Dissimilatory nitrate reduction to ammonium (DNRA), not denitrification dominates nitrate reduction in subtropical pasture soils upon rewetting. *Soil Biology & Biochemistry, 125*, 340-349.

Friedl, J., Scheer, C., Rowlings, D. W., Mumford, M. T., & Grace, P. R. (2017). The nitrification inhibitor DMPP (3, 4-dimethylpyrazole phosphate) reduces N_2 emissions from intensively managed pastures in subtropical Australia. *Soil Biology & Biochemistry, 108*, 55-64.

Fry, B. (2007). *Stable isotope ecology*: Springer Science & Business Media.

Fuller, E. N., Schettler, P. D., & Giddings, J. C. (1966). New method for prediction of binary gas-phase diffusion coefficients. *Industrial & Engineering Chemistry, 58*, 18-27.

Galloway, J. N., Dentener, F. J., Capone, D. G., Boyer, E. W., Howarth, R. W., Seitzinger, S. P., Asner, G. P., Cleveland, C., Green, P., & Holland, E. (2004). Nitrogen cycles: past, present, and future. *Biogeochemistry, 70*, 153-226.

Galloway, J. N., Townsend, A. R., Erisman, J. W., Bekunda, M., Cai, Z., Freney, J. R., Martinelli, L. A., Seitzinger, S. P., & Sutton, M. A. (2015). Transformation of the nitrogen cycle: recent trends, questions, and potential solutions. *Science, 320*, 889-892.

Ghani, A., Dexter, M., & Perrott, K. W. (2003). Hot-water extractable carbon in soils: a sensitive measurement for determining impacts of fertilisation, grazing and cultivation. *Soil Biology & Biochemistry, 35*, 1231-1243.

Ghani, A., Müller, K., Dodd, M. B., & Mackay, A. D. (2010). Dissolved organic matter leaching in some contrasting New Zealand pasture soils. *European Journal of Soil Science, 61*, 525-538.

Gliński, J., & Stępniewski, W. (1985). *Soil aeration and its role for plants*: CRC Press, Inc.

Gould, I. J., Quinton, J. N., Weigelt, A., De Deyn, G. B., & Bardgett, R. D. (2016). Plant diversity and root traits benefit physical properties key to soil function in grasslands. *Ecology Letters, 19*, 1140-1149.

Granger, J., Sigman, D. M., Lehmann, M. F., & Tortell, P. D. (2008). Nitrogen and oxygen isotope fractionation during dissimilatory nitrate reduction by denitrifying bacteria. *Limnology and Oceanography, 53*, 2533-2545.

Granger, J., Sigman, D. M., Needoba, J. A., & Harrison, P. J. (2004). Coupled nitrogen and oxygen isotope fractionation of nitrate during assimilation by cultures of marine phytoplankton. *Limnology and Oceanography, 49*, 1763-1773.

Granger, J., & Wankel, S. D. (2016). Isotopic overprinting of nitrification on denitrification as a ubiquitous and unifying feature of environmental nitrogen cycling. *Proceedings of the National Academy of Sciences, 113*, E6391-E6400.

Groffman, P. M., Altabet, M. A., Böhlke, J. K., Butterbach-Bahl, K., David, M. B., Firestone, M. K., Giblin, A. E., Kana, T. M., Nielsen, L. P., & Voytek, M. A. (2006). Methods for measuring denitrification: diverse approaches to a difficult problem. *Ecological Applications, 16*, 2091-2122.

Groffman, P. M., Butterbach-Bahl, K., Fulweiler, R. W., Gold, A. J., Morse, J. L., Stander, E. K., Tague, C., Tonitto, C., & Vidon, P. (2009). Challenges to incorporating spatially and temporally explicit phenomena (hotspots and hot moments) in denitrification models. *Biogeochemistry, 93*, 49-77.

Grybos, M., Davranche, M., Gruau, G., Petitjean, P., & Pédrot, M. (2009). Increasing pH drives organic matter solubilization from wetland soils under reducing conditions. *Geoderma, 154*, 13-19.

Gu, C., & Riley, W. J. (2010). Combined effects of short term rainfall patterns and soil texture on soil nitrogen cycling ? A modeling analysis. *Journal of Contaminant Hydrology, 112*, 141-154.

Hale, S. S., Paul, J. F., & Heltshe, J. F. (2004). Watershed landscape indicators of estuarine benthic condition. *Estuaries, 27*, 283-295.

Hamill, K. D., & McBride, G. B. (2003). River water quality trends and increased dairying in Southland, New Zealand.

Heathwaite, A. L., & Johnes, P. J. (1996). Contribution of nitrogen species and phosphorus fractions to stream water quality in agricultural catchments. *Hydrological processes, 10*, 971-983.

Heaton, T. H. E. (1986). Isotopic studies of nitrogen pollution in the hydrosphere and atmosphere: A review. *Chemical Geology: Isotope Geoscience section, 59*, 87-102.

Heil, J., Vereecken, H., & Brüggemann, N. (2016). A review of chemical reactions of nitrification intermediates and their role in nitrogen cycling and nitrogen trace gas formation in soil. *European Journal of Soil Science, 67*, 23-39.

Hergoualc'h, K., Skiba, U., Harmand, J., & Oliver, R. (2007). Processes responsible for the nitrous oxide emission from a Costa Rican Andosol under a coffee agroforestry plantation. *Biology & Fertility of Soils, 43*, 787-795.

Hesser, F. B., Franko, U., & Rode, M. (2010). Spatially distributed lateral nitrate transport at the catchment scale. *Journal of Environmental Quality, 39*, 193-203.

Hewitt, A. E. (1998). *New Zealand soil classification*. Lincoln, NZ: Manaaki Whenua Press.

Hewitt, A. E. (2010). New Zealand soil classification. *Landcare research science series*.

Hochstein, L. I., & Tomlinson, G. A. (1988). The enzymes associated with denitrification. *Annual Reviews in Microbiology, 42*, 231-261.

Högberg, P. (1997). Tansley review no. 95 ^{15}N natural abundance in soil–plant systems. *The New Phytologist, 137*, 179-203.

Horneck, D. A., & Miller, R. O. (1998). Determination of total nitrogen in plant tissue. In Y. P. Kaira (Ed.), *Handbook of referenece methods for plant analysis* (pp. 75-83). CRC Press, New York

Howarth, R. W., & Marino, R. (2006). Nitrogen as the limiting nutrient for eutrophication in coastal marine ecosystems: evolving views over three decades. *Limnology & Oceanography, 51*, 364-376.

Hübner, H. (1986). *Isotope effects of nitrogen in the soil and biosphere In Handbook of EnVironmental Isotope Geochemistry: The Terrestrial EnVironment*: Elsevier: Amsterdam, The Netherlands.

Hughes, B., Wilson, K., Rissmann, C., & Rodway, E. (2016). Physiographics of Southland: Development and application of a classification system for managing land use effects on water quality in Southland. *Environment Southland Technical Report Publication*.

Hutchinson, G. L., & Davidson, E. A. (1993). Processes for production and consumption of gaseous nitrogen oxides in soil. *Agricultural ecosystem effects on trace gases and global climate change*, 79-93.

Ibendahl, G., & Fleming, R. A. (2007). Controlling aquifer nitrogen levels when fertilizing crops: a study of groundwater contamination and denitrification. *Ecological modelling, 205*, 507-514.

IPCC. (2014a). *Climate Change 2014: Synthesis Report. Contribution of Working Groups I, II and III to the Fifth Assessment Report of the Intergovernmental Panel on Climate Change*. [Core Writing Team, R.K. Pachauri and L.A. Meyer (eds.)]. IPCC, Geneva, Switzerland, 151 pp. .

IPCC. (2014b). International Panel on Climate Change. *In: Climate Change 2013: The Physical Science Basis. Contribution of Working Group I to the Fifth Assessment Report [Stocker, T.F., D. Qin, G.-K. Plattner, M. Tignor, S.K. Allen, J. Boschung, A. Nauels, Y. Xia, V. Bex and P.M. Midgley (eds.)]. Cambridge University Press, Cambridge, United Kingdom and New York, NY, USA*.

Jahangir, M. M. R., Khalil, M. I., Johnston, P., Cardenas, L. M., Hatch, D. J., Butler, M., Barrett, M., O'flaherty, V., & Richards, K. G. (2012). Denitrification potential in subsoils: A mechanism to reduce nitrate leaching to groundwater. *Agriculture, Ecosystems & Environment, 147*, 13-23.

Jarvie, H. P., Oguchi, T., & Neal, C. (2002). Exploring the linkages between river water chemistry and watershed characteristics using GIS-based catchment and locality analyses. *Regional Environmental Change, 3*, 36-50.

Jarvis, S. C., & Hatch, D. J. (1994). Potential for denitrification at depth below long-term grass swards. *Soil biology and biochemistry, 26*, 1629-1636.

Jia, B., & Zhou, G. (2009). Integrated diurnal soil respiration model during growing season of a typical temperate steppe: Effects of temperature, soil water content and biomass production. *Soil Biology & Biochemistry, 41*, 681-686.

Junk, G., & Svec, H. J. (1958). The absolute abundance of the nitrogen isotopes in the atmosphere and compressed gas from various sources. *Geochimica et Cosmochimica Acta, 14*, 234-243.

Kay, B. D. (2018). Soil structure and organic carbon: a review. In *Soil Processes and the Carbon Cycle* (pp. 169-197): CRC Press.

Keeney, D., & Fillery, J. (1979). Effect of temperature on the gaseous nitrogen products of denitrification in a silt loam soil. *Soil Sci. Soc. Am. J, 43*, 1124-1128.

Kelliher, F. M., West, P. J. S., & Moir, J. L. (2015). Soil carbon stock beneath an established irrigated pasture grazed by dairy cattle. *New Zealand Journal of Agricultural Research, 58*, 78-83.

Kendall, C. (1998). Tracing nitrogen sources and cycling in catchments. *Isotope tracers in catchment hydrology*, 519-576.

Kendall, C., & Aravena, R. (2000). Nitrate Isotopes in Groundwater Systems. In *Environmental Tracers in Subsurface Hydrology* (pp. 261-297): Springer.

Kendall, C., & Caldwell, E., &. (1998). *Fundamentals of isotope geochemistry. In "Isotope tracers in Catchment Hydrology."(Eds C. Kendall and JJ McDonnell.) pp 51–86*: Elsevier: Amsterdam.

Kendall, C., Elliott, E. M., & Wankel, S. D. (2007). Tracing anthropogenic inputs of nitrogen to ecosystems. *Stable isotopes in ecology and environmental science, 2*, 375-449.

Khalil, K., Mary, B., & Renault, P. (2004). Nitrous oxide production by nitrification and denitrification in soil aggregates as affected by O 2 concentration. *Soil Biology and Biochemistry, 36*, 687-699.

King, C., McEniry, J., Richardson, M., & O'Kiely, P. (2012). Yield and chemical composition of five common grassland species in response to nitrogen fertiliser application and phenological growth stage. *Acta Agricultura Scandinavica, Section B - Soil & Plant Science, 62*, 644-658.

King, R. S., Baker, M. E., Whigham, D. F., Weller, D. E., Jordan, T. E., Kazyak, P. F., & Hurd, M. K. (2005). Spatial considerations for linking watershed land cover to ecological indicators in streams. *Ecological Applications, 15*, 137-153.

Knowles, R. (1982). Denitrification. *Microbiological reviews, 46*, 43.

Kool, D. M., Dolfing, J., Wrage, N., & Van Groenigen, J. W. (2011a). Nitrifier denitrification as a distinct and significant source of nitrous oxide from soil. *Soil Biology and Biochemistry, 43*, 174-178.

Kool, D. M., Van Groenigen, J. W., & Wrage, N. (2011b). Source determination of nitrous oxide based on nitrogen and oxygen isotope tracing: dealing with oxygen exchange. In *Methods in Enzymology* (Vol. 496, pp. 139-160): Elsevier.

Korom, S. F., Schuh, W. M., Tesfay, T., & Spencer, E. J. (2012). Aquifer denitrification and in situ mesocosms: modeling electron donor contributions and measuring rates. *Journal of Hydrology, 432*, 112-126.

Kraft, B., Tegetmeyer, H. E., Sharma, R., Klotz, M. G., Ferdelman, T. G., Hettich, R. t. L., Geelhoed, J. S., & Strous, M. (2014). The environmental controls that govern the end product of bacterial nitrate respiration. *Science, 345*, 676-679.

Kritee, K., Sigman, D. M., Granger, J., Ward, B. B., Jayakumar, A., & Deutsch, C. (2012). Reduced isotope fractionation by denitrification under conditions relevant to the ocean. *Geochimica et Cosmochimica Acta, 92*, 243-259.

Kuenen, J. G., & Robertson, L. A. (1994). Combined nitrification-denitrification processes. *FEMS Microbiology Reviews, 15*, 109-117.

Lambie, S. M., Schipper, L. A., Balks, M. R., & Baisden, T. W. (2012a). Carbon leaching from undisturbed soil cores treated with dairy cow urine. *Soil Research, 50*, 320-327.

Lambie, S. M., Schipper, L. A., Balks, M. R., & Baisden, T. W. (2012b). Solubilisation of soil carbon following treatment with cow urine under laboratory conditions. *Soil Research, 50*, 50-57.

Ledgard, G. (2013). Land use change in the Southland Region. *Environment Southland Technical Report., 13*.

Ledgard, S. F., Penno, J. W., & Sprosen, M. S. (1999). Nitrogen inputs and losses from clover/grass pastures grazed by dairy cows, as affected by nitrogen fertilizer application. *The Journal of Agricultural Science, 132*, 215-225.

Leifheit, E. F., Veresoglou, S. D., Lehmann, A., Morris, E. K., & Rillig, M. C. (2014). Multiple factors influence the role of arbuscular mycorrhizal fungi in soil aggregation - a meta-analysis. *Plant & Soil, 374*, 523-537.

Linden, D. R. (1977). *Design, installation, and use of porous ceramic samplers for monitoring soil-water quality*: Dept. of Agriculture, Agricultural Research Service.

Linn, D. M., & Doran, J. W. (1984a). Effect of water-filled pore space on carbon dioxide and nitrous oxide production in tilled and nontilled soils. *Soil Science Society of America Journal, 48*, 1267-1272.

Linn, D. M., & Doran, J. W. (1984b). Effect of water-filled pore space on carbon dioxide and nitrous oxide production in tilled and nontilled soils 1. *Soil Science Society of America Journal, 48*, 1267-1272.

Liu, B., Frostegård, Å., & Bakken, L. R. (2014). Impaired reduction of N_2O to N_2 in acid soils is due to a posttranscriptional interference with the expression of nosZ. *MBio, 5*, e01383-01314.

Liu, B., Mao, Y., Bergaust, L., Bakken, L. R., & Frostegård, Å. (2013). Strains in the genus T hauera exhibit remarkably different denitrification regulatory phenotypes. *Environmental Microbiology, 15*, 2816-2828.

Liu, C.-Q., Li, S.-L., Lang, Y.-C., & Xiao, H.-Y. (2006). Using δ^{15}N-and δ^{18}O-values to identify nitrate sources in karst ground water, Guiyang, Southwest China. *Environmental science & technology, 40*, 6928-6933.

Liu, C., Wang, K., Meng, S., Zheng, X., Zhou, Z., Han, S., Chen, D., & Yang, Z. B. (2011). Effects of irrigation, fertilization and crop straw management on nitrous oxide and nitric oxide emissions from a wheat–maize rotation field in northern China. *Agriculture, Ecosystems & Environment, 140*, 226-233.

Luo, J., Tillman, R. W., & Ball, P. R. (2000). Nitrogen loss through denitrification in a soil under pasture in New Zealand. *Soil Biology & Biochemistry, 32*, 497-509.

Lycus, P., Bøthun, K. L., Bergaust, L., Shapleigh, J. P., Bakken, L. R., & Frostegård, Å. (2017). Phenotypic and genotypic richness of denitrifiers revealed by a novel isolation strategy. *The ISME Journal, 11*, 2219.

Macara, G. R. (2014). *The Climate and Weather of Southland*: NIWA.

Macleod, C. J. A., Humphreys, M. W., Whalley, W. R., Turner, L., Binley, A., Watts, C. W., Skøt, L., Joynes, A., Hawkins, S., King, I. P., & O'donovan, S. (2013). A novel grass hybrid to reduce flood generation in temperate regions. *Scientific Reports, 3*, 1683.

Maharjan, B., Venterea, R. T., & Rosen, C. (2014). Fertilizer and irrigation management effects on nitrous oxide emissions and nitrate leaching. *Agronomy Journal, 106*, 703-714.

Malcolm, B., Cameron, K., Di, H., Edwards, G., & Moir, J. (2014a). The effect of four different pasture species compositions on nitrate leaching losses under high N loading. *Soil Use and Management, 30*, 58-68.

Malcolm, B. J., Cameron, K. C., Di, H. J., Edwards, G. R., & Moir, J. L. (2014b). The effect of four different pasture species compositions on nitrate leaching losses under high N loading. *Soil Use and Management, 30*, 58-68.

Mariotti, A., Germon, J., Hubert, P., Kaiser, P., Letolle, R., Tardieux, A., & Tardieux, P. (1981). Experimental determination of nitrogen kinetic isotope fractionation: some principles; illustration for the denitrification and nitrification processes. *Plant and soil, 62*, 413-430.

Mariotti, A., Mariotti, F., Amarger, N., Pizelle, G., Ngambi, J. M., Champigny, M. L., & Moyse, A. (1980a). Nitrogen isotope fractionation during nitrate absorption and nitrogen fixation by plants. *Physiologie Végétale, 18*, 163-181.

Mariotti, A., Mariotti, F., Champigny, M. L., Amarger, N., & Moyse, A. (1982). Nitrogen isotope fractionation associated with nitrate reductase activity and uptake of NO3− by pearl millet. *Plant Physiology, 69*, 880-884.

Mariotti, A., Pierre, D., Vedy, J. C., Bruckert, S., & Guillemot, J. (1980b). The abundance of natural nitrogen 15 in the organic matter of soils along an altitudinal gradient (Chablais, Haute Savoie, France). *Catena, 7*, 293-300.

Marshall, T. J. (1959). The diffusion of gases through porous media. *Journal of Soil Science, 10*, 79-82.

Martikainen, P. J., & de Boer, W. (1993). Nitrous oxide production and nitrification in acidic soil from a Dutch coniferous forest. *Soil Biology and Biochemistry, 25*, 343-347.

Matheson, F. E., Nguyen, M. L., Cooper, A. B., Burt, T. P., & Bull, D. C. (2002). Fate of ^{15}N-nitrate in unplanted, planted and harvested riparian wetland soil microcosms. *Ecological Engineering, 19*, 249-264.

Mathieu, O., Leveque, J., Henault, C., Milloux, M. J., Bizouard, F., & Andreux, F. (2006). Emissions and spatial variability of N_2O, N_2 and nitrous oxide mole fraction at the field scale, revealed with ^{15}N isotopic techniques. *Soil Biology and Biochemistry, 38*, 941-951.

McIlvin, M. R., & Altabet, M. A. (2005). Chemical conversion of nitrate and nitrite to nitrous oxide for nitrogen and oxygen isotopic analysis in freshwater and seawater. *Analytical Chemistry, 77*, 5589-5595.

McLaren, R. G., & Cameron, K. C. (1996). *Soil science: sustainable production and environmental protection*. Retrieved from <Go to ISI>://CABI:19971904200

Mengis, M., Schif, S. L., Harris, M., English, M. C., Aravena, R., Elgood, R. J., & MacLean, A. (1999). Multiple geochemical and isotopic approaches for assessing ground water NO_3^- elimination in a riparian zone. *Groundwater, 37*, 448-457.

Menneer, J. C., Ledgard, S. F., McLay, C., & Silvester, W. (2005). Animal treading stimulates denitrification in soil under pasture. *Soil Biology and Biochemistry, 37*, 1625-1629.

Miller, A. E., Schimel, J. P., Meixner, T., Sickman, J. O., & Melack, J. M. (2005). Episodic rewetting enhances carbon and nitrogen release from chaparral soils. *Soil Biology & Biochemistry, 37*, 2195-2204.

Miller, C. J., Yesiller, N., Yaldo, K., & Merayyan, S. (2002). Impact of Soil Type and Compaction Conditions on Soil Water Characteristic. *Journal of Geotechnical and Geoenvironmental Engineering, 128*, 733-742.

Millington, R. J., & Quirk, J. P. (1961). Permeability of porous solids. *Transactions of the Faraday Society, 57*, 1200-1207.

Minet, E., Coxon, C., Goodhue, R., Richards, K., Kalin, R., & Meier-Augenstein, W. (2012). Evaluating the utility of ^{15}N and ^{18}O isotope abundance analyses to identify nitrate sources: A soil zone study. *Water research, 46*, 3723-3736.

Minitab®18.1.0.0. (2018). Statistical Software (Version 18.1.0.0): Minitab Inc. Retrieved from https://www.minitab.com/en-us/

Moir, J., Cameron, K., & Di, H. (2007). Effects of the nitrification inhibitor dicyandiamide on soil mineral N, pasture yield, nutrient uptake and pasture quality in a grazed pasture system. *Soil Use and Management, 23*, 111-120.

Moir, J., Cameron, K., & Di, H. (2016). Potential pasture nitrogen concentrations and uptake from autumn or spring applied cow urine and DCD under field conditions. *Plants, 5*, 26.

Moir, J. L., Cameron, K. C., Di, H. J., & Fertsak, U. (2011). The spatial coverage of dairy cattle urine patches in an intensively grazed pasture system. *Journal of Agricultural Science, 149*, 473-485.

Moir, J. L., Edwards, G. R., & Berry, L. N. (2013). Nitrogen uptake and leaching loss of thirteen temperate grass species under high N loading. *Grass and Forage Science, 68*, 313-325.

Moldrup, P., Chamindu Deepagoda, T., Hamamoto, S., Komatsu, T., Kawamoto, K., Rolston, D. E., & de Jonge, L. W. (2013). Structure-dependent water-induced linear reduction model for predicting gas diffusivity and tortuosity in repacked and intact soil. *Vadose Zone Journal, 12*.

Moldrup, P., Olesen, T., Gamst, J., Schjønning, P., Yamaguchi, T., & Rolston, D. E. (2000). Predicting the gas diffusion coefficient in repacked soil water-induced linear reduction model. *Soil Science Society of America Journal, 64*, 1588-1594.

Moldrup, P., Olesen, T., Komatsu, T., Schjønning, P., & Rolston, D. (2001). Tortuosity, diffusivity, and permeability in the soil liquid and gaseous phases. *Soil Science Society of America Journal, 65*, 613-623.

Monaghan, R. M., & Smith, L. C. (2004). Minimising surface water pollution resulting from farm-dairy effluent application to mole-pipe drained soils. II. The contribution of preferential flow of effluent to whole-farm pollutant losses in subsurface drainage from a West Otago dairy farm. *New Zealand Journal of Agricultural Research, 47*, 417-428.

Morley, N., & Baggs, E. (2010). Carbon and oxygen controls on N 2 O and N 2 production during nitrate reduction. *Soil Biology and Biochemistry, 42*, 1864-1871.

Moyano, F. E., Kutsch, W. L., & Schulze, E. D. (2007). Response of mycorrhizal, rhizosphere and soil basal respiration to temperature and photosynthesis in a barley field. *Soil Biology & Biochemistry, 39*, 843-853.

Moyano, F. E., Manzoni, S., & Chenu, C. (2013). Responses of soil heterotrophic respiration to moisture availability: An exploration of processes and models. *Soil Biology & Biochemistry, 59*, 72-85.

Mudge, P. L., Schipper, L. A., Ghani, A., Upsdell, M., & Baisden, W. T. (2013). Changes in natural N abundance in pastoral soils receiving differing amounts of superphosphate fertilizer and irrigation for 50 Years. *Soil Science Society of America Journal, 77*, 830-841.

Müller, M. M., Sundman, V., & Skujinš, J. (1980). Denitrification in low pH spodosols and peats determined with the acetylene inhibition method. *Applied and environmental microbiology, 40*, 235-239.

Murray, P., Hatch, D., Dixon, E., Stevens, R., Laughlin, R., & Jarvis, S. (2004). Denitrification potential in a grassland subsoil: effect of carbon substrates. *Soil Biology and Biochemistry, 36*, 545-547.

Nadelhoffer, K. J., & Fry, B. (1994). Nitrogen isotope studies in forest ecosystems. *Stable isotopes in ecology and environmental science. Blackwell, Oxford, 316*.

Needoba, J. A., Sigman, D. M., & Harrison, P. J. (2004). The mechanism of isotope fractionation during algal nitrate assimilatin as illuminated by the $^{15}N/^{14}N$ of intracellular nitrate. *Journal of Phycology, 40*, 517-522.

Neira, J., Ortiz, M., Morales, L., & Acevedo, E. (2015). Oxygen diffusion in soils: Understanding the factors and processes needed for modeling. *Chilean Journal of Agricultural Research, 75*, 35-44.

Nestler, A., Berglund, M., Accoe, F., Duta, S., Xue, D., Boeckx, P. l., & Taylor, P. (2011). Isotopes for improved management of nitrate pollution in aqueous resources: review of surface water field studies. *Environmental Science & Pollution Research, 18*, 519-533.

Nikolenko, O., Jurado, A., Borges, A. V., Knöller, K., & Brouyère, S. (2018). Isotopic composition of nitrogen species in groundwater under agricultural areas: a review. *Science of the Total Environment, 621*, 1415-1432.

NIWA. (n.d). CliFlo:The National Climate Database. Retrieved October 2015, from National Institute of Water and Atmospheric Research Ltd http://cliflo.niwa.co.nz/

Nömmik, H. (1956). Investigations on denitrification in soil. *Acta Agriculturae Scandinavica, 6*, 195-228.

Ocampo, C. J., Oldham, C. E., & Sivapalan, M. (2006). Nitrate attenuation in agricultural catchments: Shifting balances between transport and reaction. *Water Resources Research, 42*.

Oelmann, Y., Kreutziger, Y., Bol, R., & Wilcke, W. (2007). Nitrate leaching in soil: Tracing the NO3− sources with the help of stable N and O isotopes. *Soil Biology and Biochemistry, 39*, 3024-3033.

Olsen, S. R., Cole, C. V., & Watanabe, F. S. (1954). Estimation of available phosphorus in soils by extraction with sodium bicarbonate. In *Circular. United States Department of Agriculture* (pp. 19)

Ostrom, N. E., Knoke, K. E., Hedin, L. O., Robertson, G. P., & Smucker, A. J. M. (1998). Temporal trends in nitrogen isotope values of nitrate leaching from an agricultural soil. *Chemical Geology, 146*, 219-227.

Owens, J. (2016). *Understanding how pasture irrigation influences soil nitrous oxide fluxes and nitrous oxide reductase*. Lincoln University.

Owens, J., Clough, T. J., Laubach, J., Hunt, J. E., & Venterea, R. T. (2017). Nitrous oxide fluxes and soil oxygen dynamics of soil treated with cow urine. *Soil Science Society of America Journal, 81*, 289-298.

Owens, J., Clough, T. J., Laubach, J., Hunt, J. E., Venterea, R. T., & Phillips, R. L. (2016). Nitrous oxide fluxes, soil oxygen, and denitrification potential of urine-and non-urine-treated soil under different irrigation frequencies. *Journal of Environmental Quality, 45*, 1169-1177.

Parfitt, R., Stevenson, B. A., Dymond, J. R., Schipper, L. A., Baisden, W. T., & Ballantine, D. (2012). Nitrogen inputs and outputs for New Zealand from 1990 to 2010 at national and regional scales. *New Zealand Journal of Agricultural Research, 55*, 241-262.

Parfitt, R. L., Baisden, T. W., Ross, C. W., Rosser, B. J., Schipper, L. A., & Barry, B. (2013). Influence of erosion and deposition on carbon and nitrogen accumulation in resampled steepland soils under pasture in New Zealand. *Geoderma, 192*, 154-159.

Parsons, A. J., Rowarth, J. S., & Newton, P. C. D. (2009). Managing pasture for animals and soil carbon*New Zealand Grassland Association.* Symposium conducted at the meeting of the Proceedings of the New Zealand Grassland Association

Parsons, A. J., Thornley, J. H. M., Newton, P. C. D., Rasmussen, S., & Rowarth, J. S. (2013). Soil carbon dynamics: the effects of nitrogen input, intake demand and off-take by animals. *Science of The Total Environment, 465*, 205-215.

Patrick Jr, W., & Gotoh, S. (1974). The role of oxygen in nitrogen loss from flooded soils. *Soil Science, 118*, 78-81.

Payne, W. (1973). Reduction of nitrogenous oxides by microorganisms. *Bacteriological Reviews, 37*, 409.

Payne, W. J., Riley, P., & Cox, C. (1971). Separate nitrite, nitric oxide, and nitrous oxide reducing fractions from Pseudomonas perfectomarinus. *Journal of bacteriology, 106*, 356-361.

Pearson, L., Rissmann, C., & Lindsay, J. (2018). Waituna Catchment: Physiographic Risk Assessment. *Land & Water Science Report, 2*.

Pellerin, B. A., Downing, B. D., Kendall, C., Dahlgren, R. A., Kraus, T. E., Saraceno, J., Spencer, R. G., & Bergamaschi, B. A. (2009). Assessing the sources and magnitude of diurnal nitrate variability in the San Joaquin River (California) with an in situ optical nitrate sensor and dual nitrate isotopes. *Freshwater Biology, 54*, 376-387.

Penman, H. L. (1940). Gas and vapour movements in the soil: I. The diffusion of vapours through porous solids. *The Journal of Agricultural Science, 30*, 437-462.

Peterson, M., Curtin, D., Thomas, S., Clough, T., & Meenken, E. (2013). Denitrification in vadose zone material amended with dissolved organic matter from topsoil and subsoil. *Soil Biology and Biochemistry, 61*, 96-104.

Pett-Ridge, J., Petersen, D. G., Nuccio, E., & Firestone, M. K. (2013). Influence of oxic/anoxic fluctuations on ammonia oxidizers and nitrification potential in a wet tropical soil. *FEMS Microbiology Ecology, 85*, 179-194.

Phillips, R. L., McMillan, A. M. S., Palmada, T., Dando, J., & Giltrap, D. J. (2015). Temperature effects on N_2O and N_2 denitrification end-products for a New Zealand pasture soil. *New Zealand Journal of Agricultural Research, 58*, 89-95.

Putz, M., Schleusner, P., Rütting, T., & Hallin, S. (2018). Relative abundance of denitrifying and DNRA bacteria and their activity determine nitrogen retention or loss in agricultural soil. *Soil Biology & Biochemistry, 123*, 97-104.

Qin, S., Hu, C., Clough, T. J., Luo, J., Oenema, O., & Zhou, S. (2017). Irrigation of DOC-rich liquid promotes potential denitrification rate and decreases $N_2O/(N_2O+ N_2)$ product ratio in a 0–2 m soil profile. *Soil Biology & Biochemistry, 106*, 1-8.

Ravishankara, A. R., Daniel, J. S., & Portmann, R. W. (2009). Nitrous oxide (N_2O): the dominant ozone-depleting substance emitted in the 21st century. *Science, 326*, 123-125.

Reverey, F., Ganzert, L., Lischeid, G., Ulrich, A., Premke, K., & Grossart, H. P. (2018). Dry-wet cycles of kettle hole sediments leave a microbial and biogeochemical legacy. *Science of the Total Environment, 627*, 985-996.

Rissmann, C. (2011). *Regional Mapping of Groundwater Denitrification Potential and Aquifer Sensitivity*. doi:10.13140/2.1.3412.5606

Rissmann, C. (2012). *The Extent of Nitrate in Southland Groundwaters Regional 5 Year Median (2007–2012 (June))*. doi:10.13140/2.1.1184.3361

Rissmann, C., Pearson, L., Lindsay, J., Beyer, M., Marapara, T., Badenhop, A., & Martin, A. (2018). Integrated landscape mapping of water quality controls for farm planning-applying a high resolution physiographic approach to the Waituna Catchment, Southland Symposium conducted at the meeting of the Farm environmental planning-Science, policy and practice.(Eds. LD Currie and CL Christensen) http://flrc.massey.ac. nz/workshops/18/Manuscripts/Paper_Rissmann_2018. pdf. Occasional Report

Rissmann, C., Rodway, E., Beyer, M., Hodgetts, J., Snelder, T., Pearson, L., Killick, M., Marapara, T., Akbaripasand, A., & Hodson, R. (2016). Physiographics of Southland Part 1: Delineation of key drivers of regional hydrochemistry and water quality Technical Report.

Robertson, G. P., & Groffman, P. M. (2007). Nitrogen Transformations. In E. A. Paul (Ed.), *Soil Microbiology, Ecology and Biochemistry* (3 ed., pp. 341-362): Academic press.

Robinson, D. (2001). δ 15 N as an integrator of the nitrogen cycle. *Trends in Ecology & Evolution, 16*, 153-162.

Rock, L., Ellert, B., & Mayer, B. (2011). Tracing sources of soil nitrate using the dual isotopic composition of nitrate in 2 M KCl-extracts. *Soil Biology and Biochemistry, 43*, 2397-2405.

Rogers, K. M., Turnbull, R. E., Martin, A. P., Baisden, T. W., & Rattenbury, M. S. (2017). Stable isotopes reveal human influences on southern New Zealand soils. *Applied Geochemistry, 82*, 15-24.

Rolston, D. E. (1986). Gas flux. *Methods of Soil Analysis: Part 1—Physical and Mineralogical Methods*, 1103-1119.

Rolston, D. E., & Moldrup, P. (2002). 4.3 Gas Diffusivity. *Methods of Soil Analysis: Part 4 Physical Methods*, 1113-1139.

Romano, N., Dane, J., & Hopmans, J. (2002). Water Retention and Storage: Suction table. In (pp. 692-698)

Romera, A. J., Levy, G., Beukes, P. C., Clark, D. A., & Glassey, C. B. (2012). A urine patch framework to simulate nitrogen leaching on New Zealand dairy farms. *Nutrient Cycling in Agroecosystems, 92*, 329-346.

Ruser, R., Flessa, H., Russow, R., Schmidt, G., Buegger, F., & Munch, J. C. (2006). Emission of N^2O, N^2 and CO_2 from soil fertilized with nitrate: effect of compaction, soil moisture and rewetting. *Soil Biology & Biochemistry, 38*, 263-274.

Rütting, T., Boeckx, P., Müller, C., & Klemedtsson, L. (2011). Assessment of the importance of dissimilatory nitrate reduction to ammonium for the terrestrial nitrogen cycle. *Biogeosciences, 8*, 1779-1791.

Ryden, J. C. (1986). Gaseous Losses of Nitrogen from Grassland. In *Nitrogen Fluxes in Intensive Grassland Systems* (pp. 59-73): Springer.

Savard, M. M., Paradis, D., Somers, G., Liao, S., & van Bochove, E. (2007). Winter nitrification contributes to excess NO_3^- in groundwater of an agricultural region: A dual-isotope study. *Water Resources Research, 43*.

Schipper, L. A., Baisden, W. T., Parfitt, R. L., Ross, C., Claydon, J. J., & Arnold, G. (2007). Large losses of soil C and N from soil profiles under pasture in New Zealand during the past 20 years. *Global Change Biology, 13*, 1138-1144.

Schipper, L. A., Dodd, M. B., Pronger, J., Mudge, P. L., Upsdell, M., & Moss, R. A. (2013). Decadal changes in soil carbon and nitrogen under a range of irrigation and phosphorus fertilizer treatments. *Soil Science Society of America Journal, 77*, 246-256.

Schipper, L. A., Parfitt, R. L., Ross, C., Baisden, T. W., Claydon, J. J., & Fraser, S. (2010). Gains and losses in C and N stocks of New Zealand pasture soils depend on land use. *Agriculture, Ecosystems & Environment, 139*, 611-617.

Schipper, L. A., Percival, H. J., & Sparling, G. P. (2004). An approach for estimating when soils will reach maximum nitrogen storage. *Soil Use & Management, 20*, 281-286.

Schullehner, J., & Hansen, B. (2014). Nitrate exposure from drinking water in Denmark over the last 35 years. *Environmental Research Letters, 9*, 095001.

Schullehner, J., Hansen, B., Thygesen, M., Pedersen, C. B., & Sigsgaard, T. (2018). Nitrate in drinking water and colorectal cancer risk: A nationwide population-based cohort study. *International Journal of Cancer, 143*, 73-79.

Sebestyen, S. D., Boyer, E. W., Shanley, J. B., Kendall, C., Doctor, D. H., Aiken, G. R., & Ohte, N. (2008). Sources, transformations, and hydrological processes that control stream nitrate and dissolved organic matter concentrations during snowmelt in an upland forest. *Water Resources Research, 44*.

Seiler, R. L. (2005). Combined use of $\delta^{15}N$ and $\delta^{18}O$ of nitrate and $\delta^{11}B$ to evaluate nitrate contamination in groundwater. *Applied Geochemistry, 20*, 1626-1636.

Seitzinger, S., Harrison, J. A., Böhlke, J., Bouwman, A., Lowrance, R., Peterson, B., Tobias, C., & Drecht, G. V. (2006). Denitrification across landscapes and waterscapes: a synthesis. *Ecological Applications, 16*, 2064-2090.

Selbie, D. R., Buckthought, L. E., & Shepherd, M. A. (2015). The challenge of the urine patch for managing nitrogen in grazed pasture systems. In *Advances in agronomy* (Vol. 129, pp. 229-292): Elsevier.

Sgouridis, F., Heppell, C. M., Wharton, G., Lansdown, K., & Trimmer, M. (2011). Denitrification and dissimilatory nitrate reduction to ammonium (DNRA) in a temperate re-connected floodplain. *Water Research, 45*, 4909-4922.

Shearer, G., & Kohl, D. H. (1988). Nitrogen isotopic fractionation and ^{18}O exchange in relation to the mechanism of denitrification of nitrite by Pseudomonas stutzeri. *Journal of Biological Chemistry, 263*, 13231-13245.

Sherlock, R. R., & Goh, K. M. (1984). Dynamics of ammonia volatilization from simulated urine patches and aqueous urea applied to pasture I. Field experiments. *Fertilizer Research, 5*, 181-195.

Shiels, D. R. (2010). Implementing landscape indices to predict stream water quality in an agricultural setting: An assessment of the Lake and River Enhancement (LARE) protocol in the Mississinewa River watershed, East-Central Indiana. *Ecological Indicators, 10*, 1102-1110.

SIDDC. (2017). New Zealand Dairy Statistics 2016-17. Livestock Improvement Corporation Limited and Dairy NZ Limited. Retrieved January 2018, from LIC-Dairy NZ https://www.lic.co.nz/about/dairy-statistics/

Sigman, D., Casciotti, K., Andreani, M., Barford, C., Galanter, M., & Böhlke, J. (2001). A bacterial method for the nitrogen isotopic analysis of nitrate in seawater and freshwater. *Analytical chemistry, 73*, 4145-4153.

Sigman, D. M., Granger, J., DiFiore, P. J., Lehmann, M. M., Ho, R., Cane, G., & van Geen, A. (2005). Coupled nitrogen and oxygen isotope measurements of nitrate along the eastern North Pacific margin. *Global Biogeochemical Cycles, 19*.

Šimek, M., Brůček, P., Hynšt, J., Uhlířová, E., & Petersen, S. O. (2006). Effects of excretal returns and soil compaction on nitrous oxide emissions from a cattle overwintering area. *Agriculture, Ecosystems & Environment, 112*, 186-191.

Šimek, M., Jíšová, L., & Hopkins, D. W. (2002). What is the so-called optimum pH for denitrification in soil? *Soil Biology and Biochemistry, 34*, 1227-1234.

Six, J., Bossuyt, H., Degryze, S., & Denef, K. (2004). A history of research on the link between (micro) aggregates, soil biota, and soil organic matter dynamics. *Soil & Tillage Research, 79*, 7-31.

Smid, A., & Beauchamp, E. (1976). Effects of temperature and organic matter on denitrification in soil. *Canadian Journal of Soil Science, 56*, 385-391.

Smith, C., Wilcock, R., Vant, W., Smith, D., & Cooper, A. (1993). Towards sustainable agriculture: Freshwater quality in New Zealand and the influence of agriculture (Prepared for Ministry of Agriculture and Fisheries and Ministry for the Environment). *Hamilton, New Zealand: National Institute of Water & Atmospheric Research*.

Smith, K. A., Ball, T., Conen, F., Dobbie, K. E., Massheder, J., & Rey, A. (2003). Exchange of greenhouse gases between soil and atmosphere: interactions of soil physical factors and biological processes. *European Journal of Soil Science, 54*, 779-791.

Smith, V. H., Wood, S. A., McBride, C. G., Atalah, J., Hamilton, D. P., & Abell, J. (2016). Phosphorus and nitrogen loading restraints are essential for successful eutrophication control of Lake Rotorua, New Zealand. *Inland Waters, 6*, 273-283.

Šnajdr, J., Valášková, V., Merhautová, V., Herinková, J., Cajthaml, T., & Baldrian, P. (2008). Spatial variability of enzyme activities and microbial biomass in the upper layers of Quercus petraea forest soil. *Soil Biology & Biochemistry, 40*, 2068-2075.

Snelder, T., Hughes, B., Wilson, K., & Dey, K. (2016). Physiographic Zones for the Southland Region: Classification system validation and testing report. *Water Land People Report prepared for Environment Southland.*, 60.

Song, B., Lisa, J. A., & Tobias, C. R. (2014). Linking DNRA community structure and activity in a shallow lagoonal estuarine system. *Frontiers in Microbiology, 5*, 460.

Soussana, J. F., Loiseau, P., Vuichard, N., Ceschia, E., Balesdent, J., Chevallier, T., & Arrouays, D. (2004). Carbon cycling and sequestration opportunities in temperate grasslands. *Soil Use & Management, 20*, 219-230.

Spohn, M., Klaus, K., Wanek, W., & Richter, A. (2016). Microbial carbon use efficiency and biomass turnover times depending on soil depth–Implications for carbon cycling. *Soil Biology & Biochemistry, 96*, 74-81.

Stark, C. H., & Richards, K. G. (2008). The continuing challenge of agricultural nitrogen loss to the environment in the context of global change and advancing research. *Dynamic Soil, Dynamic Plant, 2*, 1-12.

Stein, L. Y. (2011). Heterotrophic nitrification and nitrifier denitrification. In B. B. Ward, D. J. Arp & M. G. Klotz (Eds.), *Nitrification*: American Society for Microbiology Press.

Stein, L. Y. (2019). Insights into the physiology of ammonia-oxidizing microorganisms. *Current Opinion in Chemical Biology, 49*, 9-15.

Stenger, R., Barkle, G., Burgess, C., Wall, A., & Clague, J. C. (2008). Low nitrate contamination of shallow groundwater in spite of intensive dairying: the effect of reducing conditions in the vadose zone-aquifer continuum. *Journal of Hydrology (New Zealand), 47*, 1.

Stenger, R., Clague, J., Woodward, S., Moorhead, B., Burbery, L., & Canard, H. (2012). Groundwater assimilative capacity-an untapped opportunity for catchment-scale nitrogen management. *Advanced Nutrient Management: Gains from the Past-Goals for the Future*.

Stepniewski, W. (1981). *Oxygen diffusion and strength as related to soil compaction. II. Oxygen diffusion coefficient* (Vol. 14)

Stevenson, B. A., Parfitt, R., Schipper, L. A., Baisden, W. T., & Mudge, P. (2010). Relationship between soil $\delta^{15}N$, C/N and N losses across land uses in New Zealand. *Agriculture, ecosystems & environment, 139*, 736-741.

Stokes, A., Atger, C., Bengough, A. G., Fourcaud, T., & Sidle, R. C. (2009). Desirable plant root traits for protecting natural and engineered slopes against landslides. *Plant & Soil, 324*, 1-30.

Tiedje, J. M., Sexstone, A. J., Myrold, D. D., & Robinson, J. A. (1983). Denitrification: Ecological Niches, Competition and Survival. *48*, 569-583.

Trost, B., Prochnow, A., Drastig, K., Meyer-Aurich, A., Ellmer, F., & Baumecker, M. (2013). Irrigation, soil organic carbon and N_2O emissions. A review. *Agronomy for Sustainable Development, 33*, 733-749.

Uchida, Y., Clough, T. J., Kelliher, F. M., & Sherlock, R. R. (2008). Effects of aggregate size, soil compaction, and bovine urine on N_2O emissions from a pasture soil. *Soil Biology and Biochemistry, 40*, 924-931.

Ueda, S., Ohno, H., Ogura, N., Katase, T., & Watanabe, K. (2006). Nitrate decrease with isotopic fractionation in riverside sediment column during infiltration experiment. *Water, Air, & Soil Pollution, 174*, 47-61.

Van Cleemput, O., & Baert, L. (1984). Nitrite: a key compound in N loss processes under acid conditions? *Plant and Soil, 76*, 233-241.

Van Cleemput, O., & Patrick, W. (1974). Nitrate and nitrite reduction in flooded gamma-irradiated soil under controlled pH and redox potential conditions. *Soil Biology and Biochemistry, 6*, 85-88.

van der Weerden, T. J., Kelliher, F. M., & de Klein, C. A. M. (2012). Influence of pore size distribution and soil water content on nitrous oxide emissions. *Soil Research, 50*, 125-135.

Van Kessel, J. (1977). Factors affecting the denitrification rate in two water-sediment systems. *Water Research, 11*, 259-267.

Venterea, R. T. (2007). Nitrite-driven nitrous oxide production under aerobic soil conditions: kinetics and biochemical controls. *Global Change Biology, 13*, 1798-1809.

Venterea, R. T., Clough, T. J., Coulter, J. A., Breuillin-Sessoms, F., Wang, P., & Sadowsky, M. J. (2015). Ammonium sorption and ammonia inhibition of nitrite-oxidizing bacteria explain contrasting soil N 2 O production. *Scientific Reports, 5*, 12153.

Wada, E., & Hattori, A. (1978). Nitrogen isotope effects in the assimilation of inorganic nitrogenous compounds by marine diatoms. *Geomicrobiology Journal, 1*, 85-101.

Warneke, S., Schipper, L. A., Bruesewitz, D. A., & Baisden, W. T. (2011). A comparison of different approaches for measuring denitrification rates in a nitrate removing bioreactor. *Water research, 45*, 4141-4151.

Watanabe, I., & Furusaka, C. (1980). Microbial ecology of flooded rice soils. In *Advances in microbial ecology* (pp. 125-168): Springer.

Webb, J., Sylvester-Bradley, R., & Seeney, F. M. (1997). The effects of site and season on the fate of nitrogen residues from root crops grown on sandy soils. *Journal of Agricultural Science, 128*, 445-460.

Weier, K. L., Doran, J. W., Power, J. F., & Walters, D. T. (1993). *Denitrification and the Dinitrogen/Nitrous Oxide Ratio as Affected by Soil Water, Available Carbon, and Nitrate* (Vol. 57). doi:10.2136/sssaj1993.03615995005700010013x

Wells, N. S. (2013). *Stable isotopes as indicators of nitrate attenuation across landscapes*. Lincoln University.

Wells, N. S., Baisden, W. T., & Clough, T. J. (2015). Ammonia volatilisation is not the dominant factor in determining the soil nitrate isotopic composition of pasture systems. *Agriculture, Ecosystems & Environment, 199*, 290-300.

Wells, N. S., Baisden, W. T., Horton, T., & Clough, T. J. (2016). Spatial and temporal variations in nitrogen export from a New Zealand pastoral catchment revealed by stream water nitrate isotopic composition. *Water Resources Research*.

White, J., & Hodgson, J. G. (1999). *New Zealand Pasture and Crop Science*: Oxford University Press.

Widory, D., Kloppmann, W., Chery, L., Bonnin, J., Rochdi, H., & Guinamant, J.-L. (2004). Nitrate in groundwater: an isotopic multi-tracer approach. *Journal of Contaminant Hydrology, 72*, 165-188.

Wijler, J., & Delwiche, C. (1954). Investigations on the denitrifying process in soil. *Plant and Soil, 5*, 155-169.

Woods, R., Cameron, K., Edwards, G., Di, H., & Clough, T. (2016). Does gibberellic acid reduce nitrate leaching losses from animal urine patches. *Integrated nutrient and water management for sustainable farming*.

Woodward, S. J., Stenger, R., & Bidwell, V. J. (2013). Dynamic analysis of stream flow and water chemistry to infer subsurface water and nitrate fluxes in a lowland dairying catchment. *Journal of Hydrology, 505*, 299-311.

Wrage-Mönnig, N., Horn, M. A., Well, R., Müller, C., Velthof, G. L., & Oenema, O. (2018). The role of nitrifier denitrification in the production of nitrous oxide revisited. *Soil Biology & Biochemistry, 123*, A3-A16.

Wrage, N., Van Groenigen, J. W., Oenema, O., & Baggs, E. M. (2005). A novel dual-isotope labelling method for distinguishing between soil sources of N_2O. *Rapid Communications in Mass Spectrometry, 19*, 3298-3306.

Wrage, N., Velthof, G. L., Van Beusichem, M. L., & Oenema, O. (2001). Role of nitrifier denitrification in the production of nitrous oxide. *Soil biology and Biochemistry, 33*, 1723-1732.

Wriedt, G., & Rode, M. (2006). Modelling nitrate transport and turnover in a lowland catchment system. *Journal of Hydrology, 328*, 157-176.

Wu, L., McGechan, M. B., Watson, C. A., & Baddeley, J. A. (2005). Developing existing plant root system architecture models to meet future agricultural challenges. *Advances in Agronomy, 85*, 181-219.

Xue, D., Botte, J., De Baets, B., Accoe, F., Nestler, A., Taylor, P., Van Cleemput, O., Berglund, M., & Boeckx, P. (2009). Present limitations and future prospects of stable isotope methods for nitrate source identification in surface-and groundwater. *Water research, 43*, 1159-1170.

Xue, Y., Song, J., Zhang, Y., Kong, F., Wen, M., & Zhang, G. (2016). Nitrate pollution and preliminary source identification of surface water in a semi-arid river basin, using isotopic and hydrochemical approaches. *Water, 8*, 328.

Yoon, S., Cruz-García, C., Sanford, R., Ritalahti, K. M., & Löffler, F. E. (2015). Denitrification versus respiratory ammonification: environmental controls of two competing dissimilatory NO_3^-/NO_2^- reduction pathways in Shewanella loihica strain PV-4. *The ISME journal, 9*, 1093.

Zhu, X., Burger, M., Doane, T. A., & Horwath, W. R. (2013). Ammonia oxidation pathways and nitrifier denitrification are significant sources of N_2O and NO under low oxygen availability. *Proceedings of the National Academy of Sciences, 110*, 6328-6333.

Zuraidah, Y., Aminuddin, H., Jamal, T., Jamarei, O., Siti, Z. D., Osumanu, H. A., & Mohamadu, B. J. (2011). Pores reconfiguration in compacted Bernam series soil. *American Journal of Applied Sciences, 8*, 212-216.